# The Powering Performances of Large Waterjet and Propeller Driven Catamarans at Medium-Speed

by

Iwan Mustaffa Kamal

B.Eng (Hons) Mechanical Engineering (University of Plymouth, UK)
M.Eng Marine Technology (Universiti Teknologi Malaysia)

Submitted in fulfilment of the requirements for the degree of Doctor of Philosophy

**Supervisors**

Assoc. Prof. Jonathan Binns

Prof. Neil Bose

Prof. Giles Thomas

Assoc. Prof. Shuhong Chai

National Centre for Maritime Engineering and Hydrodynamics

Australian Maritime College

**University of Tasmania**

June 2016

# Declaration of Originality

I declare that this thesis contains no material which has been accepted for a degree or diploma by the University or any other institution of learning, except by way of background information and duly acknowledged in the thesis, and that, to the best of my knowledge and belief, this thesis contains no material previously published or written by another person, except where due acknowledgement is made in the text of the thesis nor this thesis contain any material that infringes copyright.

Iwan Mustaffa Kamal June 2016

# Statement of Authority of Access

This thesis may be made available for loan and limited copying in accordance with the *Copyright Act 1968.*

Iwan Mustaffa Kamal June 2016

**Abstract**

Wave-piercing catamaran builder INCAT has been developing new energy-efficient hull forms for medium speeds operation (Froude number between 0.25 to 0.50), to reduce the environmental impact of fast sea transportation. This research focused on the investigation into the performance of the potential propulsors for these new medium-speed catamarans which could either be waterjets or propellers. The challenge is in defining the appropriate speed changeover point between using waterjets and propellers for large catamarans operating in the medium speed regime.

The main approach in determining which propulsor is more efficient was to perform experimental model testing of a self-propelled catamaran using a towing tank. These tests were done for both propeller and waterjet propulsion. A single demihull test using the tank wall as the plane of symmetry was employed rather than using the whole catamaran model in order to maximise the size of the model.

The comparison of these two types of propulsion required new studies in several areas. A study was made as to investigate the magnitude of the scale effect on the small propeller used in the self-propulsion test. A method of scale effect correction was proposed as the scale effect corrections on the propeller proposed by ITTC 1978 method are inappropriate for corrections over large scales for variations in propulsors. The self-propulsion test (SPT) only method was chosen over the traditional ITTC 1978 method as some of the empirical approximation in the ITTC 1978 method were not applicable; uncertainty analysis revealed that the SPT method has lower uncertainties than the traditional ITTC 1978 method.

The two catamaran models had a different hullform designed to the specific propulsion method. So both of these catamarans could not be directly compared as the length to displacement ratios and the wetted surface area ratio were not identical. Therefore comparative methods that can adequately compare these two catamarans were sought. Three approaches were made in order to assess the merit of the waterjet and the propeller as the propulsor for the medium-speed catamaran: an approach using the propulsive efficiency, an approach using transport efficiency or transport factor and an approach using a scaling to a similar size method. The study on the propulsive efficiency showed that the propeller catamaran is more efficient than the waterjet catamaran up to a Froude number of 0.33. In the transport efficiency approach, the propeller catamaran was found to be more efficient than the waterjet catamaran up to a Froude number of 0.44, at higher speeds waterjets become superior. Similar results were found using the scaling to a similar size method. These findings suggest that the propeller propulsion is considered to be the best option for a large energy-efficient catamaran operating in the medium-speed regime. Finally, methods of improving the ship powering prediction method for catamarans are proposed, based on the reasons for the variation in Froude number cross-overs from the different comparison techniques.

# Acknowledgement

All praise to Allah ASWJ, the Most Gracious and the Most Merciful, Who has created mankind with knowledge, wisdom and power. The process of doing a PhD, earning a doctorate and writing a thesis is long and arduous – and it is certainly not done single-handedly. Therefore I would like to acknowledge a group of people that have been an important part of me in completing this PhD research project. This thesis is based on research carried out from 2012 – 2015 in the National Centre for Maritime Engineering and Hydrodynamics, Australian Maritime College at the University of Tasmania.

First and foremost, I would like to thank my supervisors Assoc. Prof. Jonathan Binns (Australian Maritime College), Prof. Neil Bose (Australian Maritime College), Prof. Giles Thomas (University College London) and Assoc. Prof. Shuhong Chai (Australian Maritime College) for the help and encouragement they have provided during the course of this project. Their insight, feedback and advice were influential and essential throughout the project and the thesis writing process.

I would also like to thank Gary Davidson and rest of the staff at Incat Tasmania and Revolution Design Pty Ltd for all their support in this project.

My special thanks are also extended to those people who assisted with the design, instrumentation, manufacturing and testing of the single demihull propeller driven Incat catamaran model:

- AMC Towing Tank staffs and technicians, Dr Gregor Macfarlane, Tim Lilienthal, Kirk Meyer and Liam Honeychurch for their support and assistance during model experiments at the Australian Maritime College Towing Tank.

- AMC Technical Support staff Michael Underhill, Jock Ferguson and Rowan Carins for their valuable experience and technical support during towing tank experiments.

- Stuart Philips, the model maker, for the construction of the catamaran model hull.

I would also like thank to my fellow postgraduate and project team members at the National Centre for Maritime Engineering and Hydrodynamics, Australian Maritime College Konrad Zürcher and Max Haase for all the discussions, sharing ideas and the valuable assistance that they have provided during the course of this project. It has been my pleasure to work with them in this project.

I would also like to thank for the help received from Mrs. Fatin Zawani Zainal Azaim of Universiti Kuala Lumpur, Malaysian Institute of Marine Engineering Technology, Lumut, Malaysia for her help in proof-reading this thesis.

Finally and most importantly, I would like to thank my wife Syima and sons Amir, Imran and Danish who have been my source of strength and inspiration.

This research has been conducted as part of a collaborative research project between Incat Tasmania Pty Ltd, Revolution Design Pty Ltd, Wartsila Corporation, MARIN and the Australian Maritime College at the University of Tasmania with support from the Australian Research Council's Linkage Project funding scheme. Project ID: LP110100080

# Table of Contents

# List of Figures

# List of Tables

# Nomenclature

| | |
|---|---|
| $A$ | propeller disc area in $m^2$ |
| $A_D$ | developed blade area of propeller in $m^2$ |
| $A_E$ | expanded blade area of propeller in $m^2$ |
| $Ai$ | cross-section area at station i – waterjet in $m^2$ |
| $A_O$ | propeller disc area in $m^2$ |
| $A_X$ | maximum transverse area in $m^2$ |
| $A_T$ | transom immersed area in $m^2$ |
| $B_{Mx}$ | bias error in the resistance measurements |
| $B_Q$ | bias error in the propeller torque |
| $B_{QAD}$ | bias error in the A/D converter in the torque measurements |
| $B_{Qcf}$ | bias error in the torque transducer calibration |
| $B_{Qw}$ | bias error in the individual weights used in the torque calibration |
| $B_T$ | bias error in the thrust measurements |
| $B_{TAD}$ | bias error in the A/D converter in the thrust measurements |
| $B_{Tcf}$ | bias error in the thrust transducer calibration |
| $B_{Tw}$ | bias error in the individual weights used in the thrust calibration |
| $B_{WL}$ | breadth at waterline in m |
| $B_{WL,\ DH}$ | breadth at waterline (demihull) in m |
| $c$ | chord length of propeller blades in m |
| $c$ | volt increment in the mass/volt relation calibration curve |
| $c_{0.7}$ | chord length of propeller blades at radius 0.7R in m |
| $C_A$ | model-ship correlation allowance |
| $C_{AA}$ | still-air resistance coefficient |
| $C_B$ | block coefficient |
| $C_{FD}$ | coefficient form of skin friction corrrection between model and full scale |
| $C_F$ | frictional resistance coefficient |

| | |
|---|---|
| $C_{FM}$ | model's fricitional resistance coefficient |
| $C_{FS}$ | ship's frictional resistance coefficient |
| $C_{np}$ | shaft speed correlation factor for contant power |
| $C_P$ | prismatic coefficient |
| $C_R$ | residual resistance coefficient |
| $C_{TM}$ | model's total resistance coefficient |
| $C_T$ | total resistance coefficient |
| $C_{TS}$ | ship's total resistance coefficient |
| $D$ | propeller diameter in m |
| $D_M$ | model propeller diameter in m |
| $D_S$ | ship's propeller diameter in m |
| $DLR$ | displacement over length ratio |
| $E_1$ | energy flux at station 1, point of tangency at forward end of waterjet inlet |
| $E_1$ | transport efficiency |
| $E_3$ | transport efficiency |
| $E_7$ | energy flux at station 7, a point behind the nozzle where the static pressure coefficient in the jet is zero – vena contracta |
| $F_D$ | skin friction correction between model and full scale in N |
| $F_G$ | gross towing force of the waterjet driven model in N |
| $F_M$ | towing force for the model in N |
| $F_{nh}$ | Depth Froude number |
| $F_R$ | Froude number |
| $F_{T=0}$ | towing force at zero propeller thrust in N |
| $g$ | gravitational acceleration in m/s$^2$ |
| $h_J$ | height above undisturbed free surface relative to the waterjet unit centreline in m |
| $J$ | advance coefficient of propeller |
| $J_M$ | advance coefficient of model propeller |
| $J_O$ | advance coefficient corresponding to $K_{TO}$ at the thrust 'identity' |

| | |
|---|---|
| $J_P$ | advance coefficient based on the towing speed of the model |
| | $V$ |
| $J_S$ | advance coefficient of ship propeller |
| $J_{TS}$ | operating value of the advance coefficient of the ship |
| | *propeller* |
| $k$ | form factor |
| $k_S$ | mean amplitude of surface roughnessof the hull in m |
| $K_{FD}$ | towing force coefficient |
| $K_Q$ | propeller torque coefficient |
| $K_{Qcorr}$ | corrected propeller torque coefficient |
| $K_{QP}$ | propeller torque coefficient in the behind condition |
| $K_{QO}$ | open water propeller torque coefficient at the ‘thrust identity’ |
| $K_{QO}$ | open water propeller torque coeffcient |
| $K_{QS}$ | full-scale propeller torque coefficient |
| $K_{QOS}$ | full-scale open water propeller torque coefficient |
| $K_{QP}$ | propeller torque coefficient in the behind condition |
| $K_T$ | propeller thrust coefficient |
| $K_{Tcorr}$ | corrected propeller thrust coefficient |
| $K_{TO}$ | open water propeller thrust coefficient at the ‘thrust identity’ |
| $K_{TO}$ | open water propeller thrust coefficient |
| $K_{TOS}$ | full-scale open water propeller thrust coefficient |
| $K_{TP}$ | propeller thrust coefficient in the behind condition |
| $K_{TS}$ | operating value of the thrust coefficient of the ship propeller |
| $L$ | ship length in m |
| $L_{WL}$ | length on waterline in m |
| $m_i$ | mass increment in the mass/volt relation curve of the load |
| | cell calibration in kg |
| $m_x$ | resistance measured in the data acquisition system in kg |
| $n$ | number of repeated measurements in the time series data |
| | taken from the data acquisition system |
| $n$ | propeller shaft speed in rev/sec |
| $n_M$ | model propeller shaft speed in rev/sec |

| | |
|---|---|
| $n_S$ | ship propeller shaft speed in rev/sec |
| $N$ | propeller shaft speed in rev/min |
| $P$ | geometrical pitch of propeller in m |
| $P$ | power in kW |
| $P_B$ | brake power of the engine in kW |
| $P_D$ | delivered power in kW |
| $P_{DS}$ | delivered power for the ship in kW |
| $P_E$ | effective power for the ship in kW |
| $P_{JSE}$ | effective waterjet system power in kW |
| $P_{PE}$ | waterjet pump effective power in kW |
| $P_S$ | shaft power in kW |
| $P_T$ | thrust power in kW |
| $\bar{q}$ | mean of individual measurement in the data acquisition system |
| $q_k$ | individual measurement in the data acquisition system |
| $Q$ | propeller torque in Nm |
| $Q_j$ | volume flow rate through the jet |
| $Q_M$ | model propeller torque in Nm |
| $Q_O$ | open water propeller torque in Nm |
| $Q_S$ | ship propeller torque in Nm |
| $r$ | local radius at a propeller blade fraction in m |
| $r_B$ | propeller boss radius in m |
| $R$ | propeller radius in m |
| $R_{BH}$ | bare-hull resistance in N |
| $R_C$ | resistance of the model corrected for the water temperature at the time of the self-propulsion test in N |
| $R_e$ | Reynolds number |
| $R_F$ | frictional resistance in N |
| $R_{n0.7}$ | local Reynolds number at propeller radius 0.7R |
| $R_N$ | Reynolds number |
| $R_T$ | total resistance in N |
| $R_{TM}$ | total resistance of the model in N |

| | |
|---|---|
| $R_{TS}$ | total resistance of the ship in N |
| $s$ | gradient of the mass/volt relation curve |
| $s/L$ | twin-hull separation ratio |
| $S_S$ | wetted surface area for ship's hull in $m^2$ |
| $S_M$ | wetted surface area for model's hull in $m^2$ |
| $S_{DH}$ | wetted surface area for single demihull in $m^2$ |
| $t$ | thrust deduction fraction |
| $t^*$ | thrust deduction fraction obtained from the $F$-$T$ slope |
| $T$ | ship draft in m |
| $TE$ | transport efficiency |
| $T_{F=0}$ | thrust at zero towing force in N |
| $T_G$ | gross thrust of the waterjet in N |
| $T_M$ | model propeller thrust in N |
| $T_O$ | open water propeller thrust in N |
| $T_S$ | ship propeller thrust in N |
| $u$ | uncertainty value in the towing tank measurement |
| $U_{CT}$ | overall uncertainties in the total resistance coefficient |
| $U_{nS}$ | overall uncertainties in the ship's shaft speed |
| $U_{PD}$ | overall uncertainties in the delivered power |
| $U_{QS}$ | overall uncertainties in the ship's propeller torque |
| $U_x$ | local velocity at the propeller disc area |
| $U_{inf}$ | free stream velocity |
| $U_\infty$ | model forward speed |
| $v_i$ | volt increment in the mass/volt relation calibration curve |
| $V$ | forward speed or towing speed or freestream velocity in m/s |
| $V_A$ | advance speed in m/s |
| $V_i$ | inlet velocity – waterjet in m/s |
| $V_j$ | jet velocity – waterjet in m/s |
| $V_M$ | model speed in m/s |
| $V_S$ | ship speed in m/s |
| $w$ | wake fraction |
| $w_M$ | wake fraction of the model |

| | |
|---|---|
| $w_{QM}$ | wake fraction of the model obtained using 'torque identity' |
| $w_S$ | wake fraction of the ship |
| $w_T$ | nominal wake of the ship |
| $\bar{w}_T$ | mean nominal wake of the ship |
| $w_{TM}$ | wake fraction of the model |
| $w_{TS}$ | wake fraction of the ship |
| $W$ | vessel's deadweight in tonnes |
| $W_d$ | vessel's deadweight in tonnes |
| $W_D$ | vessel's deadweight in kg |
| $z$ | sinkage in m |
| $z_{aft}$ | aft sinkage in m |
| $z_{fwd}$ | forward sinkage in m |
| $Z$ | number of propeller blades |
| $\Delta$ | ship's displacement in tonnes |
| $\Delta_M$ | model displacement in kg |
| $\Delta_S$ | full scale displacement in kg |
| $\Delta C_D$ | increment in drag coefficient between model and full scale |
| $\Delta\ C_F$ | frictional resistance due to roughness |
| $\Delta K_Q$ | scale correction on open water propeller torque coefficient |
| $\Delta K_T$ | scale correction on open water propeller thrust coefficient |
| $\Delta M$ | change in the momentum flux - waterjet |
| $\Delta V$ | increment in speed due to blockage |
| $\eta$ | efficiency |
| $\eta_D$ | propulsive efficiency |
| $\eta_H$ | hull efficiency |
| $\eta_i$ | intake efficiency - waterjet |
| $\eta_{INT}$ | total interaction efficiency of waterjet |
| $\eta_{inst}$ | waterjet pump installation efficiency |
| $\eta_n$ | nozzle efficiency - waterjet |
| $\eta_O$ | open water propeller efficiency |
| $\eta_{pump}$ | pump efficiency - waterjet |
| $\eta_P$ | pump element efficiency - waterjet |

| | |
|---|---|
| $\eta_R$ | relative rotative efficiency |
| $\eta_S$ | shaft transmission efficiency |
| $\eta_T$ | overall propulsive efficiency |
| $\lambda$ | scale ratio |
| $\upsilon$ | kinematic viscosity in $m^2/s$ |
| $\pi$ | pi |
| $\rho$ | water density in $kg/m^3$ |
| $\rho_M$ | fresh water density for model in $kg/m^3$ |
| $\rho_S$ | sea water density for ship in $kg/m^3$ |
| $\varsigma_{57}$ | outlet loss factor between station 5, behind stator – pump exit and station 7, point behind the nozzle where the static pressure coefficient in the jet is zero – vena contracta |
| $\sigma_{0.7R}$ | local cavitation number at 0.7R propeller radius |
| $\tau_C$ | thrust loading coefficient of propeller |
| $\varphi$ | propeller pitch angle in degrees |
| $\phi$ | misalignment angle of the load cell in degrees |
| $\phi$ | propeller disc area circumferential angle relative to propeller directrix in degrees |

# Abbreviations

| | |
|---|---|
| ABS | Acrylonitrile butadiene styrene |
| A/D | Analog to Digital |
| AMC | Australian Maritime College |
| AMTI | Advanced Mechanical Technology Inc. |
| ASME | American Society of Mechanical Engineers |
| AWJ | Advanced Waterjet |
| BAR | Blade Area Ratio |
| CAD | Computer Aided Drawing |
| CFD | Computational Fluid Dynamics |
| $CO_2$ | Carbon Dioxide |
| CNC | Computer Numerical Controlled |
| CPP | Controllable Pitch Propeller |
| DAQ | Data Acquisition |
| EEDI | Energy Efficiency Design Index |
| FPP | Fixed Pitch Propeller |
| FS | Full-scale |
| FTV | Fisheries Training Vessel |
| GE | General Electric |
| HSD | Hardanger Sunnhorlandske Dampskipsselskap |
| HSV | High-Speed Vessel |
| ID | Identification |
| IMO | International Maritime Organization |
| INSEAN | Istituto Nazionale Per Studi Ed Esperienze Di Architettura Navale, Roma, Italy |
| ISO | International Organization for Standardisation |
| ITTC | International Towing Tank Conference |
| JHSV | Joint High Speed Vessel |
| LDV | Laser Doppler Velocimetry |
| LVDT | Linear Variable Differential Transformer |
| KAMEWA | Karlstad Mekaniska Werkstads AB |
| MARIN | Maritime Research Institute of Netherlands |
| MARPOL | International Convention for the Prevention of Pollution from Ships |
| MCM | Monte Carlo Method |

| | |
|---|---|
| MCR | Maximum Continuous Rating |
| MEPC | Marine Environment Protection Committee |
| MIT | Massachusetts Institute of Technology |
| MS | Model scale |
| MTU | Motoren und Turbinen Union GmbH |
| NACA | The National Advisory Committee for Aeronautics |
| NSRDC | The Naval Ship Research and Development Center |
| NSWCCD | The Naval Surface Warfare Centre, Carderock Division |
| PC | Personal Computer |
| QPC | Quasi-Propulsive Coefficient |
| RANS | Reynolds Averaged Navier Stoke |
| RoPax | Roll-On-Roll-Off-Passenger Ship |
| RSS | Root-Sum Square |
| SEEMP | Ship Energy Efficiency Management Plan |
| SEE | Standard error in the regression equation |
| SLS | Selective Laser Sintering |
| SPT | Self-propulsion Test |
| SSS | Short Sea Shipping |
| STL | Stereolithography |
| TSM | Taylor Series Method |
| WJ | Waterjet |
| WPC | Wave-Piercing Catamaran |

# Chapter 1

## Introduction

Transport accounts for 26% of global $CO_2$ emissions, according to Chapman (2007) and is one of the few industrial sectors where emissions are still growing. As a result of changes in environmental protection laws regarding marine pollution, as defined by the International Convention for the Prevention of Pollution from Ships (MARPOL), and the steady increase of fuel costs, the focus for new vessel designs must be on reducing emissions (Psaraftis et al., 2009). As a consequence, the market for fuel-efficient vessels is increasing.

Tasmanian-based shipbuilder Incat, which is renowned as a pioneer in wave-piercing catamaran technology, is developing the next generation of energy-efficient medium-speed catamarans. This work includes designing new hull forms and investigating feasible propulsion systems for efficient operation at medium speeds. The medium-speed regime is defined to be at Froude number from 0.25 to 0.50.

Normally these catamarans operate at high speeds of greater than 35 knots or at a Froude number of greater than 0.5. But the next generation of energy-efficient medium speed catamarans are expected to operate below a Froude number of 0.5 with a higher deadweight capacity. A key technical challenge in developing medium-speed catamarans is in choosing the appropriate propulsion type. Waterjets are used for high-speed vessel due to high efficiency when operating at speeds over Froude number 0.5, however their performances at medium speeds are less defined and need to be investigated. Davidson et al. (2011) stated that as the high speed requirement is reduced (in combination with a higher deadweight target for medium speed vessels) propellers will likely become progressively more efficient than waterjets. Therefore defining the appropriate changeover point between using waterjets and propeller for large medium-speed catamarans is a challenge. There is still uncertainty in how this high-speed design ship can operate in the medium-speed region, especially in terms of the powering performance. The research in the powering performance of wave-piercing

catamarans at medium-speed regime is still deficient and there is still a gap of knowledge in determining the changeover point between using waterjets and propellers for large medium speed catamarans. Therefore, the main investigative approach to answer the question which propulsion system is more efficient at the medium-speed regime was an experimental study of a self-propelled catamaran by calm water self-propulsion tests using the Australian Maritime College (AMC) towing tank. Self-propulsion tests for both screw propeller and waterjet propulsion were carried out to determine the powering requirement at various ship speeds.

This research aims to answer the following research questions:

1. Will the propeller be more efficient in comparison with the waterjets propulsion in propelling the medium speed catamarans?
2. What is the most accurate way to extrapolate to full scale for the medium-speed catamaran?
3. At what speed is the changeover point between both propulsors?
4. Is it possible to make an equal comparison between both systems?
5. What is the method to be used to make a 'fair basis' comparison?

To date, there was no literature found which addresses and provides solutions to these problems based on a physical experimental study, see Section 1.6, Waterjet versus Propeller – Previous Investigation**.** This novel investigation, which explores the powering performance of waterjets and propellers at medium speed region for large catamarans, is expected to give an insight to ship designers in the selection of the most efficient propulsor to large medium-speed catamarans.

## 1.2 Medium-speed regime

The speed regime is characterised by the Froude number $F_R = V / \sqrt{gL}$ where $V$ is the ship speed in m/s, $L$ is the ship's length in metre and g is the gravitational acceleration in m/s$^2$. Depending on the Froude number, the speed regime can be subdivided into low, medium or high. The medium speed regime in this thesis is defined to be at Froude number from 0.25 to 0.50 as shown in Figure 1.2. The speed past Froude number 0.5 can be considered as high-speed where the hull enters the planing regime.

## 1.3 Motivation – industry need

Shipbuilders and ship operators are very concerned about the impact of fuel price increases, emission reductions and regulatory amendments on their markets. The International Maritime Organization (IMO), through the Marine Environment Protection Committee (MEPC) has created further controls by adding a new chapter into the MARPOL Annex VI Regulations for the prevention of air pollution from ships. This makes the Energy Efficiency Design Index (EEDI) mandatory for

new ships, and the Ship Energy Efficiency Management Plan (SEEMP) for all ships. Detailed information on EEDI can be found in IMO (2012), IMO (2013), Kristensen and Hagemeister (2011), Tzannatos and Stournaras (2014) and Hasan (2011). As EEDI and SEEMP are made mandatory, ferry operators across the globe are forced to act and share their responsibility to minimise the impact of climate change. It is highly expected that the demand for large fuel-efficient catamaran ferry will increase. To support this demand, Revolution Design and Incat are committed to the evolution and the development of large fuel-efficient catamarans for the international commercial market. Seizing this opportunity offered by the new demand in the marketplace, will be fundamental to their continuing positions as a ship design and shipbuilding leaders.

With the move in promoting short sea shipping across the globe, the need for medium speed ferries are expected to increase (Mulligan & Lombardo, 2006). This is especially true for most of the shipping trade in Europe, where short sea shipping is one of the main features in the European Union's transportation policy. To encourage sustainable transportation, the European Community has established policy, such as short sea shipping (SSS) as reported by Becker et al. (2004). Becker further commented that with the SSS, the needs for speed are becoming less important. If this is true, the type of transport could be shifted from using high speed vessels (HSV) to medium-speed vessels. As SSS will be the obvious choice for future Europe's sustainable transportation, medium-speed ferry would be preferred than the high-speed vessel (HSV).

For these reasons, there is an important need for research into the powering performance of large medium-speed catamaran, i.e. waterjet and propeller propelled, which will allow for more correct decision in making the right choice of propulsors at the medium-speed regime.

## 1.4 Wave-Piercing Catamaran and the fast ferry industry

Since 1990, the size of the catamarans has grown as the available engine power has expanded from 7,000 kW to 19,000 kW (Wartsila, 2014). The larger vessels of Ro-Pax type can now carry trucks and coaches. Some catamaran car ferries such as the 99 metre high speed vessel Francisco operated by the Argentine-Uruquayan ferry company Buquebus, could surpass 58 knots when powered by the two 22MW GE LM2500 gas turbines, see Figure 1.1. It is anticipated that the designers will continue to improve the wave-piercing catamaran and to expand the range of the capabilities, including having large catamarans operating at the medium speed regime.


**Figure 1.1** The 99m Lopez Mena (Francisco) at the Incat Shipyard. Photo courtesy of Kim Clifford.

## 1.5 Possible propulsion system for wave-piercing catamarans

### Propeller propulsion

Numerous catamarans are in commercial operation using screw propellers (Armstrong, 2004). Most of them are using the fixed pitch propeller (FPP) and the controllable pitch propeller (CPP) type. One of the most recent catamarans that uses propellers is the 80 metre *Auto Express 80 Aremiti Ferry II* owned by the French Polynesian Aremiti Ferry. Built in 2013 by Austal Ships, the 480 tonnes deadweight Ro-Ro passenger ferry is driven by four fixed pitch propellers at speeds up to 20 knots. The *Spirit of Kangaroo Island* is a 50 metre medium speed vehicle ferry which was built at Austal Ships. It is propelled by two five-bladed fixed pitch propellers at 16.3 knots at 100% MCR (Austal, 2004).

The CPP application in catamarans can be found in the 42 metre ferry *Draupner* owned by Hardanger Sunnhorlandske Dampskipsselskap (HSD) with maximum speed of 35 knots. The passenger ferry with a deadweight capacity of 53.5 tonnes was equipped with two Servogear CPP. For details of more recent catamarans see Goubault and Allison (2004).

### Waterjet propulsion

Waterjet propulsion is the standard choice in propelling high-speed catamarans. The system normally consists of an impeller rotating inside a shroud which draws water upstream via a tunnel

from outside and discharges it astern as a jet at high velocity. The waterjet type will normally lie into either axial flow type or the mixed flow type (Carlton, 2007, p.359).

Incat's large catamaran ferries are all equipped with waterjet propulsion as the majority of these vessels are designed for high-speed operations. Normally one or two units are installed per demihull depending of the breadth of the demihull. Most of the Incat's wave-piercing catamarans operate at speeds 30 to 40 knots. A recent example is the 99m Ro-Pax catamaran ferry as mentioned earlier. The ferry *Lopez Mena*, is driven by two Wartsila LJX 1720 SR waterjets powered by two 22MW GE LM2500 gas turbines ("Passenger Ship Technology," 2012). A plot of the current Incat's catamaran fleet in terms of its waterline length with respect to the Froude number is shown in Figure 1.2.

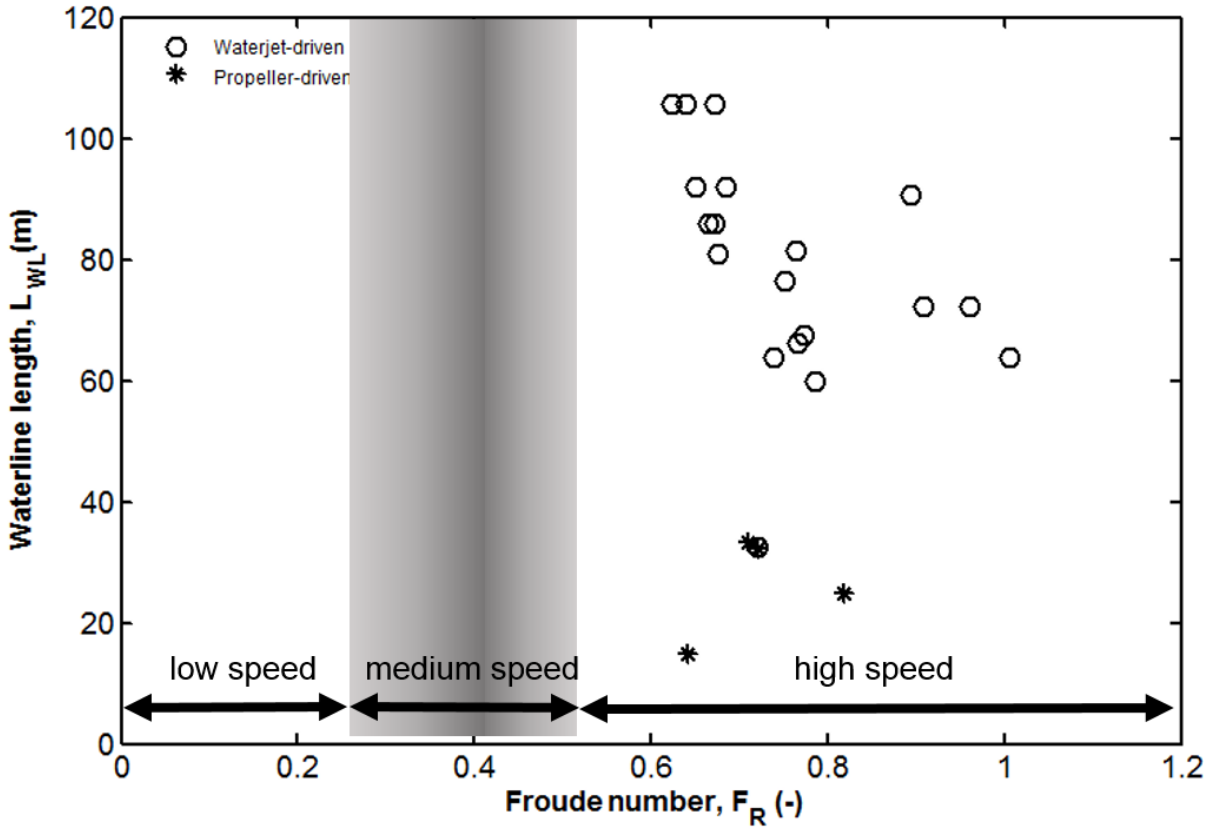


**Figure 1.2** Incat's current catamaran fleet

## 1.6 Waterjets versus propeller – previous investigations

High speed craft have been propelled by waterjets which have proved to be very efficient and offer a number of advantages over propellers (Davidson et al., 2011). But once the high speed requirement is reduced, propellers can become progressively more competitive. Therefore in this section, previous investigations comparing the performance of waterjet propulsion with screw propeller propulsion were discussed.

Haglund et al. (1982) analysed the performance of waterjet propulsion in comparison with ordinary propeller propulsion for three different types of high speed craft. In the first case study, a 30 metre catamaran ferry called JET CAT, a prototype vessel owned by AB Marinteknik of Sweden, was tested in model and full scale. The 73 tonnes displacement ferry was propelled by two KaMeWa water jet units, one in each demihull, with each unit driven by an MTU diesel engine of 1165 kW at 1865 rpm. Haglund et al. (1982) reported the ferry achieved 32.9 knots at 1119 kW on each pump shaft with the waterjet unit efficiency close to 60%. A comparison with controllable pitch propellers (CPP) was made theoretically. With the two propellers installed and with assumptions made on the propulsion factors, the power requirements of the propeller were roughly equal to that of waterjet propulsion. Haglund et al. (1982) added that one of the drawbacks of using propellers for this ferry was that the draught of the vessel would increase by 1 metre. In the second case study, a 210 tonnes displacement naval vessel was selected. The monohull vessel was fitted with three fixed pitch propellers of the sub-cavitating wide-bladed type. The performance of the propellers was compared with the vessel's performance with triple waterjets units. Haglund et al. (1982) concluded that in the speed range of 32 – 40 knots, the three units of the waterjets require 0.5 – 1.0% less power than the propellers. The overall propulsive efficiency of the propellers was higher at 63.3% than the waterjets at 62.5%. For the third case study, an example of a patrol boat with a displacement of 70 tonnes was chosen. It was fitted with three wide-bladed propellers and its performance was compared with a patrol boat installed with three waterjets units. Haglund at al. (1982) reported that to run at 27 knots, the required power is 5% higher for the propeller driven patrol boat than the waterjet driven boat.

Svensson (1987) did a performance comparison using a 35 metre twin-shaft patrol boat. The actual vessel was built with KaMeWa waterjets units and went for sea trials for full scale measurements. The hull was also model tested without any appendages. The performance of the vessel fitted with fixed pitch propellers (FPP) was assumed using the open water propeller efficiency based on model tests in KaMeWa's cavitation tunnels. Svensson used propulsion factors based on Bailey (1982) statistical data. For the 35 metre patrol boat, Svensson concluded that the waterjet performance was superior to the expected performance of the FPP installations. Svensson also made some comparison using larger patrol boats with a displacement between 250 to 300 tonnes. At 15 knots the waterjets gives 4% higher fuel consumption compared to the FPP. At 22 knots the waterjets and the FPP would have equal fuel consumption. At 28 knots and above, the waterjets have 8% lower fuel consumption than FPP.

Hugel (1992) reported the comparison of various propulsors for a destroyer, where the waterjets outperformed the conventional propeller. However the plots of the propulsive coefficients against the thrust coefficients, $C_T$ were created by numerical means, specifically using propeller Lifting Line computer program developed by Professor J.E. Kerwin's propeller design group in the Department of Ocean Engineering, MIT and not from experimental means. For the waterjet

performance, the information was obtained from the Swedish waterjet manufacturer, KaMeWa, or now known as Rolls Royce.

Allison (1993) made comparisons of propellers with waterjet propulsors using simple momentum theory. Assuming that the disc diameter of the propeller is relatively similar to the waterjet pump flange diameter, Allison showed that the horsepower required by the propeller is less than that for the waterjet. Allison further commented that the waterjet power could be less than the propeller, if the installation effects were taken into account. The installation effects, according to Allison, include the reduction of thrust required due to the absence of the appendage drag for the waterjet ship, change of displacements and wake absorption.

Alexander (1995) made comparison of the propulsion power available and the engine rpm against boat speed for waterjets and propellers. This was based on estimations and assumptions from the study of a 42.7 ft (13 metre) monohull craft. This study estimated the power and shaft speed relationship and the propulsive coefficient for the craft when it was fitted with either two Hamilton (39 kW impeller rating) waterjets or two 26 inches (0.66 metre) diameter Gawn Series propellers. Alexander concluded that the propellers generally have the advantages as propulsors up to 25 knots, and there is an overlap with the waterjets up to approximately 35 knots. Alexander also concluded that a waterjet shaft speed is independent with reference to the vessel speed, while propeller shaft speed is intimately linked to the boat speed.

Giles et al. (2010) conducted a comparison of an advanced submerged waterjet called AWJ-21™ developed by Rolls Royce Naval Marine against a conventional propeller. The propulsive coefficients for the waterjet were calculated using an empirical method based on the first principles methodology developed by Terwisga (1996) and a "momentum flux" method as recommended by International Towing Tank Conference (ITTC). The propulsion prediction for the conventional propulsion form was obtained using appendage allowance, wake fraction, thrust deduction and relative rotative efficiency estimated from past data. The comparison between the total shaft powers was presented as $P_s/V_s^3$ with respect to the ship speed, $V_s$ in knots to make the relative difference in power levels through the speed range clearer. Giles et al. (2010) reported that at 18 knots the AWJ-21™ form had a 15% higher power requirement than the conventional propeller. Giles et al. added that at 30 knots the power was comparable. Giles et al. considered other factors in choosing a propulsor for a modern frigate platform such as shaft speed, specific fuel consumption, stern design and the effect on the propulsion train. In order to derive the approximation for the specific fuel consumption, an annual time based operating profile of the ship has to be estimated. Once the operating profile was estimated, based on the engine manufacturer's data, the specific fuel consumption across the speed range can be plotted. In the stern design, several parameters were being compared such as the power plant seat height above baseline, shaft rake angle, propeller hull clearance and minimum shaft length required.

In general, a hull designed for waterjet propulsion will have a larger submerged transom stern area, since the waterjets should be submerged at least to the shaft line at low speed in order to properly prime the waterjet unit. This is not necessary for propellers, so the transom stern area is usually significantly smaller. A submerged transom could be an advantage or disadvantage depending on the vessel's speed as reported by Kiss and Compton (1989). In their investigation, five transom shapes and their corresponding after-bodies were designed to examine the effect of draft and beam at the transom on ship resistance. The forebody was held constant for all five designs. It was found that a deep transom causes up to 2% increase in effective horsepower at high speeds. However at low speeds, below Froude number of 0.38, the deep transom shows a marginal advantage in effective horsepower of as much as 1%. It was also found that a shallow transom causes up to 2% decrease in effective horsepower at high speeds above Froude number of 0.38. At low speeds, below Froude number of 0.38, the shallow transom shows an addition to the effective horsepower of as much as 2%. The submerged transom of the waterjet hull used in this research was much deeper than the combatants used in Kiss and Compton (1989) investigations. Furthermore, the comparison in this thesis was completed for speed below Froude number 0.35. Therefore, the deep transom stern of the waterjet hull could have increased the resistance of the hull. The influence of submerged transom area is further discussed in Section 6.4.

Waterjet hulls are normally less directionally stable than propeller driven hulls due to the lack of rudder(s). In a waterjet installation, the jet intake is flush with the hull bottom and there are no conventional rudders or other appendages such as struts. The directional instability of waterjet hulls are controlled by vectoring the jetstream to port or starboard with an external nozzle. At slower speeds the absence of underwater appendages may result in ship handling problems in the form of 'wandering' but this usually can be compensated by the helmsman by applying small and frequent helm corrections.

Waterjets are also prone to ventilation especially when operating in waves. The ventilation of waterjets can be avoided with a good hull design. The stepped hull design should be avoided, as the air created by the steps could be drawn into the jets. Some asymmetric hull shapes may require some consideration to prevent ventilation of the jet from the tunnel side of the hull. Catamarans with air delivered below the waterline for reduced hull resistance may be not suitable with waterjet propulsion.

It is well known that waterjets are preferred for vessels operating in high speed regime above 30 knots, where a conventional screw propeller in the high speed regime are unable to overcome the associated issues of cavitation (Bulten, 2008). However, in this study it was assumed that the waterjet and propeller were respectively designed to reduce cavitation to acceptable limits where the focus of this study is on the performance changes in the waterjet and propeller propulsion. The study of the cavitation on the screw propeller used in this study are presented in Section 6.12 Cavitation consideration.

Therefore, in determining which propulsor is more efficient, it is necessary to look into other factors as mentioned above apart from the overall propulsive efficiency and the delivered shaft power alone. The summary of the findings from the researchers mentioned earlier are listed in Table 1.1.

**Table 1.1** Summary of previous investigations on waterjet versus propeller.

| Author | Method | Propeller performance | Waterjet performance |
|---|---|---|---|
| Haglund et al. (1982) | Waterjets were tested in model scale and full scale.<br><br>CP propeller performance was theoretically estimated. | Equivalent power was estimated at 32.9 knots.<br><br>63% overall propulsive efficiency | Achieved 32.9 knots at 1119kW.<br><br>62.5% overall propulsive efficiency |
| Svensson (1987) | Waterjets were tested in full-scale sea trials.<br><br>Fixed pitch propeller (FPP) performance was estimated based on statistical data. | Overall propulsive efficiency was assumed<br><br>58% at 13 knots. | Overall propulsive efficiency was measured at 51% at 13 knots |
| Hugel (1992) | Propeller performance was estimated using numerical methods. Waterjet performance was based on manufacturer data | No clear data available | No clear data available |
| Allison (1993) | Performance of both propulsors were estimated using momentum theory. | At speed of 35 knots, the power required was at 1219 kW. The overall propulsive efficiency was 66%. | At speed 35 knots, the power required was at 1338 kW. The overall propulsive efficiency was 60%. |
| Alexander (1995) | Performance of both propulsors was estimated using manufacturer data. | At speed of 25 knots, the power required was at 537 kW.<br><br>At 32 knots , both power were similar | At speed 25 knots, the power required was at 597 kW.<br><br>At 32 knots , both power were similar |
| Giles et al. (2010) | Performance of both of propulsors was estimated using empirical method | At 30 knots , both power were similar | At 18 knots, the waterjet required 15% higher power than the propeller. |

All the previous investigations of waterjets versus propellers mentioned above were based on assumptions and theoretical calculations. Furthermore, all the comparisons made earlier were on small vessels. There was no previous experimental work that could support the investigation of the

powering performance of the waterjet and propeller driven large medium-speed catamarans, hence a novel investigation based on model testing was required.

## 1.7 Ship powering performance and efficiency

### Ship resistance

It is not the aim here to elaborate in details on ship resistance theory. This can be found in Lammeren (1948), Saunders (1957a), Manen and Oossanen (1988), Molland et al. (2011) and Larsson and Hoyte (2010). However, an elementary account is included here. The resistance faced by a catamaran due to its movement through water may be resolved into two principal components. This is based on the work of William Froude (Froude, 1872, 1874; Manen & Oossanen, 1988), who introduced the so-called Froude assumption in 1867, separating the total resistance into frictional resistance and residual resistance components and proposing that the resistance test to be conducted based on identical Froude numbers, with a correction for the different Reynolds number effects.

In order to improve the traditional method, the ITTC Resistance and Propulsion Performance Committee adopted the following method in 1978, introducing the form factor concept as the performance prediction method for single-screw ships (Lindgren et al., 1978).

$$C_{TS} = C_{FS}(1+k) + \Delta C_F + C_A + C_R + C_{AAS} \tag{1.1}$$

where $C_T$ is the total resistance coefficient, $k$ is the form factor, $C_F$ is the frictional resistance coefficient, $\Delta C_F$ is the additional frictional resistance due to roughness, and $C_{AA}$ is the air-resistance coefficient. Subscript $S$ denotes full-scale ships. In Equation 1.1, the ITTC has adopted of separating the frictional resistance and the residual resistance. In this research, the ITTC'57 correlation line was utilised as the frictional resistance coefficient, i.e.,

$$C_F = \frac{0.075}{(\log R_e - 2)^2} \tag{1.2}$$

and

$$R_e = \frac{VL}{\upsilon} \tag{1.3}$$

where $R_e$ is the Reynolds number, $V$ is the ship speed, $L$ is the ship length, and $\upsilon$ is the kinematic viscosity. Other frictional lines have been proposed by Grigson (1993) and Katsui et al. (2005a). These is discussed in detail in Chapter 2. The total resistance of the model is separated into the frictional resistance and the residual resistance. This is done by subtracting the total resistance in model scale with the frictional resistance of the model using Equation 1.2.

$$C_R = C_{TM} - C_{FM}(1+k) \tag{1.4}$$

Based on Froude's assumption of similarity, the model residual resistance coefficient $C_R$ is similar in full scale i.e. $C_{RS} = C_{RM}$. The $(1+k)$, one plus the form factor is normally obtained from a series of low Froude number speed resistance tests using the Prohaska method (Watson, 1998). This method in obtaining the form factor is discussed in Chapter 2.

**Propulsive efficiency**

The propulsive efficiency of a propulsion system is of prime importance as it is a measure of the power supplied to the propulsor per amount of the delivered power from the propulsor. The overall propulsive efficiency which is found in Manen and Oossanen (1988) and Molland et al. (2011) is defined as

$$\eta_T = \eta_H \eta_O \eta_R \eta_S \tag{1.5}$$

where $\eta_H$ is the hull efficiency, $\eta_O$ is the open water propeller efficiency, $\eta_R$ is the relative rotative efficiency and $\eta_S$ is the shaft transmission efficiency. In this research the shaft transmission efficiency will be neglected, as attention will only be focused on the hydrodynamic performance of the catamarans. Furthermore, it will be impossible to measure the shaft transmission losses in the model scale. Therefore a more meaningful measure of efficiency, which is the quasi-propulsive coefficient (QPC) will be used. The QPC is the ratio of the useful power obtained, $P_E$, to the power actually delivered to the propeller, $P_D$ (Manen & Oossanen, 1988). It is defined as

$$\eta_D = \frac{P_E}{P_D} \tag{1.6}$$

The values in the numerator and the denominator are predicted from the towing tank model tests. The effective power, $P_E$ is obtained from the calm water bare hull resistance test and the delivered power $P_D$ is obtained from the self-propulsion test. Further details on the experimental model tests are explained in Chapter 2. The propulsion efficiencies and its associated power are shown schematically in Figure 1.3. Details on the other efficiencies can be found in Manen and Oossanen (1988) and Molland et al. (2011).

The propulsion efficiency of waterjets differs from the propeller propulsion efficiency. Although the general definition of the overall propulsive efficiency is defined as $\eta_D = P_E/P_D$, a more detailed numerical determination of the overall propulsive efficiency can be define as

$$\eta_D = \frac{\Delta MV}{P_{PE}} = \frac{\rho Q_j \left[ V_j - V\left(1-w\right) \right] V \eta_{pump} \eta_{inst}}{\frac{1}{2}\rho Q_j \left[ \frac{V_j^2}{\eta_n} - \eta_i V^2 \left(1-w\right)^2 \right]} \tag{1.7}$$

where $V$ is the velocity of the vessel, $V_j$ is the jet velocity, $\Delta M$ is the change in the momentum flux, $P_{PE}$ is the pump effective power, $\eta_{pump}$ is the pump element efficiency and $\eta_{inst}$ is the waterjet pump installation efficiency, $\eta_i$ is the intake efficiency, $\eta_n$ is the nozzle efficiency and $Q_j$ is the is the volume flow rate through the jet. The details on the waterjet efficiencies and its associated parameters such as the intake efficiency, nozzle efficiency and others can be found in Bose (2008) and Zürcher et al. (2013). The schematic diagram of the waterjet propulsion definition is shown in Figure 1.4.

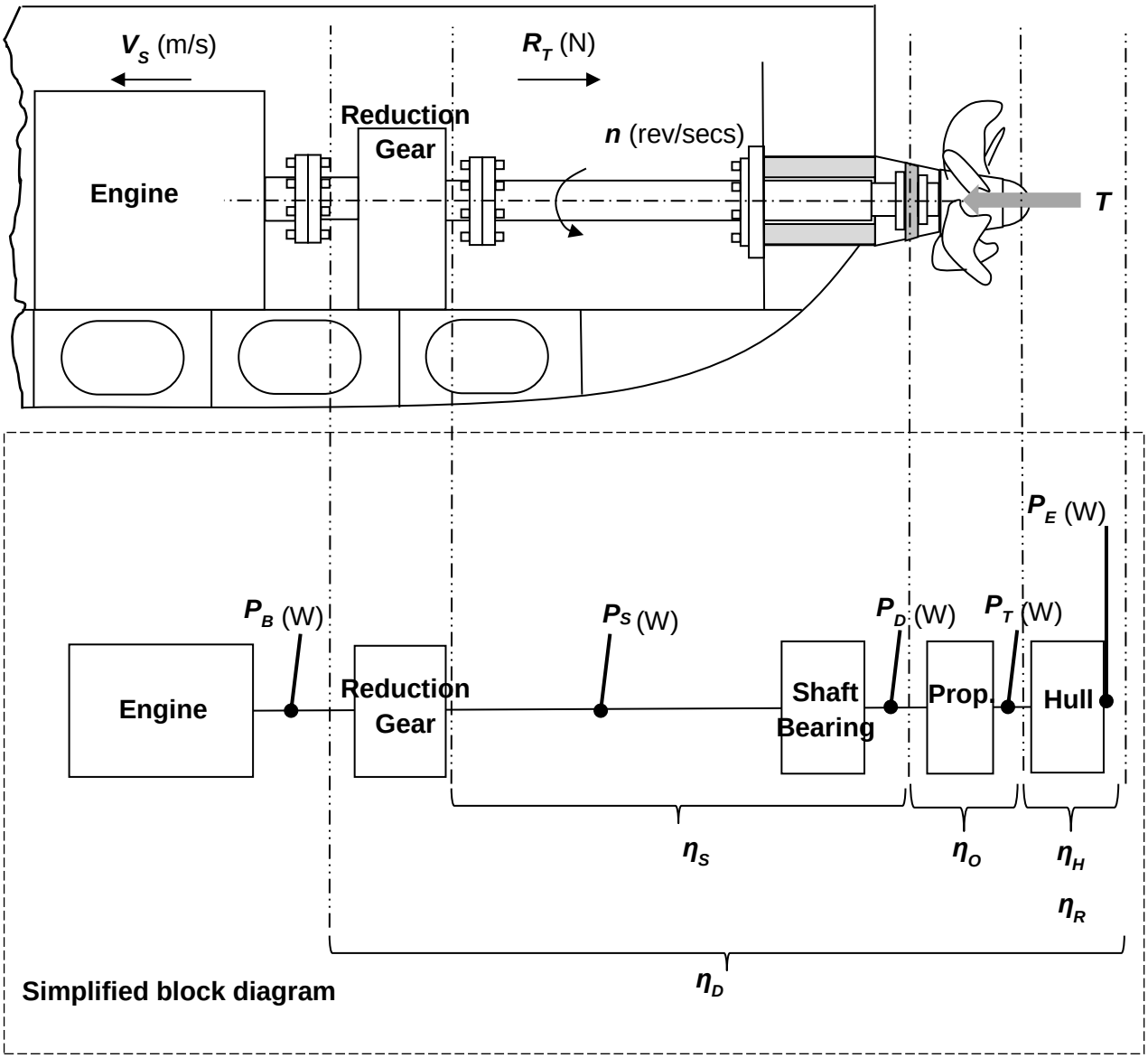


**Notes:**

| | | | |
|---|---|---|---|
| $n$ | propeller shaft speed in rev/sec | $T$ | ship propeller thrust in N |
| $P_B$ | brake power of the engine in kW | $V_S$ | ship speed in m/s |
| $P_D$ | delivered power in kW | $\eta_D$ | propulsive efficiency |
| $P_{DS}$ | delivered power for the ship in kW | $\eta_H$ | hull efficiency |
| $P_E$ | effective power for the ship in kW | $\eta_O$ | open water propeller efficiency |
| $P_T$ | thrust power for the ship in kW | $\eta_R$ | relative rotative efficiency |
| $P_S$ | shaft power for the ship in kW | $\eta_S$ | shaft transmission efficiency |
| $R_T$ | total resistance in N | | |

**Figure 1.3** The propeller propulsion power transmission.

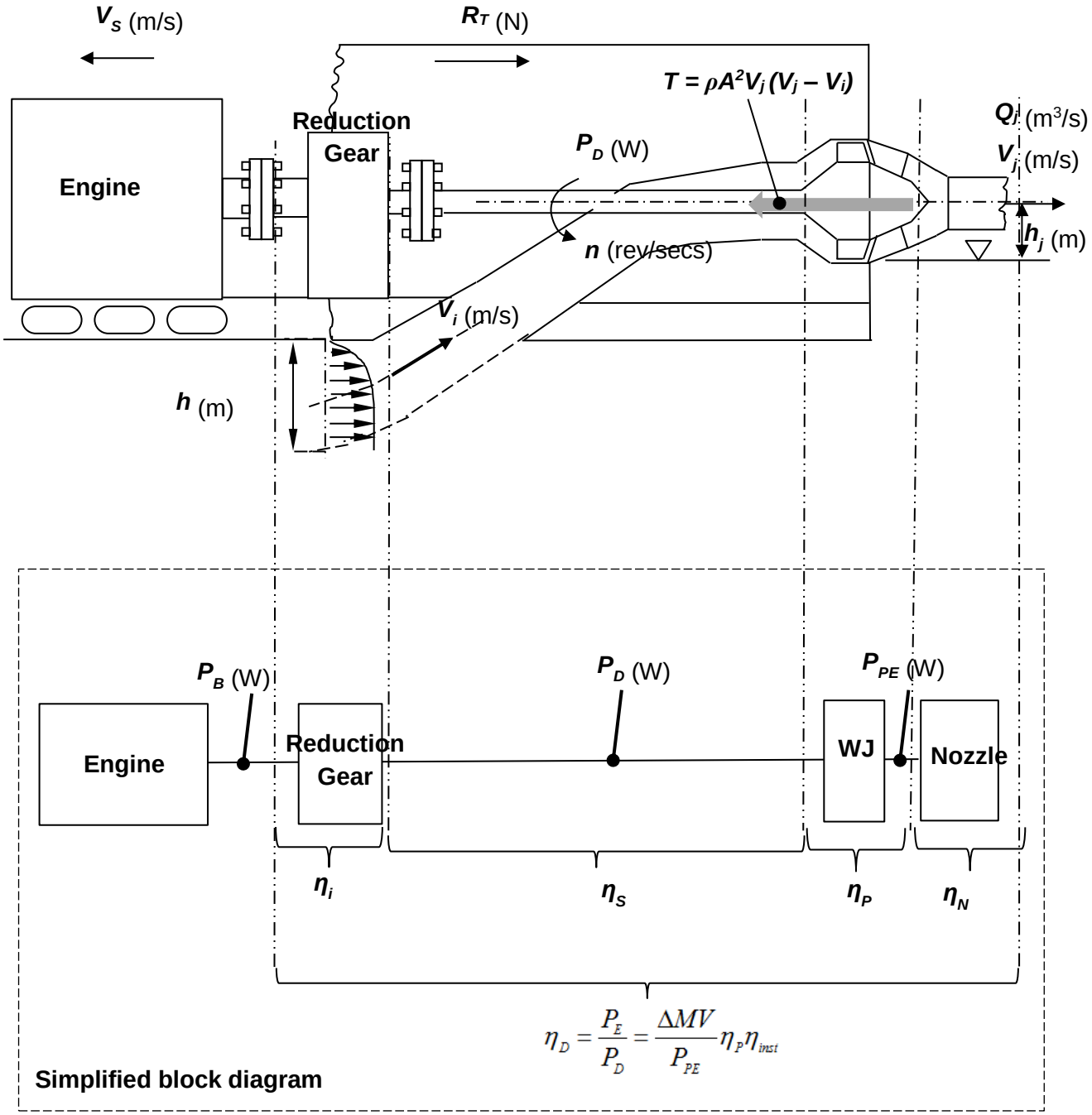


**Notes:**

| | | | |
|---|---|---|---|
| $h_J$ | height above undisturbed free surface relative to the waterjet centreline in m | $V_i$ | inlet velocity – waterjet in m/s |
| $n$ | propeller shaft speed in rev/sec | $V_j$ | jet velocity – waterjet in m/s |
| $P_B$ | brake power of the engine in kW | $V_S$ | ship speed in m/s |
| $P_D$ | delivered power in kW | $\eta_D$ | propulsive efficiency |
| $P_E$ | effective power for the ship in kW | $\eta_i$ | intake efficiency - waterjet |
| $P_{PE}$ | waterjet pump effective power in kW | $\eta_{inst}$ | waterjet pump installation efficiency |
| $R_T$ | total resistance in N | $\eta_N$ | nozzle efficiency - waterjet |
| $T$ | impeller thrust in N | $\eta_P$ | pump element efficiency - waterjet |
| | | $\eta_S$ | shaft transmission efficiency |

**Figure 1.4** The waterjet propulsion power transmission.

## 1.8 Research programme

This research programme was supported by the Australian Research Council Linkage Project 'Powering Optimisation of Large Energy-Efficient Medium Speed Multi-Hulls', Project ID: P1101000080. This programme was divided into a series of projects:

1. To develop new hull forms of large fuel-efficient medium speed catamarans. The new hull forms needed to be hydrodynamically efficient in the medium speed region. Computational fluid dynamics (CFD) was used to evaluate design alterations to develop hull forms with minimum calm water resistance for such vessels. This research was conducted by Haase (2015b).
2. To develop an extrapolation procedure for predicting the waterjet powering performance based on thrust measurements. This method which deviates from the normal extrapolation procedure for waterjet does not require the waterjet system test results. This research was conducted by Zürcher (2015).
3. To evaluate the performance of both waterjet and propeller driven catamaran operating at medium-speed. This task was taken by the author. The powering performance results of the waterjet driven catamaran were taken from Zürcher (2015). The author conducted the model testing experiments of the propeller driven catamaran. This initial study was constricted to a single experimental case study and the scope does not include any CFD case study. Then the author made a comparative study on the powering performance of both waterjet and screw propulsion at medium speed. Problems associated with the experiments were investigated such as scale effects on the model propeller and uncertainty analysis of the experiments. As both of the waterjet and the propeller driven catamarans cannot be directly compared as the length to displacement ratio and the wetted surface area ratio are not the same, comparative methods that can compare these two catamarans equally were established. The author has derived several approaches to assess the merit of the waterjet and the propeller as the propulsor for the medium-speed catamaran. These were based on three methods, an approach using the propulsive efficiency, an approach using a transport efficiency or a transport factor and an approach using a scaling to a similar size method. The author had published some of the findings of this research which can be found in Mustaffa Kamal et al. (2015). The amount of work in this thesis was more on the experimentation work and synthesising of the work of Zürcher (2015) and Haase (2015a). At the early stage of the project, it was decided that the experimentation work on the waterjet and the propeller hull self-propulsion test need to be separated to two separate projects, considering the tremendous amount of work involved in running the self-propulsion test for the waterjet hull and the propeller driven hull. This thesis was more focused on the comparison of the performance of the waterjet hull and the propeller with different hull. The challenge in this research was on how to compare these two different

hulls and synthesising the work of Zürcher (2015), Haase (2015a) and others in a rigorous and academic way to make solid conclusions. One of the example of the synthesising work was the work on wake scaling. The wake fraction data was obtained from the work of Haase (2015a). The raw data was then integrated into one nominal wake fraction using the method which can be found in Carlton (2007) and Molland et al. (2011). Then the nominal wake fraction values for the model scale and the full scale were used for wake scaling, using the wake scaling formula $1 - w_{TM} / 1 - w_{TS}$ (Bose, 2008).

## 1.9 Outline of the thesis

This thesis consists of five parts forming an extensive investigation into the powering performance of propeller and waterjet driven large medium-speed catamarans. Chapter 2 explains experiments consisting of model testing, i.e. calm water resistance test, open water propeller test and self-propulsion test. The preliminary powering design, inclusive of propeller design and bracket design is explained in Appendix A.5.

Chapter 3 explains the Reynolds scale effect study on a small propeller. This study was necessary as small propellers, with diameters ranging from 110 mm to 120 mm were used in the towing tank experiments. The problem of conducting a self-propulsion test using a small propeller is that the propeller is operating at a lower Reynolds number and due to this it is expected that there are Reynolds scale effect affecting the performance of the small propeller. This scale effect is essentially viscous in nature, and it is mainly due to boundary layer phenomena dependent on Reynolds number. Namely the flows over the small model propeller in open water test or in the self-propulsion test are in a laminar boundary layer. Whilst turbulent boundary layer flows are fully developed over the blade of full scale propellers. This difference in the model scale to the full scale performance is known as the Reynolds scale effects.

Chapter 4 explains the uncertainty analysis study of the experimental results. The uncertainty analysis was done to identify which sources of error had the most influence on the total uncertainty in the measurements as well as to ascertain the overall level of uncertainty in the measurements during these tests, i.e. calm water resistance test, open water propeller test and self-propulsion test. These results later will provide guidance for uncertainty analysis of similar tests at other testing facilities.

Chapter 5 presents the powering performance of the propeller-driven catamaran. These results include the thrust deduction fraction, the wake fraction, the delivered power and the overall propulsive efficiency.

The comparative study between the propeller-driven catamaran and the waterjet driven catamaran is given in Chapter 6. The results were compared in terms of the thrust deduction fraction, wake fraction, overall propulsive efficiency, transport efficiency and Admiralty coefficient. In the

end, discussions were made in discussing which propulsor are the best for the medium-speed operation of the Incat catamaran ferry.

In Chapter 7, the conclusions to the work are outlined, including the implications of the research to vessel designers and hydrodynamic researchers. Recommendations for future work are also presented.

## 1.10 The novelty aspects of this research

The key contribution of this work is that it provides clear case study-based conclusions into the powering performance of propeller driven catamarans and waterjet driven catamarans in the medium speed regime. Currently, there is insufficient information in the powering performance of large wave-piercing catamaran operating at medium speed for either propulsion system. The powering results for both propulsion system which are presented in this thesis provide useful data for the ship designers in the development of a new fleet of medium-speed highly efficient vessels. The testing of both propulsion system provides invaluable information on the crossover point between both propulsors. In establishing these design points, a number of research questions have been answered including:

1. Will the propeller be more efficient in comparison with the waterjets propulsion in propelling the medium speed catamarans?
2. What is the most accurate way to extrapolate to full scale for the medium-speed catamaran?
3. At what speed is the changeover point between both propulsors?
4. Is it possible to make an equal comparison between both systems?
5. What is the method to be used to make a ‘fair basis’ comparison?

The last three questions here have required the use of 3 methods of comparison. These methods were: (1) an approach using the propulsive efficiency; (2) an approach using a transport efficiency or a transport factor and (3) an approach using a scaling to a similar size method. A final conclusion was required combining the effects of these three methods.

Primary of the research contributions outside of the design case study, is the creation of a modified extrapolation procedure for large wave-piercing catamarans. This research has proved that the extrapolation to full scale using the ITTC 1978 recommended procedure did not work properly for large wave-piercing catamarans. It has been shown that the combination of the three discrete tests, calm water resistance, open water and self-propulsion test provides unrealistic wake fractions of the model (e.g. negative values of the wake fractions), thrust deduction fractions that have large scatter with respect to the Froude number and the propeller scale effects correction proposed in the ITTC 1978 procedure leads to inadequate propeller scale effects correction.

On the issue of wake scaling, the model wake fractions are believed to be small, such that the value of the advance coefficient in behind the model is too close to the value of the advance coefficient in the open water. This results were calculated using the equation $w_{TM} = 1 - J_O/J_P$ and the wake scaling formula $w_{TS} = (t + 0.04) + (w_{TM} - t - 0.04). (1+ k) C_{FS} + \Delta C_F/ (1 + k) C_{FM}$ which was originally based on the work of Sasajima et al. (1966) in the ITTC 1978 procedure. This approach did not work properly for the medium-speed catamaran powering prediction. In discussing the large scatter of the thrust deduction fraction, the large scatter increases significantly at lower Froude numbers. It is believed that incorrect flow conditions existed at the lower Froude numbers and contributed to lower total drag to the model hence contributing to large scatter in the lower Froude numbers. On the issue of propeller scale effect, the propeller scale effect correction proposed in the ITTC 1978 procedure leads to inadequate corrections to the propeller torque and thrust coefficients. These corrections are not adequate as discussed in Chapter 3, where a propeller scale effect study was done by conducting propeller open water tests. The results of the open water tests then were compared with propeller coefficients results from a larger 'geosim' propeller which acts as a benchmark.

The modified extrapolation procedure for large wave-piercing catamarans was based on an extrapolation procedure that used only the self-propulsion test results. This extrapolation procedure is known as 'the self-propulsion test only method' in this thesis. This self-propulsion test only method was used instead of the recommended ITTC 1978 procedure. Two changes were introduced in the self-propulsion test only method, the first modification is by introducing a wake scaling calculation using CFD and the second modification is introducing an alternative method in correcting propeller scale effects.

Finally, novel contribution was required in the areas of wake fraction and propeller force scaling. For the issue of wake scaling a method integrating Computational Fluid Dynamics (CFD) simulated wake fractions in model scale and in full scale was introduced in the self-propulsion test only method. These values of the wake fraction circumferential and radial distributions in model scale and in full scale were integrated over the propeller disk radius in order to obtain the nominal mean wake fraction. The values of the nominal mean wake fractions in model scale and in full scale were later used for the wake scaling formula $1 - w_{TM} / 1 - w_{TS}$. For the issue of propeller force scaling, an alternative method of propeller scale effect correction proposed by Benedek (1985) was used. This alternative method approximation is similar to Froude's method used to calculate the resistance of the ship. In this method, it was assumed that only the friction force coefficient on the blade surface is different on the full-scale propeller, as compared to its model. However the pressure distribution along the blade section of the full-scale propeller and its model is considered similar. Therefore the normal force affecting the blade section and the pressure resistance of viscous origin can be recalculated without correction. This research has proved that the alternative method of propeller scale effect correction proposed as above correlates better to the results of a benchmark propeller which was based on a larger 'geosim' propeller running at Reynolds number

*Re 2.0 x* $10^6$ than the propeller scale effect correction method proposed in the ITTC 1978 procedure.

# Chapter 2

# Experimentation

## 2.1 Introduction

This chapter presents the details of the methodology in answering the research questions which were explained in Chapter 1, which is the model testing experimentation. This chapter describes the bare hull resistance test, self-propulsion test, open water test, and the testing set-up in addition to the data analysis itself. All of the tests were conducted at the AMC's towing tank of 100m in length, 3.55 metre in width, 1.5 meter in depth and has a maximum towing carriage speed of 4.6 m/s.

The primary aim of these three discrete tests was to investigate the full scale powering parameters such as the delivered power, thrust deduction fraction, wake fraction and the overall propulsive efficiency.

## 2.2 The ITTC 1978 powering prediction procedure

In 1978, a committee was formed for the 1978 ITTC conference to develop a ship powering prediction method that could be recommended as standard for the towing test institutions all over the world. The committee discussed the results of different methods used in major facilities at the time. The results were compared with full-scale trial data. The committee then combined a selection of techniques to form the 1978 Powering Prediction method for Single Screw Ships (Manen & Oossanen, 1988). The method used the test results from a scaled geometrically similar model of a full-scale vessel. Using scaling principles as well as empirical formulae to correct for scaling effects due to physical testing limitations, this method predicted the full-scale operating parameters of the model e.g. delivered power, thrust and overall propulsive efficiency. These full-scale operating parameters were the important parameters in this research.

In a traditional towing tank tests the model values of the Froude number, $F_R = V/\sqrt{gL}$ and the Reynolds number, $R_e = VL/\upsilon$ cannot be tested simultaneously. Practically, the model experiment can only comply to the Froude number, but not the Reynolds number. If a model experiment has to comply with Reynolds number, it will result in very impossible high speeds during the model experiments. For this reason, model experiments with ship models are always carried out maintaining a constant Froude number, while maintaining a constant Reynolds number is neglected and required some corrections for this omission.

This dynamical dissimilarity between the model and full-scale means that the results cannot simply be multiplied by a scaling factor. The ITTC 1978 method recommends a number of factors developed to account for these differences, such as a frictional resistance coefficient, a wake scaling and an air resistance scaling among others (Lindgren et al., 1978). The ITTC 1978 method used the results of three physical tests which are a calm water resistance test, a propeller open water test and a self-propulsion test. The resistance test is a bare hull tow test without any appendages, the propeller open test is a test with the model propeller operating in uniform flow without the model hull and the self-propulsion test is a test with the ship model equipped with appendage(s) and propeller(s) operating in the model wake. The details of each physical test are described in this chapter.

## 2.3 Single demihull testing

Based on the findings of Rovere (1997), a choice was made in applying his novel technique in carrying out the model experiments. Rovere tested a catamaran with its single demihull in the towing tank travelling in close proximity to the tank wall, with the demihull distance relative to the towing tank wall equal to half of the catamaran hull spacing. Rovere's test was done in the same AMC's towing tank facilities. The test was performed using a full catamaran model and an equivalent demihull with different hull spacing to model-length ratio. The tank wall acted as a plane of symmetry for the catamaran, and thereby reflected the waves generated by the demihull to provide correct interference and blockage effects from the non-existent hull. This method was chosen as to make the ship model as large as possible, which increased the accuracy of the full-scale results by increasing the force magnitude measurement to a level of increasingly accurate measurement.

Furthermore, with the current AMC's towing tank dimension, a full whole catamaran model, say with a scale ratio of 1 to 50, will be too small for the self-propulsion test instrumentation and propulsion train components. Rovere (1997) found that by using a single demihull, the results of the wave-making resistance were in close agreement with the results tested in a whole catamaran model. A schematic illustration of this novel technique of catamaran testing is shown in Figure 2.1 and Figure 2.2, with the view facing aft of the catamaran. This set-up at the AMC towing tank used the port side

demihull, with a designated hull separation *s*, depending on the hull type. In order to validate this testing technique, Haase et al. (2012b) replicated the testing of a single demihull catamaran and used the towing tank wall as a symmetry plane in a RANS CFD simulation. The results have close agreement to the wave-making resistance prediction with variations of hull separation spacing, found in Rovere (1997).

One may questioned on how accurate or straight is the AMC's tank wall? If it is not straight, it is a source of error. The error is very minimal as this was supported by the work of Rovere (1997) where the difference between the demihull testing and the full catamaran model testing is small. Rovere (1997) commented that there is close agreement between the catamaran and the equivalent demihull wave-making resistance results, and that the full catamaran and demihull show a general trend for an increase of wave-making resistance with an increase in hull spacing as shown in Figure 3 through 6 in Rovere (1997).

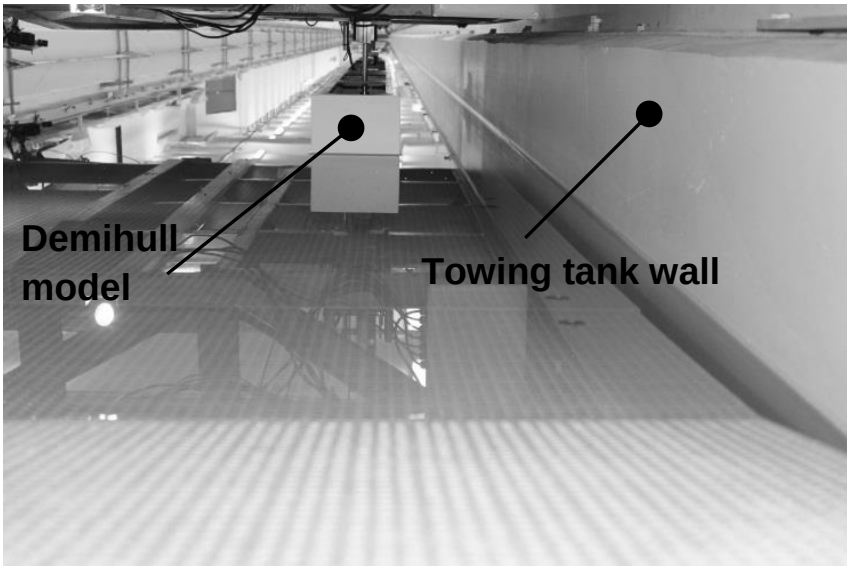


**Figure 2.1** The single demihull model of the catamaran in the towing tank in close proximity to the towing tank.

## 2.4 The Incat ship models

The project 'Powering Optimisation of Large Energy-Efficient Medium Speed Multi-Hulls' was conducted as part of a collaborative project between Incat Tasmania Pty Ltd, Revolution Design Pty Ltd, Wärtsilä Corporation, MARIN, and AMC. The two hulls that were chosen for this project, were the HSV-2 Swift, 98m waterjet hull which was an existing hull and the 130m propeller driven hull which was an entirely new design designed by Revolution Design Pty Ltd and Stuart Friezer Marine. It should be noted that these two hulls *L/B, B/T, s/L* and displacement to length ratios were not similar as listed in Table 2.1. It will be an ideal case, if the waterjet and the propeller driven hull were tested with a similar *L/B, B/T, s/L* and displacement to length ratios. It would be significantly

more interesting if the same ship hull had been redesigned, in the afterbody, to accommodate waterjet propulsion. But this was not the intention at that time, as these two hulls were both designed by Incat and Revolution Design as realistic alternatives and were not simple geometric scales. Even though if the propeller driven hull and the waterjet driven hull were more similar in size, the hulls would be different as a waterjet hull is very different from a propeller driven one. Therefore, in order to make an equal 'scientific' comparison that could be used for other studies as well, three methods of comparison were conducted in this research. These methods were: (1) an approach using the propulsive efficiency; (2) an approach using a transport efficiency or a transport factor and (3) an approach using a scaling to a similar size method. A further detailed discussions of this equal 'scientific' comparison of the two quite different medium-speed catamarans are discussed in Chapter 6. Therefore the results of this study apply strictly to the specific ship forms tested and should only be used as applicable to similar catamaran vessels with caution. In order to obtain accurate results for a given hull form, individual comparative tests with that hull form should be done.

Two separate programs were conducted, one for the propeller driven catamaran, and the other one for the waterjet driven catamaran. The propeller driven catamaran were tested at two displacements, 2,500 tonnes and 3,640 tonnes, and the HSV-2 Swift, 98m waterjet driven catamaran was tested at only one displacement, which was at 1,500 tonnes. See Table 2.1 for the main particulars of the two catamarans. The 98m waterjet catamaran testing was done in a separate program and was conducted by Zürcher (2015).

The 130m propeller driven catamaran was an entirely new hull designed by Revolution Design Ltd and Stuart Friezer Marine. The demihull was asymmetric and the stern was designed to accommodate a propeller with a built-in trim tab.

The 98m wave-piercing catamaran was designed by Revolution Design Pty. Ltd and built by INCAT Tasmania in 2003. Zürcher in his PhD thesis was looking for a new approach in extrapolating waterjet self-propulsion test result based only on the self-propulsion test and bare hull resistance data, without the need of a waterjet system test. A typical waterjet powering normally consists of a waterjet system test, a resistance and a self-propulsion test (Dang et al., 2013). The selection of this 98m wave-piercing catamaran in Zürcher's research was made because of the availability of a complete set of sea trials data carried out the Naval Surface Warfare Centre Carderock Division with the sea trials conducted up to 40 knots in 2004.

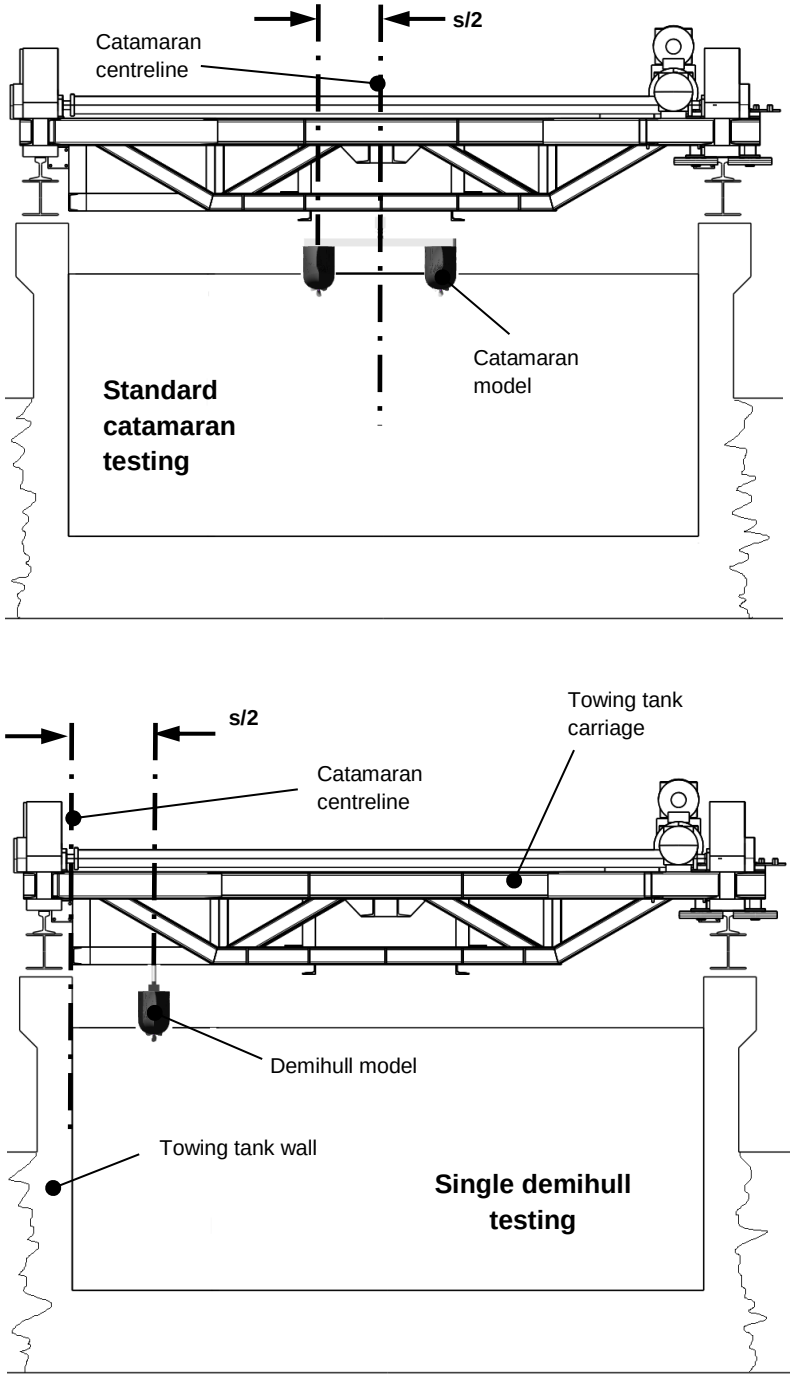


**Figure 2.2** Standard whole catamaran located at the centre of the towing tank (top) and single demihull testing with the demihull located half a demihull centreline distance off the towing tank (bottom)

**Table 2.1** Main particular of the 130m propeller driven and the 98m waterjet driven wave piercing catamaran where FS stands for full scale and MS for model scale particulars. *Note: s/2 is half of the separation distance between the demihull centreline and the vessel centreline.

| | | **Waterjet driven (1,500t)** | | **Propeller driven (2,500t)** | | **Propeller driven (3,640t)** | |
|---|---|---|---|---|---|---|---|
| **Particular** | **Unit** | FS | MS | FS | MS | **FS** | **MS** |
| **$L_{WL}$** | m | 92.9 | 4.3 | 124.8 | 4.3 | 122.6 | 4.23 |
| **$B_{WL,DH}$** | m | 4.5 | 0.21 | 6.35 | 0.22 | 6.4 | 0.22 |
| **T** | m | 3.3 | 0.15 | 3.23 | 0.11 | 4.1 | 0.14 |
| **$S_{DH}$** | $m^2$ | 704.5 | 1.51 | 995.8 | 1.18 | 1,216.9 | 1.45 |
| **Δ** | t (kg) | 1,500 | (145) | 2,500 | (100) | 3,640 | (146) |
| **s/L** | - | 0.238 | | 0.197 | | 0.2 | |
| **$B_{WL,DH}$/T** | - | 1.364 | | 1.97 | | 1.56 | |
| **L/$B_{WL,DH}$** | - | 20.64 | | 19.53 | | 19.15 | |
| **DLR** | - | 10.31 | | 11.68 | | 10.12 | |
| **$C_B$** | - | 0.592 | | 0.476 | | 0.552 | |
| **$A_T/A_X$** | | 0.62 | | 0.23 | | 0.39 | |

*Note: $S_{DH}$ = Wetted surface area, s/L = separation ratio, DLR = Displacement /Length ratio, $A_T/A_X$ = transom immersion ratio.*

## 2.5 Towing tank facilities

All of the tests were conducted at the AMC's towing tank. The carriage runs on a pair of rails on the top of both sides of the towing tank walls. The towing tank wall was constructed out of concrete and a study was made to check the straightness of the tank wall by Zürcher (2015). The rails extend over the wet dock, where the model was trimmed according to the static trim testing conditions. The walls of the wet dock were built in glass which was helpful for the model static trim adjustments and ballasting process.

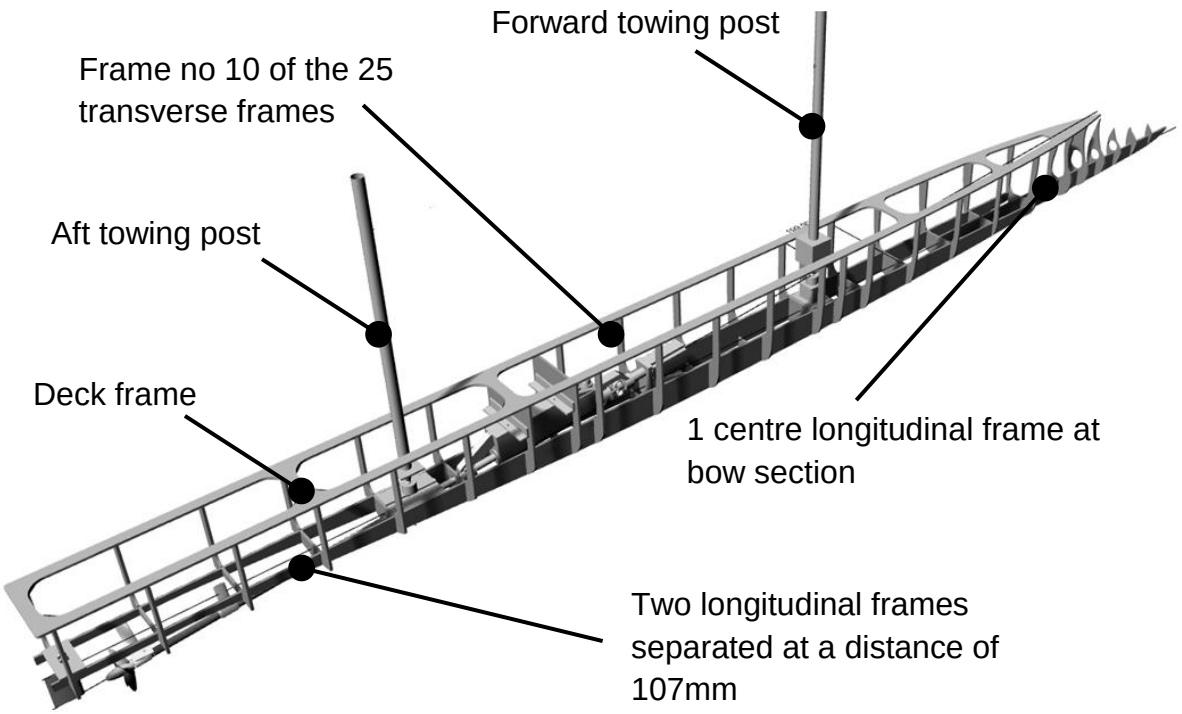


**Figure 2.3** Assembled view of the 130m propeller catamaran without the hull body. The internal structure of the model consists of two longitudinal frames, one short centre longitudinal frames at the bow section, 25 transverse frames, and one deck frame**.**

## 2.6 Towing system

The tow post system in the carriage consists of two towing post frames and two stainless steel towing posts, two Linear Variable Differential Transformer (LVDT) sensors and a dyno bed. The forward towing post, free to slide in a vertical linear bearings, was connected to the AMTI load cell for the resistance force measurements. The load cell was fastened to a universal ball joint mount as shown in Figure 2.3 and Figure 2.5. The mount itself was fastened to the model by means of bolts and nuts. The aft towing post was mounted to the universal joint on a linear slider.

## 2.7 Model turbulence stimulator set-up

Turbulence stimulators fitted at the bow of a ship model are necessary because ship models tested in a towing tank at Reynolds numbers which are normally two magnitudes less than at full scale. Due to the small 'angle of entrance' of this single demihull bow, the ITTC (2011d) procedure that recommends the location of the turbulence stimulator would not be valid for this type of hull. In the ITTC (2011d), the Figure 1 on page 1 identify the location of trip studs back from the stem which was influenced by the angle of entry and the model size. For the 130m propeller driven catamaran demihull, as the half angle of entrance is less than $10^{o}$, the procedure recommends for the studs to be kept as far forward as possible. It was a concern that the turbulent flow could be returning back to

laminar somewhere aft of the trip studs especially at low speeds. Therefore, further investigation was carried out in locating the laminar-turbulent transition point, where the turbulence stimulator studs should be located.

Zürcher (2015) used the momentum thickness theory in determining the suitable location of the stimulator studs. The momentum thickness theory can be found in Preston (1958) and McCarthy et al. (1976). Through experimental data from the study of the boundary layer thickness, Preston suggested that the lower limit of a fully developed turbulent boundary layer is at $R_\theta$ = 320. Using Reynolds number based on the lower limit of a fully developed turbulent boundary layer and the minimum and maximum expected model testing speeds, the two positions of the turbulence stimulators can be calculated. The distances *x*, from the most forward perpendicular end of the model can be calculated as:

$$x = \left( \frac{R_{e\theta} \upsilon}{U_\infty 0.664} \right)^2 \frac{U_\infty}{\upsilon} \tag{2.1}$$

where $R_{e\theta}$ is the Reynolds number based on the momentum thickness theory at the lower limit of a fully developed turbulent boundary layer at $R_\theta$ = 320, $\upsilon$ is the kinematic viscosity of fresh water at 1.033 x $10^{-6}$ $m^2/s$ and $U_\infty$ is the model testing speeds.

Following the method used by Zürcher (2015), the distances from the most forward perpendicular end of the model for the minimum and the maximum model testing speeds were calculated to be 72 and 434 mm. These distances were in the wave piercing bow area. The turbulence stimulator types are 'studs' and the stud diameter, height and spacing recommended by ITTC can be found in ITTC (2011d). ITTC (2011d) recommends a stud with a diameter of 3 mm, height of 3 mm and a spacing of 20 mm. The stud's double row setup arrangement on the wave piercing bow is shown in Figure 2.4.

The drag correction due to the effect of turbulence studs on model resistance was based on the work of Hughes and Allan (1951), Hoerner (1965) and Molland et al. (1996). According to Molland et al. (1996) there are three main points that must be taken into consideration in calculating the effect of turbulence studs on model resistance which are (1) the additional drag on the model due to the presence of studs, (2) the increase in the momentum thickness of the boundary layer due to the presence of the studs and (3) the laminar region in front of the studs. A detailed study on the additional drag due to the turbulence stud and the calculations on the drag correction is described in Appendix E. The drag corrections were applied to all measured resistance data as described in Appendix E although the study indicates that the net correction to the model resistance would be relatively small. The corrections were calculated to be about 0.82% to 2.54% of the measured resistance.

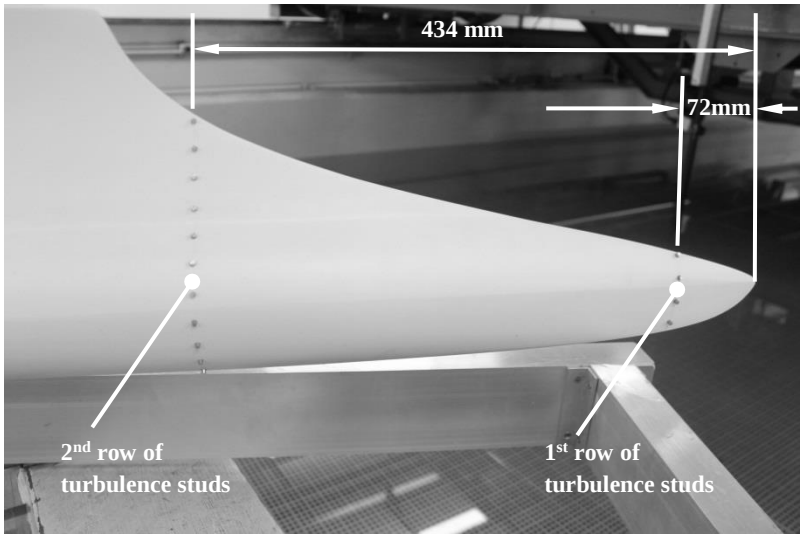


**Figure 2.4** The double row of the turbulence stimulator set-up in the bow region of the Incat model.

## 2.8 Calm water bare hull resistance test experiment

The calm water resistance test was done according to the ITTC 1978 guidelines as described by ITTC (2011b). The main aim of this calm water resistance test was to determine the full scale resistance force $R_{TS}$ and the wave making resistance coefficient, $C_R$. The sinkage and the running trim were also measured in this test. The resistance test was made at two displacements i.e. 2,500 tonnes and 3,640 tonnes. The test was also conducted in three trim settings. i.e. at 0 degrees, at 0.5 degrees and -0.5 degrees. The test was conducted from Froude number *Fr* 0.20 to 0.46. Each run was repeated at least three times for the purpose of calculating the standard deviation in the uncertainty analysis.

The testing of the bare hull resistance followed the method and procedures recommended by ITTC (2011b) . The only difference to the ITTC recommended procedures is that in this research, a single demihull was tested instead of the full vessel as mentioned earlier in this chapter. The resistance test was also conducted at low speed, i.e. Froude number below 0.2, to obtain the one plus form factor *(1 + k)* using Prohaska method.

## 2.9 Arrangement of the model in the towing tank

The model was attached to the carriage in the towing tank. The model was attached and linked to the carriage by means of two towing posts. The model was without appendages such as rudder and propeller brackets. The forward towing post was located 2365 mm from the transom of the model. The load cell for measuring the resistance force was attached at the end of the forward towing

post and fastened to the pin joint of the model as shown in Figure 2.5. The aft towing post was attached and fastened to a slider joint which permits the heaving motions of the model. The distance between the forward and the aft post was 1396mm. The demihull centreline was positioned at 424mm from the towing tank wall. This was achieved by moving the dyno bed from its original position to the new position which was in close proximity to the tank's wall. The 2.3 metre long dyno bed was fastened to the structural frames of the carriage by means of customised made bolt clamps. This was necessary as there was no possible means of having holes for the fastening bolts.

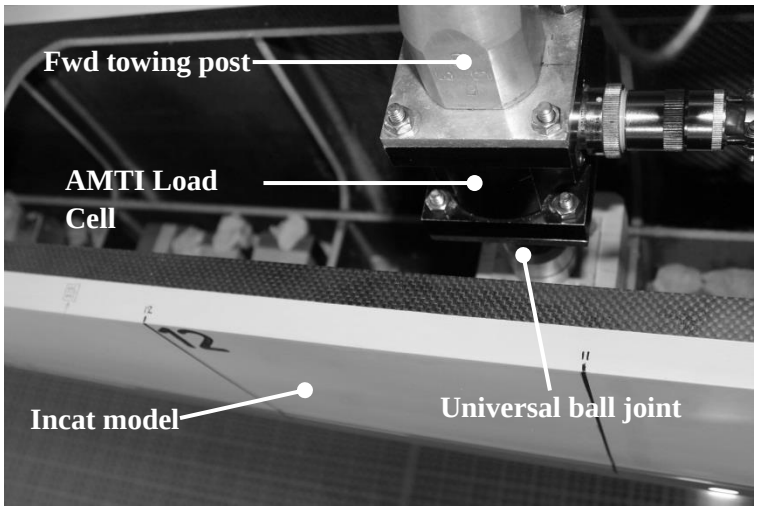


**Figure 2.5** The attachment of the forward towing post, the AMTI load cell and the pin joint of the propeller driven Incat model.

## 2.10 Instrumentation of the calm water resistance test

In the calm water resistance test, the measured variables were the model speed, the total resistance force, the sinkage forward and aft, the running trim and running sinkage and the towing tank water temperature as shown in Figure 2.6. The mentioned variables are listed in Table 2.2 with its measured units, measuring instrumentation and its filter setting. The model speeds were measured by a rotary pulse generator attached to a dedicated wheel of the towing tank carriage. The sinkage and the running trim was calculated from the measured running sinkage fore and aft. The sinkage fore and aft were measured using two Schaevitz 5000 DC-EC Linear Variable Differential Transformers (LVDT). The sinkage was calculated by taking the average values of the forward and aft LVDT readings. The running trim of the model was calculated by taking the arc tangent of the length of the forward LVDT to the aft LVDT. The total resistance forces were measured using an Advanced Mechanical Technology, Inc. (AMTI) load cell. The load cell was located on the forward carriage post as shown in Figure 2.5.

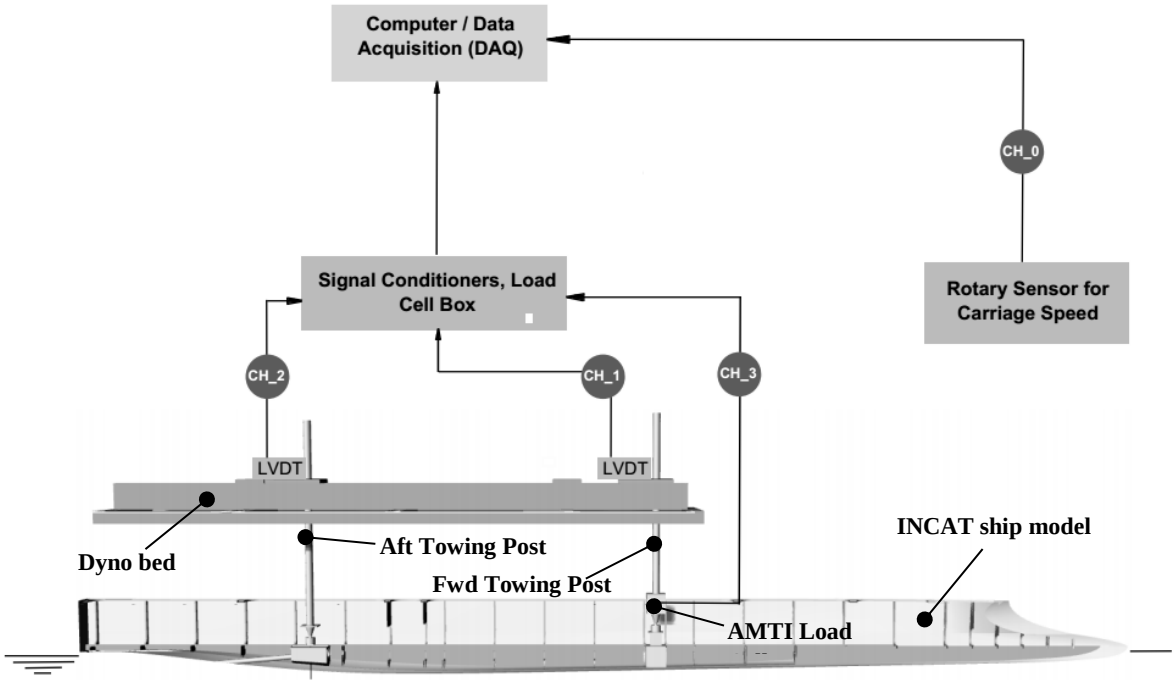


**Figure 2.6** The resistance test arrangement in the towing tank. There were 4 channels used for the calm water resistance testing.

**Table 2.2** The variables measured, units and the instrumentation used in the calm water test.

| **Variables** | **Instrumentation** | **Units** | **Calibration max. to** | **Filter** |
|---|---|---|---|---|
| **Model speed** | Rotary pulse generator | m/s | Direct | - |
| **Total resistance** | AMTI load cell | grams | 6000 grams | 1 Hz |
| **Sinkage** | LVDT - Fwd and Aft | mm | ± 60 mm | 1 Hz |
| **Running trim** | LVDT – Fwd and Aft | mm | ± 60 mm | 1 Hz |
| **Water temperature** | Thermometer | $^{o}$C | - | - |

## 2.11 Friction line

In this research, only two friction lines were used for extrapolation calculations. The two friction lines considered were the ITTC 1957 model ship correlation line (Manen & Oossanen, 1988) and a frictional line described by Grigson (1993). A detail explanation and implementation of the Grigson's friction line can also be found in Bose (2008). In this thesis as explained later in Chapter 5,

it was decided that the Grigson's line was chosen in favour of the ITTC57 correlation line because of two reasons. The first is to be consistent with the waterjet extrapolations which used Grigson's line. The second is that the 1 + k using the Grigson's line are expected to be more consistent in model and full scale than the ITTC57 correlation line (Couser et al., 1997).

## 2.12 Correlation allowance, $C_A$

In the original ITTC 1978 method, the roughness correction was a part of the correlation allowance $C_A$ (ITTC, 1999a). The original ITTC 1978 adopted the well-known Bowden-Davison formula (Bowden & Davidson, 1974) where in the 15th ITTC, this correlation allowance was accepted as the expression of correlation allowance $C_A$, intended for use when extrapolating ship resistance. This coefficient is a function of the mean hull roughness, average peak of peak-to-trough roughness height measured over 50 mm sampling lengths on the hull surface as shown in Equation 2.2.

$$C_A = \left[ 105 \left( \frac{k_s}{L_{WL}} \right)^{\frac{1}{3}} - 0.64 \right] \times 10^{-3} \tag{2.2}$$

In 2008, the 25th ITTC Performance Prediction Committee (Steen et al., 2008, p. 419) proposed a separation of this value into two independent coefficients, to allow for the effects from newly developed hull coating systems. The two separate coefficients are $C_A$ and $\Delta C_F$ (ITTC, 2014). In the new recommended procedures, the correlation allowance is shown in Equation 2.3 and the roughness allowance is shown in Equation 2.4.

$$C_A = \left(5.68 - 0.6 \log R_e\right) \times 10^{-3} \tag{2.3}$$

$$\Delta C_F = 0.044 \left[ \left( \frac{k_s}{L_{WL}} \right)^{\frac{1}{3}} - 10 R_e^{-\frac{1}{3}} \right] + 0.000125 \tag{2.4}$$

Using the correlation allowance recommended in ITTC (1999a) or ITTC (2014) results in a higher correlation allowance than that normally used for catamaran towing tank testing. It was decided in this research to use a correlation allowance that was used by other towing tank facilities that have conducted model tests on Incat's wave piercing catamaran. The Maritime Research Institute of Netherlands (MARIN) performed a calm water resistance test for the Joint High Speed Vessel (JHSV) 112m wave piercing catamaran in 2008. The tests carried out by the Maritime Research Institute Netherlands (MARIN) used a correlation allowance $C_A$ of 0.00035 and this value was used in this research (Marin, 2008). The Marin's correlation allowance was used directly and no conversion was made to the Marin's correlation allowance to suit the extrapolation used in this thesis. The Marin

extrapolation method (Marin, 2008) is actually similar to the ITTC'78 method of the 2011 version, procedure 7.5-0.2.03-01.4 (ITTC, 2014), except the formulation is not in coefficient or non-dimensional form and the absence of roughness allowance and the air resistance, where

$$R_{TS} = \left[R_{TM} - R_{FM}(1+k)\right]\lambda^3 \frac{\rho_S}{\rho_M} + R_{FS}(1+k) + R_{Allowance} \tag{2.5}$$

The resistance component $R_W$ can be scaled following Froude's similarity law;

$$\frac{R_{WS}}{R_{WM}} = \lambda^3 \frac{\rho_S}{\rho_M} \tag{2.6}$$

Therefore;

$$R_{TS} = \left[R_{WM}\right]\frac{R_{WS}}{R_{WM}} + R_{FS}(1+k) + R_{Allowance} \tag{2.7}$$

Thus;

$$C_{TS} = C_{FS}(1+k) + C_{WS} + C_A \tag{2.8}$$

Therefore the equation 2.8 is similar to the ITTC'78 procedure. But the main point is that the correlation allowance used in the extrapolation should be the same for both waterjet and propeller driven configuration for making a fair comparison.

## 2.13 Form factor using Prohaska plot

The form factor, *k* was derived using the Prohaska's method (Lindgren et al., 1978; Tanibayashi et al., 1984) . This was done by testing the model at a very low Froude number. The speed selected for the testing ranged from Froude number 0.1 to 0.2. According to Hughes (1954), by running at low speed, the residual resistance $C_R$ which consists of wave resistance and air resistance are negligible as they tend to be zero. As the wave resistance and air resistance are close to zero, the total resistance is left with only the component of the viscous resistance where the total resistance coefficient can be written as $C_{TM} = (1 + k)\, C_{FM}$.

Using the Prohaska's method, $C_{TM}/C_{FM}$ was plotted with respect to variation in $F_R^n / C_{FM}$ as shown in Figure 2.7. The exponent *n* is normally chosen in the order of 2 to 9, so that the data points fall on a line that is as straight as possible. In this study, an exponent order of 4 was used. The Prohaska's low speed testing was done using the lightest displacement at 2,500 tonnes and at level trim. Two frictional formulation lines were used to determine the coefficient of frictional resistance,

which were the Grigson's frictional line (Grigson, 1993) and ITTC 1957 model-ship correlation line (ITTC, 2011b). The total model resistance coefficient was calculated using $C_{TM} = R_{TM} / 1/2 \rho_M S_M V_M^2$. The form factors were read from the intersections of the linear plot on the y-axis ($C_{TM}$ / $C_{FM}$) as in Figure 2.7. The one plus form factor *(1 + k)* established using the Grigson's frictional line is at 1.272 and the one plus form factor using the ITTC 1957 model-ship correlation line is at 1.195. When referring to the form factor in the successive Chapters, a one plus form factor of 1.272 was used.

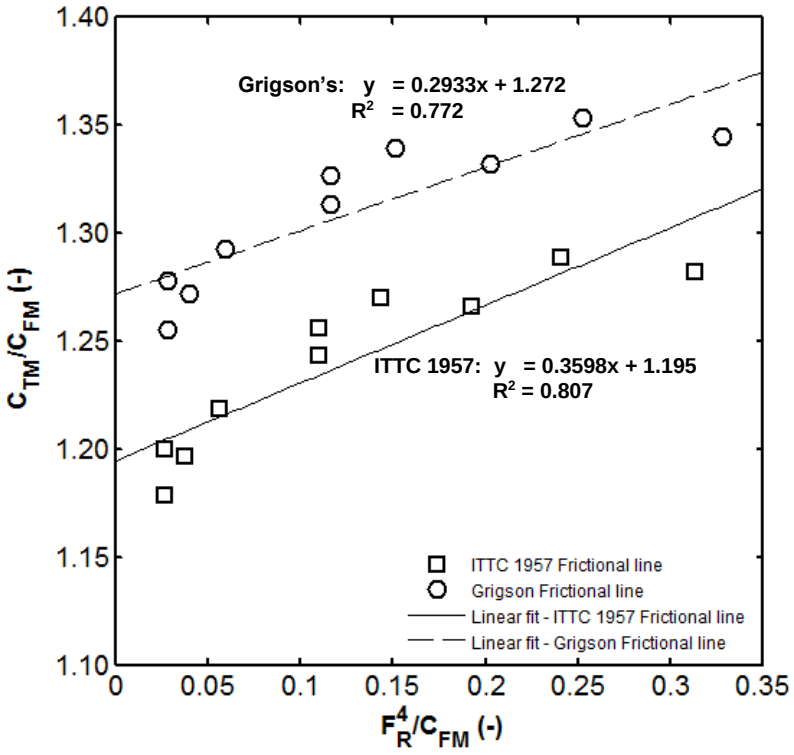


**Figure 2.7** Form factors derived using the Prohaska's method. The Grigson's frictional line and the ITTC 1957 model-ship correlation line were used to determine the coefficient of frictional resistance, $C_F$. The one plus form factors *(1 + k)* derived from the Prohaska's plot are 1.272 and 1.195 using Grigson's and ITTC 1957 line respectively.

There are some problems associated with using Prohaska's plot to find the form factor for a catamaran with a submerged transom stern. One of the problems was highlighted in Couser et al. (1997), where they questioned on the application of this Prohaska's method to transom stern vessels because of the different flow regime in the transom area. Molland et al. (1996) performed tests with the vessel trimmed by the bow to emerge the transom. This was done by having a sufficient bow down trim to raise the transom above the still water line. This was similarly done by Zürcher (2015) in getting the form factor for the waterjet driven catamaran, where in getting the form factor using Prohaska's method, the waterjet model was significantly trimmed by aft. This method of raising the transom above the waterline was originally put forward by Bailey (1976) where in further discussion in Insel and Molland (1992), form factors of the order of 1.55 were found at normal trim and 1.37 with the transom emerged. In Zürcher (2015), form factors of the order of 1.45 were found at normal

trim and 1.14 with the transom emerged. For the propeller driven catamaran, form factors of the order of 1.27 were found at normal trim and 1.195 with the transom emerged.

Another common problem is the accuracy of the load cell in measuring such a low force magnitude at lower speed (Froude number below 0.2). This will always remain a problem in determining form factors using Prohaska's method, where the resistance shows some scattering at low speeds.

## 2.14 Blockage and finite depth correction

The shallow-depth effects or the blockage effects were taken into account in the resistance analysis by making some blockage corrections to the resistance test results. The detail explanation on the blockage effects and blockage corrections can be found in Maruo (1948), Kinoshita (1954), Emerson (1959), Hughes (1961) and Kim (1962). The blockage corrections were calculated according to the ITTC recommendations and guidelines (ITTC, 2011b). The blockage corrections in ITTC (2011b) were based on the work of Schuster (1955), Scott (1970) and Tamura (1972).

Zürcher (2015) made comparison on the three blockage corrections using the formulae given by Schuster, Scott and Tamura in the 98m waterjet driven catamaran resistance results. Zürcher commented that only the Tamura and the Schuster blockage corrections were valid in correcting the resistance results. Zürcher reported that the difference in 'uncorrected' to 'corrected' resistance ranges from 1 to 2.5% using Tamura, 1 to 12% using Schuster and 3 to 7% using Scott's corrections. Zürcher further suggested using Schuster corrections to account the blockage effects. Haase (2015a) proved that this finite depth corrections using Schuster approach is in close agreement with his CFD predictions.

In Figure 2.8, a comparison of the velocity correction factor based on Tamura's and Schuster blockage corrections was made. The Tamura's correction factor was found to be higher than the Schuster's correction factor. It was observed that the correction factor increases with speed. In this research, the Schuster method was used as to be consistent with Zürcher work. The blockage corrections in terms of speed increase were added to the carriage speed and this corrected speed is used for all calculations.

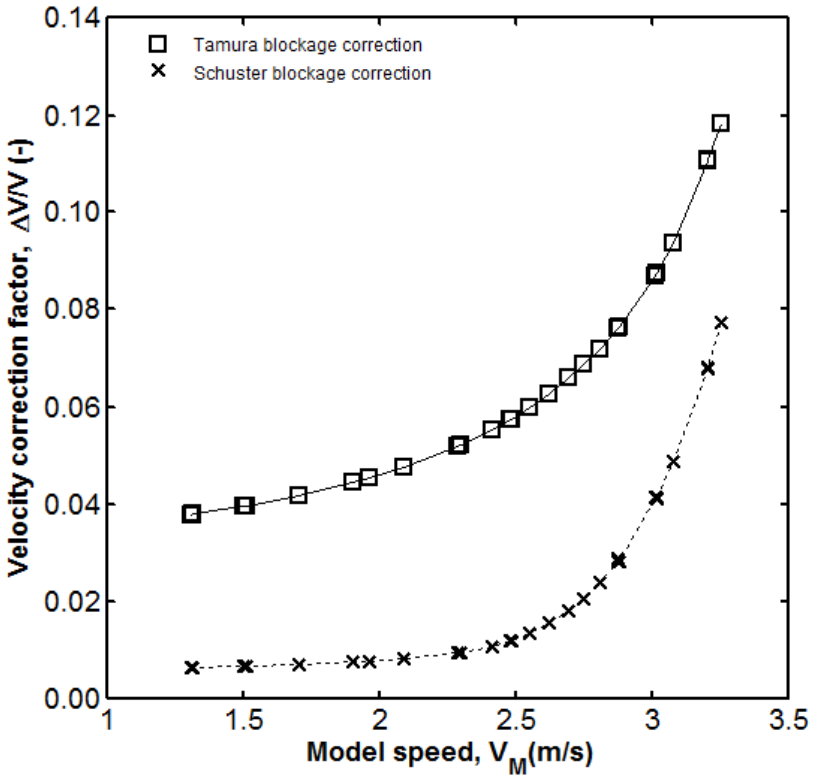


**Figure 2.8** Comparison of the velocity correction factor based on Tamura's and Schuster's blockage correction as described in the ITTC Resistance Test Guidelines 7.5-02-02-01.

## 2.15 Open water propeller test experiment

This section contains details of the open water propeller experimentation, at model scale. The open water test was carried out using the actual model of the propeller to obtain its open water characteristics. The open water characteristics were later used in the extrapolation procedures in order to derive the propulsion coefficients. The open water test was conducted in the AMC's towing tank.

One of the required data in the powering prediction is the propeller characteristics. The propeller characteristics are the forces and moments produce by the propeller which are the thrust and torque of the propeller. These forces and moments are expressed in non-dimensional terms which are the thrust coefficient, $K_T$, torque coefficient, $K_Q$ and the advance coefficient, $J$. These performance characteristics for the propeller in isolation and in uniform flow without the presence of a wake from the hull are known as open water data. The propeller open water data for the chosen propeller were measured using a propeller boat in AMC's towing tank. The model propeller was fitted on a horizontal driveway shaft and was moved through the water at an immersion of the shaft equal to at least 1.5 times of the diameter of the propeller as what has been recommended by ITTC (2002b).

The open water experiment was conducted by towing the open water boat at a steady speed while running the propeller at a constant revolution rate. The speed of the propeller boat which is the

speed of advance, $V_A$, and the revolution rate, $n$, thrust, $T$ and torque, $Q$ of the propeller were measured in each run. The measured thrust and torque were corrected using the tare thrust and torque value, i.e. the thrust and torque measured by the dynamometer when the experiment was carried out with a dummy boss of equal weight replacing the propeller.

## 2.16 Arrangement of the open water test

The test was conducted in the AMC's towing tank with the propeller boat attached to the towing tank's carriage. The propeller boat was lowered down to an immersion depth of 735 mm. The propeller dynamometer which is the force transducer that measures the thrust and torque of the propeller was fitted in the propeller boat. The dynamometer was connected to the driving electric motor through a coupling. The layout of the arrangement is illustrated in Figure 2.9 and Figure 2.10.

The propeller shaft extends at 410 mm forward from the boat to ensure that the flow around the propeller is not disturbed by the propeller boat. A fairing cap was provided at the forward end of the propeller hub as to ensure that the inflow over the propeller hub is parallel to the shaft (ITTC, 2002b).

## 2.17 Setup of equipment and instrumentation

The open water propeller experiments were conducted based on the ITTC guidelines for propeller open water tests. A similar setup as per ITTC (2002b) was used for the testing as shown in Figure 2.11. A propeller dynamometer supplied by Cussons, Type R-31 was used for measuring the propeller thrust and torque. An AM series analog inductive proximity sensor (AM9-10-1) was used to provide feedback on the shaft revolutions rate. All measured signals were stored and analysed to a desktop computer using National Instruments data acquisition card and all the measured signals were recorded as voltage, -10 volts to 10 volts. A program which was readily available in the towing tank data acquisition system which was written in LABVIEW was used as the interface in executing the data collection, recording static data, recording moving data and calibration file storage.

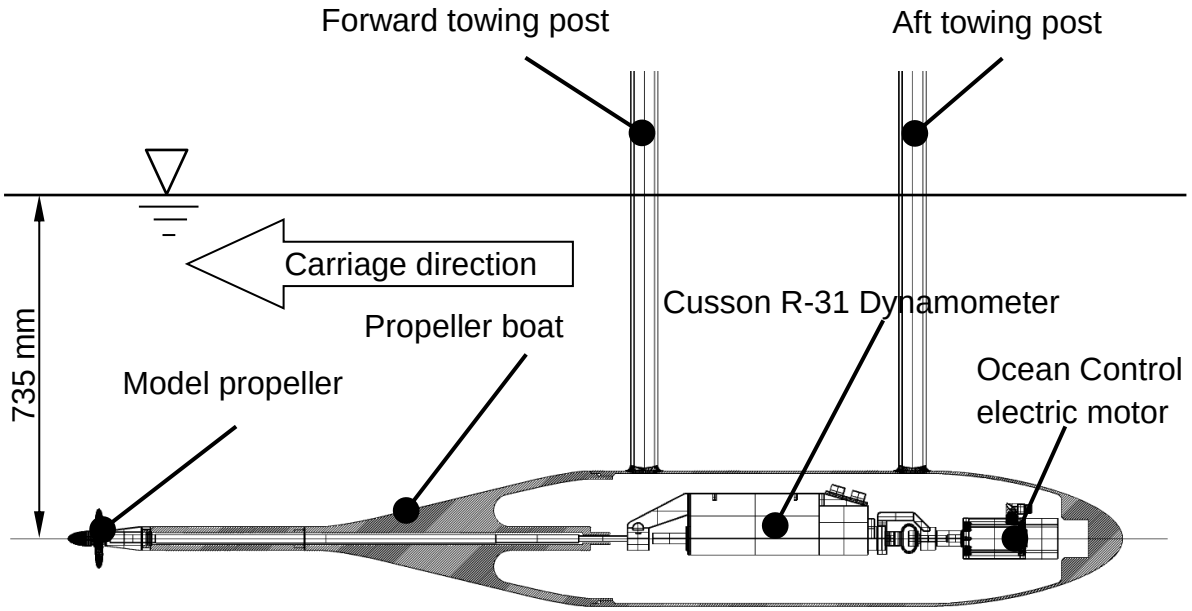


**Figure 2.9** The open water propeller test arrangement in the towing tank. The propeller boat was attached to the carriage of the towing tank. The propeller boat housed the propeller dynamometer and the driving electric motor**.**

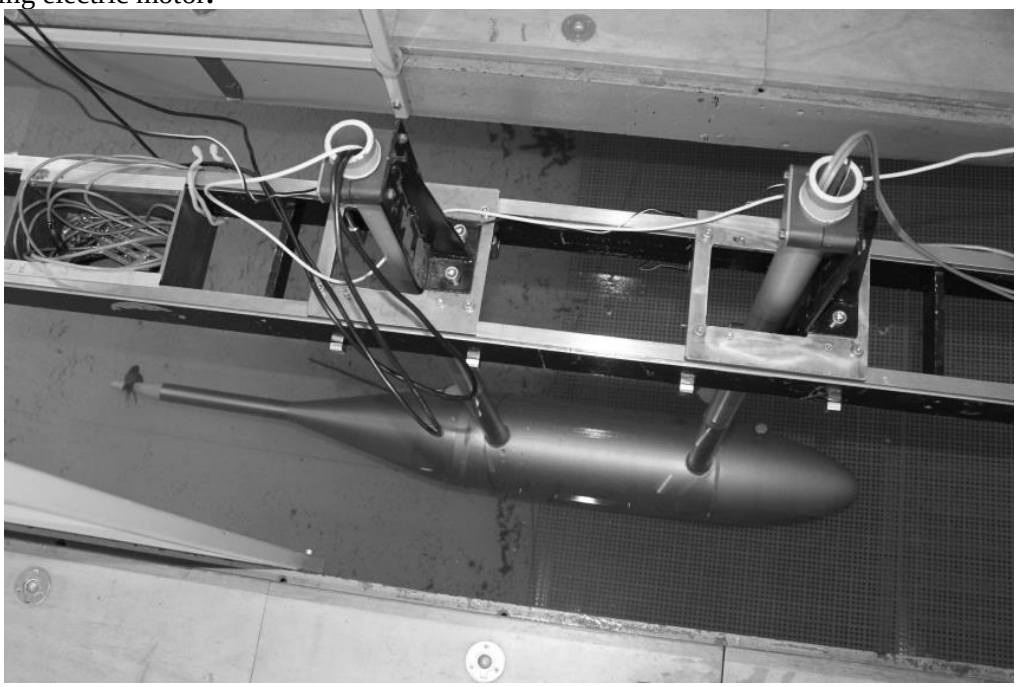

**Figure 2.10** The open water propeller test boat attached to the carriage of the towing tank. The two posts were secured to the dyno bed. The two posts were made of two aluminium tubes allowing access to the instrumentation cables and the power supply cable for the electric driving motor.

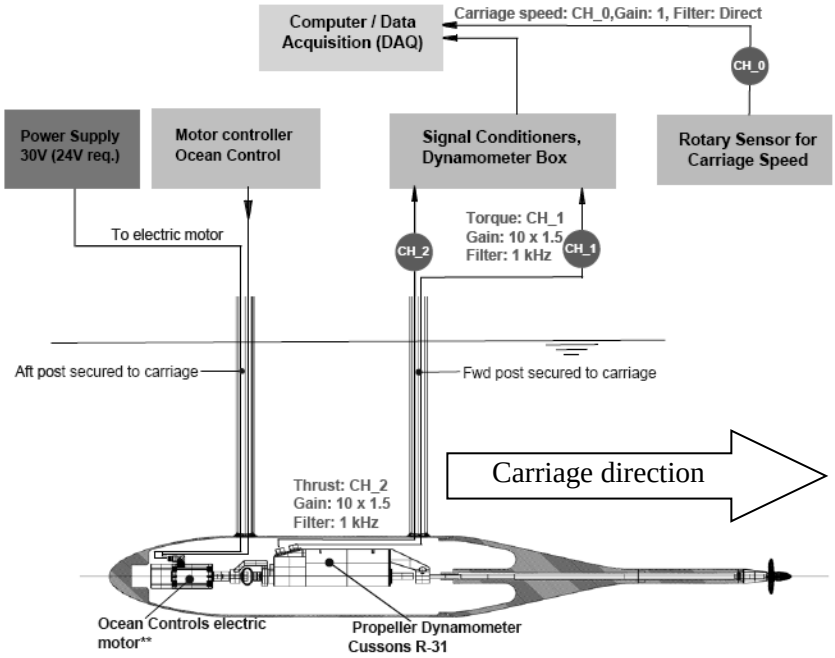


**Figure 2.11** The propeller open water test setup schematic. Four channels were used to measure (1) carriage speed (2) thrust (3) torque (4) shaft revolution rate. The shaft centerline was positioned 735mm below the water free surface. This typical setup follows the guideline recommended by ITTC 2002.

The open water tests were done using a propeller boat which contained the propeller dynamometer. All the propellers tested in the same setup with the propeller boat having an immersion depth of 735mm. This depth is necessary to reduce the proximity to the free surface effect to the propeller. This was to conform to the ITTC guidelines, which recommended that the shaft centerline immersion must be at least 1.5 times of the model propeller diameter. The propeller boat was secured to the towing tank carriage by clamping the forward and aft post using pipe brackets. These two posts were made using two aluminium hollow pipes with the pipe end fillet welded to the body of the propeller boat, allowing for the instrumentation wiring such as the thrust cable, torque cable and the proximity sensor cable to be connected to the propeller dynamometer and the proximity sensor. The propeller boat has two openings in allowing an access to the internal part of the boat for instrumentation installation purposes. The openings were through the aft and forward cones, fastened by bolts and sealed with two O-rings for avoiding water ingression into the propeller boat.

## 2.18 Self-propulsion test for propeller driven catamaran

The self-propulsion test was done using the same model as used in the calm water resistance test. This testing provides the means of directly measuring the thrust, $T$, the torque, $Q$, shaft speed $n$, and the drag of the model, $F_D$. In this experiment, the catamaran model was equipped with a model propeller, a model rudder and a propeller bracket supporting the propeller shaft. This testing was made for the purpose of assessing factors that influence the overall performance of the model

propeller operating behind the catamaran model. The testing method was also similar to the calm water resistance test using a single demihull method.

## 2.19 Arrangement of the model in the towing tank

The towing tank at AMC was arranged with the catamaran model using the wall as the symmetry centre line of the full vessel, similar to the calm water resistance test. The catamaran model was fitted with stern tubes made out of aluminium tubes, stainless steel shaft and external fittings such as the propeller bracket which was made out of brass and a rudder which was made from 3D printing out of Acrylonitrile butadiene styrene (ABS).

The brass propeller with the diameter of 120 mm was driven from inboard. The self-propelled model of the single demihull catamaran was assembled with one Cussons R-31 propeller dynamometer, one AMTI load cell for measuring the towing force, one brushless electric motor to drive the propulsion system, a one meter stainless steel shaft connecting the propulsion train to the propeller, one five bladed 120mm diameter Wageningen B-series propeller and a rectangular spade rudder with NACA 0015 section profile as shown in Figure 2.12 (Bottom). A 2 mm clearance was provided between the propeller and the bracket to prevent from any physical interference between the two parts. The rudder was locked in an amidships position, by having two stainless steel shafts as rudder stocks at the rudder top (root section) horizontal surface. These two rudder stocks were connected to the hull through two hollow tubes. The two hollow tubes were permanently fitted to the hull. This arrangement will prevent from the rudder to be rotated from the amidships position while the model running in a test.

## 2.20 Shaft inclination of the propulsion train system

The shaft was necessary to be set in an inclined position to allow some clearances between the tip of the propeller and the model hull. Furthermore, it was also necessary for the instrumentation such as the propeller dynamometer and the electric motor to have adequate spaces in the model. Initially, the options for the shaft inclination angle from the keel line were $0^o$, $2^o$, $3^o$, $5^o$ and $7^o$. These angle options were simulated in the CAD software (Rhinoceros 3D). In the CAD simulation, all the instrumentations and shaft train accessories were modelled and any physical interference of the instrumentations to the hull and the structure internal frame was checked. This option was shortlisted to $5^o$ and $7^o$ after considering the internal space available and physical interference of the instrumentations to the hull. Finally, a decision was made to use $5^o$ of shaft angle after considering the study of J. G. Peck and Moore (1974) on inclined-shaft propeller performance characteristics. Peck and Moore conducted a series of propeller open water test in a towing tank using a propeller boat with varying shaft inclinations. They used four Naval Ship Research and Development Center (NSRDC)

commercial propeller with different pitch to diameter ratio. The shaft inclinations studied were 0, 7.5 and 15 degrees for cavitation numbers ranging from 0.5 to 14.7. Peck and Moore concluded that a propeller operating at 15 degree shaft inclination is less efficient than one at either 0 or 7.5 degrees.

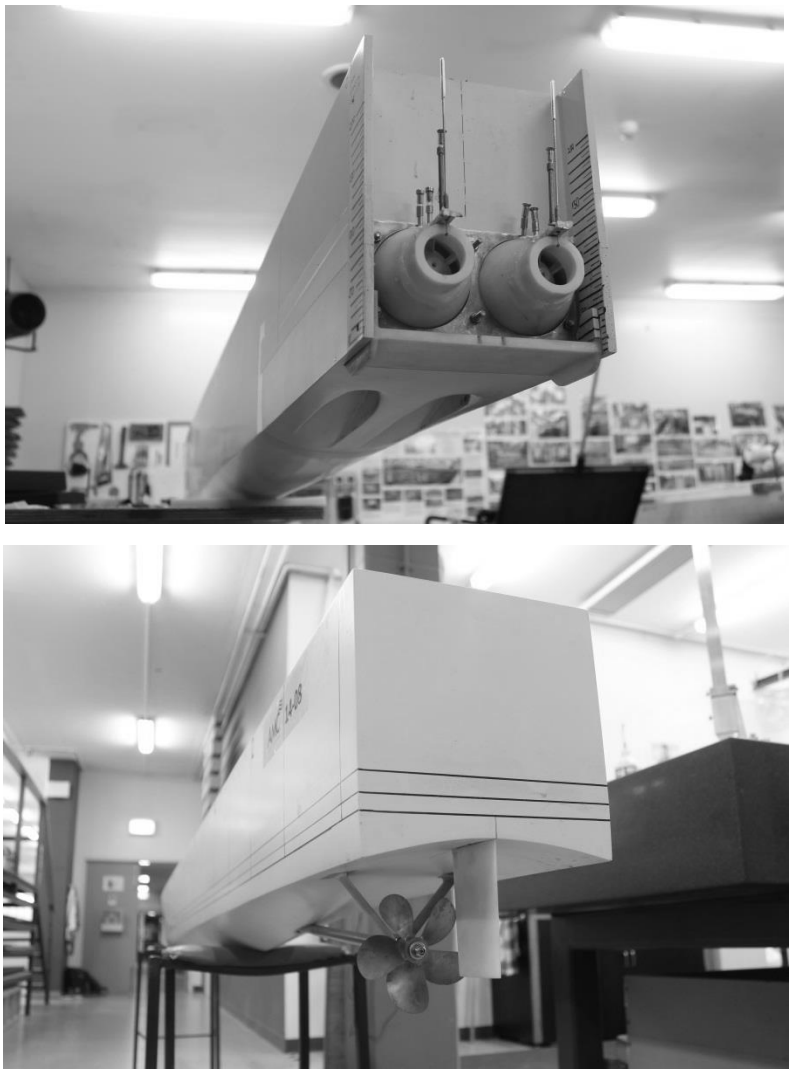

**Figure 2.12** (Top) The 3D printed waterjet propulsion unit attachment. Note the nozzles and the tunnels of the waterjet unit of the 98m waterjet driven catamaran model. (Bottom) The propeller arrangement with a support bracket and a rudder of the 130m propeller driven catamaran model.

## 2.21 Instrumentation of the self-propulsion test

The R-31 dynamometer measured the thrust, $T$ and torque, $Q$ of the model propeller. The shaft speed was measured using a proximity sensor, which senses the shaft rotational speed by picking up voltage. The AMTI load cell measures the towing force $F_M$. In addition to the instrumentation mentioned above, the forward and aft post connecting the model to the towing tank carriage was fitted

with two Schaevitz 5000 DC-EC Linear Variable Differential Transformers (LVDT) for heave and trim measurements of the models. The carriage speeds were measured by a rotary pulse generator attached to the wheel of the towing tank carriage. Seven channels of data acquisition were used as shown in Figure 2.13. The channel for the carriage speed (Channel 0) was linked directly to the Data Acquisition System (DAQ), with the rest of the channels (Channel 1 – Channel 6) were linked to the DAQ via an amplifier and a filter unit. The details of the calibration limits and the filter used in each of the instrumentation are presented in Table 2.3. The sample rate for the data acquisition was set at 800 Hz.

**Table 2.3** The variables measured, units and the instrumentation used in the self-propulsion test.

| **Variables** | **Instrumentation** | **Units** | **Calibration max. to** | **Filter** |
|---|---|---|---|---|
| **Model speed** | Rotary pulse generator | m/s | Direct | - |
| **Total resistance** | AMTI load cell | grams | 6000 grams | 1 Hz |
| **Thrust** | R-31 Dynamometer | grams | 6000 grams | 1 Hz |
| **Torque** | R-31 Dynamometer | Nm | 1.5 Nm | 1 Hz |
| **Sinkage** | LVDT - Fwd and Aft | mm | $\pm$ 60 mm | 1 Hz |
| **Running trim** | LVDT – Fwd and Aft | mm | $\pm$ 60 mm | 1 Hz |
| **Water temperature** | Thermometer | $^{o}$C | - | - |

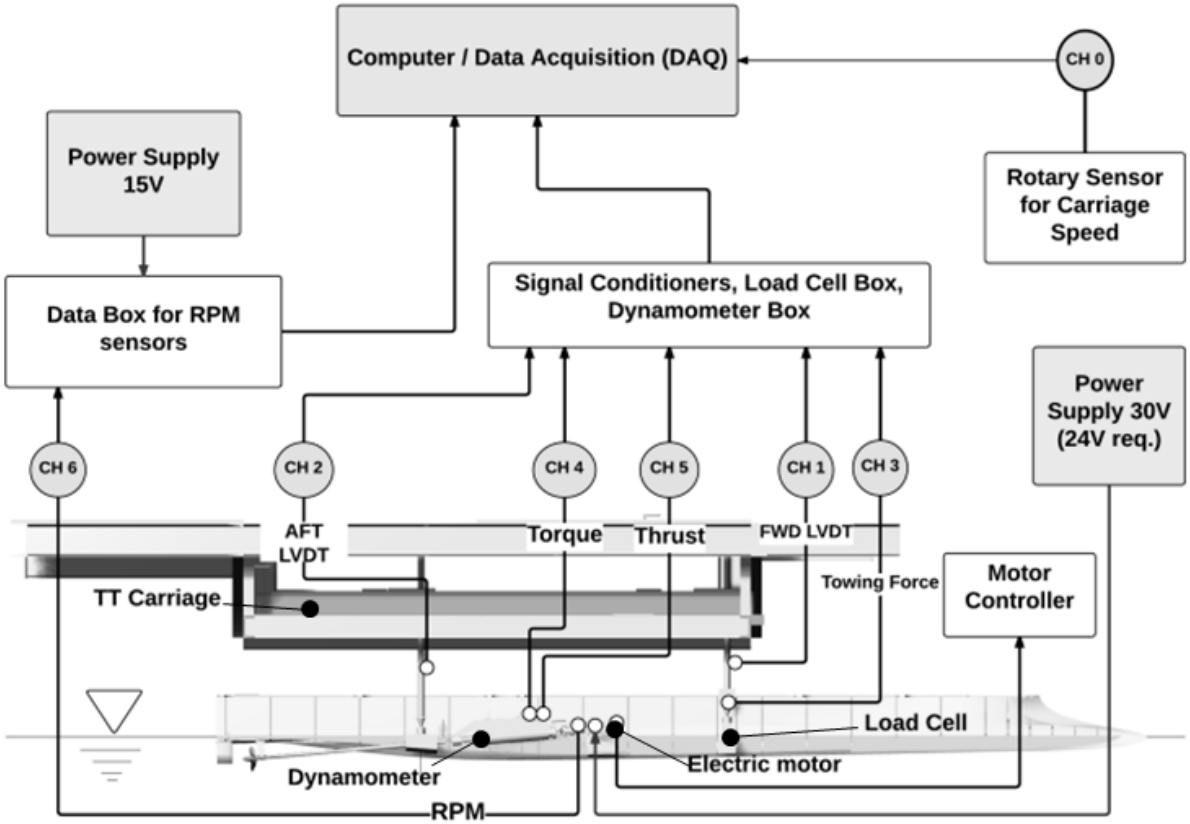


**Figure 2.13** Data acquisition setup for the propeller driven self-propulsion test.

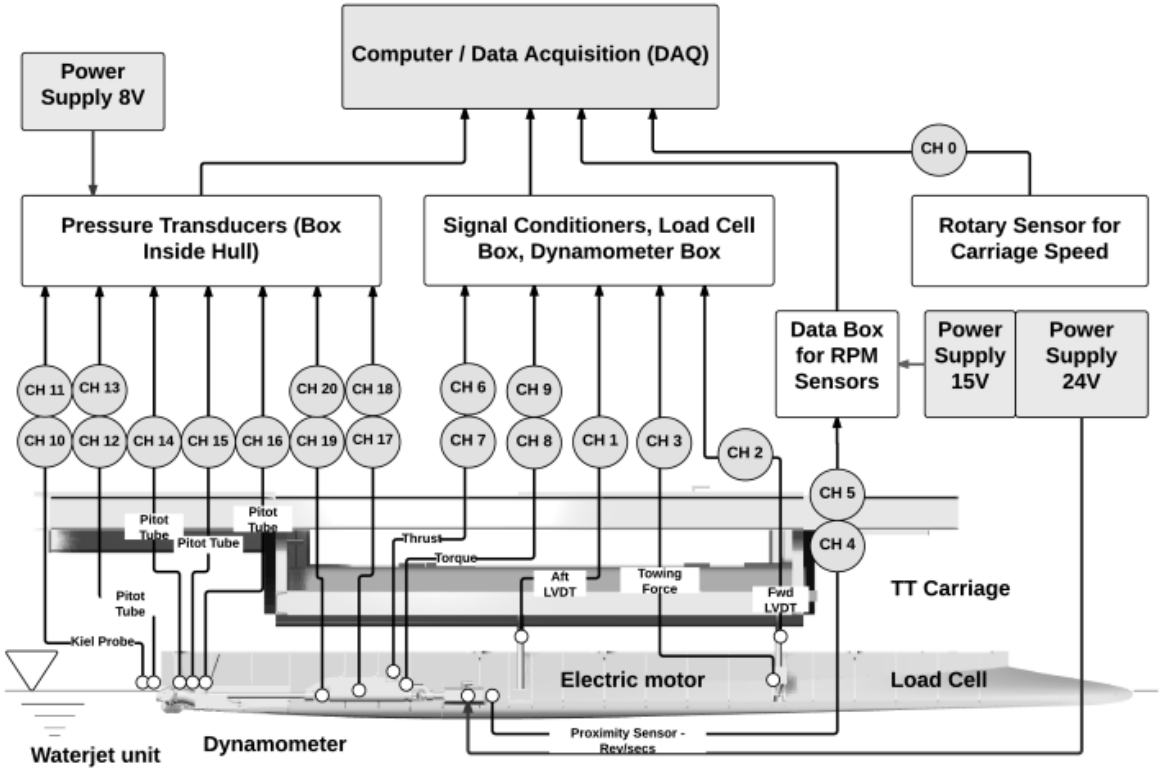


**Figure 2.14** Data acquisition setup for the waterjet driven self-propulsion test.

All the instruments mentioned above were calibrated regularly with the LVDTs and the AMTI load cell calibrated on a daily basis. The calibration procedures for the LVDTs and the AMTI load cell in the self-propulsion test are similar to the calibrations in the calm water resistance test. The calibration of the R-31 dynamometer follows the similar steps as in the propeller open water test, see Appendix A - Experiment Set-up.

## 2.22 The experiments of the waterjet driven hull

The full scale vessel for the waterjet propulsion testing is an Incat Tasmania designed and built vessel named HSV-2 Swift (Hull 061) as mentioned in the beginning of this chapter. As presented in Table 2.1, the model to the full-scale ratio of the tested single demihull is 21.6 and the model length is 4.3 m at the waterline. Zürcher (2015) carried out the experimental testing which consists of (1) Flow rate measurement testing, (2) Bare hull resistance testing, (3) Waterjet self-propulsion test.

The waterjet testing was carried out by Zürcher using the load varied ("British method") model self-propulsion testing where the model speed was put constant and a series of runs were carried out at different shaft speeds in the over and underloaded conditions relative to the self-propulsion point similar to the method conducted in the self-propulsion test for the 130m propeller driven catamaran. Zürcher used two model waterjets fitted in a single demihull model which was scaled geometrically from a full scale waterjet unit taken from LIPS Jet LJ120E. Zürcher fabricated the model waterjets as a 3D printed hull section, which was attached to the model demihull as shown in Figure 2.12 (Top).

A schematic representation of the demihull model showing how Zürcher arranged the experimental setup of the two model waterjets and the data acquisition system is shown in Figure 2.14. The data acquisition system and sensors for the model waterjet were employed based on the recommended ITTC propulsive performance prediction procedures for waterjet propelled vessels (ITTC, 2011c). ITTC recommends Laser Doppler Velocimetry (LDV) measurements for determining waterjet flow rate. But due to the lack of LDV equipment, Zürcher conducted a separate static flow rate measurement test at the AMC Model Test Basin to relate the flow rate to jet velocity measured at a single point using a Kiel probe (Zürcher et al., 2013).

The detail of the experimental work of the waterjet driven catamaran, the waterjet performance extrapolation and the full results can be found in Zürcher et al. (2013) and Zürcher (2015).

## 2.23 Results of the experiment

The model experimental results of the three physical model tests, i.e. bare hull resistance test, propeller open water test, self-propulsion test, are listed in Appendix F – Model experimental results. The extrapolated results of the resistance test and the self-propulsion test of the 130m propeller driven catamaran are discussed in Chapter 5.

## 2.24 Extrapolating the results to full-scale – ITTC 1978 method

The ITTC 1978 method was used to extrapolate the results of the three physical model tests, i.e. bare hull resistance test, propeller open water test, self-propulsion test, to full scale power as in ITTC (2001). The detailed procedure of the entire ITTC1978 extrapolation analysis can also be found in Manen and Oossanen (1988) and Bose (2008). The steps shown here are similar to Molloy (2006).

The 'British' method used in the self-propulsion test requires the interpolation of the self-propulsion point for the model tested. The method used here involves the plotting of the non-dimensional towing force coefficient $K_{FD}$ from the self-propulsion test results against the advance coefficient, $J_P$. At the intersection of the $K_{FD}$ curve where $K_{FD} = F_D / \rho_M n_M^2 D_M^4$ (Bose, 2008) and the curve of the required towing force coefficient by using, $K_{FD} = \left(C_{FD} S_S / 2D_S^2\right) J_P^2$ (Bose, 2008), the towing force at the self-propulsion point was obtained.

The results of the tow force at the self-propulsion-point, taking an example of the propeller driven catamaran at Froude number 0.29 are shown in Figure 2.15 (a). Once the advance coefficient, $J_P$, at the model self-propulsion point was obtained using the curve of $K_{FD}$ and $K_{FD}/J_P^2$, the values of the propeller coefficients, in the behind condition, $K_{TP}$ and $K_{QP}$, can be found from the results of the self-propulsion test as shown in Figure 2.15 (b). Then, using the "thrust identity" method, the value of $K_{TP}$ was used to find the value of advance coefficient, $J_O$ and the torque coefficient, $K_{QO}$ in the results of the open water test of the propeller. An example is included in Figure 2.16 (a).

Corrections were made to the model open water thrust and torque coefficients, $K_{TO}$ and $K_{QO}$, to obtain the full-scale open water propeller thrust and torque coefficients, $K_{TOS}$ and $K_{QOS}$. The operating point of the full-scale propeller can be found from the intersection of the curves of $K_{TOS}$, $K_{QOS}$ and the requirement for thrust given in the form of $K_T/J^2 = S_S.C_{TS}/2D_S^2(1-t)(1-w_{TS})^2$ (Bose, 2008). This intersection leads to the operating values of $K_{TS}$, $K_{QS}$ and $J_{TS}$, of the ship propeller, Figure 2.16 (b). Then it is possible to calculate the delivered power $P_{DS}$ where $P_{DS} = 2\pi\rho_S D_S^5 n_S^3 K_{QS} / \eta_R$.

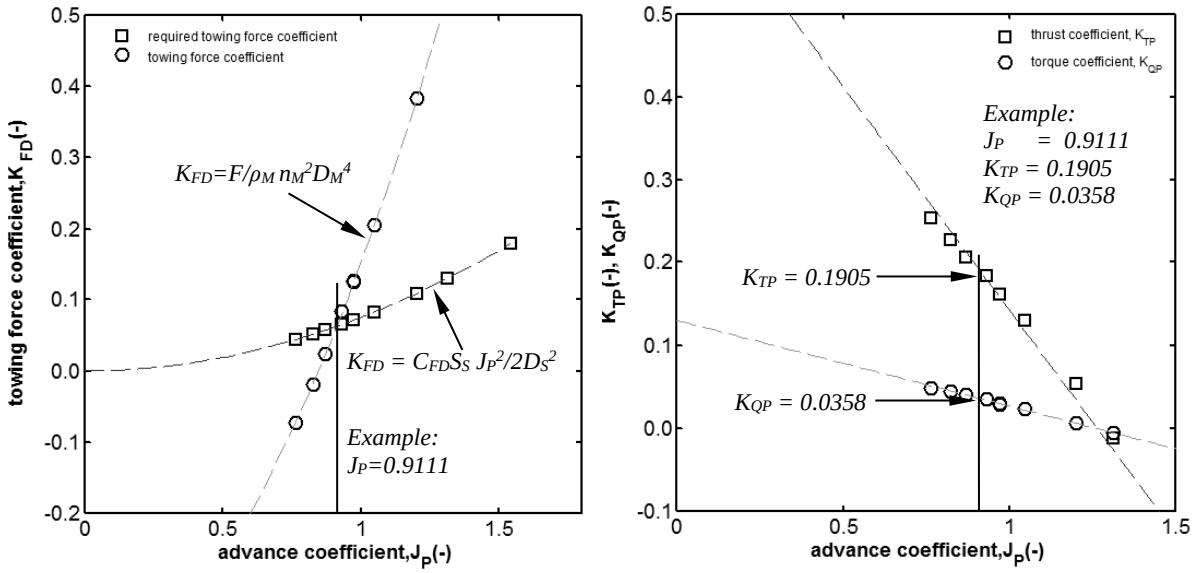


**(a)** **(b)**

**Figure 2.15 (a)** Plot of the $K_{FD}=F_D/\rho_M n_M^2 D_M^4$ curve and the $K_{FD} = C_{FD}S_S J_P^2/2D_S^2$ curve showing the tow force interpolation to obtain the model self-propulsion point. **(b)** The value of $J_P$ was used to find $K_{TP}$ in the self-propulsion test results, example using INCAT 130m propeller driven catamaran data at Froude number 0.29.

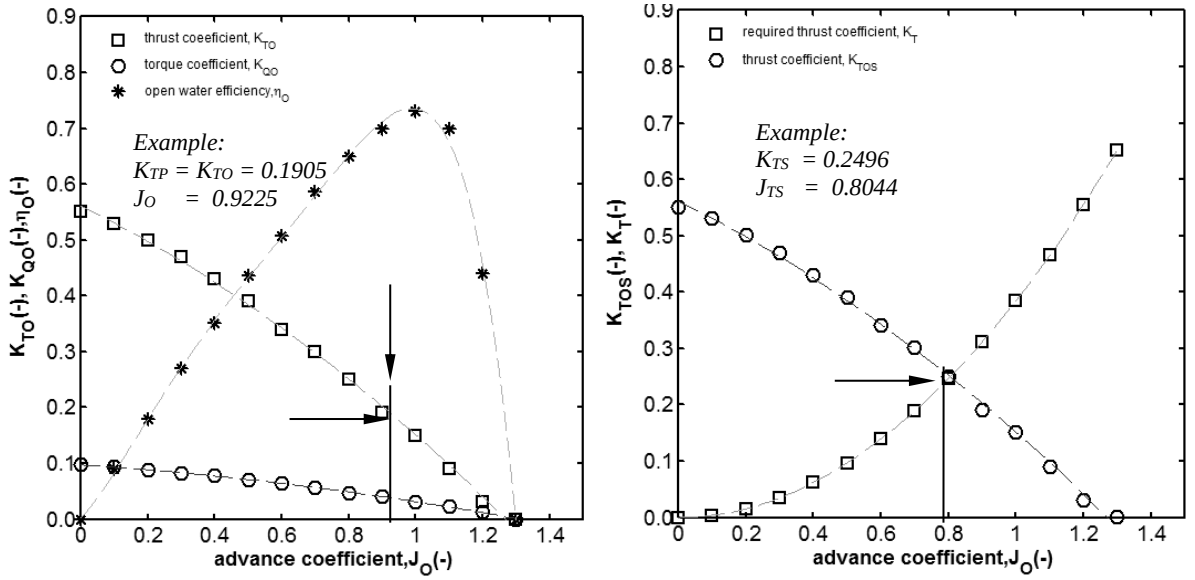


**(a)** **(b)**

**Figure 2.16 (a)** Using the 'thrust identity' method, the value of $K_{TP}$ was assumed to be identical to $K_{TO}$ to obtain advance coefficient, $J_O$ and torque coefficient, $K_{QO}$ from the open water test results **(b)** Using the intersection of the $K_{TOS}$ curve from the open water data and $K_{TS}$ curve from the equation to obtain the operating values of $K_{TS}$ and $J_{TS}$ - An example using INCAT 130m propeller driven catamaran data at Froude number 0.29.

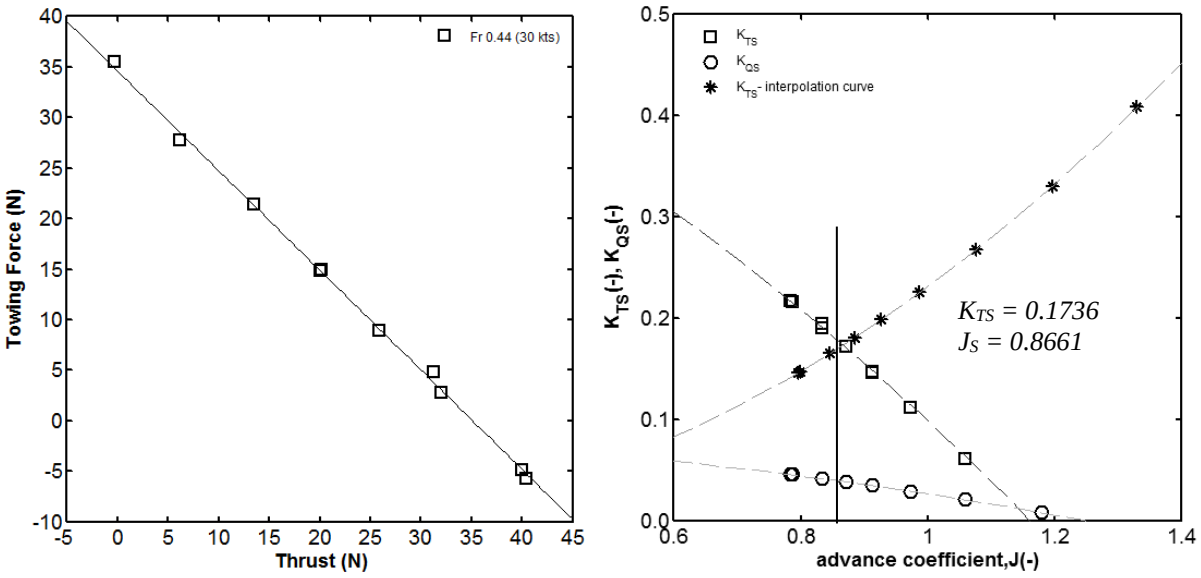


**(a)** **(b)**

**Figure 2.17 (a)** An example of a linear plot of towing force with respect to the thrust, an example was taken from the results of the 130m propeller driven catamaran at *Fr* 0.44 and displacement 3,640 tonnes. **(b)** Ship propeller operating point determination, to find the advance coefficient of the propeller, an example is taken from the results of the 130m propeller driven catamaran at *Fr* 0.44 and displacement 3,640.

## 2.25 The self-propulsion test only extrapolation method

Another method that was used in this study to extrapolate the towing tank results to full scale was the self-propulsion test only method. In this method the resistance test and the propeller open water test are not required. The method uses the results from a load varied self-propulsion test alone. This extrapolation method is based solely on results from the load-varying self-propulsion tests. This work is based on the work of Holtrop (2001), Bose and Molloy (2001a), Schmiechen (1991) and Kracht (1991). This method only works with the British method or the load-varied method of self-propulsion test only as the name implies. The self-propulsion test only method seeks to predict full scale power based on the load varying self-propulsion test only. Hence it is not necessary to conduct an open water test or a resistance test to obtain all information needed for completing the procedure. This method was based on the recommendation to the ITTC from the 22nd ITTC Specialist Committee on Unconventional Propulsors. The committee stated the following:

"….a powering performance prediction for a ship equipped with unconventional propulsors should be tested as unit, and not broken down into component tests of hull, propulsors etc" (Bose et al., 1999).

The first step was to plot the propeller thrust against the towing force for every speed tested as shown in Figure 2.17 (a). From the plot of the towing force with respect to the thrust, the thrust deduction fraction, *t*, was obtained from a linear regression line fitted through the points, where the line can be described by $F_M = -T_M(1-t^*) + F_{T=0}$ (Bose, 2008). The thrust deduction fraction was

obtained using the linear regression line slope of – *(1- t)*, where for an example, a regression line of *y = -0.9857x + 34.59*, has a slope of – *(1 – t)* equal to – *0.9857*. Therefore the value of *t* can be calculated where – *(1 – t) = - 0.9857*, giving the value of *t* equal to *0.0143*. Then the full scale thrust was calculated from:

$$T_S = T_M \lambda^3 \frac{\rho_S}{\rho_M}$$
$$= \left( \frac{F_{T=0} - F_M}{1-t} \right) \lambda^3 \frac{\rho_S}{\rho_M} \quad (2.9)$$

where $\lambda$ is the scale factor, $\rho$ is the density and $T$ and $F$ are any coordinates on the line. The next step was to determine the ship propeller operating point. The operating point was interpolated from the intersection of the full scale thrust and torque coefficients. A wake scaling is needed, to take into account the wake scale effects. These can be done by adjusting the advance coefficients of the plot by $J_S = J\left(1-w_M/1-w_S\right)$. The full-scale ship propeller operating point was found using the interpolation equation $K_{TS} = J^2$. $T_S/2\rho D_S^2 V_S^2$ which intersect with the ship thrust coefficient, $K_{TS}$, an example is shown in Figure 2.17 (b). Once the full scale thrust and the ship propeller operating point are determined, then these can be used to calculate the shaft speed, the full scale torque and the delivered power.

## 2.26 The waterjet thrust based extrapolation method (Zürcher, 2015)

The waterjet performance extrapolation was partially based on standard ITTC waterjet extrapolation procedures, but deviates from the common method of conducting the water-jet system test. This new method of extrapolation can be found in Zürcher (2015). In this method, the gross thrust $T_G$ is the main component of the waterjet performance extrapolation. The mass flow rate $\rho Q_J$ was measured in the flow rate measurements and the inlet wake fraction *w* had been determined by carrying out boundary layer measurements at ITTC momentum flux station at ahead of the inlet. Waterjet self-propulsion test results were used to establish self-propulsion points for each tested speed. Model self-propulsion points were corrected for frictional differences between model and full scale vessels using towing force $F_G$ equation (Zürcher, 2015). Self-propulsion points result in thrust, mass flow rate, torque and shaft revolution values for each of the tested speeds were then determined. The thrust was then extrapolated to full scale using the equation found in Bose (2008, p. 17).

Zürcher used the momentum flux energy method to calculate the delivered power $P_D$. Zürcher then calculate the overall propulsive efficiency using the values of the effective power $P_E$, the pump effective power $P_{PE}$, is the pump efficiency $\eta_{pump}$ and the installation efficiency $\eta_{inst}$.

# Chapter 3

# The Reynolds scale effect on small propeller and its correction method

## 3.1 Introduction

This chapter presents the investigation of the Reynolds scale effect study on small propellers. This study is necessary as small propellers with diameters ranging from 110 mm to 120 mm were used in the self-propulsion tests.

The values of torque and thrust coefficients of any propeller are different from the corresponding values of its model. This difference is known as scale effect and it alters the powering prediction of the vessel. The scale effect could jeopardise the reliability of a result if not taken into account correctly. Therefore, it is prime importance to study the propeller scale effect on the self-propulsion test performance.

Bazilevski (2001) studied variations in flow regimes, similar to scale effect, using trip wires of 0.1 mm diameter which were placed at 10% of blade chord. With the unmodified blades, the scatter of measured efficiency was 13.6% and by using the turbulence stimulation, the scatter is reduced to 1.5%. Bazilevski (2001) proposed a stimulator drag allowance semi-empirical formula developed by Tagori (1963) and Katzman et al. (1972). Boorsma (2000) investigated using model propellers of which the leading edge was roughened. Using a sample of 5 correlation cases of fixed pitch propeller, it was shown by Boorsma that the use of flow-tripping on the model propellers reduced the dispersion of the rotation rate correlation factor for constant power, $C_{np}$, from 2.4 to 1.7 per cent. Jessup et al. (2002) concluded that although the results look promising, the retested sample of correlation cases was too small.

Bazilevski (2001) listed several experimental investigations of propeller blade flow over a wide range of Reynolds numbers using propeller models with diameters between 168 and 355 mm. Flow visualizations show boundary layer flow is mainly laminar on both pressure and suction sides of Reynolds number below $1 \times 10^6$. At higher Reynolds number, the laminar portion on the suction side

is progressively reduced and tends to disappear. On the pressure side, the laminar boundary layer is more stable. Between Reynolds number 1 x $10^6$ and 1 x $10^7$ a fully developed turbulent boundary layer is established on both sides. Jessup et al. (2002) also recommended that to perform open water tests at higher shaft rotation rate than the value required by Froude number identity for achieving closer similarity to full scale conditions. The Naval Surface Warfare Centre, Carderock Division, NSWCCD presented the threshold above in which the propeller performance is independent of Reynolds number which is at *Re* of about 1.15 x $10^6$, see Figure 6.1 in Jessup et al. (2002). From the literature mentioned above, it can be concluded that the scale effects can be minimised by either rotating the model propeller at higher Reynolds number above the threshold presented by NSWCCD or by implementing turbulence stimulation. Alternatively the scale effects can be corrected using semi-empirical formulas which can be found in Benedek (1985), Kuiper (1992) and ITTC (2014).

## 3.2 Method of investigation

In order to study the scale effect of a propeller having a small diameter, in the range of 100 mm – 120 mm, which was used for the Incat's propeller driven wave-piercing catamaran model self-propulsion test, propeller scale effects experiments were conducted in AMC's towing tank. To investigate the scale effect on a small propeller, the model propellers were tested in open water conditions, without the presence of the wake of the hull. This experimental study which is called the open water test was completed for two different Reynolds numbers. The results of the open water test were then compared with with the results of propeller coefficients of a larger geometrically similar or 'geosim' propeller with a diameter of 220 mm found in Kuiper (1992).

## 3.3 Model propeller

The model propellers selected for this investigation were three sets of propellers with different pitch settings of FTV Bluefin and a Wageningen B-series propeller. The FTV Bluefin full scale propeller is an Ulstein AB (now Rolls-Royce Ltd) controllable pitch propeller. As there were no available documented drawings and blade contour of the FTV Bluefin propeller, the blade contour had to be 3D scanned during the periodically scheduled dry-docking of the Bluefin at the Southern Marine Shiplift Pty Ltd, Kings Wharf, Invermay on 14 February 2013. The propeller scanning was done by Lester Franks, a 3D scanning, metrology and engineering survey firm, using a FARO Focus$^{3D}$ laser scanner. The laser scanner has an accuracy of $\pm$ 2mm. The Bluefin propeller was scanned at 100%, 80% and 60% pitch settings. Using the scanned data, the propellers were remodelled in CAD and manufactured by 3D printing in Acrylonitrile butadiene styrene (ABS). The Bluefin propellers were

printed in two sets of sizes, the first set consists of three propellers, each with different pitch settings with a diameter of 110mm, and the second set consists of three propellers, each with different pitch settings, with a diameter of 220mm. For the Wageningen B-series propeller, its geometry and blade contour was found in Kuiper (1992, pp. 38 - 50). The B-series propeller was CNC machined out of brass by Danford Engineering, Melbourne. The Bluefin and the Wageningen propeller's main particulars are detailed in Table 3.1.

**Table 3.1** Main particulars for the FTV Bluefin and the Wageningen B-series propeller. There were six Bluefin propellers with different sizes and pitch settings and a Wageningen B5.75 propeller used for this scale effect study.

| **Propeller** | **Bluefin CP** | | | | | | **Wageningen B5.75** | |
|---|---|---|---|---|---|---|---|---|
| **Diameter (mm)** | Ø110 | | | Ø220 | | | Ø120 | |
| **No of blades, *Z*** | 4 | | | | | | 5 | |
| **B.A.R, $A_E/A_O$** | 0.5 | | | | | | 0.75 | |
| **P/D** | 0.93 | 0.75 | 0.57 | 0.93 | 0.75 | 0.57 | 1.2 | |
| **Pitch (%)** | 100 | 80 | 60 | 100 | 80 | 60 | - | |
| **Re** | 98,000 | | | 200,000 | | | 119,000 | 228,000 |
| **Material** | Acrylonitrile butadiene styrene | | | | | | Brass | |

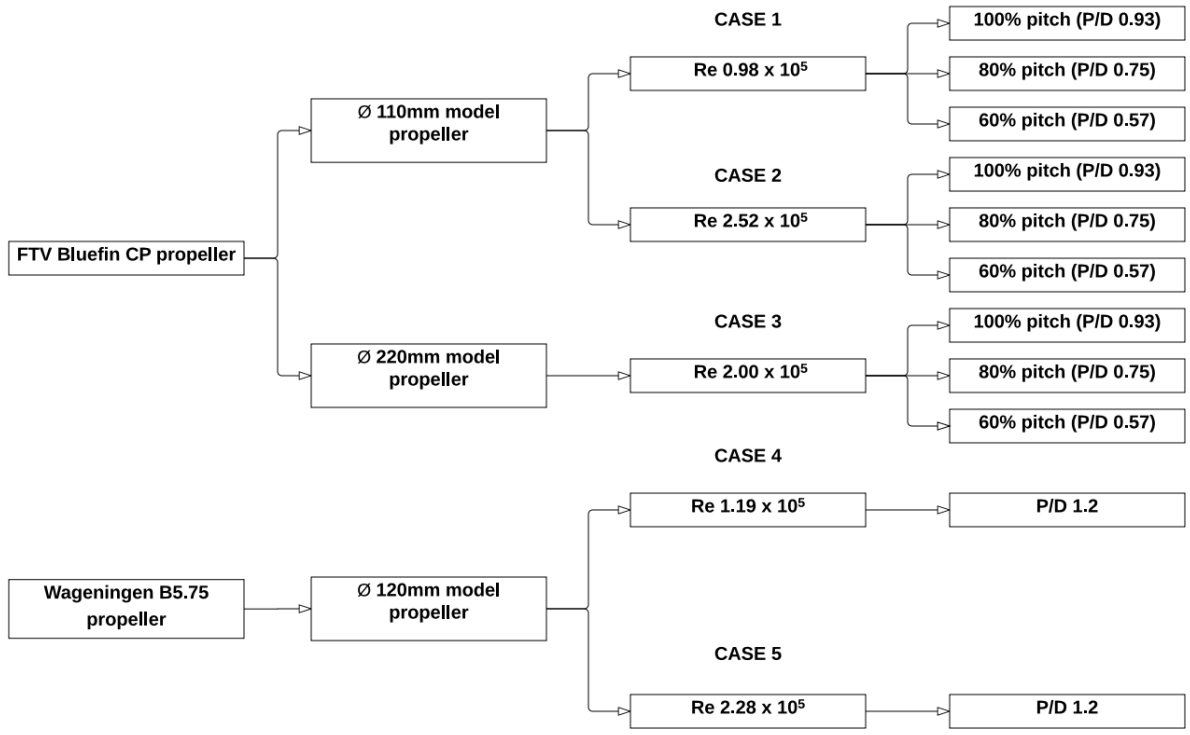


**Figure 3.1** The Reynolds scale effect case study. The 4 bladed FTV Bluefin propellers were tested in 3 case situations and the 5 bladed Wageningen B5.75 propeller was tested in 2 case situations.

## 3.4 The open water test procedure

In the open water test, the values measured were the advance speed $V_A$ or the carriage speed, the propeller thrust $T$, the propeller torque $Q$ and the propeller shaft revolution rate $n$. These values were non-dimensionalised as in Equation 3.1, 3.2, 3.3 and 3.4. The non-dimensional thrust coefficient of the tested model propeller can be represented as:

$$K_{TO} = \frac{T_O}{\rho n^2 D^4} \tag{3.1}$$

where $n$ is the rotation speed, $D$ is the diameter of the model propeller and $T_O$ is the thrust measured by the propeller dynamometer in the open water towing tank test. The non-dimensional torque coefficient of the tested model propeller can be represented as:

$$K_{QO} = \frac{Q_O}{\rho n^2 D^5} \tag{3.2}$$

where $Q_O$ is the torque measured by the propeller dynamometer in the open water test. The advance speed $V_A$, can be represented in non-dimensional form of:

$$J_O = \frac{V_A}{nD} \tag{3.3}$$

The open water efficiency of the model propeller which is the most important parameter in this study, can be represented by:

$$\eta_O = \frac{J_O}{2\pi}\frac{K_T}{K_Q} \tag{3.4}$$

In the open water test, the experiments were carried out at a constant propeller rate of revolution with the speed of advance, i.e. the carriage speed covering the range of the advance ratio from $J$ = 0 to the $J$ corresponding to $K_T$ = 0, with at least one run with negative thrust. At the beginning and at the end of the test program, the friction in the bearings of the propeller shaft was measured. This was done by replacing the model propeller with a blade-less hub. The friction in the bearings was measured by measuring the torque at varied carriage speed covering the range of the advance ratio from $J$ = 0 to the $J$=1.0. The shaft revolution rate was set to be similar to the actual speed required for testing. The average value of the measured torque was used as a tare value in order to subtract additional torque from the mean test value of the shaft torque caused by the bearing friction in the shafting system.

Two shaft speeds were chosen in order to investigate the Reynolds scale effect, one in the low Reynolds number regime, i.e. $Re$< 200,000 and the other one in the high Reynolds number regime i.e. $Re$>200,000. This was based on the ITTC guidelines that the local Reynolds number, $R_{n0.7}$ at the 0.7 relative radius should be not less than 200,000. In a self-propulsion test, especially testing with a small model hull and a small model propeller, testing in the low Reynolds number regime is unavoidable. Therefore, in order to investigate the scale effect in the low Reynolds number, the shaft

rotation speed was chosen to be at 11 revolutions per second which was at *Re* 98,000. The shaft rotation speed for testing at high Reynolds number was chosen to be at 28 revolutions per second which was at *Re* 252,000. The local Reynolds number can be found from Kuiper (1992, p. 81) and Bose (2008, p. 10):

$$R_{e_{0.7}} = \frac{c_{0.7}\sqrt{V_A^2 + (0.7\pi nD)^2}}{\upsilon} \tag{3.5}$$

where $c$ is the chord length of the propeller blades at 0.7 relative radius, $V_A$ is the local advance speed, $n$ is the propeller shaft revolution rate, $D$ is the propeller diameter and $\upsilon$ is the kinematic viscosity of water.

## 3.5 Experimental results

### FTV Bluefin propeller (Case 1, Case 2 and Case 3)

The results were presented in a non-dimensionalised form of the thrust coefficient $K_{TO}$, torque coefficient $K_{QO}$, and the open water efficiency $\eta_O$, plotted with respect to the advance coefficient $J_O$. The open water test results of the Ø110mm diameter Bluefin propellers tested at Reynolds number *Re* 0.98 x $10^5$ (Case 1), were compared with the results of Bluefin propellers tested at Reynolds number *Re* 2.52 x $10^5$ (Case 2) and Ø220mm diameter Bluefin propellers tested at Reynolds number *Re* 2.0 x $10^5$ (Case 3), see Figure 3.2, 3.3 and 3.4.

In Figure 3.2 (a), the torque coefficient of the propeller in Case 1 was lower than the propeller in Case 2 (small prop) and Case 3 (large prop). The efficiency of the propeller in Case 1 was higher than the propeller in Case 2 and 3 from $J$ = 0 to $J$ = 0.85. In Figure 3.2 (b) it is observed that the thrust of the propeller tested in Case 1 was lower than the results of propeller in Case 2, from $J$ = 0 to $J$ = 0.5. The thrust differences between these two results (Case 1 and Case 2) were not that significant beyond $J$ = 0.5. The thrust of the propeller tested in Case 1 was also lower than the thrust of the 'geosim' large propeller tested in Case 3 from $J$ = 0 to $J$ = 0.5. Then beyond $J$ = 0.5, the thrust of the propeller in Case 3 was observed to be higher than the thrust of the propeller in Case 1.

In Figure 3.3 (a) for the 80% pitch propeller, the torque of the propeller in Case 1 was lower than the torque coefficient of the propeller in Case 2 and 3. The values of the torque were found to be more scattered than the other two propeller results (Case 2 and 3). In Figure 3.3 (b), the thrust coefficient of the propeller in Case 1 was also found to be lower than the thrust of the propeller in Case 2 and 3. The open water efficiency of the propeller in Case 1 was lower at low advance coefficient ($J$ = 0 to $J$ = 0.17) but higher at the mid-region advance coefficient ($J$ =0.17 to $J$=0.6).

In Figure 3.4 (a) for the 60% pitch propeller, the torque coefficient of the propeller in Case 1 was found to be significantly higher than the torque coefficient of the propeller in Case 2 and 3. In Figure 3.4 (b) the thrust coefficient of the propeller in Case 1 was found to be lower than the thrust coefficient of the propeller in Case 2 and 3. The open water efficiency of the propeller in Case 1 was also lower than the propeller in Case 2 and 3.

### Wageningen B5.75 propeller (Case 4 and Case 5)

The B5.75 propeller was tested in two Reynolds numbers which were at *Re* 1.19 x $10^5$ (Case 4) and *Re* 2.28 x $10^5$ (Case 5). In Figure 3.5 (a), the torque coefficient of the propeller in Case 4 was higher than the torque coefficient of the propeller in Case 5 (from $J$ = 0.1 to $J$ = 1.1). The thrust coefficient of the propeller in Case 4 was lower than the thrust coefficient of the propeller in Case 5 as shown in Figure 3.5 (b). The open water efficiency of the propeller in Case 4 was lower than the efficiency of the propeller in Case 5, especially at $J$ = 0.5 to $J$ = 1.2.

## 3.6 Discussion of the results

The results of the FTV Bluefin propeller (Case 1, Case 2 and 5), shows some huge scatter of the propeller coefficient and the propeller open water efficiency with respect to the Reynolds number as shown in Figure 3.6 and Figure 3.7. From all the results mentioned above, it was clear that the propeller running at slower speeds (lower Reynolds number) produced less torque (blade section drag) than the propeller operating at higher Reynolds number and the propeller in a larger scale (the 'Geosim' propeller, Case 3) except for the case of the 60% pitch propeller. This peculiar result was opposite to what theory has dictated, where theoretically a body or in this case the blade sections of the propeller rotates at lower Reynolds number the frictional drag coefficient will tend to be higher than the frictional drag coefficient at a higher Reynolds number. Such an example can clearly be seen in the results of series of lift and drag test (wind-tunnel test) of the NACA wing section by Abbott and Doenhoff (1959), where the wing sections tested in a higher Reynolds number resulted in a lower sectional drag coefficient than the wing section tested in a lower Reynolds number. It was suspected that the lower torque coefficient at the lowest Reynolds number suggested that there exists a wide extent of laminar flow around the blades of the Bluefin propeller. This suggested that the flow around the blade followed the Blasius (1908) line of laminar flow.

It was also suspected that the propeller blade section deflection causing these inconsistent results. This deflection was suspected to have altered the blade geometric pitch and the mean line (camber line) of the propeller blade section. This inconsistency was proven by plotting the propeller

coefficient ($K_T$, $K_Q$ and $\eta_O$) variation with respect to the Reynolds number, see Figure 3.6 and Figure 3.7. It was noticeable that the propeller coefficient of the Bluefin propeller fluctuates significantly with respect to the Reynolds number, and was not consistent as shown in Figure 3.6 and Figure 3.7. The alteration to the blade geometric pitch changes the velocity and the pressure gradients, which change the flow transition from laminar to turbulent flow or vice versa. This was supported by the findings of Muller et al. (2009), where the flow on the NACA profile 66-009 was computed using RANS at different Reynolds number for different angles of attack.

This deflection and bending issues were also found by Bazzi and Benedetti (2009). Bazzi and Benedetti conducted open water experiments at INSEAN towing tanks for propellers manufactured using the Selective Laser Sintering (SLS) technique similar to the Bluefin's propeller. Bazzi and Benedetti used ABS and bronze powders as the materials for the propellers to be tested. They reported that there were large variations in the thrust and torque coefficients compared with a similar propeller, manufactured in bronze (casting).

The results of the Wageningen B5.75 propeller (Case 4 and 5) however, shows some consistent propeller coefficient with respect to the Reynolds number as shown in Figure 3.8, Figure 3.9 and Figure 3.10. The torque coefficient were found to be higher at the lower Reynolds number for advance ratio J = 0.2, 0.4, 0.8 and 1.0. This correlates with the results of series of lift and drag test of the NACA wing section by Abbott and Doenhoff (1959), where the wing sections tested in a higher Reynolds number resulted in a lower sectional drag coefficient than the wing section tested in a lower Reynolds number. The lower torque coefficient at advance ratio $J = 1.2$ at the lowest Re suggested that there exists a wide extent of laminar flow around the blades at lower Reynolds number.

In conclusion, the results of the open water test of the Bluefin's propeller were unreliable. One of the major issues using ABS material for the model propeller is the blade deflection that altered the blade geometric pitch and mean camber line. Therefore, a decision was made, to use a bronze propeller in the self-propulsion test for the Incat propeller driven catamaran.

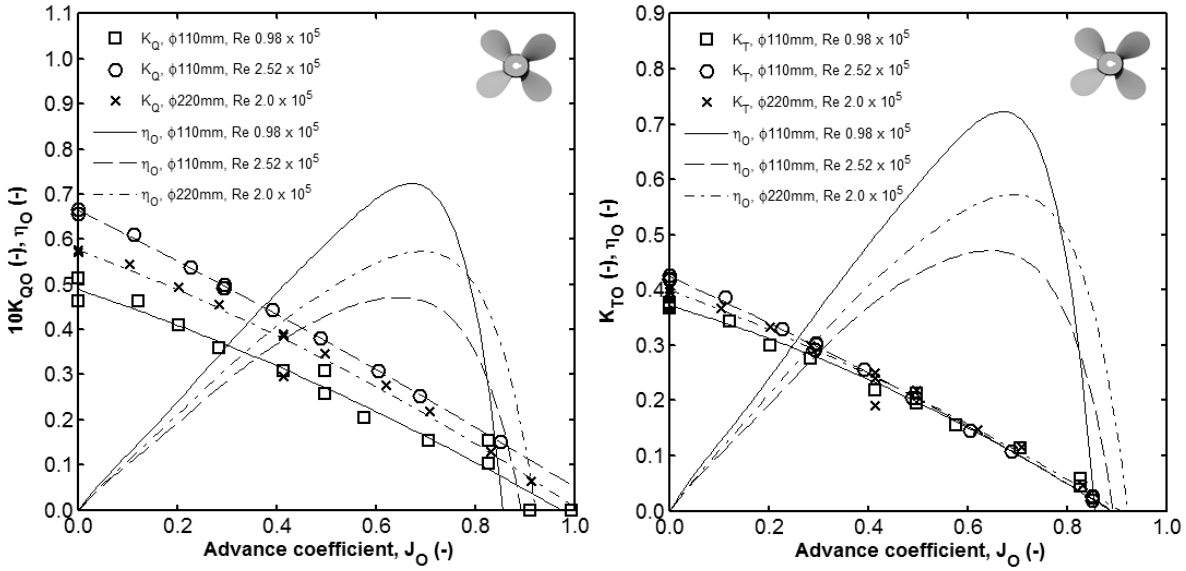


**(a)** **(b)**

**Figure 3.2** The results of the 100% pitch (P/D 0.93) of the FTV Bluefin CP propeller **(a)** The open water efficiency and the torque coefficient **(b)** The open water efficiency and the thrust coefficient. *Inset at upper left corner: The 4 bladed FTV Bluefin CP propeller.*

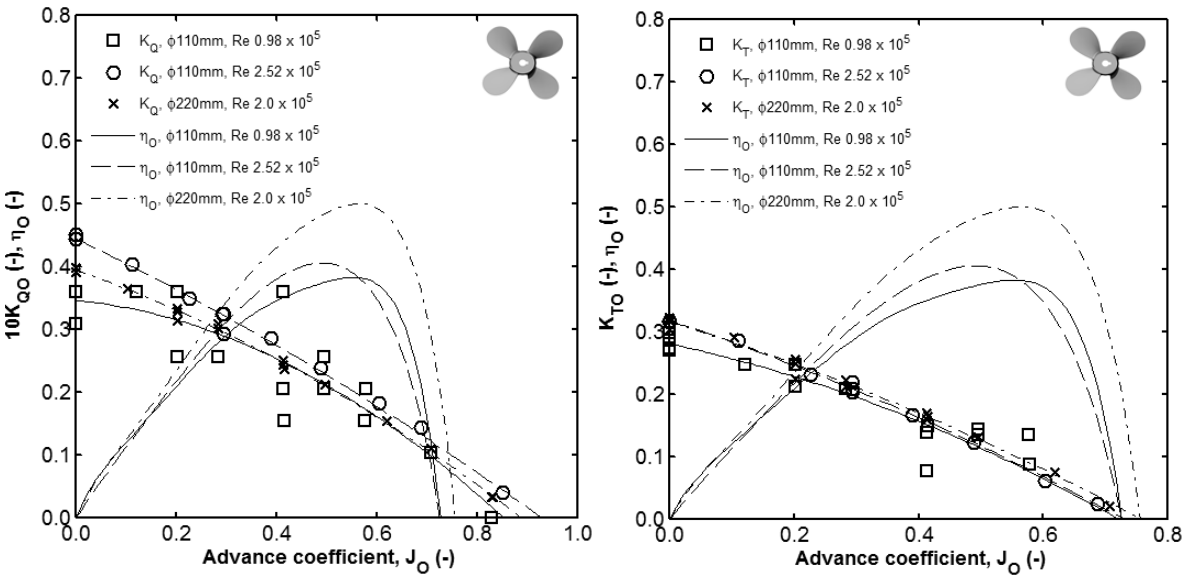


**(a)** **(b)**

**Figure 3.3** The results of the 80% pitch (P/D 0.75) of the FTV Bluefin CP propeller **(a)** The open water efficiency and the torque coefficient **(b)** The open water efficiency and the thrust coefficient. *Inset at upper left corner: The 4 bladed FTV Bluefin CP propeller.*

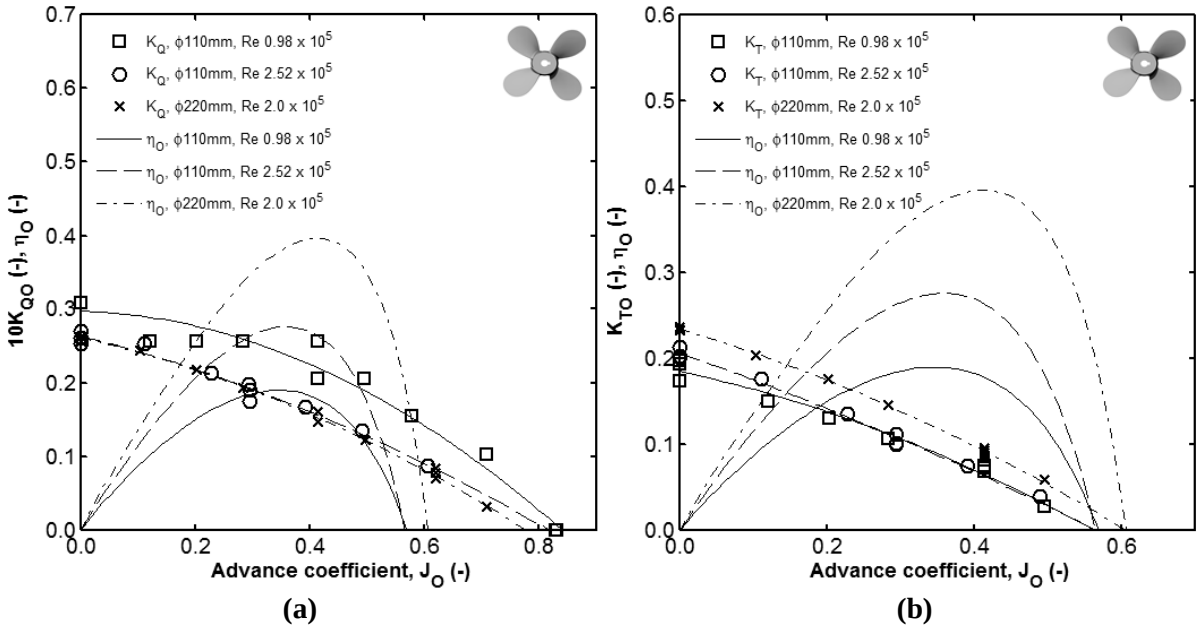


**Figure 3.4** The results of the 60% pitch (P/D 0.57) of the FTV Bluefin CP propeller **(a)** The open water efficiency and the torque coefficient **(b)** The open water efficiency and the thrust coefficient. *Inset at upper left corner: The 4 bladed FTV Bluefin CP propeller.*

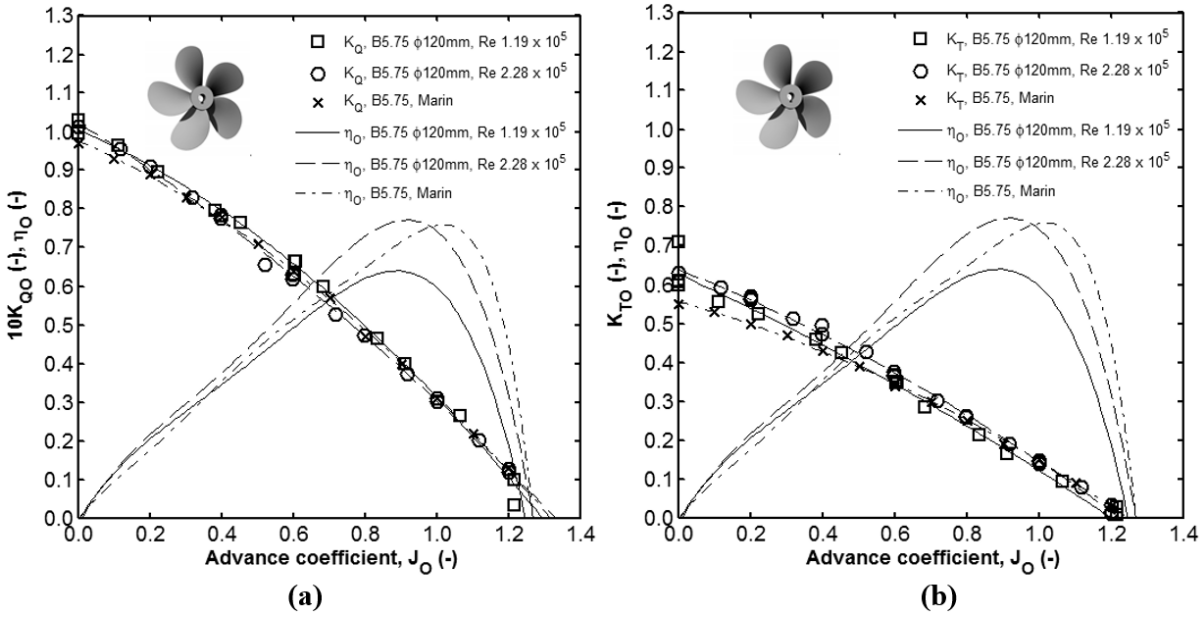


**Figure 3.5** The results of the Wageningen B-5.75 propeller (P/D 1.2) tested in two Reynolds number. The results were compared with the results of the same propeller tested by Marin (Kuiper, 1992) **(a)** The open water efficiency and the torque coefficient **(b)** The open water efficiency and the thrust coefficient. *Inset at upper right corner: The 5 bladed Wageningen B5.75 P/D 1.2 propeller.*

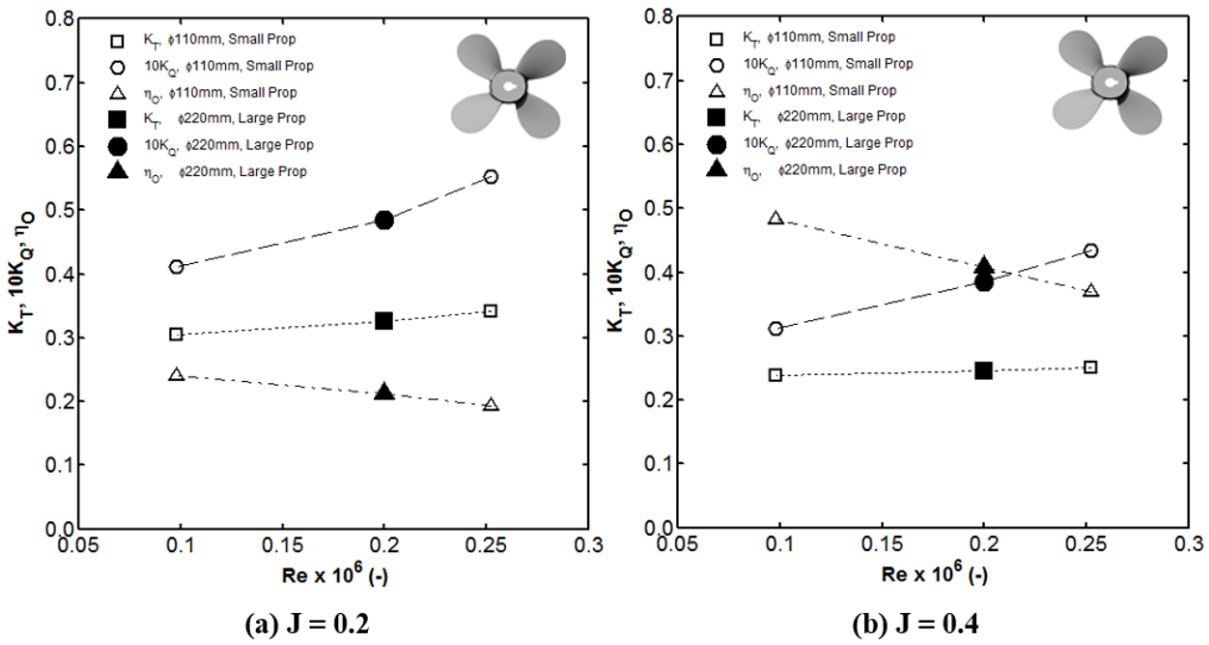


**Figure 3.6** Open water coefficients of the FTV Bluefin CP propeller (100% pitch) with respect to the Reynolds number. This results are at advance coefficient **(a)** J = 0.2 **(b)** J = 0.4. *Notes*: *Hollow marker - (small prop), Solid markers - (large prop). Inset at upper left corner: The 4 bladed FTV Bluefin CP propeller.*

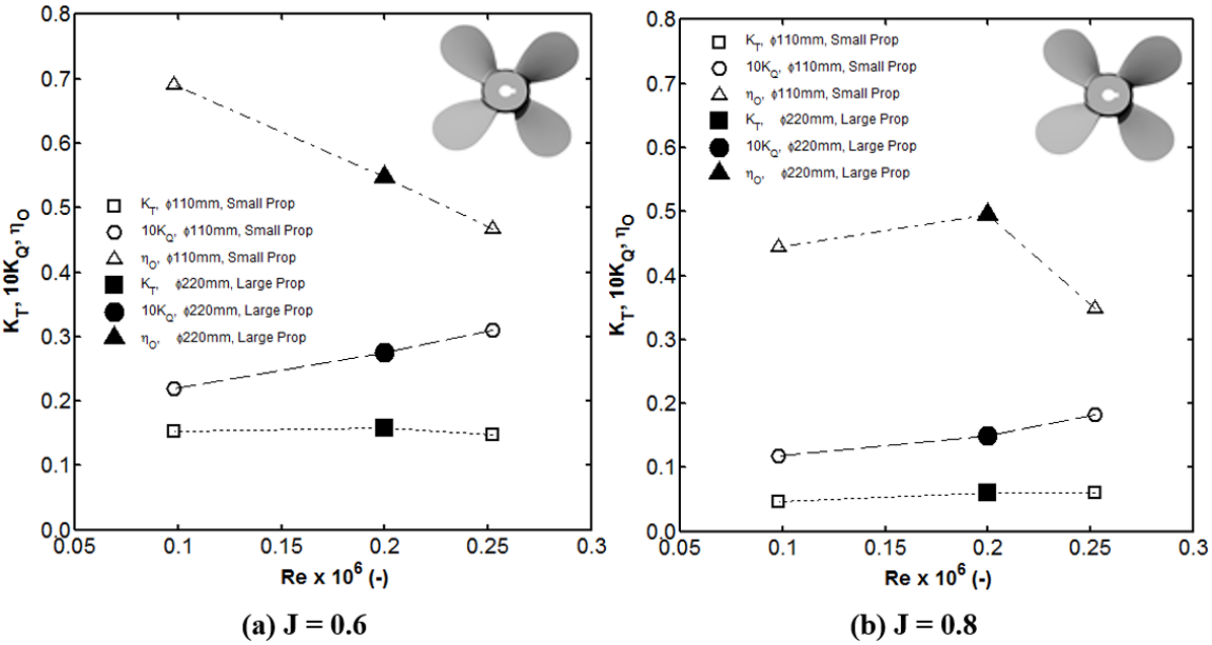


**Figure 3.7** Open water coefficients of the FTV Bluefin CP propeller (100% pitch) with respect to the Reynolds number. This results are at advance coefficient **(a)** J = 0.6 **(b)** J = 0.8. *Notes*: *Hollow marker - (small prop), Solid markers - (large prop). Inset at upper left corner: The 4 bladed FTV Bluefin CP propeller.*

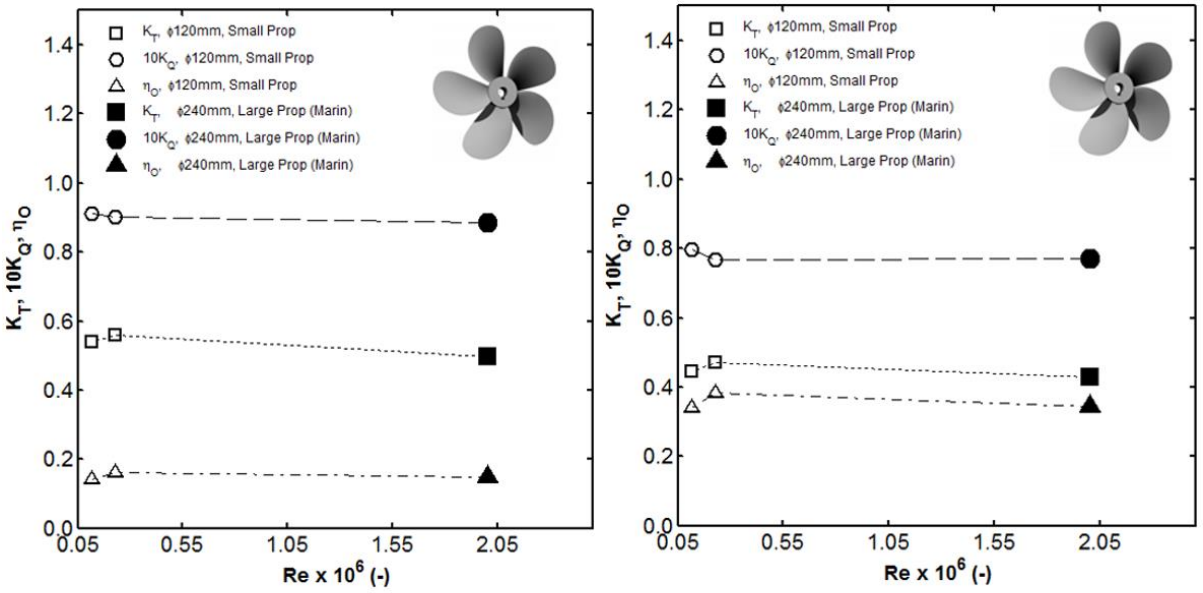


**(a) J = 0.2** **(b) J = 0.4**

**Figure 3.8** Open water coefficients of the Wageningen B5.75 propeller with respect to the Reynolds number. This results are at advance coefficient **(a)** J = 0.2 **(b)** J = 0.4. *Notes*: *Hollow marker - (small prop), Solid markers - (large prop). Inset at upper right corner: The 5 bladed Wageningen B5.75 P/D 1.2 propeller.*

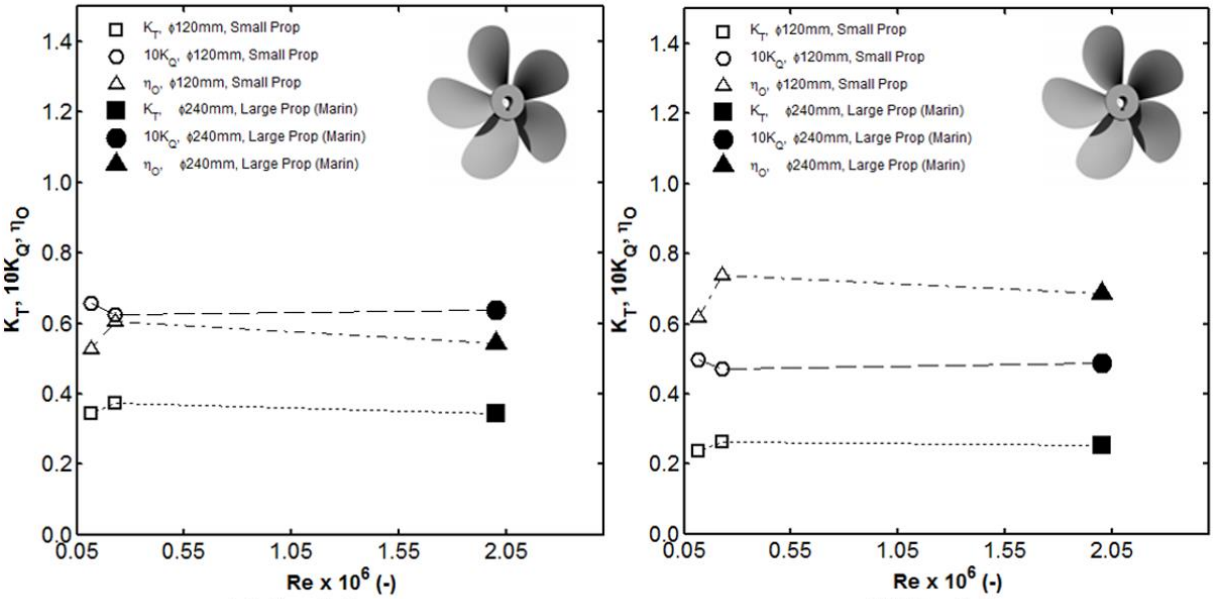


**(a) J = 0.6** **(b) J = 0.8**

**Figure 3.9** Open water coefficients of the Wageningen B5.75 propeller with respect to the Reynolds number. This results are at advance coefficient **(a)** J = 0.6 **(b)** J = 0.8. Notes: Hollow marker - (small prop), Solid markers - (large prop). *Inset at upper right corner: The 5 bladed Wageningen B5.75 P/D 1.2 propeller.*

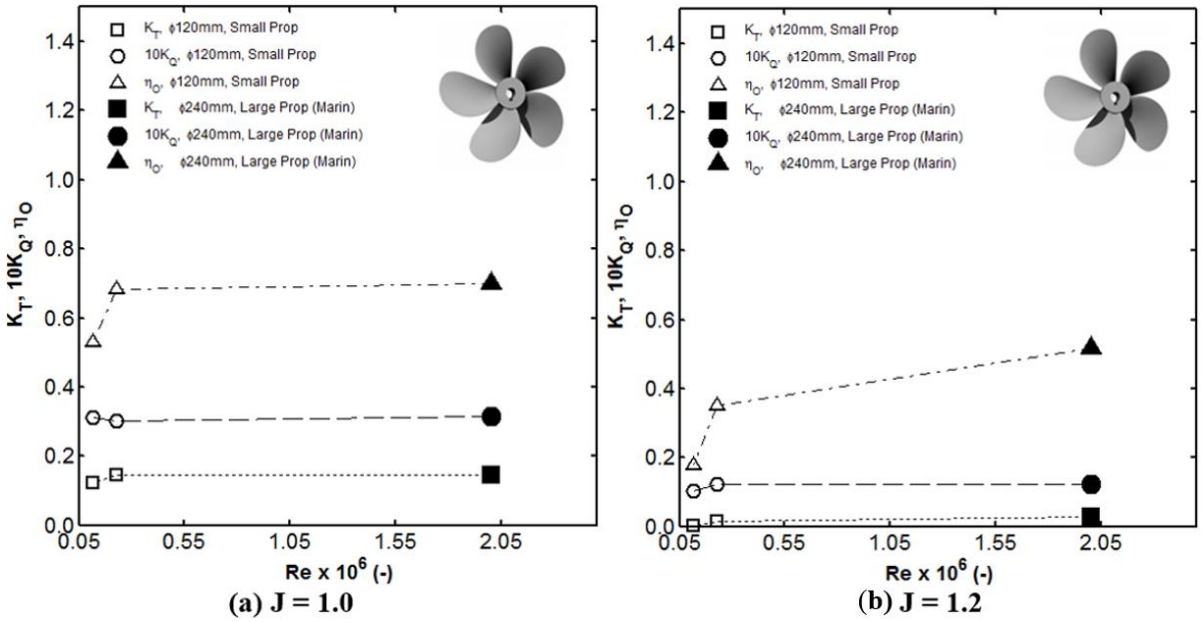


**Figure 3.10** Open water coefficients of the Wageningen B5.75 propeller with respect to the Reynolds number. This results are at advance coefficient **(a)** J = 1.0 **(b)** J = 1.2. *Notes*: *Hollow marker - (small prop), Solid markers - (large prop). Inset at upper right corner: The 5 bladed Wageningen B5.75 P/D 1.2 propeller.*

## 3.7 The Reynolds scale effect corrections

Two methods of correction were applied to the propeller coefficients of the Wageningen B5.75 propeller. The corrected propeller coefficients using the two methods were compared with the propeller coefficients of a larger geometrically similar or 'geosim' propeller with a diameter of 220 mm found in Kuiper (1992). At the end, these two correction methods were evaluated in terms of correlation to the 'benchmark' propeller coefficients found in Kuiper (1992).

In the first approach, the correction recommended by ITTC1978 was used. This can be found in Manen and Oossanen (1988, p. 156) and ITTC (2014). The standard ITTC 1978 procedure uses two corrections, one for the thrust coefficient $K_T$ and one for the torque coefficient $K_Q$. These corrections are taking into account the influence of the Reynolds number, the thickness-chord ratio $t/c$, the number of blades $Z$ and the pitch-diameter ratio $P/D$. The corrections were applied to the open water thrust coefficient $K_{TO}$ and torque coefficient $K_{QO}$ to obtain the full-scale thrust and torque coefficients. These corrections lead to small changes in the values as illustrated in Figure 3.11 (a) and 3.12 (a).

In the second approach, a method proposed by Benedek (1985) was used. The Benedek's corrections also used two corrections, one for the thrust coefficient $K_T$ and one for the torque coefficient $K_Q$. The Benedek's corrections are taking into account the influence of the developed blade area ratio $A_D/A_O$, the advance ratio $J$, and the pitch angle $\varphi$. Benedek's approximation is similar to Froude's method used to calculate the resistance of the ship. It was assumed that only the friction

force coefficient on the blade surface is different on the propeller, as compared to its model and the pressure distribution along the blade section of the propeller and its model is considered similar. The decrease of the thrust coefficient is a function of the developed blade area, the differences in the frictional resistance coefficient on the blade surface, the advance coefficient and the geometrical pitch angle of the propeller. The increase of the torque coefficient is also a function of the similar parameters as mentioned above. Benedek (1985) described the decrease of the thrust coefficient as

$$\Delta K_T = \frac{\pi}{4}\frac{A_D}{A_O}\left(C_{FS} - C_{FM}\right)\left[J^2 + \left(0.75\pi\right)^2\right]\sin\varphi \tag{3.6}$$

where $A_D$ is the developed area of the propeller blades, $A_O$ is the propeller disk area, $C_{FS}$ is the frictional resistance coefficient of the full-scale propeller blades, $C_{FM}$ is the frictional resistance coefficient of the model propeller and $J$ is the advance coefficient. The pitch angle φ is given as $\varphi = arc\ tan\ (P/0.75.D.\pi)$. The increase of the torque coefficient

$$\Delta K_Q = \frac{\pi}{4}\frac{A_D}{A_O}\left(C_{FS} - C_{FM}\right)\left[J^2 + \left(0.75\pi\right)^2\right]0.375\cos\varphi \tag{3.7}$$

The frictional resistance coefficient of the propeller blades was obtained using the formula given in the ITTC78 procedure for the drag coefficient in the model scale and in full scale. The frictional coefficient for the model propeller blade at 0.75 radius fraction can be found using the formula proposed by Aucher (1974)

$$C_{FM} = 2\left(1 + 2\frac{t}{c}\right)\left[\frac{0.044}{\left(\mathrm{Re}_{nco}\right)^{\frac{1}{6}}} - \frac{5}{\left(\mathrm{Re}_{nco}\right)^{\frac{2}{3}}}\right] \tag{3.8}$$

The Reynolds number used in Equation 3.8 was found using the local Reynolds number at the 0.75 radius fractions of the propeller blades. The frictional coefficient for the full scale propeller blade at 0.75 radius fraction can be found using the Schlichting flat-plate formula with some measures of surface roughness $k_p$ to give the appropriate drag increase,

$$C_{FS} = 2\left(1 + 2\frac{t}{c}\right)\left[1.89 + 1.62\log\frac{c}{k_p}\right]^{-2.5} \tag{3.9}$$

The corrected coefficients can be found by adding and subtracting the value of $K_T$ and $K_Q$ respectively, i.e. $K_{Tcorr} = K_T - \Delta K_T$ and $K_{Qcorr} = K_Q + \Delta K_Q$. The corrections using Equation 3.6 and 3.7 were found to correlate with the thrust and torque coefficient found in Kuiper (1992) than the ITTC

1978 method, see Figure 3.11 (b) and 3.12 (b). The propeller coefficients found in Kuiper is based on a 'geosim' propeller with diameter of 220 mm and running at Reynolds number *Re 2.0 x* $10^6$. This much larger 'geosim' propeller acts as a benchmark to the 120 mm diameter smaller propeller. The aim is to get the corrected propeller coefficients of the smaller 'geosim' propeller as close as possible to propeller thrust and torque coefficient of the larger 'geosim' propeller. Therefore the corrections method proposed by Benedek was chosen over the corrections recommended by the ITTC procedure no 7.5-0.2.03-01.4 (ITTC, 2011a).

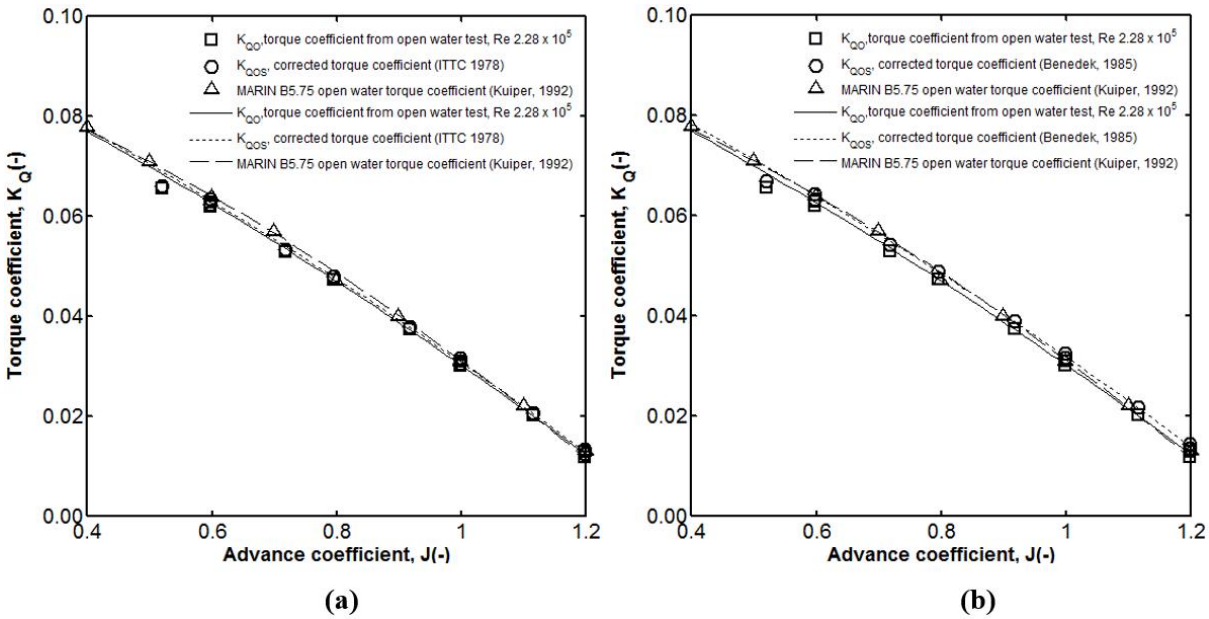


**Figure 3.11** Correction in model torque (a) using ITTC 1978 method (b) method proposed by Benedek (1985).

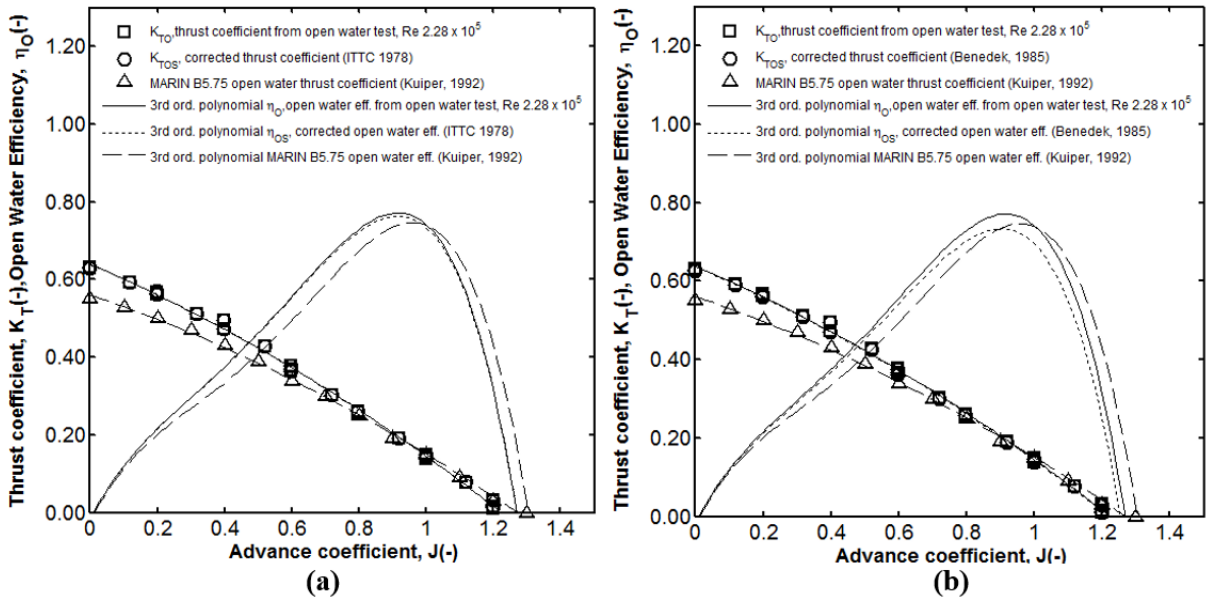


**Figure 3.12** Correction in thrust coefficient and open water efficiency (a) using ITTC 1978 method (b) method proposed by Benedek (1985).

## 3.8 Summary

In this chapter, a study on the scale effect on torque and thrust of a number of small screw propellers for the self-propulsion test ship model was discussed. The method consists of testing the small propellers at two Reynolds numbers, with the first at a normal shaft speed usually used in a self-propulsion test and the second, at a higher rate of shaft speed running above Reynolds number 200,000. Using similarity laws these coefficients were compared as to quantify the scale effect. The coefficients from the small propeller model were also compared against a larger geometrical similar propellers coefficient found in Kuiper (1992). From this study the followings were concluded:

1. The variation of thrust coefficients between the propeller operating at Reynolds number 119,000 and 228,000 were ranged from 1 to 14%.
2. The variation of torque coefficients between the propeller operating at Reynolds number 119,000 and 228,000 were ranged from 1 to 13% except at the higher advance coefficient.
3. The corrections proposed by ITTC 1978 (ITTC, 2014; Manen & Oossanen, 1988) leads to small changes to the propeller coefficients.
4. The correction method proposed by Benedek (1985) correlates better with a larger 'geosim' propeller (Kuiper, 1992) than the corrections made by the standard ITTC1978 method.
5. The correction method proposed by Benedek (1985) was chosen for propeller scale effect corrections in the ITTC 1978 and the Self-propulsion test only extrapolation procedures.

# Chapter 4

# Uncertainty Analysis

## 4.1 Introduction

This chapter describes the application of uncertainty analysis in assessing the reliability of the results obtained from the towing tank testing. Even though the powering prediction of scale model tests is currently the most reliable method available for the purpose, verification studies or uncertainty analyses are required to provide confidence in the accuracy of the results. The uncertainty analysis was also done to identify which sources of error had the most influence on the total uncertainty in the measurements as well as to ascertain the overall level of uncertainty in the measurements during the model testing, i.e. calm water resistance test, open water propeller test and self-propulsion test. It will also provide a guide for the uncertainty analysis of further tests of the 130m propeller driven catamaran conducted at other testing facilities.

However, the conventional uncertainty analysis recommended by the 22$^{nd}$ ITTC (ITTC, 1999b) using the Taylor series method (TSM) is almost prohibitive for ship model to ship extrapolation by the ITTC 1978 method, as the ITTC 1978 extrapolation procedures are complex and involve many steps. In other words the ITTC 1978 procedure is not differentiable by analytical means. One alternative approach to such problems is by applying the Monte Carlo method (MCM) in the uncertainty analysis as demonstrated in Bose et al. (2005), Molloy (2006) and Mustaffa Kamal et al. (2013). Furthermore, with the computing power and speed available nowadays, it has become feasible to perform an uncertainty analysis directly using Monte Carlo simulation that could involve up to 1,000,000 iterations.

The way Monte Carlo methods are used in the uncertainty analysis is by assuming a variation in the inputs to a data reduction equation and then calculating the variation in the output for a given number of trials (Bose, 2008). The variation in the inputs is given an assumed range of a given normal distribution with a set standard deviation. This is achieved using a Gaussian random generator which is easily available in any computer program languages or spreadsheet (Coleman & Steele, 1999).

Often 10,000 to 50,000 iterations are used for assigning new randomised inputs to the data reduction equations (Mustaffa Kamal et al., 2013). Then the uncertainty of the output is obtained as the distribution in the values of the output from the iterations made. The work carried out in this study was based on work presented in Molloy (2006) and Mustaffa Kamal et al. (2013) utilising Monte Carlo simulation work. Other references on the concept of the Monte Carlo method can be found in Fishman (1996) and Robert and Casella (2004).

## 4.2 The current standard in uncertainty analysis for experimental model testing

The recent procedure for experimental model testing uncertainty analysis can be found in ITTC (2008) which now uses type 'A' and type 'B' uncertainties based on the ISO (1995) model. The type 'A' evaluation of uncertainty is a method of evaluation of uncertainty by the statistical analysis of series of observations. The type B evaluation is a method of evaluation of uncertainty by means other than the statistical analysis of series of observations.

Prior to ISO (1995), the old procedure ITTC (1999b) used the bias and the precision error breakdown. These terms of bias and precision errors were adapted from the work of Moffatt (1982). Precision errors are found from repeated measurements and bias errors are systematic errors and these errors are not found from repeated measurements. This approach was adopted by the American Society of Mechanical Engineers (ASME) where the ASME PTC 19.1 was first published in 1985. The revised ASME PTC 19.1 – 1998 used the terms 'bias uncertainty' and 'precision uncertainty'. However in the latest revision in ASME 2005, the terms 'bias uncertainty' and precision uncertainty' were avoided and replaced by 'systematic' and 'random' uncertainties.

Both approaches using type 'A' and 'B' or bias and precision error breakdown would end-up with the same results. Therefore in this research, the approach using the bias and precision error was chosen. What is most important is that all major sources of uncertainty are taken into account in the uncertainty analysis.

## 4.3 Uncertainty analysis using the Monte Carlo method

The Monte Carlo method can be applied in the uncertainty analysis of a complicated data reduction equation such as the ITTC 1978 extrapolations. Bose et al. (2005) described the methodology steps are:

1. Estimate the precision errors in the experimental measured values such as thrust, torque, towing force and shaft speed from the data acquisition system (DAS). This is done by calculating the standard deviation of the mean of the individual measurements in the time series data taken from the DAS. Multiply the standard deviation with 1.96 to find the uncertainty for 95% confidence level.

2. Determine the bias and precision error sources and combine these two error sources using Root-sum-square (RSS) method.
3. Create a Gaussian (or other) error distribution of the bias and precision errors.
4. Create a calculation model by using data reduction equations.
5. Setup simulations consisting of N number of simulations, in which bias and precision error values are assigned randomly complying with Gaussian error distributions.
6. Calculate the result and its distribution, i.e. calculate mean and standard deviation from N simulations.
7. Multiply the standard deviation with 1.96 to find the total uncertainty (for 95% confidence level)

## 4.4 Programming the Monte Carlo simulation

In programming the Monte Carlo simulation, the initial approach was to program the ITTC 1978 and the self-propulsion test only extrapolation procedure, see Appendix C – Matlab Code, with the three different sets of test data imported into the main body of the program (Mustaffa Kamal et al., 2013). The first input file contained the results of the resistance test: which contained the data of the velocity of the model, $V_M$ in m/s and the resistance of the model through the water, $R_{TM}$ in Newton (N). Using the MATLAB polynomial function (Gilat, 2010; Hahn & Valentine, 2007), the resistance test data were then converted into an equation using a 2$^{nd}$ order regression equation.

The second input file imported to the main program contained the results of the open water test. The test results were entered into the main program in the form of $J=V_A/nD$, $K_T = T/\rho n^2D^4$, $K_Q = Q/\rho n^2D^5$ (Manen & Oossanen, 1988) 1988). The coefficient of $K_T$ and $K_Q$ were also converted to 2$^{nd}$ order polynomial equations through regression.

The third input file contained the results of the self-propulsion test in the form of velocity of the model, $V_M$ in m/s, the propeller shaft revolution rate, $n_M$ in rev/sec, the propeller thrust in N, the propeller torque, $Q_M$ in Nm and the towing force, $F_M$ in N were also imported into the main program. There was also a fourth file of inputs containing other information such as the model particulars, the test temperatures and viscosities, the form factor and the correlation allowances.

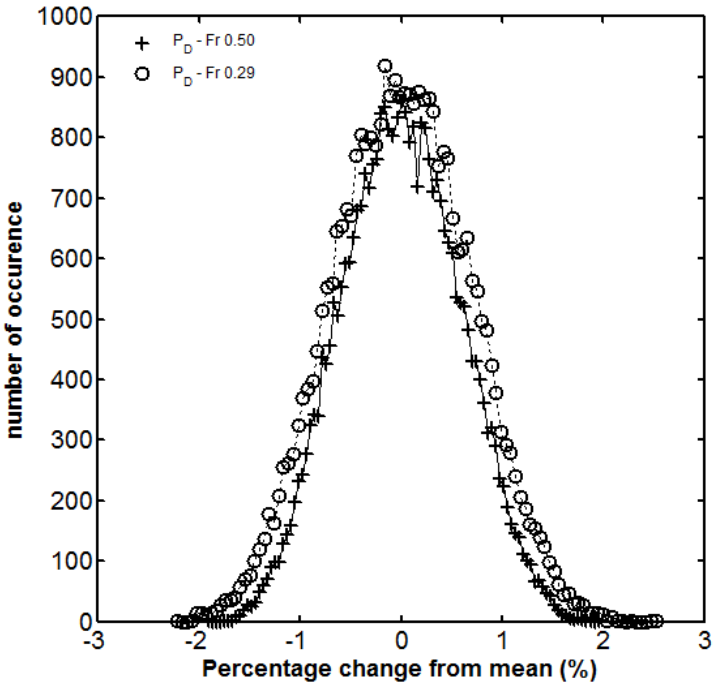


**Figure 4.1** The uncertainty distribution of the delivered power for Froude number 0.50 and 0.29, simulated using the Monte Carlo method, plotted as the percentage change from the mean values.

Then, the randomisation using the Monte Carlo simulation was applied directly to each input, where the input values in the data reduction equation are randomly varied by a predetermined uncertainty using the bias and precision error which will be explained in the next section. Then a distribution of the uncertainty results is obtained (Coleman & Steele, 1999). The equation referred to here is the set of non-linear equations that form the extrapolation method itself. The original values, for instance the propeller thrust $T_M$, in the self-propulsion test was assigned to a standard deviation and distributed normally. The randomiser in the program randomly varied each test result with a standard deviation according to the bias limits determined earlier. This process was repeated for a large number of times specified by the user, and in this study, 33,000 numbers of iteration were chosen as this number is usually sufficient (Bose, 2008; Coleman & Steele, 1999). For every iteration on the resistance test values of $V_M$ and $R_{TM}$, a new regression equation was calculated using the new data and this new regression equation was the new input into the ITTC 1978 extrapolation program. An example of the uncertainty propagation distribution simulated using the Monte Carlo method is shown in Figure 4.1.

A similar process was applied to randomise the open water test data. These data were converted into a regression equation, and at each randomisation, a new regression equation was calculated and this new regression was input to the program. This process was also repeated 33,000 times. Similarly the self-propulsion test data was randomised although the test runs were less numerous than the resistance test or the open water test. The data for $K_{QP}$, $K_{TP}$, $J_P$, $K_{FD}$ and $n_M$ were also converted into a regression equation, and a new regression was calculated at each randomisation.

## 4.5 Precision error

The precision limits were obtained for resistance, towing force, thrust and torque measurements as listed in Table 4.1 and 4.2. The precision limits were obtained by calculating the standard deviation of repeated test measurements i.e. resistance, towing force, torque and thrust measurements. The precision error in the test measurements were calculated using the equation;

$$u\left(\bar{q}\right)=\sqrt{\frac{\sum_{k=1}^{n}\left(q_k-\bar{q}\right)^2}{n(n-1)}} \tag{4.1}$$

where $q_k$ is the individual measurements such as thrust, torque, towing force and shaft speed from the data acquisition system (DAS), $\bar{q}$ is the mean or average of the individual measurements and $n$ is the number of repeated measurements in the time series data taken from the DAS. The equation 4.1 is defined as the standard uncertainty or the estimated standard deviation of the mean.

## 4.6 Bias error sources in the experimental measurements

The bias error limits in each measurement were predetermined following the procedures given in ITTC (2002b). An example case is presented as the followings to explain the basic measurement errors. The details of the bias error for each variable are tabulated in Table 4.1 and 4.2. The explanation on how the bias errors were obtained is in Appendix B – Uncertainty Analysis.

## 4.7 Overall uncertainty comparison between TSM and MCM

The value of the overall uncertainty using the Monte Carlo Method (MCM) was compared against the value of the overall uncertainty using the Taylor Series Method (TSM) in order to validate the effectiveness of the Monte Carlo method. The overall uncertainty for the total resistance coefficient, $C_T$ was chosen for the comparative study as shown in Figure 4.2 in terms of the percentage of the overall uncertainty of the total resistance coefficient, $U_{CT}$ over the original value of the total resistance coefficient, $C_T$. The values of the $U_{CT}$ computed using the Monte Carlo method was in close agreement with the value of the $U_{CT}$ calculated using the Taylor Series method.

**Table 4.1** Bias and precision errors for each variable

| Variable | Bias error | | Precision error | |
|---|---|---|---|---|
| **Model length** | Manufacturing error: ± 0.001m<br>Overall: ± 0.001m | | - | |
| **Model wetted surface area** | Manufacturing error: ± 0.00041$m^2$<br>Overall: ± 0.00041$m^2$ | | - | |
| **Propeller diameter** | Manufacturing error: ± 0.0001m<br>Overall: ± 0.0001m | | - | |
| **Tank water temperature** | Overall: ± 0.5°C | | - | |
| **Water density** | Density-temperature relation: ± 0.0410kg/$m^3$<br>Data reduction error ± 0.0700kg/$m^3$<br>Overall: ± 0.660kg/$m^3$ | | - | |
| **Viscosity** | Overall: ± 4.52E-09 $m^2$/s | | - | |
| **Carriage speed (Self-propulsion test)** | Overall: ± 0.2% of nominal speed | | **3640t** | **2500t** |
| | | Fr 0.26 | ± 0.014 m/s | ± 0.012 m/s |
| | | Fr 0.29 | ± 0.009 m/s | ± 0.012 m/s |
| | | Fr 0.32 | ± 0.013 m/s | ± 0.012 m/s |
| | | Fr 0.35 | ± 0.011 m/s | ± 0.011 m/s |
| | | Fr 0.38 | ± 0.013 m/s | ± 0.010 m/s |
| | | Fr 0.40 | ± 0.012 m/s | ± 0.012 m/s |
| | | Fr 0.44 | ± 0.012 m/s | ± 0.014 m/s |
| **Carriage speed (Resistance test)** | Overall: ± 0.2% of nominal speed | | **3640t** | **2500t** |
| | | Fr 0.20 | ± 0.007 m/s | ± 0.006 m/s |
| | | Fr 0.23 | ± 0.009 m/s | ± 0.006 m/s |
| | | Fr 0.26 | ± 0.012 m/s | ± 0.008 m/s |
| | | Fr 0.32 | ± 0.008 m/s | ± 0.009 m/s |
| | | Fr 0.38 | ± 0.011 m/s | ± 0.009 m/s |
| | | Fr 0.44 | ± 0.008 m/s | ± 0.009 m/s |
| | | Fr 0.46 | ± 0.014 m/s | ± 0.009 m/s |
| | | Fr 0.49 | ± 0.007 m/s | ± 0.012 m/s |
| **Resistance** | Calibration error: ± 0.006 kg<br>Curve fit bias error: ± 0.046 kg<br>Load cell misalignment: ± 0.00018 kg<br>Towing force inclination: ± 0.0006 kg<br>Overall: ± 0.046kg | | **3640t** | **2500t** |
| | | Fr 0.20 | ± 0.063 kg | ± 0.037 kg |
| | | Fr 0.23 | ± 0.160 kg | ± 0.041 kg |
| | | Fr 0.26 | ± 0.209 kg | ± 0.060 kg |
| | | Fr 0.32 | ± 0.112 kg | ± 0.066 kg |
| | | Fr 0.38 | ± 0.144 kg | ± 0.091 kg |
| | | Fr 0.44 | ± 0.206 kg | ± 0.122 kg |
| | | Fr 0.46 | ± 0.153 kg | ± 0.081 kg |
| | | Fr 0.49 | ± 0.085 kg | ± 0.081 kg |

**Table 4.2** Bias and precision limits for each variable (continued)

| Variable | Bias error | | Precision error | |
|---|---|---|---|---|
| **Towing force** | Calibration error: | | **3640t** | **2500t** |
| | ± 0.006 kg | Fr 0.26 | ± 0.177 kg | ± 0.039 kg |
| | Curve fit bias error: | Fr 0.29 | ± 0.065 kg | ± 0.041 kg |
| | ± 0.046 kg | Fr 0.32 | ± 0.105 kg | ± 0.092 kg |
| | Load cell misalignment: | Fr 0.35 | ± 0.162 kg | ± 0.080 kg |
| | ± 0.00018 kg | Fr 0.38 | ± 0.150 kg | ± 0.107 kg |
| | Towing force inclination: | Fr 0.40 | ± 0.203 kg | ± 0.052 kg |
| | ± 0.00016 kg | Fr 0.44 | ± 0.178 kg | ± 0.106 kg |
| | Overall: ± 0.046kg | | | |
| **Thrust** | Weight calibration error: | | **3640t** | **2500t** |
| | ± 0.006kg | Fr 0.26 | ± 0.015 kg | ± 0.017 kg |
| | A/D converter bias: | Fr 0.29 | ± 0.016 kg | ± 0.013 kg |
| | ± 0.00153kg | Fr 0.32 | ± 0.028 kg | ± 0.016 kg |
| | Transducer calibration: | Fr 0.35 | ± 0.038 kg | ± 0.024 kg |
| | ± 0.043kg | Fr 0.38 | ± 0.034 kg | ± 0.019 kg |
| | Overall: ± 0.043kg | Fr 0.40 | ± 0.045 kg | ± 0.012 kg |
| | | Fr 0.44 | ± 0.032 kg | ± 0.031 kg |
| **Torque** | Weight calibration error: | | **3640t** | **2500t** |
| | ± 0.0003 Nm | Fr 0.26 | ± 0.007 Nm | ± 0.006 Nm |
| | A/D converter bias: | Fr 0.29 | ± 0.005 Nm | ± 0.004 Nm |
| | ± 0.0008 Nm | Fr 0.32 | ± 0.004 Nm | ± 0.006 Nm |
| | Transducer calibration: | Fr 0.35 | ± 0.007 Nm | ± 0.008 Nm |
| | ± 0.0004 Nm | Fr 0.38 | ± 0.007 Nm | ± 0.007 Nm |
| | Overall: ± 0.0009 Nm | Fr 0.40 | ± 0.009 Nm | ± 0.006 Nm |
| | | Fr 0.44 | ± 0.009 Nm | ± 0.008 Nm |
| **Open water advance velocity** | Overall: ± 0.2% of nominal speed | J = 0.00 | ± 0.0028 m/s | |
| | | J = 0.20 | ± 0.0076 m/s | |
| | | J = 0.40 | ± 0.0060 m/s | |
| | | J = 0.60 | ± 0.0080 m/s | |
| | | J = 0.80 | ± 0.0088 m/s | |
| | | J = 1.00 | ± 0.0100 m/s | |
| **Open water torque** | Weight calibration error: | J = 0.00 | ± 0.040 Nm | |
| | ± 0.0001 Nm | J = 0.20 | ± 0.034 Nm | |
| | A/D converter bias: | J = 0.40 | ± 0.032 Nm | |
| | ± 0.0004 Nm | J = 0.60 | ± 0.029 Nm | |
| | Transducer calibration: | J = 0.80 | ± 0.026 Nm | |
| | ± 0.0008 Nm | J = 1.00 | ± 0.024 Nm | |
| | Overall: ± 0.0009 Nm | | | |
| **Open water thrust** | Weight calibration error: | J = 0.00 | ± 0.229 kg | |
| | ± 0.006kg | J = 0.20 | ± 0.122 kg | |
| | A/D converter bias: | J = 0.40 | ± 0.140 kg | |
| | ± 0.00153kg | J = 0.60 | ± 0.129 kg | |
| | Transducer calibration: | J = 0.80 | ± 0.122 kg | |
| | ± 0.043kg | J = 1.00 | ± 0.140 kg | |
| | Overall: ± 0.043kg | | | |

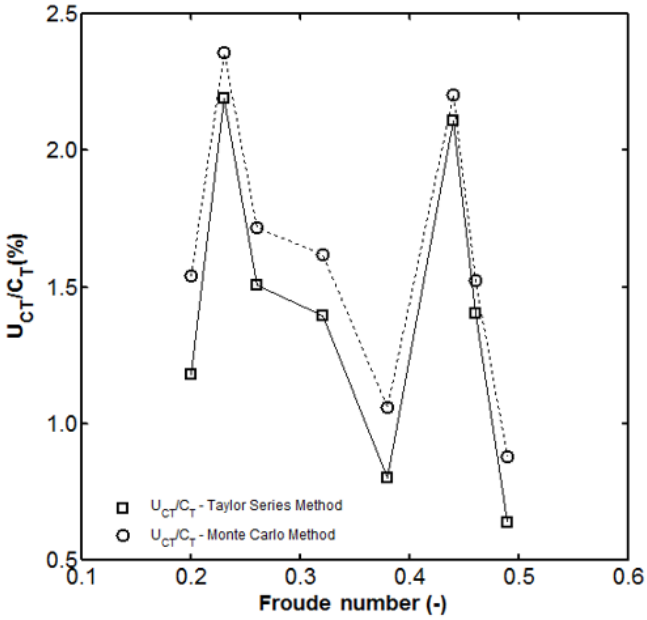


**Figure 4.2** The percentage of the overall uncertainty in the total resistance coefficient, $U_{CT}$ over the original value of the total resistance coefficient, $C_T$. The overall uncertainty results which were obtained using the Taylor Series and the Monte Carlo method were compared.

## 4.8 Overall uncertainty in the full-scale predicted power

The overall uncertainty in the delivered power was determined using the Monte Carlo simulation. Figure 4.3 (a) and (b) are the plots of the extrapolated delivered power for two displacements at 3,640 and 2,500 tonnes. The uncertainties in the values of the delivered power are shown as error bars on the plots. The error bar represents a 95% confidence level of the uncertainties in the delivered power. The standard deviation in the delivered power extrapolated using the ITTC 1978 method was found to be higher than the delivered power extrapolated using the self-propulsion test only method especially at higher Froude number. The uncertainties percentage error in the delivered power using the ITTC 1978 method is ranged from $\pm$ 8.9% to $\pm$ 18.73% depending on the Froude number. The uncertainties percentage error using the SPT method is ranged from $\pm$ 4.8% to $\pm$ 15.6% depending on the Froude number.

The overall uncertainty in the ship torque is shown in Figure 4.4 (a) and 4.4 (b). The uncertainties in the ship torque extrapolated using the ITTC 1978 method were also found to be larger than the uncertainties in the ship torque extrapolated using the self-propulsion test only method. The uncertainties percentage error in the ship torque using the ITTC 1978 method is ranged from $\pm$ 6% to $\pm$ 17% depending on the Froude number. The uncertainties percentage error using the SPT method is ranged from $\pm$ 2% to $\pm$ 12% depending on the Froude number.

The high uncertainties in the results extrapolated using the ITTC 1978 method are mainly due to the regression and the interpolation error exists in the extrapolation process. The overall uncertainty percentage error for the delivered power and ship torque are shown in Figure 4.5 (a) and (b). The

results of the uncertainty analysis for other parameters such as the ship thrust and the ship's shaft speed are shown in the Appendix B – Uncertainty Analysis.

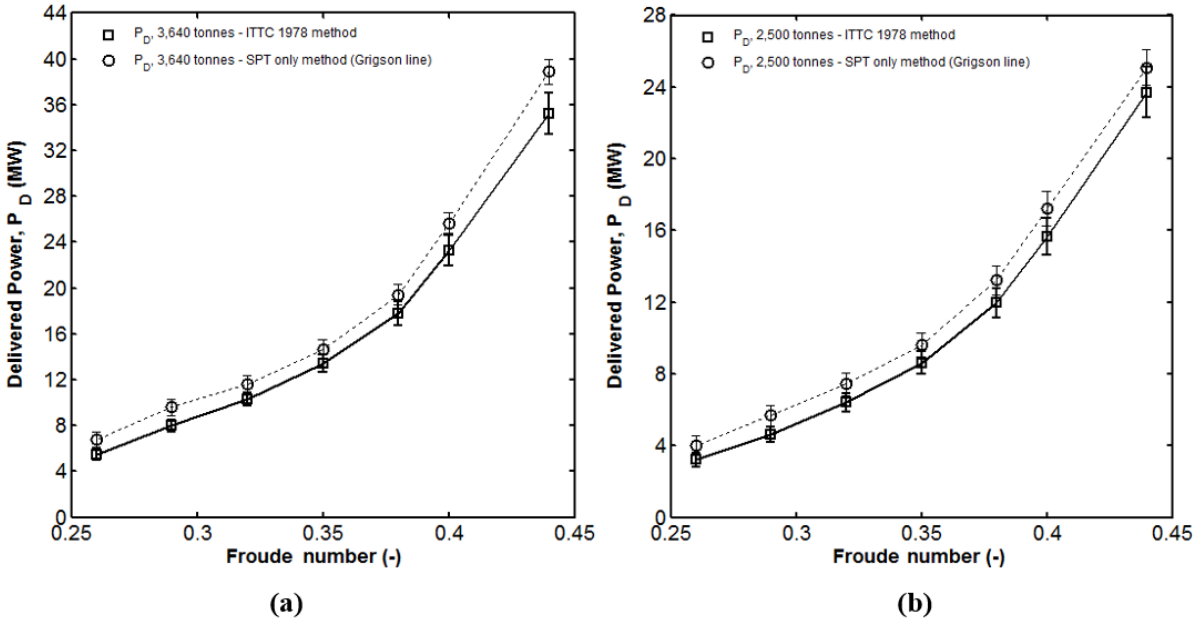


**Figure 4.3** The delivered power for two displacements of the 130m propeller driven WP catamaran. **(a)** Displacement 3,640 tonnes **(b)** Displacement 2,500 tonnes. Error bars show 95% confidence bands.

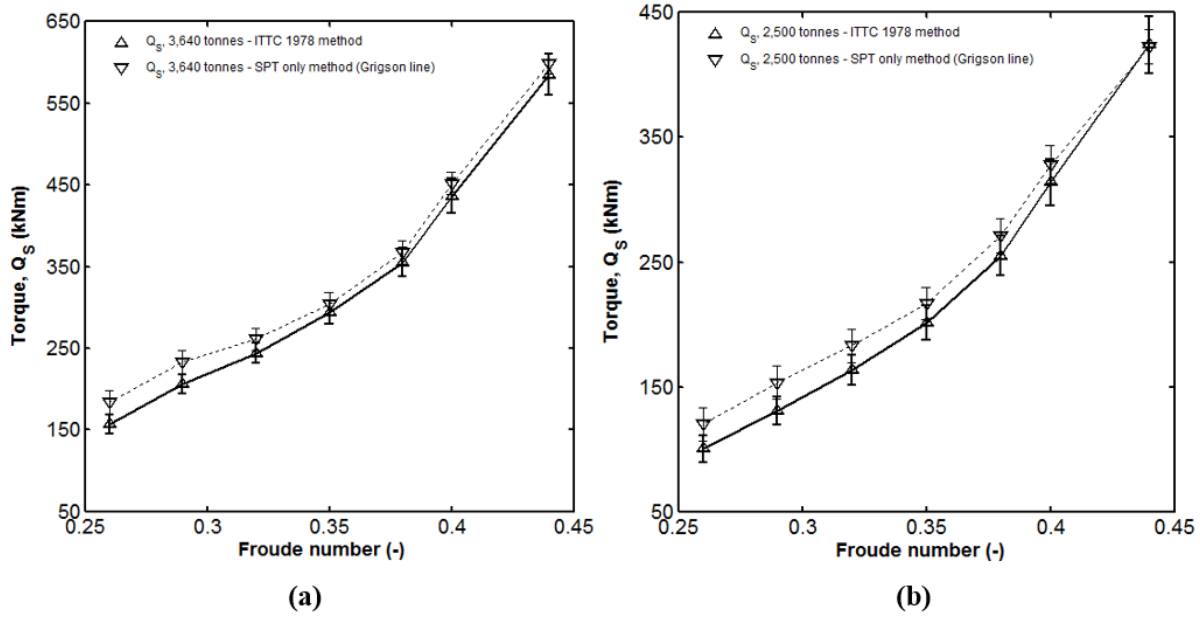


**Figure 4.4** The ship torque for two displacements of the 130m propeller driven WP catamaran. **(a)** Displacement 3,640 tonnes **(b)** Displacement 2,500 tonnes. Error bars show 95% confidence bands.

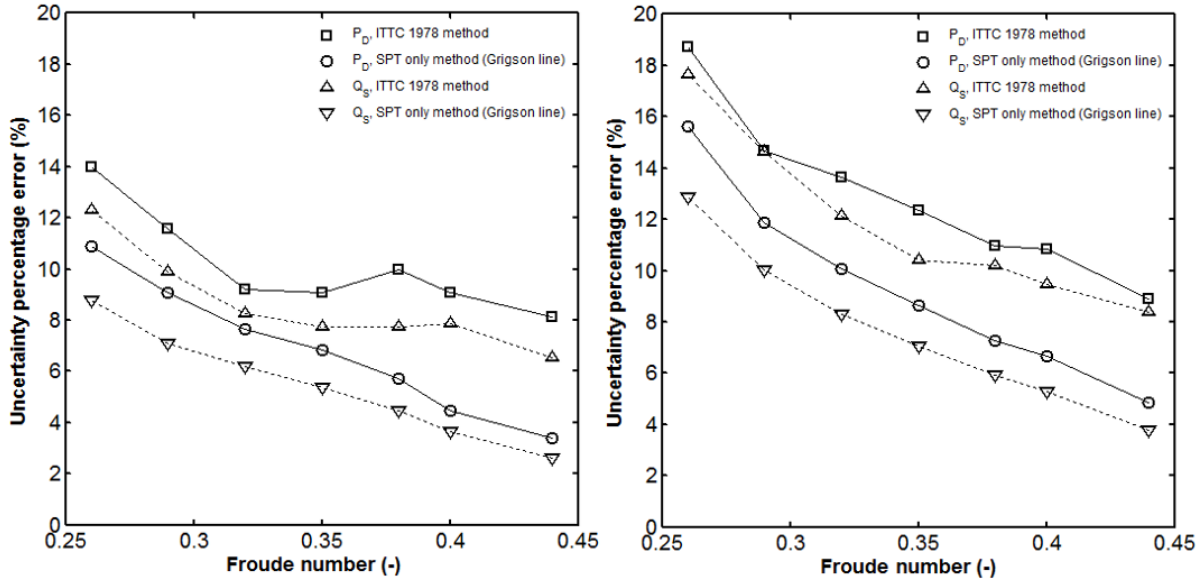


**Figure 4.5** The uncertainty percentage error for the delivered power, the ship's thrust and the ship torque, which were extrapolated using the ITTC 1978 method and the self-propulsion test only method. **(a)** Displacement 3,640 tonnes **(b)** Displacement 2,500 tonnes**.**

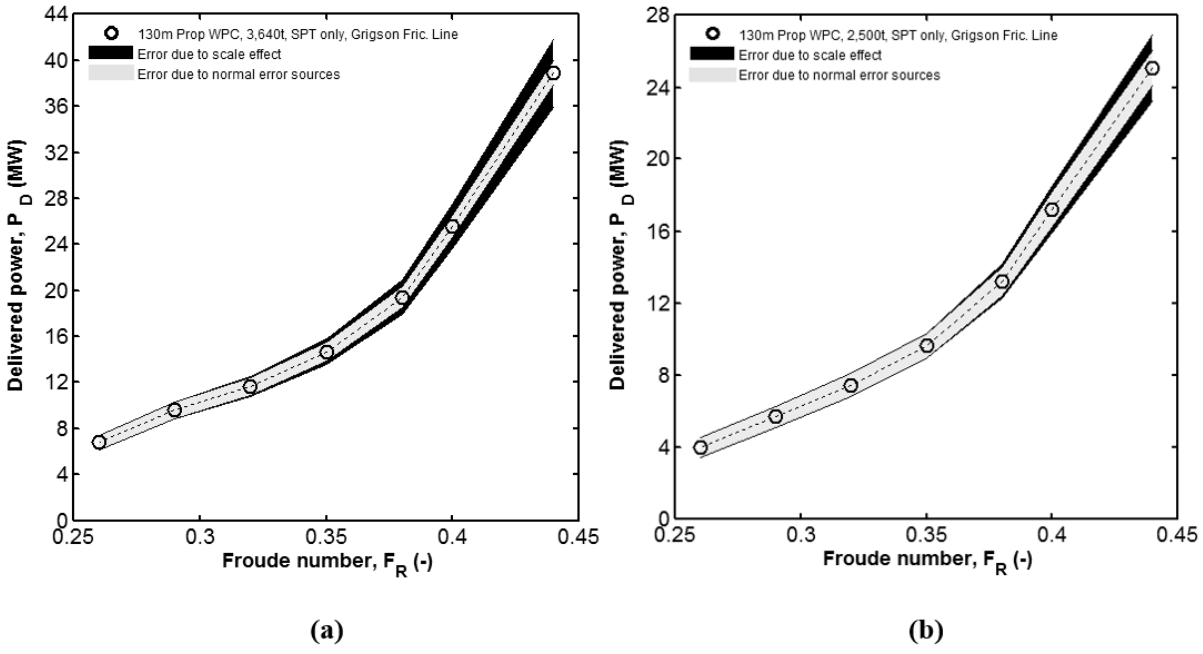


**Figure 4.6** The error due to the influence of propeller scale effect in the delivered power for two displacements of the 130m propeller driven WP catamaran. **(a)** Displacement 3,640 tonnes **(b)** Displacement 2,500 tonnes. Error shaded plot show 95% confidence bands. Both cases were extrapolated using SPT only extrapolation method.

## 4.9 The uncertainty due to influence of the propeller scale effect

There are uncertainties that are not yet quantified such as the influence of the uncertainty of small model propellers. The uncertainty associated with the small propeller scale effect could not be neglected as this is without doubt is one of the sources of error in the uncertainty of the full-scale predicted power.

Therefore an uncertainty analysis to investigate the influence of the propeller scale effect to the predicted full-scale delivered power when extrapolated using the SPT only method were performed using the Monte Carlo method. The standard deviation of the input propeller torque and thrust were varied in the range of 0.024Nm to 0.040Nm and 0.140kg to 0.229kg respectively depending on the advance ratio. The standard deviation or the error sources due to the scale effect of the input torque and thrust are tabulated in Table 4.3. It should be noted that most of the time, the advance ratio at the self-propulsion point during the extrapolation are in between 0.8 to 1.0.

When the propeller torque and the propeller thrust were varied using the error sources with the addition of errors due to the propeller scale effect as in Table 4.3, there was a substantial increases of the full-scale predicted delivered power, especially at higher Froude number. The error in the predicted delivered power is shown in Figure 4.6. The uncertainties percentage error in the delivered power due to the error sources from the propeller scale effect is ranged from $\pm$ 8.77% to $\pm$ 19.25% for the 3,640 tonnes catamaran. The uncertainties percentage error in the delivered power is ranged from $\pm$ 8.85% to $\pm$ 16.04% for the 2,500 tonnes catamaran. On average, there are 1 to 3 percent increases in the uncertainty percentage error of the delivered power when the error sources from the propeller scale effect were included.

**Table 4.3** Error sources in the model propeller torque and thrust due to the propeller scale effect

| **Variable** | **Standard error sources** | | **Error sources inclusive of propeller scale effect** | |
|---|---|---|---|---|
| **Propeller torque** | J = 0.00 | $\pm$ 0.040 Nm | J = 0.00 | $\pm$ 0.045 Nm |
| | J = 0.20 | $\pm$ 0.034 Nm | J = 0.20 | $\pm$ 0.045 Nm |
| | J = 0.40 | $\pm$ 0.032 Nm | J = 0.40 | $\pm$ 0.045 Nm |
| | J = 0.60 | $\pm$ 0.029 Nm | J = 0.60 | $\pm$ 0.045 Nm |
| | J = 0.80 | $\pm$ 0.026 Nm | J = 0.80 | $\pm$ 0.043 Nm |
| | J = 1.00 | $\pm$ 0.024 Nm | J = 1.00 | $\pm$ 0.041Nm |
| **Propeller thrust** | J = 0.00 | $\pm$ 0.229 kg | J = 0.00 | $\pm$ 0.419 kg |
| | J = 0.20 | $\pm$ 0.122 kg | J = 0.20 | $\pm$ 0.465 kg |
| | J = 0.40 | $\pm$ 0.140 kg | J = 0.40 | $\pm$ 0.326 kg |
| | J = 0.60 | $\pm$ 0.129 kg | J = 0.60 | $\pm$ 0.326 kg |
| | J = 0.80 | $\pm$ 0.122 kg | J = 0.80 | $\pm$ 0.233 kg |
| | J = 1.00 | $\pm$ 0.140 kg | J = 1.00 | $\pm$ 0.233 kg |

## 4.10 Summary

An uncertainty analysis on the towing tank tests were performed using the Monte Carlo method. This method was validated against the Taylor series method and the results obtained using the Monte Carlo method shows good agreement with the Taylor series method results.

The uncertainty analysis was done to assess the uncertainty in the full-scale predicted power. But in order to achieve this, the uncertainty errors of each test need to be determined prior to the estimation of the uncertainty error for the full scale predicted power i.e. calm water resistance test, the open water propeller test and the self-propulsion test. The uncertainty results for the self-propulsion tests are presented in the Appendix B – Uncertainty Analysis. The measurement system and the facility bias and precision errors were briefly described and were provided in Table 4.1 and 4.2 for future reference. This information is useful for future improvements in the uncertainty measurements and assessment of repeated test performed in other towing tank facilities. The level of the uncertainties percentage error in the delivered power extrapolated using the ITTC method is ranged from $\pm$ 8.9% to $\pm$ 18.73%. The uncertainties percentage error using the SPT method is ranged from $\pm$ 4.8% to $\pm$ 15.6% depending on the Froude number. The level of the uncertainties percentage error in the full scale torque extrapolated using the ITTC 1978 method is ranged from $\pm$ 6% to $\pm$ 17%. The uncertainties percentage error using the SPT method is ranged from $\pm$ 2% to $\pm$ 12% depending on the Froude number.

There were a substantial increases of the full-scale predicted delivered power, especially at higher Froude number, when the propeller torque and the propeller thrust were varied using the error sources with the addition of errors due to the propeller scale effect. The uncertainties percentage error in the delivered power due to the error sources from the propeller scale effect is ranged from $\pm$ 8.77% to $\pm$ 19.25% for the 3,640 tonnes catamaran. The uncertainties percentage error in the delivered power is ranged from $\pm$ 8.85% to $\pm$ 16.04% for the 2,500 tonnes catamaran. On average there are 1 to 3 percent increases in the uncertainties percentage error of the delivered power when the error sources from the propeller scale effect were included.

The steps used in the Monte Carlo simulation, were much easier than the conventional uncertainty analysis. Perhaps the only difficult step in this process was the identification and quantification of the elemental bias errors that affect each of the measured variables. The quantification of the uncertainties in the input parameters will remain as a difficult issue. Finally, the Monte Carlo method has proved to be very effective for uncertainty analysis, especially in a high non-linear data reduction process such as the self-propulsion test full scale extrapolation.

# Chapter 5

# The powering performance of the propeller driven catamaran

## 5.1 Introduction

This chapter presents the results on the powering performance of the 130m propeller driven catamaran. The comparisons between the 130m propeller driven catamaran with the 98m waterjet catamaran are presented later in Chapter 6. The results presented here are the thrust deduction fraction, the wake fraction, the delivered power, the shaft revolution rate, the overall propulsive efficiency, the residual drag or resistance, the sinkage and the running trim. The results presented in this chapter are at displacement of 2,500 and 3,640 tonnes. The predicted delivered power extrapolated using the ITTC 1978 method were compared with the predicted delivered power extrapolated using the self-propulsion test only method (SPT method) It will be discussed, on which method is more accurate in predicting the propulsion factors.

At the beginning of this chapter, the study on the scale effect of the ship's wake is presented. This study is necessary as the wake scaling ratio need to be known for the self-propulsion test only method. Conclusions are made at the end of this chapter on the overall results of the powering performance of the propeller driven catamaran.

Conclusions made in this chapter are discussing on why self-propulsion test method (SPT method) is much more reliable in predicting the propulsion factors than the ITTC1978 procedure.

## 5.2 The wake fractions using the thrust identity and the torque identity method

In the self-propulsion test only extrapolation method, the wake fraction is not needed to extrapolate the propulsion factors to full-scale, only the wake scaling ratio of the model and the ship has to be known prior to the extrapolation procedure. The wake fraction in the model scale can be obtained either using the 'thrust identity' or the 'torque identity' method (Bose, 2008). The method recommended by the ITTC 1978, 7.5-02-03-01.4 procedure in finding the model wake fraction, $w_{TM}$ , is as in Equation 5.1,

$$w_{TM} = 1 - \frac{J_O D_M n_M}{V_M} = 1 - \frac{J_O}{J_P} \tag{5.1}$$

In Equation 5.1, $D_M$ is the model propeller diameter in the self-propulsion test, $n_M$ is the revolution speed of the propeller, $V_M$ is the towing speed of the ship model and $J_O$ is the value of advance coefficient corresponding to the same value of $K_{TO}$ (thrust identity method) or $K_{QO}$ (torque identity method) in the results from the open water test of the propeller.

There were some issues in using these methods to obtain the wake fraction. The wake fractions obtained using the 'thrust identity' and the 'torque identity' methods as shown in Figure 5.1 (a) and (b) were somewhat strange, exhibiting for some cases unrealistic wake fractions (e.g. negative values of the wake fractions). It was also strange that the curve of the thrust coefficient in the open water condition crosses the curve of the thrust coefficient in the behind model condition. These variations can be account for with the uncertainties in these curves, where normally the curves are expected to be paralleled to each other.

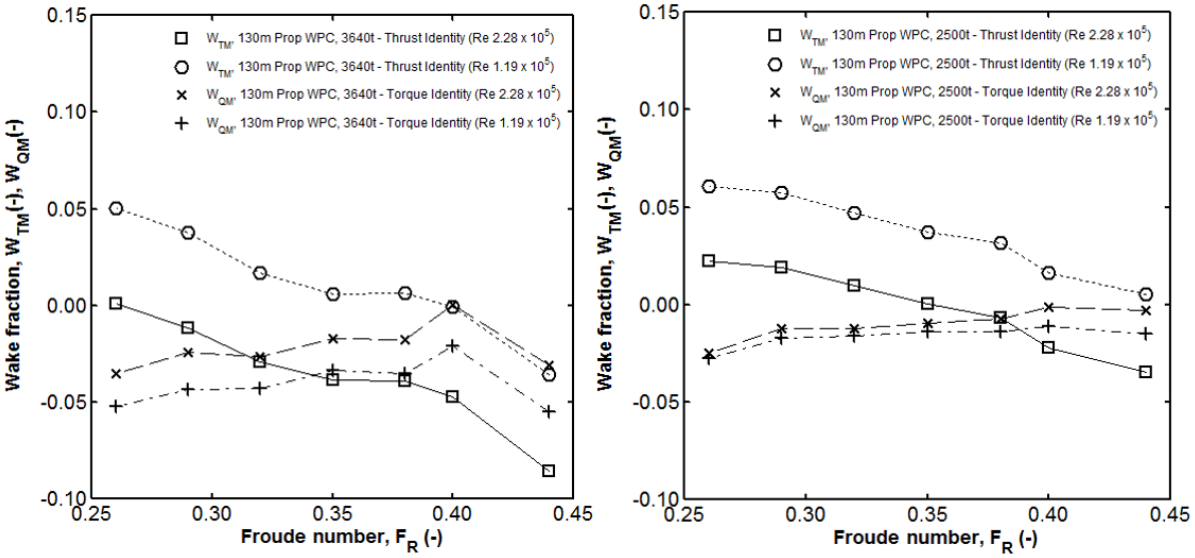


**(a)** **(b)**

**Figure 5.1** Comparison of the wake fractions obtained using the 'thrust identity' and the 'torque' identity method. The wake fractions are for model tested at displacements of **(a)** 3,640 and **(b)** 2,500 tonnes using propeller open water characteristics tested at *Re* 1.19 x $10^5$ and *Re* 2.28 x $10^5$.

The wake fractions are believed to be small as the propeller in the behind of the catamaran stern is operating in a less obstructed flow, as a results of approximately 50 – 60 % of the propeller disc area is located below the baseline of the catamaran. In other words, approximately 50 – 60% of the incoming flow into the propeller disc area is not disturbed by the hull aft end shape of the catamaran. As the value of the advance coefficient in the behind the model is too close to the value of the advance coefficient in the open water, sometimes it is not possible for equation 5.1 to work properly. In conclusion to these, as the wake fractions are quite small, an alternative method was

sought in order to obtain the wake fractions. An additional experiment using CFD RANS was conducted to obtain the relative answer to the wake fractions.

## 5.3 The wake fractions obtained using RANS

The ITTC 1978 recommended wake fraction approximation as in Equation 5.1 is not valid for the medium-speed catamaran powering prediction. This formula was originally derived for large single screw ships. Based on these experiences, further powering predictions will only be based on the CFD simulated wake fractions.

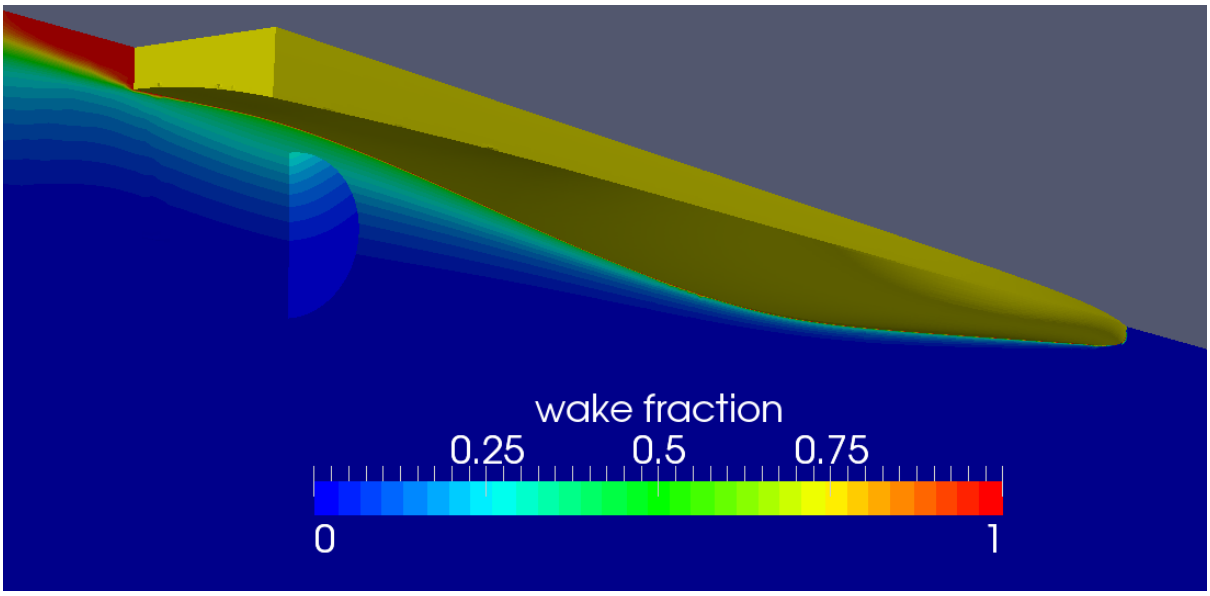


**Figure 5.2** The nominal wake in model scale**,** the wake fractions are given in $1 - U_x/U_{inf}$, at $R_e$ = $7.54 \times 10^6$.

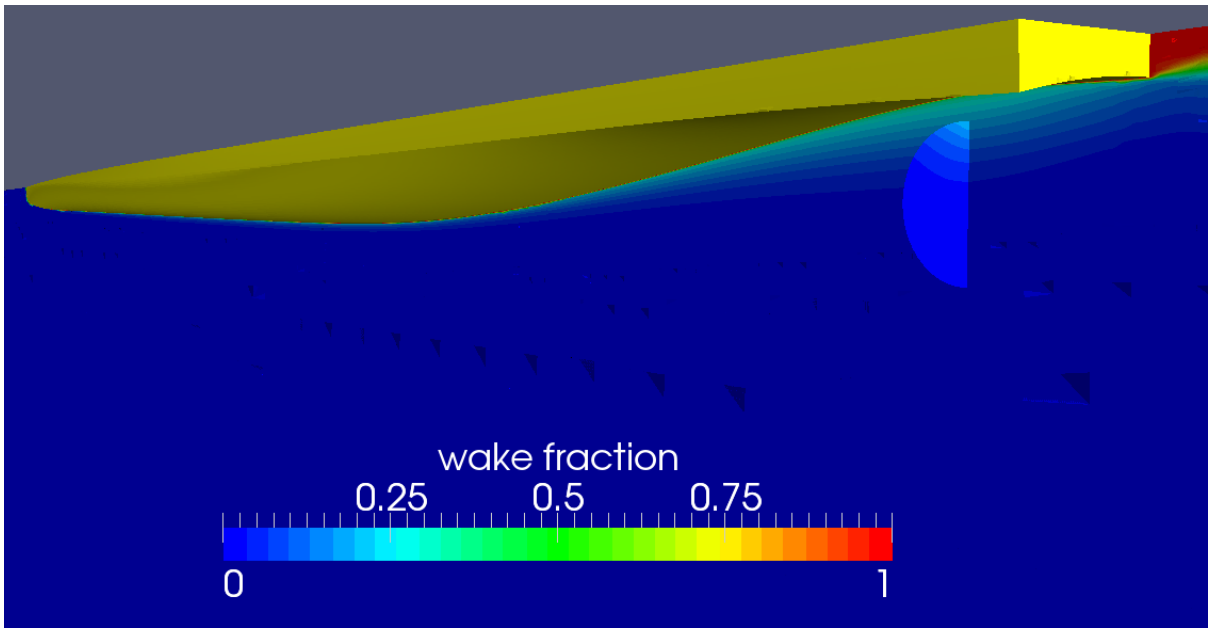


**Figure 5.3** The nominal wake in full scale, the wake fractions are given in $1 - U_x/U_{inf}$, at $R_e$ = $1.11 \times 10^9$ .

The reliability of computational fluid dynamics has improved recently. This includes in predicting the nominal and the effective wake behind a ship or a model. Most of the CFD solvers use the Reynolds Averaged Navier Stokes Equation or RANS (Bertram, 2000). Choi and Kinnas (2001) reported that they were able to predict the effective wake based on a finite volume approach. They demonstrated that the predicted total velocity field correlates very well with the results from experiments. Another example can be found in Sanchez-Caja and Pylkkanen (2007), where they used RANS to compute the velocity field at the location of the propulsion unit and at the same time taking into account the influence of the free surface on the effective wake. Nowadays, CFD and physical testing are now being used side by side by most of researcher and design house worldwide. Most of the CFD commercial package are now are easily accessible and user-friendly (Bertram, 2000) (Campana et al., 2011) (Broberg & Orych, 2011) (Stern et al., 2013) (Korkmaz et al., 2015). The most recent developments in the wake scaling using RANS reported by the specialist committee on scaling of wake field in the 26th ITTC in Rio de Janeiro can be found in Fu et al. (2011). Therefore, with this proven ability of CFD in predicting the wake behind a model or a ship, RANS-based CFD simulation was used to compute the velocity field at the propeller disc area of the propeller driven catamaran. What is important here is the wake scaling, $(1 - w_M)/ (1 - w_S)$, so it does not matter if either the nominal wake fractions or the effective wake fractions were used in the wake scaling calculation. A comparative study on the nominal and the effective wake fields which can be found in Regener et al. (2017) proved that the wake scaling either using nominal wake or the effective wake were found to be similar.

The CFD simulation was taken from the work of Haase (2015a). Haase has validated the simulation in model scale by comparing the predicted values of the total resistance, trim and sinkage to the values measured during model testing of Incat's wave-piercing catamaran carried out at AMC's towing tank. He has worked on various full scale and model scale RANS-based CFD simulation for a series of Incat wave-piercing catamaran. The CFD simulation was done using OpenFOAM in model scale and full scale, using the finite volume method as shown in Figure 5.2 and 5.3. In the simulation, the nominal wake occurring in the propeller disk area at the stern of the catamaran was calculated, as shown in Figure 5.4(a) and (b). These values were then integrated by the author of this thesis over the propeller disk radius in order to obtain the nominal mean wake as proposed by Carlton (1994) and Molland et al. (2011):

$$\bar{w}_T = \frac{\int_{r_B}^{R} r \int_0^{2\pi} w_T \, d\phi \, dr}{\pi\left(R^2 - r_B^2\right)} \tag{5.2}$$

where $R$ is the propeller radius and $r_B$ is the boss radius.

The integration of the wake in model scale results in a wake fraction of 0.03 and the integration of the wake in full scale results in a wake fraction at 0.015 as listed in Table 5.1. The wake fractions in the model scale were considered quite small at 0.03, which was expected from a

propeller plane centre which is operating below the baseline of the hull. These values were used for the wake scaling formula $1-w_{TM}\ /\ 1-w_{TS}$ (Bose, 2008) and it was calculated to be at 0.98.

**Table 5.1** Wake fraction values in model and full scale for the 130m propeller driven catamaran.

| | **Wake fraction, $w_T$** | ***1 – $w_T$*** |
|---|---|---|
| **Model scale** | 0.03 | 0.97 |
| **Full scale** | 0.015 | 0.985 |

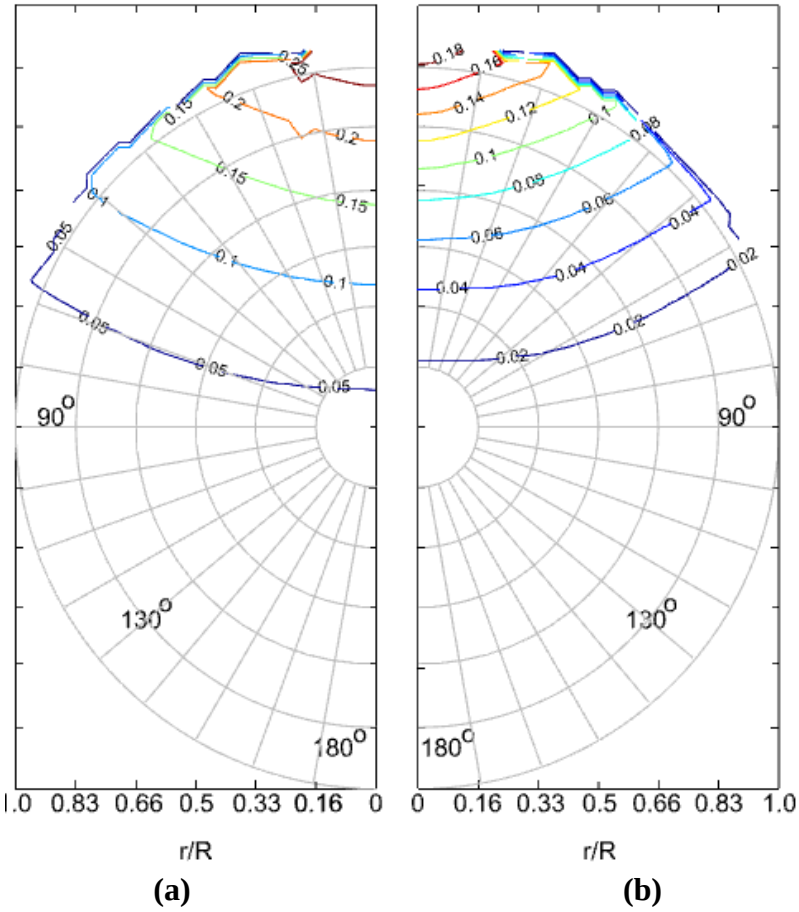


**Figure 5.4 (a)** The nominal wake in model scale **(b)** The nominal wake in full scale

The wake scaling proposed by ITTC which was based on the work of Sasajima et al. (1966) doesn't work well in the wake scaling exercise for the medium-speed catamaran here. The ITTC 1978 recommended formula $w_{TS} = (t + 0.04) + (w_{TM} – t – 0.04).\ (1+ k)\ C_{FS} + \triangle C_F/\ (1 + k)\ C_{FM}$ as in the procedure 7.5-02-03-01.4, predicted higher wake fractions in the full scale than the wake fractions in the model scale. This is not normal and simply because the wake fractions in the model scale are too small and ending up presenting negative values. Therefore this ITTC 1978 recommended wake scaling formula is not valid for the medium-speed catamaran powering prediction.

## 5.4 The towing force variation with respect to thrust – the *F – T* plot

The self-propulsion tests were done using the 'British' method. In this method, the tests were done by varying the propeller thrust so that the catamaran models operate at both under and overloaded conditions relative to the self-propulsion point of the ship. These tests were repeated again for different sets of Froude numbers or model speeds. Then the towing force variation was plotted with respect to the propeller thrust as shown in Figure 5.5 (a) and 5.5 (b).

As expected, these plots were observed to be linear. The linearity of these plots agreed with those reported by Bose (2008) and Kracht (1991) for other type of vessels. These curves were also found to be linear for the results from the self-propelled test with the waterjet propelled model.

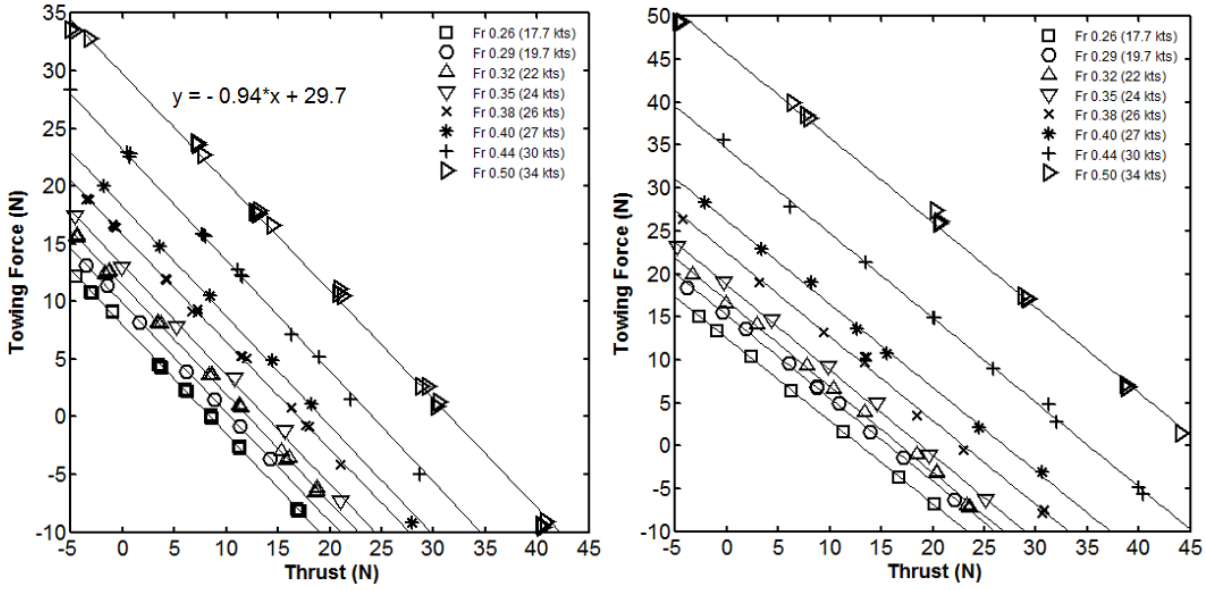


**Figure 5.5 (a)** Towing force plotted against the propeller thrust for the 130m propeller driven catamaran with the displacement of 2,500 tonnes. **(b)** Towing force plotted against the propeller thrust for the 130m propeller driven catamaran with the displacement of 3,640 tonnes.

## 5.5 The thrust deduction fraction

The thrust deduction fractions were obtained using the slope of the thrust and towing force linear regression line, where it may be obtained using;

$$F_D = F_{T=0} - T_M\left(1-t^*\right) \tag{5.3}$$

where $F_{T=0}$ is the towing force at zero propeller thrust, $F_D$ is the towing force at the self-propulsion point of the ship and $T_M$ is the model propeller thrust. When the towing force variation is plotted with respect to the propeller thrust as shown in Figure 5.5 (a) and 5.5 (b), a linear regression line can be fitted through the points at each Froude number. The fitted regression line at each Froude number normally yields a linear straight line with a negative slope of *t-1*, where *t* is the thrust deduction fraction and the y-axis intersection represents the resistance of the model in the self-propulsion condition. For example the regression line of *y = -0.94x + 29.7* for Froude number 0.50 in Figure 5.5

(a), has a slope of *t-1* which equal to *-0.94*. Therefore the value of *t* can be calculated using the equation, *t-1 = -0.94*, giving the value of *t* equal to *-0.94 + 1 = 0.06*.

ITTC (2014) in the procedure 7.5-02-03-01.4, suggested that the thrust deduction fractions can be found from the results of the separate calm water resistance test and the self-propulsion test which was also stated in Kracht (1991) and Bose (2008) where

$$t = \frac{T_M + F_D - R_C}{T_M} \tag{5.4}$$

In this formula, instead of using the towing force at zero propeller thrust, the resistance of the model measured in a separate calm water resistance test, $R_{TM}$ was used. The calm water resistance values $R_{TM}$ was then corrected as $R_C$ which is the resistance of the model corrected for the water temperature at the time of the self-propulsion test (ITTC, 2014). The propeller model thrust $T_M$ was found using the values of the thrust coefficient $K_{TP}$, which can be found from the results of the self-propulsion test, where $T_M = K_{TP}\rho n_M^2 D_M^4$. The value of the required towing force, $F_D$ was found from the intersection between the non-dimensionalised towing force from the self-propulsion test $K_{FD}$ and the parabola of the required towing force coefficient which can be found from $K_{FD}/J_P^2 = (C_{FD}S_S)/(2D_S^2)$. Note that the value of $C_{FD}$ is the required towing force coefficient and $K_{FD}$ are the values converted from the values of the towing force from the self-propulsion test. Detailed explanation on this interpolation in getting $T_M$ and $F_D$ can be found in section 2.24 in this thesis. Clearly the model thrust $T_M$ and the towing force equivalent to the self-propulsion of the ship $F_D$ were taken from a single point even though the test was conducted using the British method. This is not as accurate as getting the thrust deduction fraction from the slope of the thrust and towing force linear regression line fitted from the multiple data point from obtained from the test. In an attempt to finalise which thrust deduction fraction to be used, a comparison was made as what will be explained in the next paragraph.

The results of the thrust deduction fractions using the slope equation as in Equation 5.3 and the thrust deduction fractions using the recommendation from ITTC (2014) as in Equation 5.4 for the propeller driven catamaran were compared as shown in Figure 5.6 (a) and 5.6 (b). The results for the propeller driven catamaran were positive, as expected and range from 0.00 to 0.06 for thrust deduction using the slope (Equation 5.3). The thrust deduction fractions obtained from Equation 5.4 were higher and more scattered than the thrust deductions fractions obtained from the slope of the thrust and the towing force regression line and ranged from 0.04 to 0.348. The difference of the thrust deduction fractions ranged from 48% to 199% as listed in Table 5.2. This agrees to the large scatter of *t* found by Kracht (1991) when using the thrust deduction fractions as defined in Equation 5.4.

One might argued that the results as shown in Figure 5.6 (a) and 5.6 (b) are not comparable as the resistance test is performed without appendages, while propulsion test is performed with appendages, so that the appendage resistance, which might be significant, is included in the thrust deduction fraction in the self-propulsion test only procedure, while it is not included in the thrust

deduction fraction found from the ITTC'78 procedure. Unfortunately, there was no resistance test performed with appendages attached to the model. To investigate the appendage drag quantitatively, the appendage drag in model and full scale were calculated using equations which can be found in R. W. Peck (1976), Hoerner (1965) and Kirkman and Kloetzli (1980). Details of the equations used and the calculations are shown in Appendix D. The thrust deduction fractions with appendage drag included in the total resistance was found to be lower than the thrust deduction fractions without the appendage drag included in the total resistance as shown in Figure 5.6 (a) and (b). The thrust deduction fractions with the appendage drag included in the total resistance was found to be in close agreement with the thrust deduction fractions obtained using the slope equation especially at Froude number 0.35 to 0.45. There are still some scatter in the thrust deduction fractions especially at lower Froude numbers, $F_R$ *0.2 to* $F_R$ *0.3*. It is believe that the incorrect flow conditions existed at the lower Froude numbers and contributed to lower total drag to the un-appended model.

Conducting a resistance test for a model with its appendages has its own issues. One of main concern is the incorrect flow conditions because of low Reynolds number due to small appendages for this case, the rudder and the propeller strut bracket.

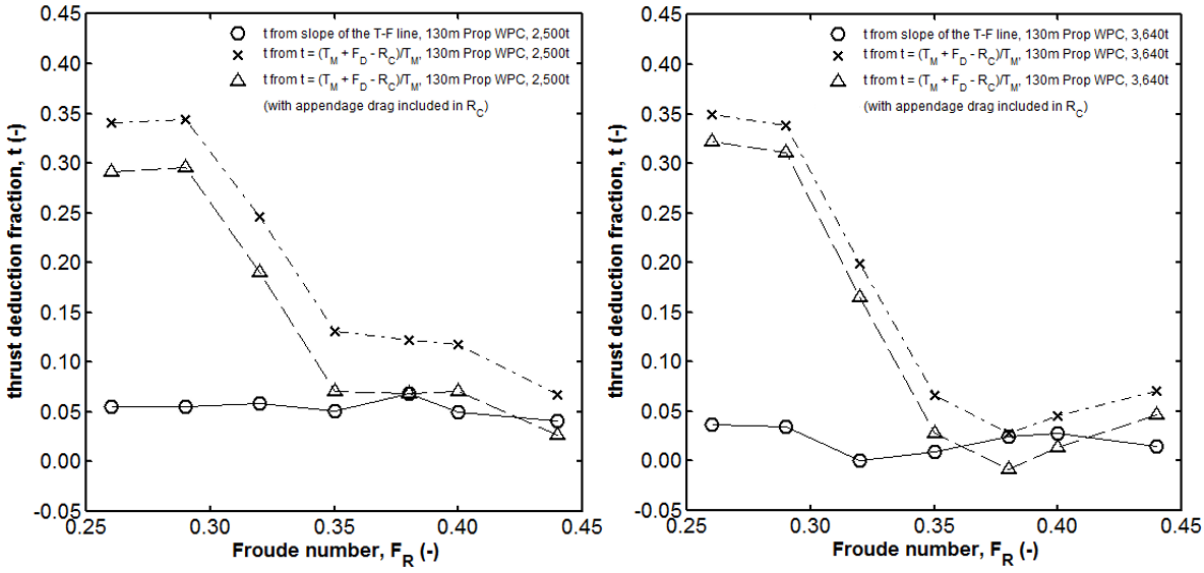


**(a)** **(b)**

**Figure 5.6** Comparison of the thrust deduction fractions obtained using *t**, Equation 5.3 and *t*, Equation 5.4 for the 130m propeller driven catamaran **(a)** Thrust deduction fraction plotted against the Froude number for the catamaran at a displacement of 2,500 tonnes. (**b)** Thrust deduction fraction plotted against the Froude number for the catamaran at a displacement of 3,640 tonnes.

The reason for the difference of the two thrust deduction fraction is likely due to the uncertainties by introducing the resistance forces from a separate test. Kracht (1991) cautioned on the using of $R_{TM}$ or $R_C$ as in Equation 5.4, as it may contain uncertainties which are significant. These were proven in Chapter 4, The Uncertainty Analysis, where the errors from the older method (ITTC1978) were higher than the errors from the SPT method. In the SPT only method, the

uncertainty was decreased by using all the multiple data points in the linear curve to find the wake fraction.

Kracht also mentioned that the different dynamic behaviour of the model and different flow around the hull and appendages (if installed) result in resistance forces which are not comparable. This was illustrated by Kracht in a plot of having a large scatter of *t* of a model with different propellers (Kracht, 1991, p.184). The thrust deduction fractions from the load-varied test (from the calculation of the slope) were more accurate since it used a linear curve fits to a multiple data points of the thrust with respect to the towing force plots. This is far more accurate than estimating the thrust deduction fraction from a single data point from the self-propulsion point of the ship in the self-propulsion point. Therefore based on evidence (large variations of *t* from ITTC traditional method as in Figure 5.6), the thrust deduction fraction obtained from the slope equation was chosen for the extrapolation to full scale. The ITTC recommended method does not work in these exercises and should not be used in the extrapolation process.

**Table 5.2** Thrust deduction fraction values for propeller driven catamaran at displacement of 2500 tonnes and 3640 tonnes

| | **2500** | **tonnes** | | | | | |
|---|---|---|---|---|---|---|---|
| **Fr** | 0.44 | 0.4 | 0.38 | 0.35 | 0.32 | 0.29 | 0.26 |
| **t*** | 0.04 | 0.05 | 0.07 | 0.05 | 0.06 | 0.05 | 0.05 |
| **t** | 0.07 | 0.12 | 0.12 | 0.13 | 0.25 | 0.34 | 0.34 |
| **Diff %** | 49.1 | 80.3 | 56.3 | 88.5 | 123.4 | 145.4 | 144.2 |
| | **3640** | **tonnes** | | | | | |
| **Fr** | 0.44 | 0.4 | 0.38 | 0.35 | 0.32 | 0.29 | 0.26 |
| **t*** | 0.01 | 0.03 | 0.02 | 0.01 | 0.0001 | 0.03 | 0.04 |
| **t** | 0.07 | 0.04 | 0.03 | 0.07 | 0.20 | 0.34 | 0.35 |
| **Diff %** | 132.5 | 48.3 | 13.8 | 155.36 | 199.8 | 163.33 | 162.6 |

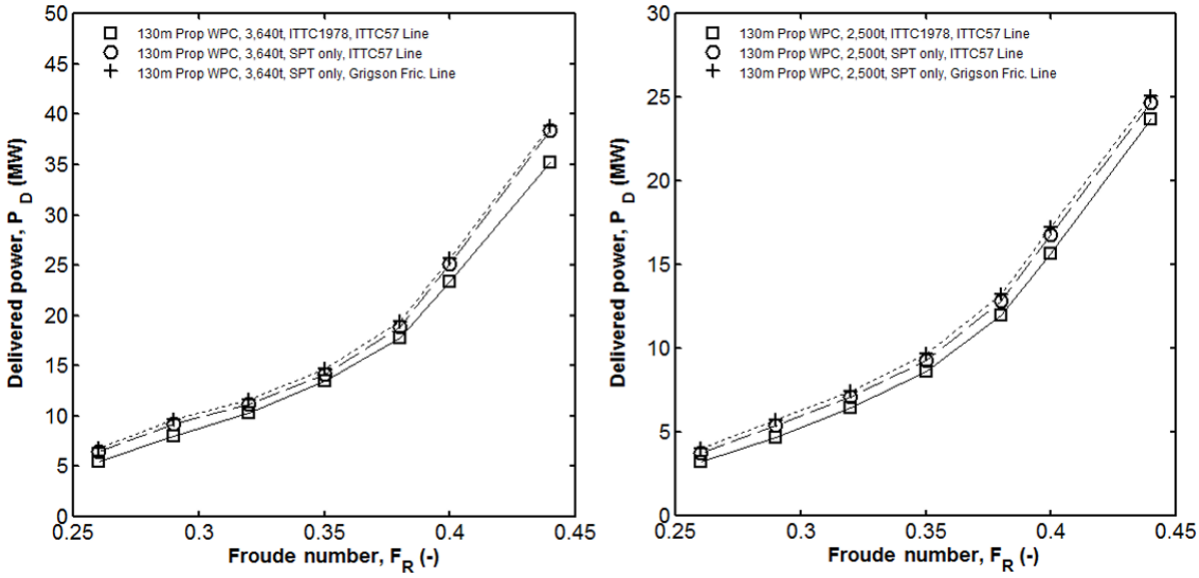


**Figure 5.7** Comparison of delivered power extrapolated using the ITTC 1978 method and the self-propulsion test (SPT) only method. **(a)** The delivered power with respect to the Froude number for the displacement of 3,640 tonnes. **(b)** The delivered power with respect to the Froude number for the displacement of 2,500 tonnes.

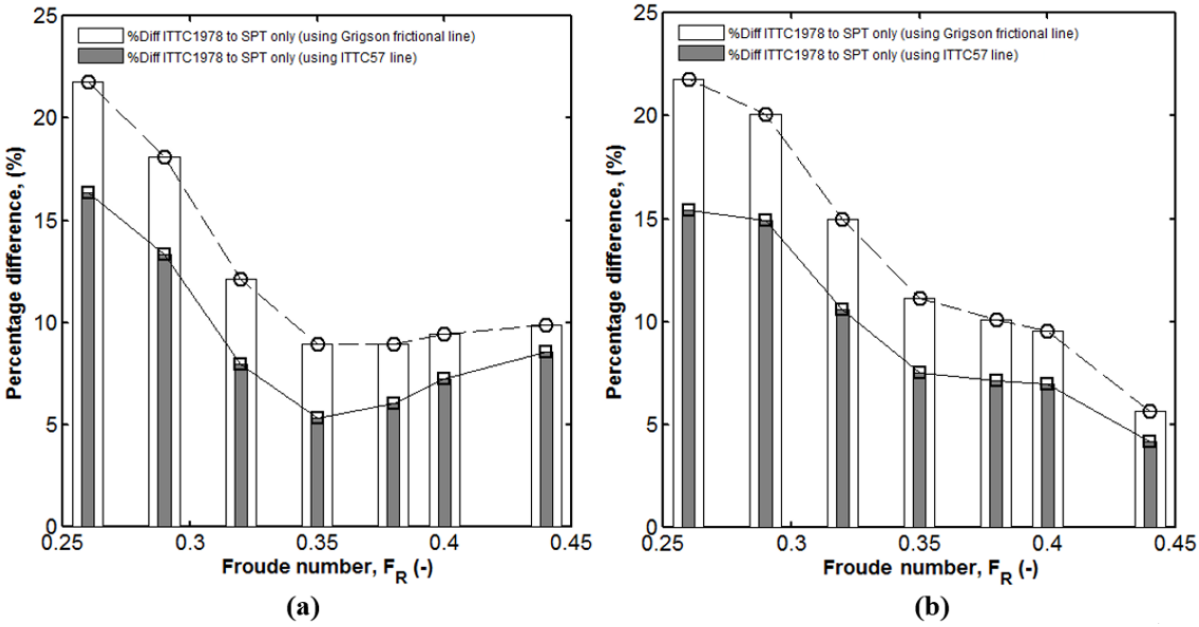


**Figure 5.8** Percentage difference of the extrapolated delivered power between the ITTC 1978 and the Self-propulsion test only method (ITTC57 model-ship correlation line and Grigson's Flat plate frictional line) at displacement of **(a)** 3,640 tonnes. **(b)** 2,500 tonnes.

## 5.6 The delivered power of the 130m propeller driven catamaran

The delivered power was extrapolated to full scale using the ITTC 1978 method and the self-propulsion test only method. There were two versions of the self-propulsion test only method. The first version was calculated using the ITTC 1957 model-ship correlation line and the second was calculated using the Grigson's formulations for turbulent flat plate friction. The correlation allowance

$C_A$ of 0.00035 was chosen as used by Marin (2008) for testing wave-piercing catamarans. Further analysis is needed in order to be confident with the choice of $C_A$. This can be achieved once the post-construction full-scale trial results are made available. The value used for the wake scaling for the self-propulsion test only method was defined to be 0.98 as in Table 5.1. This wake scaling data were obtained from a RANS numerical simulation done using OpenFOAM as mentioned in section 5.3.

In Figure 5.7 (a) and 5.7 (b), the delivered power values are plotted with respect to the Froude number for the propeller propelled catamaran at the displacement of 3640 and 2500 tonnes. The results show that the delivered power obtained using the self-propulsion test only method was higher than the ITTC 1978 method. The delivered power extrapolated using the self-propulsion test only method were 6% to 22% higher than the delivered power using the ITTC 1978 method, as shown in Figure 5.8 (a) and 5.8 (b). It shows that the variations due to frictional line change are much lesser than the variations due to the method change. Furthermore, there is a positive offset between the methods which support the idea that the correlation allowance is dependent on the extrapolation method.

The higher values of predicted delivered power extrapolated using the self-propulsion test only method (using Grigson's frictional line) was also found in Bose and Molloy (2001b). It was found that the predicted power using the 'self-propulsion test only method' was higher than the delivered power extrapolated using the ITTC1978 method. Bose and Molloy found this in the results from the self-propulsion tests and from full-scale trials for the Canadian Coast Guard R-Class icebreakers. The predictions using the 'self-propulsion method only method' done by Bose and Molloy, used the Grigson's turbulent flat-plate friction line, a correlation coefficient of 0.0006 and a form factor, obtained using low-speed resistance test results, of 0.4. The reason for the high correlation coefficient was due to the ship hull of the icebreaker which had a relatively high degree of fouling.

The question now, which method is more accurate in predicting the delivered power? Is it the delivered power extrapolated from the ITTC method or the SPT method? In the latest procedure in the extrapolation to full scale using the ITTC 1978 performance prediction method which can be found in ITTC (2014), the delivered power of each propeller is defined as $P_{DS} = 2\pi \rho_S D_S^5 n_S^3 . K_{TS} / \eta_R$. The inclusion of the relative rotative efficiency $\eta_R = K_{QO}/K_{QP}$ in the equation may lead to some error as there are uncertainties in the $K_{QO}$ from the open water propeller test. The delivered power $P_{DS} = 2 \pi K_{QS} \rho_S n_S^2 D_s^5$ obtained from the SPT method is more direct as it used the value $K_{QS}$ which was obtained from the self-propulsion test itself and not from the open water propeller test and there is no inclusion of the relative rotative efficiency. The relative rotative efficiency was introduced in the delivered power equation of the ITTC method as it was meant to keep the extrapolation in order as there will be discrepancy between the results obtained using the 'thrust identity' and the 'torque identity' method (Bose, 2008). This relative rotative efficiency is a 'fix' to make the three separate test method work and does not really have a physical meaning.

The main problem in the ITTC 1978 method is in the ship propeller operating point interpolation equation, $K_T/J^2 = S_S.C_{TS}/2.D_S^2(1-t).(1-w_{TS})^2$. This equation is used to find the operating values from the intersection of the required thrust coefficient $K_T/J^2$ and the thrust coefficient of the ship propeller $K_{TS}$. This equation used results from the three discrete tests. The $K_T/J^2$ is from the open water test, the $C_{TS}$ is from the calm water resistance test and the $(1 - t)$ and the $(1 - w_{TS})$ are from the self-propulsion test. In the SPT method, the ship propeller operating point interpolation equation is obtained from $K_{TS}/ J^2 = T_S/2\rho D_S^2 V_S^2$. The inputs for the SPT method are strictly from the self-propulsion test. Here, one can see that the method proposed by the ITTC1978 clearly assumes as negligible the interaction effects between the hull and the propeller in the behind condition. The hull interactions are taken into account using wake fraction and relative rotative efficiency in the conventional ITTC'78 procedures. But not in the self-propulsion test only method where the hull interactions are directly taken into account where the torque and thrust were taken directly without using the thrust and the torque identity method. The relative rotative efficiency used in the ITTC'78 procedure act as a corrector to the thrust – torque characteristics for a propeller working in a uniform flow to a propeller working in a variable wake. In the self-propulsion test only procedure, the thrust and torque characteristics are taken directly from the behind condition experiment.

This is in contrast with the SPT procedure where the ship propeller operating point is found from the intersection of the required thrust coefficient with the ship propeller curve in the behind condition, where the interactions between the hull and propeller are not neglected. With the presence of a working propeller in the behind of the model, the flow and the pressure field are altered at the afterbody of the model. The different flow around the hull and appendages, a propeller bracket in this case, result in resistance forces which are not comparable as mentioned by Kracht (1991) in his paper comparing the thrust deduction fractions obtained from the load-variation test and the thrust deduction fraction obtained from separately performed resistance and propulsion tests.

## 5.7 The overall propulsive efficiency

The overall propulsive efficiency was extrapolated to full scale using the ITTC 1978 method and the self-propulsion test only method. Similar to the prediction of the delivered power, two versions of the self-propulsion test only method were used, using the ITTC 1957 model-ship correlation line and using the Grigson's formulations for turbulent flat plate friction. The overall propulsive efficiency is defined as $\eta_D = P_E / P_D$ where $P_E = \frac{1}{2} C_{TS} \rho_S S_S V_S^3$ and $P_{DS} = 2\pi\rho_S D_S^5 n_S^3 . K_{TS} / \eta_R$. The overall propulsive efficiency in the SPT method is similar to the ITTC1978 method except that the $C_{TS}$ values in finding $P_E$ was obtained from the self-propulsion test and there are no inclusion of the relative rotative efficiency in the calculation of $P_{DS}$.

In Figure 5.9 (a) and 5.9 (b) the plot of the overall propulsive efficiency with respect to the Froude number for the 130m propeller driven catamaran are shown. The propulsive efficiency using the self-propulsion test only method was found to be lower than the propulsive efficiency using the ITTC1978 method; this is shown in Figure 5.10 (a) and (b) as percentage differences. The overall propulsive efficiency predicted using the self-propulsion test only method using the ITTC1957 model-ship correlation line were 1.7% to 6% lower at the displacement of 3,640 tonnes. At the displacement of 2,500 tonnes, the overall propulsive efficiency was 4.5 to 1% lower than the ITTC1978 method, except at Froude number 0.29, where the SPT method was higher at 1% than the ITTC method. The overall propulsive efficiency predicted using the self-propulsion test only method using the Grigson's formulation for the flat plate frictional line was 2.7% to 6% lower at the displacement of 3,640 tonnes and 4.5% to 1% lower at the displacement of 2,500 tonnes than the ITTC1978 prediction method except at Froude number 0.29.

The overall propulsive efficiency showed a decreasing trend as the Froude number increased in all cases. The overall propulsive efficiency here shows that there is a certain dependency of the propulsive efficiency with the speed. As described by Holtrop (2001), this dependency is primarily governed by the loading of the propulsor. The behaviour of the propulsive efficiency curve is the opposite of the $C_{TM}$ curve which increases as the speed increases.

The overall propulsive efficiency obtained from the SPT method is believed to be more realistic than the propulsive efficiency obtained from the ITTC method. As the propulsive efficiency is much dependent on the power delivered to the propulsor, it was at the best discretion to choose the propulsive efficiency using the delivered power obtained from the SPT method.

**(a)**

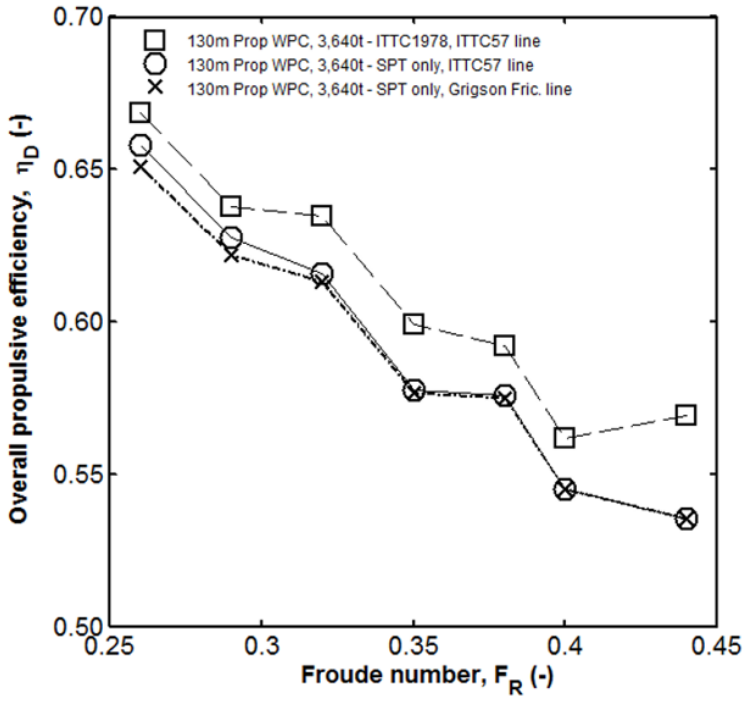


**(b)**

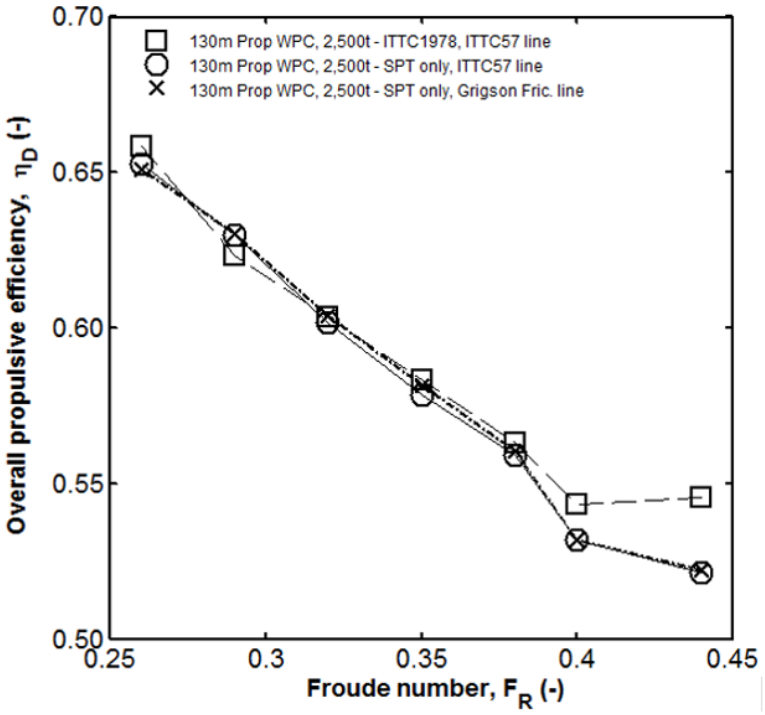


**Figure 5.9** Comparison of overall propulsive efficiency results extrapolated using the ITTC 1978 method and the self-propulsion test (SPT) only method. **(a)** The overall propulsive efficiency with respect to the Froude number for the displacement of 3640 tonnes. **(b)** The overall propulsive efficiency with respect to the Froude number for the displacement of 2500 tonnes.

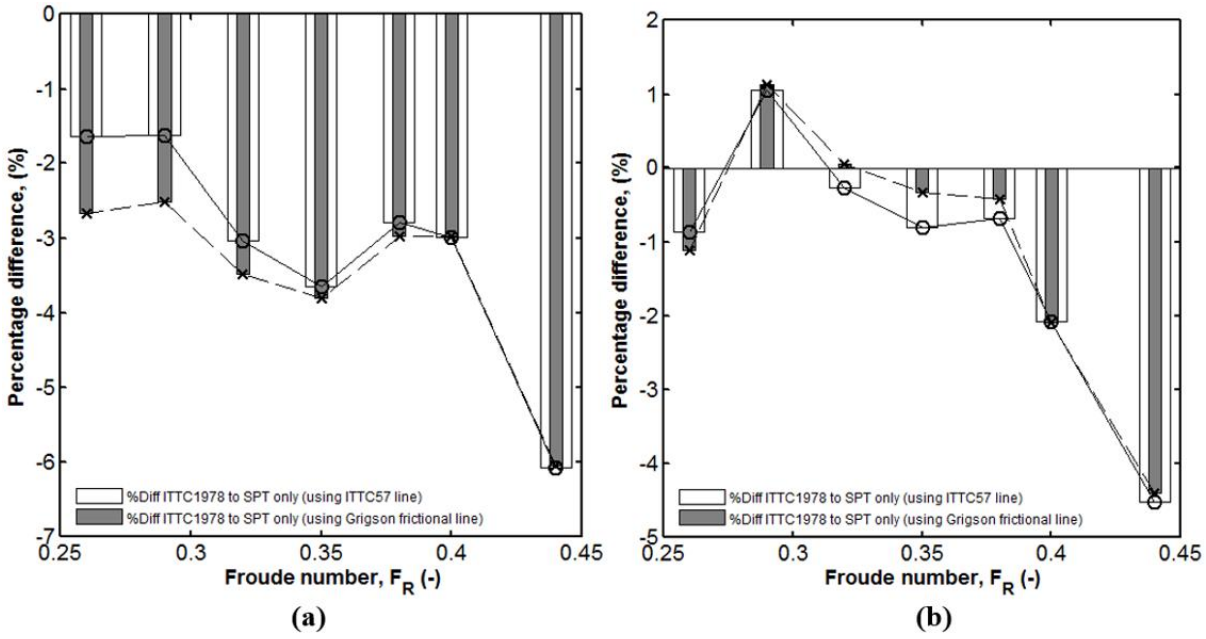


**Figure 5.10** Percentage difference in the overall propulsive efficiency between ITTC 1978 and Self-propulsion test only method at displacements of **(a)** 3,640 tonnes **(b)** 2,500 tonnes

## 5.8 The shaft revolution rate

The ITTC 1978 proposed that the shaft revolution rate can be found using the formula given in the ITTC procedure 7.5-0.2-0.3-01.4. The shaft speed is defined as $n_S = (1 - w_{TS})\, V_S / J_{TS}.D_S$ (ITTC, 2014, p. 7). In the self-propulsion extrapolation method only by using the formula given in Bose (2008, p. 19) the shaft speed is given by

$$\frac{n_S}{n_m} = \frac{V_S}{J_S D_S}\frac{J_M D_M}{V_M} = \frac{V_S}{V_M}\frac{D_M}{D_S} = \frac{1}{\sqrt{\lambda}} \tag{5.5}$$

In this equation, it is assumed that the advance coefficients are the same at model and full scale (Bose, 2008).

The shaft speeds are plotted with respect to the Froude number as shown in Figure 5.11 (a) and 5.11 (b). The shaft speeds were ranged from 2.8 rev/sec (170 rev/min) in the lower Froude number region to 5 rev/sec (300 rev/min) in the higher Froude number region. The shaft revolution rate obtained using the self-propulsion method only was higher and ranged from 1 to 5% than the shaft speed obtained using the ITTC 1978 method. There were small differences in either using the ITTC57 model-ship correlation line or the Grigson's frictional line in extrapolating the shaft speed to full scale using the SPT only method. The reasons for the differences between the predicted shaft speed obtained from the SPT method and the ITTC method, are due to the assumption made in the SPT method, where it is assumed that the advance coefficients are the same at model and full scale as shown in Equation 5.5. In the ITTC method, the underlying formula for the revolution speed of the ship propeller is given by $n_S = (1 - w_{TS})V_S / J_{TS}D_S$. The advance coefficient, $J_{TS}$, of the ship propeller is found from the intersection of the curve of the required thrust, $K_T/J^2 = S_S.C_{TS}/2.D_S^2(1\text{-}t).(1\text{-}w_{TS})^2$ and

the thrust coefficient of the ship propeller. These two different approaches in determining the shaft speed, lead to differences in the predicted shaft speed.

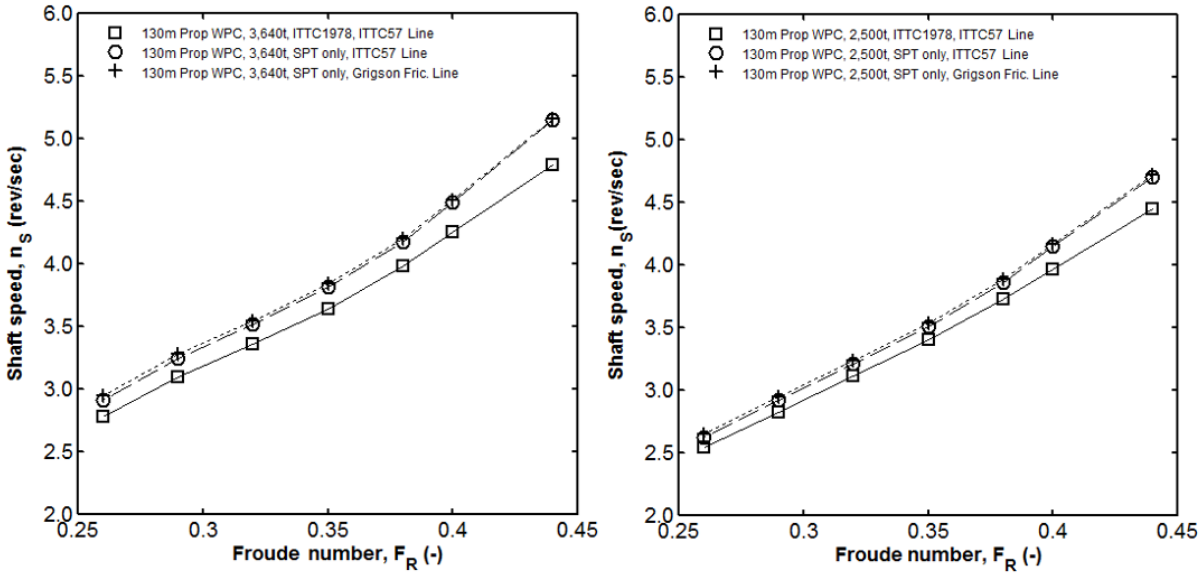


**Figure 5.11** The shaft revolution rate extrapolated using the ITTC 1978 and the Self-propulsion test only method (ITTC57 model-ship correlation line and Grigson Flat plate frictional line) at displacement of **(a)** 3,640 tonnes. **(b)** 2,500 tonnes.

## 5.9 The residual resistance

The bare hull resistance results which were taken from the calm water resistance test conducted in May, 2014 were plotted in the form of residual resistance, $C_R$ against the Froude number, as shown in Figure 5.12 (a) and 5.12 (b) for the displacement at 3,640 tonnes and 2,500 tonnes respectively. The measured residual resistance at level trim were plotted using circle markers. This residuary resistance was obtained by subtracting the values of the frictional resistance $R_F$ from the appropriate measured values of total bare hull resistance, $R_T$. It was observed that there were at least two humps visible for the 130m propeller driven catamaran. The first hump was observed at Froude number of 0.30 and the second at Froude number 0.46. This was observed in the two displacements, 3,640 and 2,500 tonnes. The hollows were observed at Froude number of 0.35. This corresponds with the observed appearance of the dry transom; see Figure 5.15, picture shown in the second column, three from the top. The detailed explanation for the transom immersion ventilation can be found in Saunders (1957a, pp. 326 - 327) and Kiss and Compton (1989). In this condition the hull will benefit by having a lower residual resistance.

### The effects of static trim to the residuary resistance

In Figure 5.12 (a) and 5.12 (b), the residual resistance reduced when the bow was trimmed down and vice versa. The reason for the reduction in the residual resistance resulted from the decrease of the wetted surface at the stern achieved when the bow was trimmed down; hence less drag was experienced by the whole hull. This was experienced by both, light and heavy displacement of the 130m propeller driven catamaran. Hence it is beneficial for the boat to be trimmed down by the bow during its operation. Even though trimming the boat by the bow is beneficial for resistance, it is usually necessary to keep some considerable trim by the stern in order to ensure adequate immersion of the propeller. A propeller operating close to the free surface has higher propeller loads and lower efficiency (Li et al., 2015). Other issues like loss of directional stability should be considered when trimming by the bow as a ship trimmed by the bow is directionally unstable as mentioned in Kobylinski (2003) and McTaggart (2016).

### The comparison between the towed resistance and the towing force $F_{T=0}$

In Figure 5.13, the towed resistance in the bare hull resistance was compared with the towing force at zero propeller thrust, $F_{T=0}$. The towing forces, $F_{T=0}$ are greater than the towed resistance in the conventional resistance test. It should be noted that the resistance test is performed with bare hull, while the zero thrust measurements in the self-propulsion test which includes the resistance and the flow disturbances caused by the appendages. It was noticed that the 'rooster tail' in the self-propulsion test was more pronounced than the one in the bare hull resistance test for the equivalent $F_{T=0}$ condition, as shown in Figure 5.14. This proved that by having a propeller operating behind the hull, it would change the flow, the separation and the pressure distribution along the hull, hence changing the resistance. The increased resistance in the self-propulsion test is also contributed by the additional drag imposed by the appendages as mentioned earlier. Another possible reason for the increase of resistance in the hull with propeller is that there is a pressure drop just before the propeller plane, resulting in increasing resistance forces moving forward.

It is ideal to have two resistance test conducted during the towing tank test programme, one without the appendage and the other with appendages. But this was impossible to be executed at that time as the AMC's towing tank was packed with other testings. Some calculations on the appendage drag in model scale and full scale were made using the common formulation which can be found in Hoerner (1965), Kirkman and Kloetzli (1980) and R. W. Peck (1976). The detail of the semi-empirical formulation used in the appendage drag calculations can be found in Appendix D in this thesis.

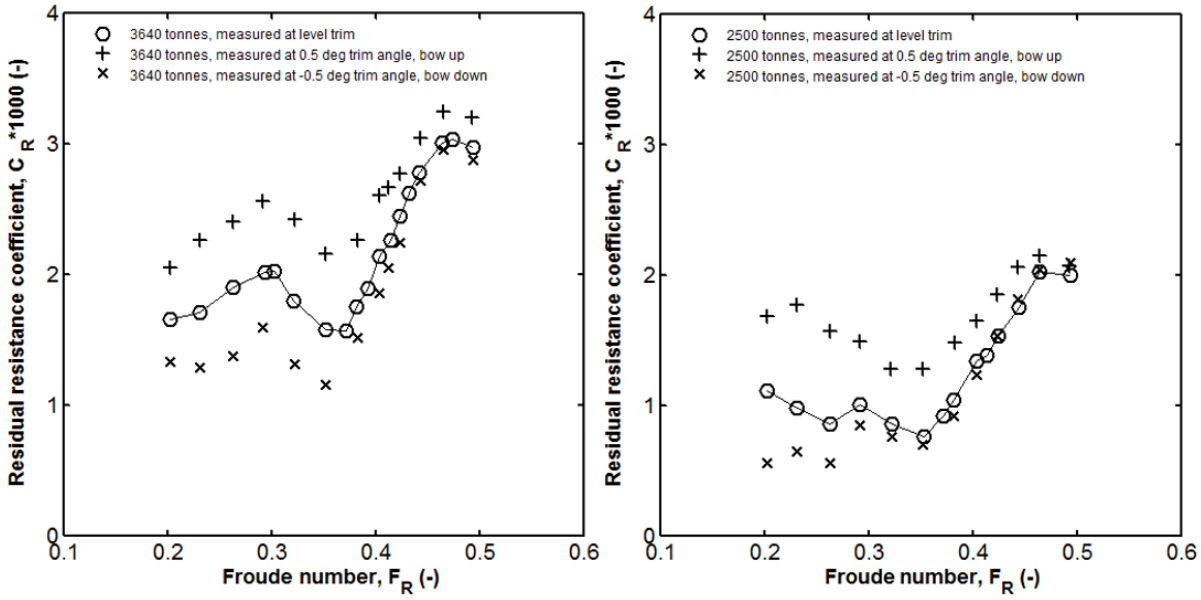


**(a)** **(b)**

**Figure 5.12** The bare hull resistance test results plotted in residual resistance, $C_R$ with respect to the Froude number showing the trim effect on the coefficient of residual resistance. **(a)** 3640 tonnes measured at 3 trim angles **(b)** 2500 tonnes measured at 3 trim angles.

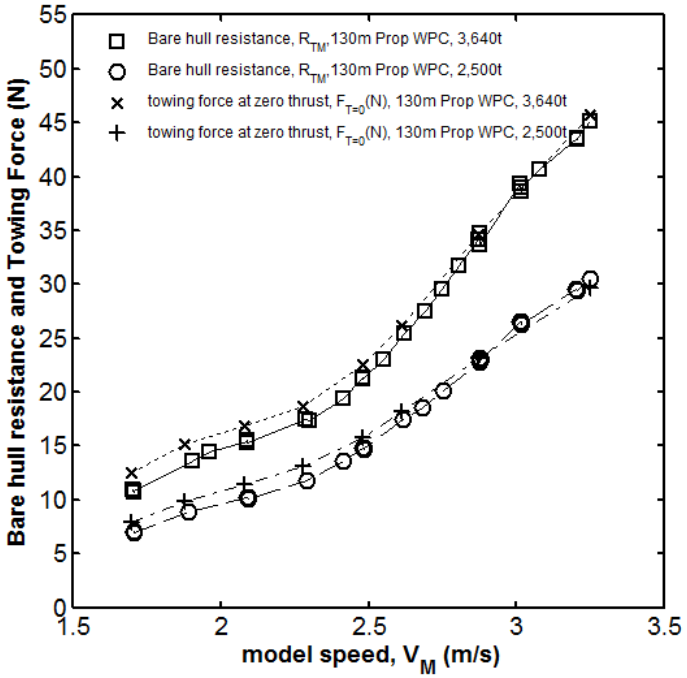


**Figure 5.13** The comparison between the total resistances of the model in the self-propulsion test and the total resistances in the bare hull resistance test.

**(a)**

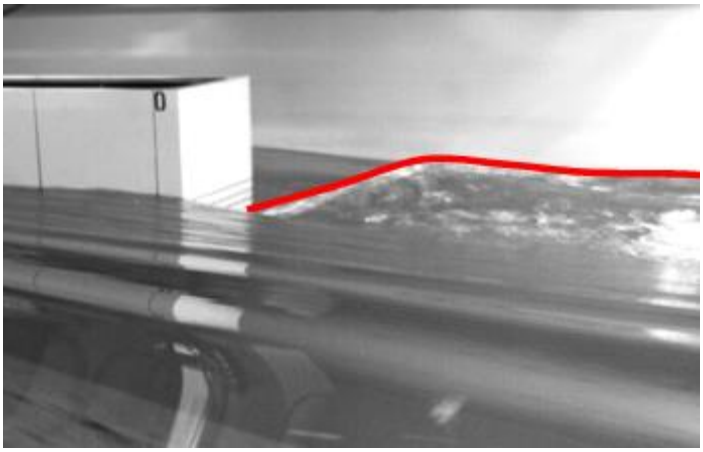

**(b)**

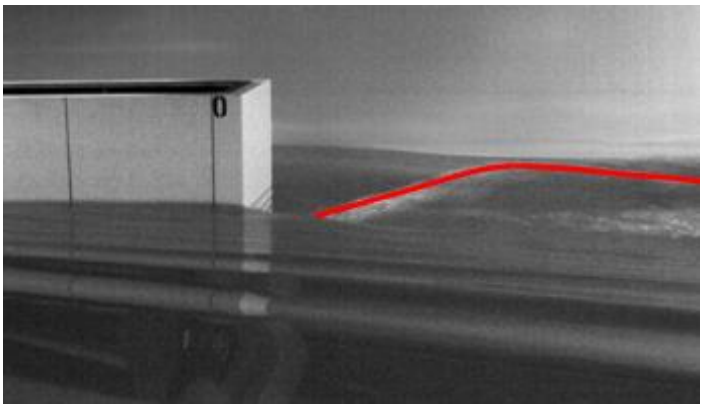

**Figure 5.14** The view of the 'rooster tail' aft of the catamaran's transom. **(a)** 3,640 tonnes Fr 0.35 from Self-propulsion point (with propeller) **(b)** 3,640 tonnes Fr 0.35 from bare hull resistance test (without propeller)

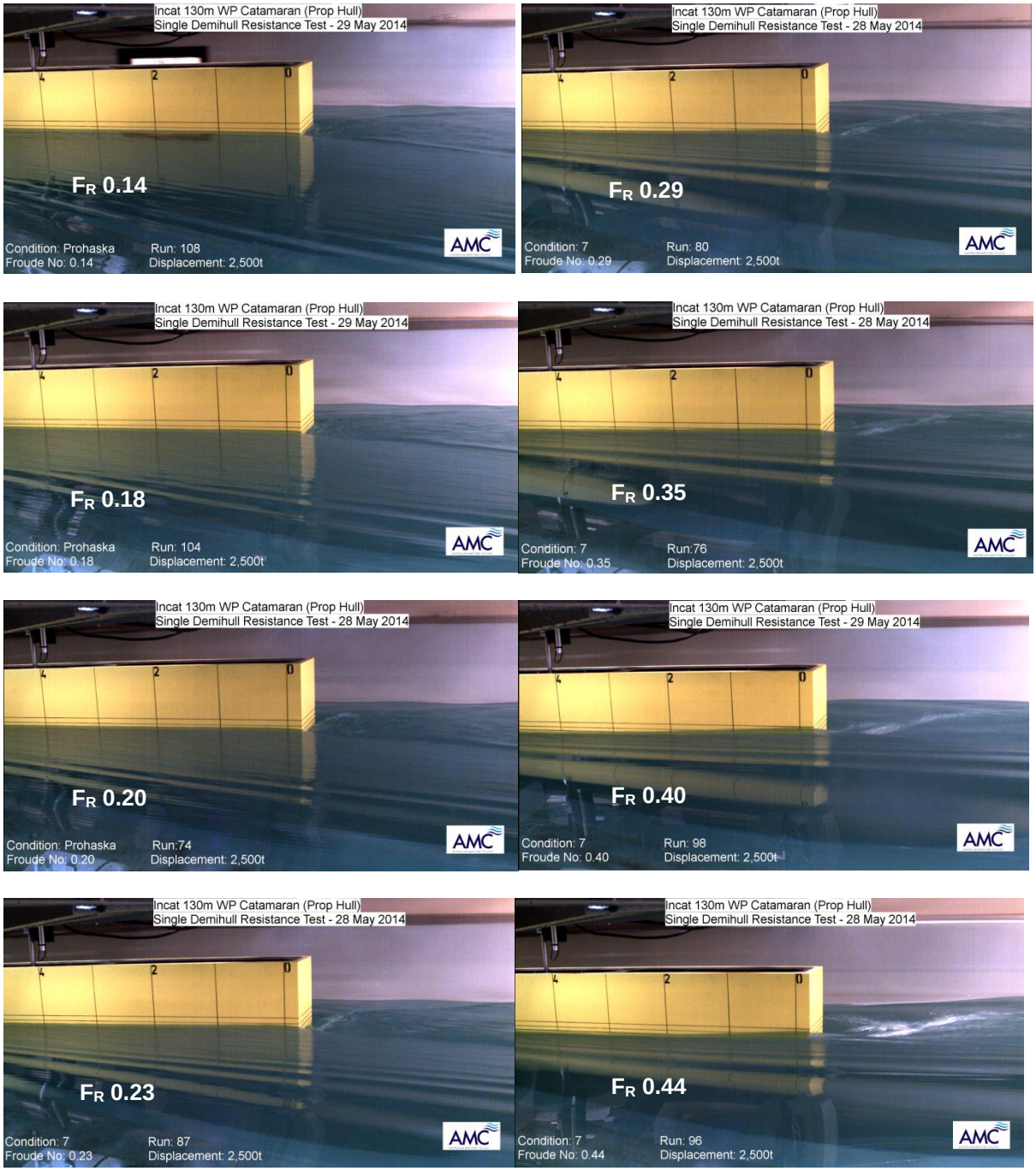


**Figure 5.15** The stern view of the transom of the 130m propeller driven catamaran. Note the transom immersion at Froude number 0.35.

## 5.10 Sinkage

The sinkage $z$ was calculated by averaging the forward sinkage, $z_{fwd}$ and aft sinkage $z_{aft}$. The sinkage $z$, have been rendered dimensionless in this study by dividing the sinkage with the ship waterline length $L_{WL}$. The dimensionless sinkage $z/L$ for the 130m propeller driven was plotted with respect to the Froude number as shown in Figure 5.16 (a) and 5.16 (b).

It was observed at low speeds, there were a slight sinkage and a slight trim by the bow as compared with at rest condition. As speed increases the movement of the bow was reversed and at Froude number of 0.47 the bow begins to rise appreciably, the stern sinks still further and the catamaran takes on a decided trim by the stern. It was observed that the maximum sinkage happened at the Froude number 0.47, which corresponds to the maximum residual resistance achieved at this Froude number. Beyond the Froude number of 0.45, the sinkage started to reduce, which corresponds to the reduction of the residuary resistance.

### The effects of the static trim to the sinkage

In Figure 5.16 (a) and (b), it was demonstrated that the sinkage increased as the trim angles were changed either in bow up or bow down position. The maximum sinkage was experienced at Froude number 0.44 to 0.45. This happened at both, light and heavy displacement of the 130m propeller driven catamaran. The sinkage happened to be less with a lighter ship displacement.

### Sinkage at self-propulsion test

In Figure 5.17 (a) and (b), the sinkage measured in the bare hull resistance was compared with the results from the self-propulsion test. The sinkage in the self-propulsion test was higher than the sinkage measured in the calm water resistance test. The variations were ranged from 16 to 20%. The variations were reduced when approaching the Froude number 0.44. It was felt that the sinkage measured in the self-propulsion test is more realistic of full-scale operating, as with a working propeller behind the hull, the pressure distribution forward to the propeller disc area is altered hence affecting the amount of sinkage on the vessel.

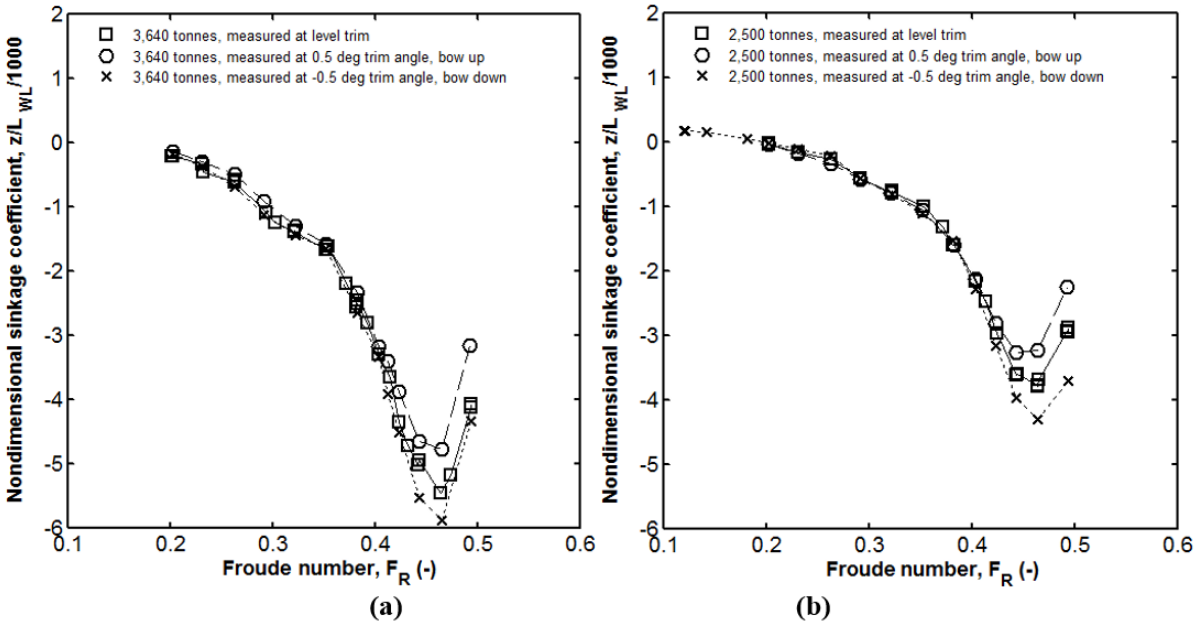


**Figure 5.16** The effects of the static trim angle at rest to the sinkage for **(a)** 130m propeller driven catamaran at displacement of 3,640 tonnes. **(b)** 130m propeller driven catamaran at displacement of 2,500 tonnes

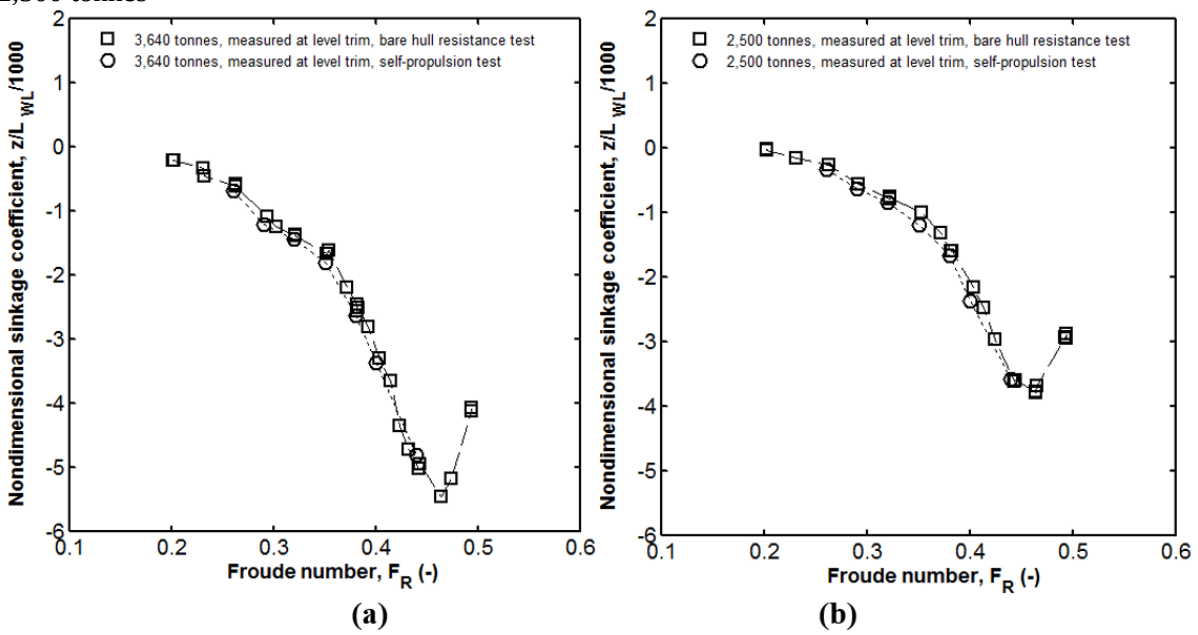


**Figure 5.17** The sinkage in dimensionless *z/L* with respect to the Froude number. Comparison of sinkage measured in bare hull resistance and self-propulsion test for; **(a)** 130m propeller driven catamaran at displacement of 3,640 tonnes **(b)** 130m propeller driven catamaran at displacement of 2,500 tonnes.

## 5.11 The running trim

The running trim was calculated by taking the inverse of the tangent of the variation of the measured forward sinkage, $z_{fwd}$ and aft sinkage $z_{aft}$ divided by the towing tank post distance. The running trim for the 130m propeller driven were plotted against Froude number as shown in Figure 5.18 (a) and (b). For clarification, the running trim in degree will be positive if the bow were raise up, and negative when the bow were pointing down. It was observed at low speeds there is a slight trim by the bow as compared with at rest condition. As speed increases the movement of the bow was further increased and at Froude number of 0.47 the bow begins to rise appreciably, the stern sinks still further and the catamaran takes on a decided trim by the stern. The maximum trim angle was at 1.33 and 1 degree for the catamaran at displacement of 3,640 and 2,500 tonnes respectively.

### The effects of the static trim to the running trim

The running trim angle was found to be lower when the bow were positively raised (bow up) or negatively pointed down (bow down), see Figure 5.18 (a) and 5.18 (b). At some point, especially at lower Froude number around 0.3 to 0.35, the running trim angle was negative. This happened in both heavy and light displacement of the 130m medium speed catamaran.

### Running trim at self-propulsion test

In Figure 5.19 (a) and 5.19 (b), the running trim measured in the self-propulsion test was found to be slightly higher than the running trim measured in the calm water resistance test. At higher Froude number ($F_r$ >0.45), the variation was found to decrease. This was observed for both heavy and light displacement medium speed catamaran.

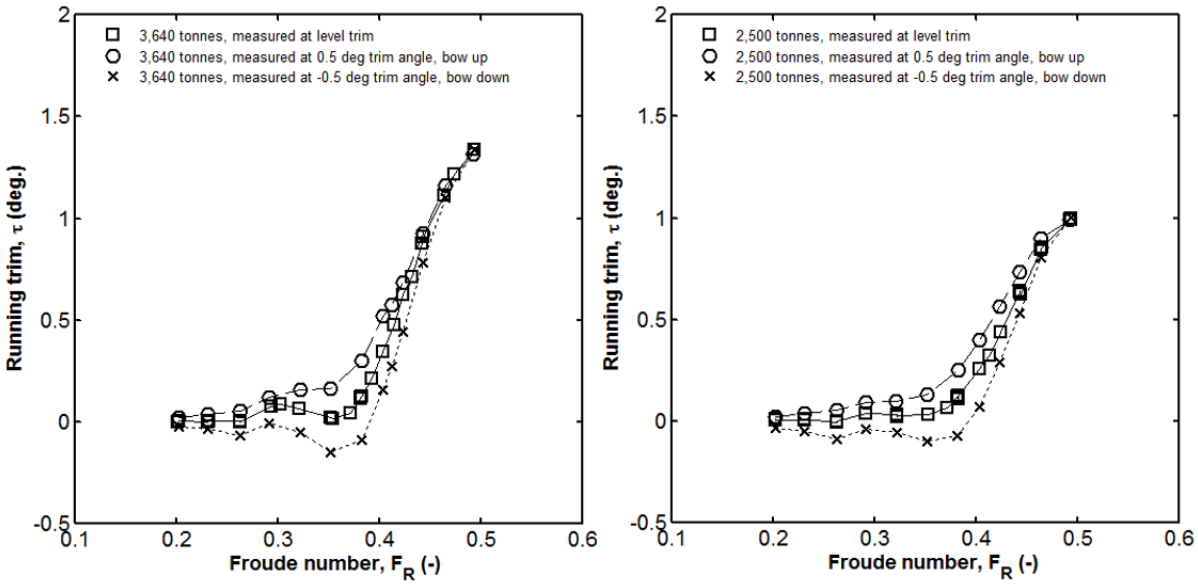


**(a)** **(b)**

**Figure 5.18** The effects of the static trim angle at rest to the running trim angle for **(a)** 130m propeller driven catamaran at displacement of 3,640 tonnes. **(b)** 130m propeller driven catamaran at displacement of 2,500 tonnes

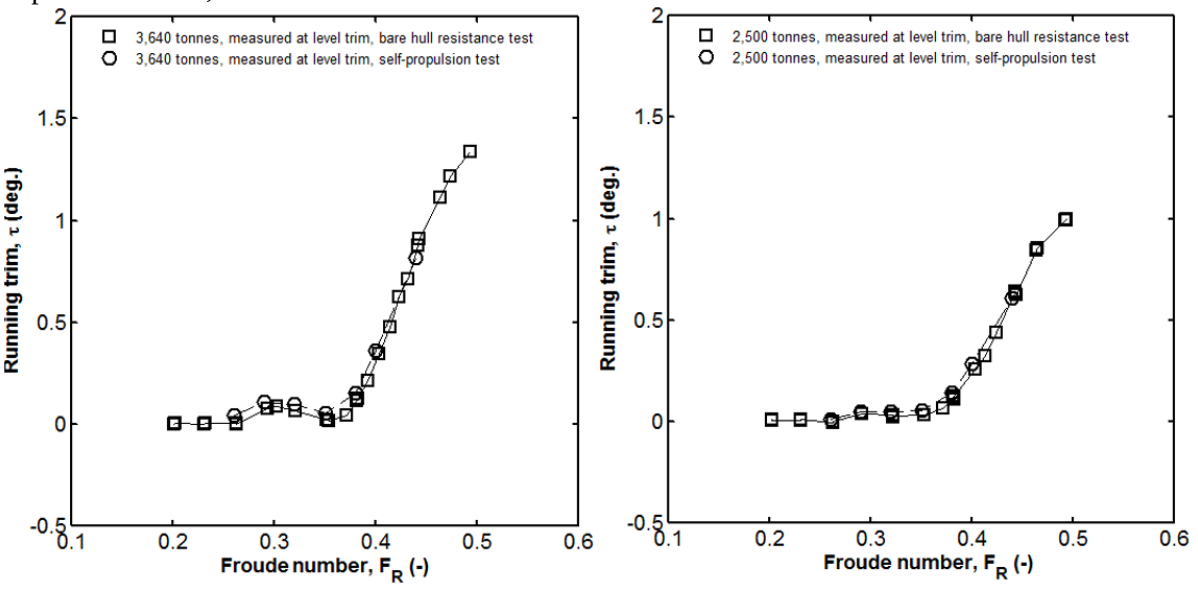


**(a)** **(b)**

**Figure 5.19** The running trim in degree with respect to the Froude number - comparison of sinkage measured in bare hull resistance and self-propulsion test for; **(a)** 130m propeller driven catamaran at a displacement of 3,640 tonnes **(b)** 130m propeller driven catamaran at a displacement of 2,500 tonnes

## 5.12 The modification of the extrapolation procedure

There are three changes or modifications in the SPT only method in order to make the prediction to full-scale, as shown in Figure 5.20. In this figure, the changes to the extrapolation procedure are highlighted in white. In this modified procedure, the wake scaling from RANS simulation was introduced. From the simulated nominal wake, the nominal wake fractions in model scale, $w_M$ and the wake scalings in full scale, $w_S$ are obtained. These wake scalings then will be the input for the advance coefficient for the full-scale propeller, where it is defined as $J_S = J\left(1-w_M\,/\,1-w_S\right)$.

In the second modification, the Grigson's line was chosen in favour of the ITTC57 correlation line as the *1 + k* using the ITTC57 correlation line increases substantially from model to ship as discussed in Raven et al. (2008), Eca and Hoekstra (2005), Garcia-Gomeza (2000) and Kouh et al. (2009). In Raven et al. (2008), CFD 'double-body flow' computations using the free-surface RANS code PARNASSOS investigating the scaling of viscous resistance were conducted. The viscous resistance of a containership 'Hamburg Test Case' and a tanker 'KVLCC2' were computed in model and in full scale. Then the computed viscous resistance coefficient were divided by the frictional resistance coefficient calculated using ITTC57 line, Grigson (1993) line and Katsui et al. (2005b) line to obtained the *1 + k*. The *1 + k* was found to be dependent of the Reynolds number using the three lines. Grigson's line shows less dependency on Reynolds number compared to ITTC57 line. One of the reasons on why *1 + k* using the Grigson's line was more consistent is that the ITTC57 line has a larger slope compared to the modern lines as proposed by Grigson (1993) and Katsui et al. (2005b). Raven et al. (2008) discussed that the ITTC57 line is higher than Grigson's line at lower Reynolds number. Grigson's line is higher than ITTC57 line at higher Reynolds number. Therefore using Grigson's line would produce a more consistent form factor than the ITTC57 line.

In the third modification, a method for propeller scale effect corrections from Benedek (1985) as explained in Chapter 3 was proposed. The Reynolds scale effect correction using the ITTC method which has been described by Lindgren et al. (1978) and Manen and Oossanen (1988) failed to provide a satisfactory correction to the small propeller used in the self-propulsion test, as explained in Chapter 3. The modification to the model propeller thrust and torque coefficients, to obtain the full-scale propeller thrust and torque coefficient, $K_{TS}$ and $K_{QS}$, are small compared to the correction proposed by Benedek (1985). Benedek's approximation is similar to Froude's method used to calculate the resistance of the ship. It was assumed that only the friction force coefficient on the blade surface is different on the propeller, as compared to its model and the pressure distribution along the blade section of the propeller and its model is considered similar. The decrease of the thrust coefficient is a function of the developed blade area, the differences in the frictional resistance coefficient on the blade surface, the advance coefficient and the geometrical pitch angle of the propeller. The increase

of the torque coefficient is also a function of the similar parameters as mentioned above. As explained in Chapter 3, the corrected coefficients using Benedek's method correlates better with the full-scale propeller coefficient.

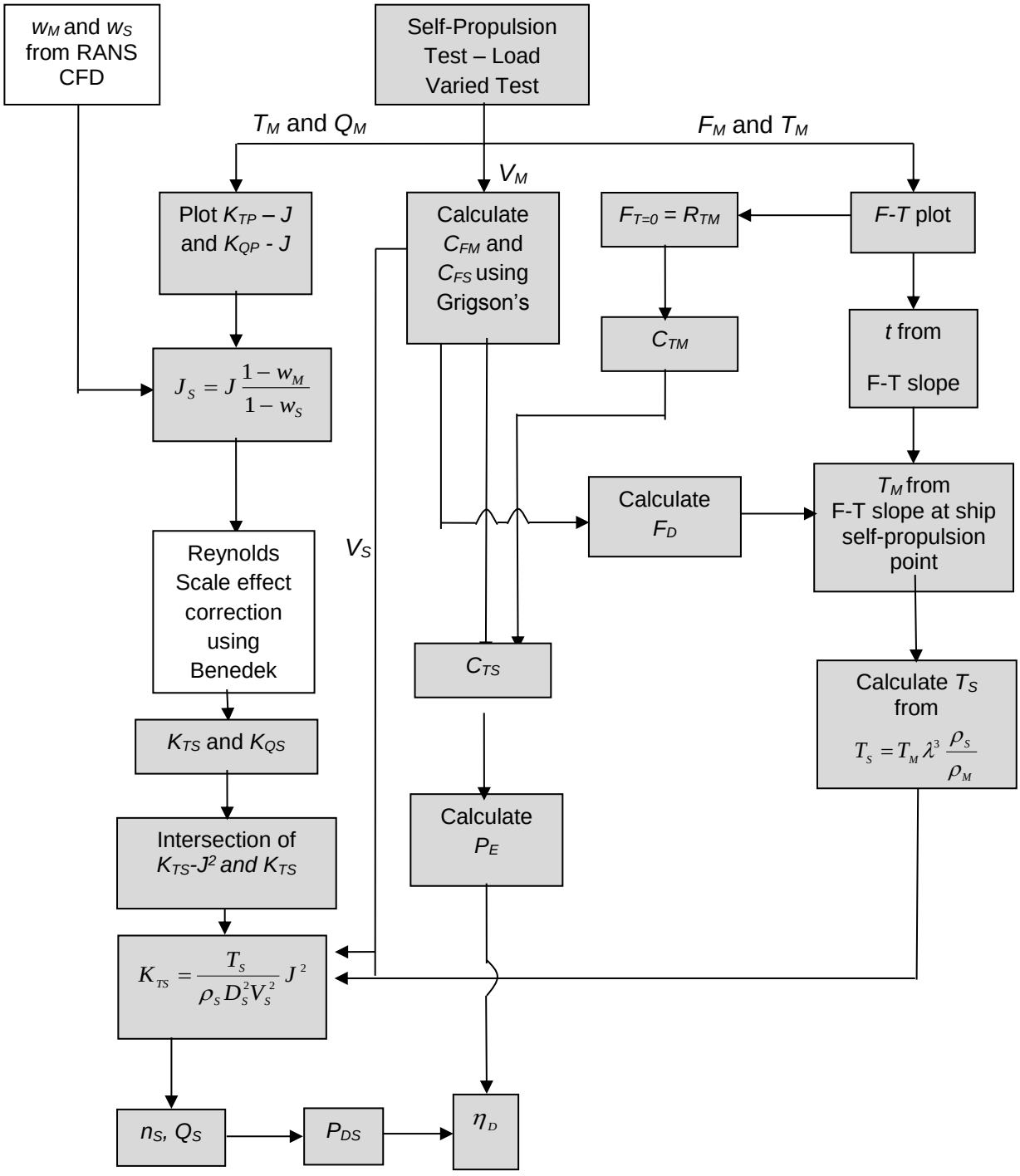


**Figure 5.20** Flowchart of the modified extrapolation procedure using the Self-Propulsion Test only method. The changes are (i) using wake scaling results from RANS (ii) using Benedek's scale effect correction for propeller thrust and torque as highlighted in white.

## 5.13 Summary

In this chapter, the results of the 130m propeller driven medium-speed catamaran were presented. The results presented in this chapter were for both heavy and light displacement of the vessel, 3,640 and 2,500 tonnes respectively. In extrapolating these results, two extrapolation methods were used, the first was the standard ITTC1978 method and the second was the method called the 'Self-propulsion test only' method or SPT method in short. The wake scaling needed for the inputs of the self-propulsion test only method was found from an in depth analysis of the results of RANS numerical simulation done on the medium-speed catamaran (Haase et al., 2012b).

The thrust deduction fraction obtained using the slope gradient from the *F-T* plot has significantly less variation with respect to Froude number than the thrust deduction fraction obtained using the recommended ITTC formula as given in Equation 5.4. The thrust deduction fraction obtained using the recommended ITTC procedure has a higher fraction at the lower Froude number range, and drops steeply at Froude number 0.35. The thrust deduction fractions from the load-varied test from the *F-T* slope were more accurate since it uses a linear curve fits to a multiple data points of the thrust with respect to the towing force plots thus significantly decreasing uncertainty in the final answer. This is far more accurate than getting the thrust deduction fraction from a single data point from the self-propulsion point of the ship in the self-propulsion point. Therefore based on this evidence, the thrust deduction fraction obtained from the slope equation was chosen for the extrapolation to full scale. The ITTC recommended procedure using the equation, $t = (T_M + F_D - R_C) / T_M$ does not work and should not be used in the extrapolation process for the medium-speed catamaran due to the inclusion of some uncertainties by introducing the resistance forces from a separate test.

The wake fraction scaling equation as proposed by ITTC (2014) does not work with small wake fractions due to the requirement to find intersection points on near parallel curves. Theoretically, the wake fraction in model scale should be larger than in full scale. The ITTC 1978 recommended wake scaling formula $w_{TS} = (t + 0.04) + (w_{TM} - t - 0.04).(1+ k) C_{FS} + \triangle C_F / (1 + k) C_{FM}$ as in the procedure 7.5-02-03-01.4, predicted higher wake fractions in the full scale than the wake fractions in the model scale. This is not physically plausible and is simply because the wake fractions in the model scale are too small and ending up presenting negative values. Therefore this ITTC 1978 recommended wake scaling procedure is not valid for the medium-speed catamaran powering prediction and it was never meant to work with this type of ship. Based on these experiences, further powering predictions will only be based on the CFD simulated wake fractions.

The delivered power obtained through the extrapolation using the self-propulsion test only method was higher than the predicted power extrapolated using the standard ITTC1978 method. The problem with the ITTC 1978 method is in the ship propeller operating point interpolation equation,

$K_T/J^2 = S_S.C_{TS}/2.D_S^2(1\text{-}t).(1\text{-}w_{TS})^2$. This equation used results from the three discrete tests. The $K_T/J^2$ is from the open water test, the $C_{TS}$ is from the calm water resistance test and the $(1 - t)$ and the $(1 - w_{TS})$ are from the self-propulsion test. In the SPT method which is based on the work of Holtrop (2001), Bose and Molloy (2001a), Schmiechen (1991) and Kracht (1991), the ship propeller operating point interpolation equation is obtained from $K_{TS}/ J^2 = T_S/2\rho D_S^2 V_S^2$. All the results for the input in the SPT method are only from the self-propulsion test. The ITTC1978 method in a way, ignored the interaction effects between the hull and the propeller in the behind condition. This is in contrast with the SPT method where the ship propeller operating point is found from the intersection of the required thrust coefficient with the ship propeller curve in the behind condition, where the interactions between the hull and propeller are not neglected.

The overall propulsive efficiency showed a decreasing trend as speed increases. The maximum efficiency is at 65% for the catamaran at displacement of 3,640 tonnes and 2,500 tonnes. The overall propulsive efficiency here shows that there is a certain dependency of the propulsive efficiency with the speed. As described by Holtrop (2001), this dependency is primarily governed by the loading of the propulsor. The behaviour of the overall propulsive efficiency curve is the opposite of the $C_{TM}$ curve which increases as the speed increases.

The Grigson's line was chosen in favour of the ITTC57 correlation line as to be consistent with the waterjet extrapolation which used Grigson's line. The other reason is that, the $1 + k$ using the ITTC57 correlation line increases substantially from model to ship as discussed in Raven et al. (2008), Eca and Hoekstra (2005), Garcia-Gomeza (2000) and Kouh et al. (2009). The $1 + k$ was found to be dependent of the Reynolds number using the ITTC57, Grigson's and Katsui lines. Raven et al. (2008) commented that the Grigson's line shows less dependency on Reynolds number compared to ITTC57 line. Therefore using Grigson's line would produce a more consistent form factor in model and in full scale than the ITTC57 line. When referring to all the extrapolated results in Chapter 6, Grigson's frictional line was used in the extrapolation procedure.

# Chapter 6

# Comparison with the waterjet propelled catamaran

## 6.1 Introduction

In this chapter, the results of the powering performance of the 130m propeller driven medium speed catamaran were compared against the 98m waterjet driven catamaran. The main aim of this exercise was to find a conclusion to the question, which propulsor is the most efficient for propelling a wave-piercing catamaran in the medium speed regime.

A comparison of full scale length to displacement ratio for the propeller and waterjet driven hulls shows that these vessels cannot be directly compared as the length to displacement and the wetted surface area ratios are not the same. In terms of length to displacement ratio, the 1,500 tonnes waterjet driven vessel and the 3,640 tonnes propeller driven vessel were the closest in ratios, 10.3 and 10.1 respectively. The 2,500 tonnes propeller driven vessel has a length to displacement ratio of 11.7, see Table 6.1.

In terms of the wetted surface area ratio, see Table 6.2, the 1,500 tonnes waterjet driven vessel and the 2,500 tonnes propeller driven vessel were identical in ratios, which is at 8.7. The length to displacement ratio was calculated using the ship waterline length divided by the displacement volume of the vessel powered by a one-third, $L_{WL}/\nabla^{(1/3)}$. The wetted surface ratios were calculated using the ship wetted surface area divided by the volumetric displacement by two-third or $S_S/\nabla^{(2/3)}$.

Therefore considering these facts, several approaches were made in order to assess the merit of the waterjet and the screw propeller as the propulsor for the medium-speed catamaran equally. These were based on three approaches, an approach using the propulsive efficiency, an approach using a transport efficiency and a transport factor and an approach using a scaling to a similar size method. The transport efficiency and transport factor approaches are thought to be necessary as the comparison in terms of propulsive efficiency is comparing only the hydrodynamic performances of both of the waterjet and propeller catamarans. This efficiency only accounts for the efficiency due to the flow physics, in terms of thrust developed by the propeller and the fact that the propeller acts behind the hull. The transport efficiency and the Telfer merit factor are efficiency representation of power-speed-deadweight relationship of a vessel. There is a difference between these two efficiencies, the propulsive efficiency and the transport efficiency. The first only accounts the dynamic similarity and the latter considered the dynamic similarity as well as the design similarity. In dynamic similarity

we are equalising the ratios of forces, but in design similarity we are looking at equalising the earning potential, which is correlated to the payload capacity of the vessel.

The results were also compared in terms of the residual drag, running trim and sinkage. The results of the 130m propeller driven catamaran were also compared against the result of the bare hull resistance test of the 130m waterjet hull tested by Duffy and Lilienthal (2010).

Further discussions were made in discussing which propulsor is the most efficient at medium-speed operation at the end of this chapter.

**Table 6.1** Length to displacement ratio showing that 1,500 and 3,640 tonnes had similar ratios.

| ***Propulsor*** | ***Displacement (t)*** | ***Length to displacement ratio*** |
|---|---|---|
| Waterjet | 1,500 | 10.3 |
| Waterjet | 1,804 | 9.5 |
| Propeller | 2,500 | 11.7 |
| Propeller | 3,640 | 10.1 |

**Table 6.2** Wetted surface ratio showing that 1,500 and 2,500 tonnes had similar ratios.

| ***Propulsor*** | ***Displacement (t)*** | ***Wetted surface ratio*** |
|---|---|---|
| Waterjet | 1,500 | 8.7 |
| Waterjet | 1,804 | 8.5 |
| Propeller | 2,500 | 8.7 |
| Propeller | 3,640 | 8.3 |

## 6.2 The towing force variation with respect to the thrust

Similar to the self-propulsion test of the propeller driven catamaran, the 98m waterjet driven catamaran was also tested using the load varying method or the 'British' method. The test was repeated so it operates at the under-load and the overload relative to the self-propulsion point of the ship. The plots of the towing force with respect to the thrust of the propeller driven catamaran were shown and explained earlier in the beginning in Chapter 5, 'Powering Performance of the Propeller Driven Catamaran'.

The plot of the towing force with respect to the thrust for the waterjet driven catamaran is shown in Figure 6.1. The self-propulsion tests were conducted by Zürcher (2015) at a displacement of 1,500 tonnes. The self-propulsion tests were conducted from Froude number 0.24 to 0.40. The plot was observed to be linear, similar to the plots of the propeller driven catamaran, although some of the slope seem to be set to be equal to the other lines. The linear fit as shown in Figure 6.1 could be

improved if more data were taken at lower shaft speeds, preferably more data until the linear fit line crosses the y-axis (towing force axis). By doing this the slope will have a better fit with additional data made available.

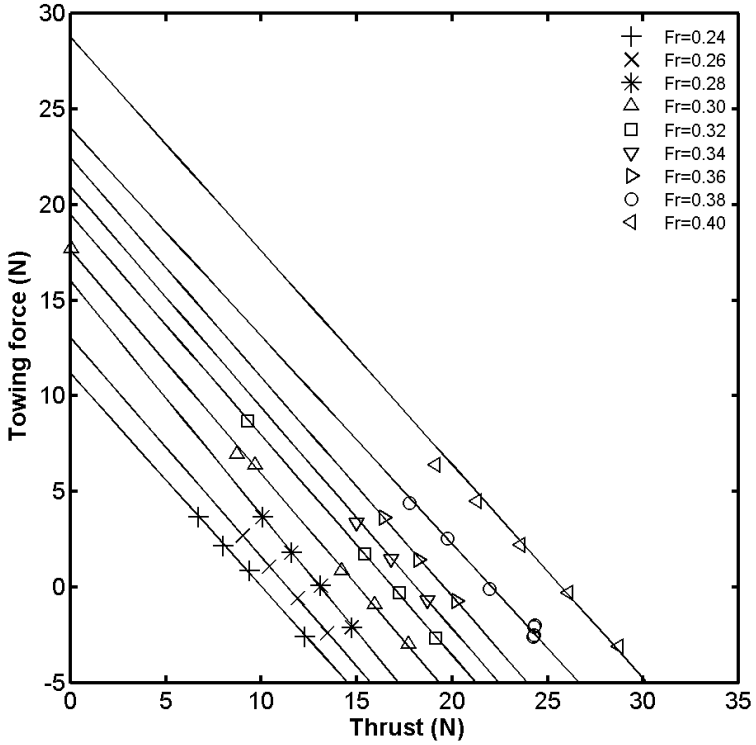


**Figure 6.1** Towing variation plotted with respect to variation in the thrust for the 98m waterjet driven catamaran with the displacement of 1,500 tonnes.

Important values from the waterjet towing force with respect to the thrust plots are the crossover of the thrust at zero resistance or zero towing force ($T_{F=0}$) and the intercept of the linear fitted curve with the y-axis defined as the zero thrust or thrust idling ($F_{T=0}$) (Zürcher, 2015). This crossover of the thrust at zero resistance ($T_{F=0}$) is the model self-propulsion point. The towing force, $F_D$ was then used to find the thrust corrected for skin friction which is then used to scale the model thrust to full scale thrust. This correction is necessary, because the normalised frictional resistance at model scale is larger than at full scale, hence an additional towing force $F_D$, has to be applied to the model. In applying the $F_D$ in the correction, Zurcher established the full-scale propulsion point by using the intersection of the towing force $F_D$ and the linear curve of the towing force and the thrust plots (using graphical method). In the SPT extrapolation method, the model thrust $T_M$ at the ship self-propulsion point was obtained using the formula $T_M = (F_{T=0} - F_D)/ (1 - t)$ from Kracht (1991), Iannone (2006), Molloy (2001) and Øyan (2012).

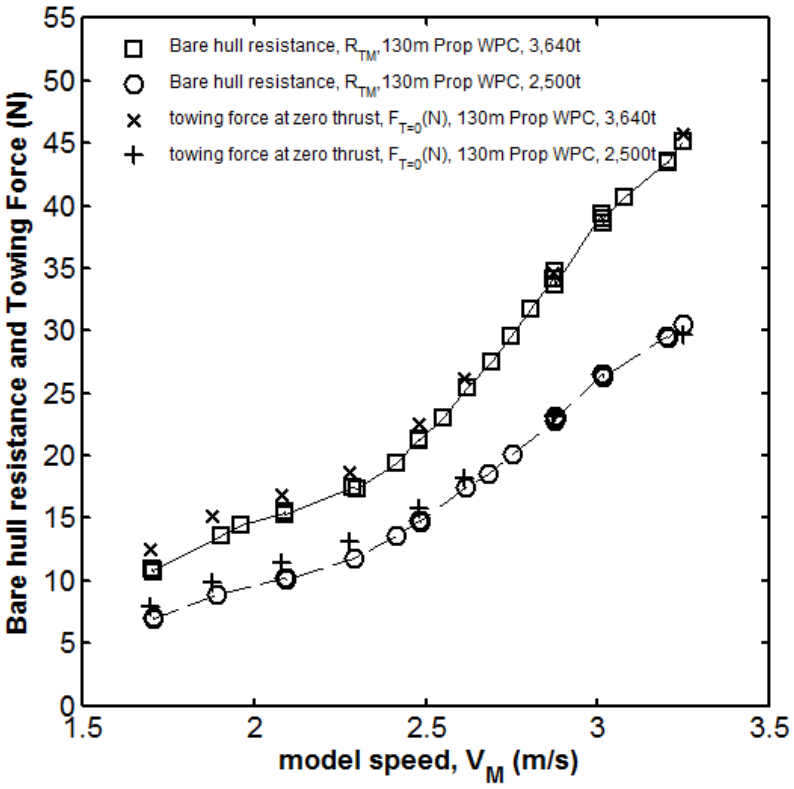


**Figure 6.2** Comparison plot showing results of the towing force measured in the self-propulsion test and the towed resistance measured in the bare-hull resistance test.

According to Bose (2008) the towing force at the zero thrust ($F_{T=0}$) in some cases has been found to be greater than the bare hull towed resistance conducted in the calm water resistance test. This was the case with the propeller driven catamaran, as shown in Figure 6.2. But this is not in the case of the waterjet catamaran, where Zürcher (2015) reported that the towing force at zero thrust ($F_{T=0}$) were below than the measured bare-hull resistance. The possible reason for this difference is due to the added drag from the rudder and the strut barrel or the propeller bracket. The wetted surface of the rudder and the propeller bracket is about 2 percent of the bare hull of the propeller catamaran. The increase in resistance in the results taken from the towing force of the self-propulsion test amounted to 2 to 13 percent. Lap (1956) in his investigation in MARIN on a number of twin-screw 6m models with shafts and bossing reported that there were increases in resistance in his investigation which amounted to some 5 to 9 percent. Mandel (1953) presented a data on appendage resistance as a percentage of bare-hull resistance for five types of ship, at three Froude numbers. He reported that for a large, medium-speed, twin screw ships at Froude number 0.208 and 0.298 with all customary appendages, the percentage increase amounted to some 8 to 14 percent.

## 6.3 The thrust deduction fraction

There is no reason why the thrust deduction should be the same for the propeller and the waterjet catamaran as they are being modelled very differently. It should be noted that this comparison is not valid as there are differences in the definition between the thrust deduction fraction for the waterjet and propeller case. In a propeller propelled vessel, the thrust deduction fraction is defined as the ratio between the towing force and the net thrust, where the net thrust is the force transmitted through the propeller shaft. In a waterjet driven vessel, it is not only the impeller shaft transmitting the thrust force to the hull but a fraction of the thrust is also transferred to the hull through the waterjet nozzle and for this reason; the gross thrust is used for the calculation of the thrust deduction fraction for a waterjet propelled vessel. The calculations for the waterjet were calculated by Zürcher (2015) using two types of thrust deduction calculations. The first equation used by Zürcher (2015) is $t = 1 - (F_{T=0} - F_M)/T_M$, where $F_{T=0}$ is the force at zero thrust, $F_M$ is the towing force and $T_M$ is the thrust at the model self-propulsion point which were found using the results of the self-propulsion test. The second equation used by Zürcher (2015) is $t = 1 - (R_{BH})/T_G$, where $R_{BH}$ is the bare-hull resistance and $T_G$ is the gross thrust which were found using the results from the bare-hull resistance test and the self-propulsion point. Thus, it is not useful to compare these two thrust deduction fractions together. However, both of these thrust deduction fractions were presented here, as to show the general trend of the thrust deduction fraction with respect to the Froude number.

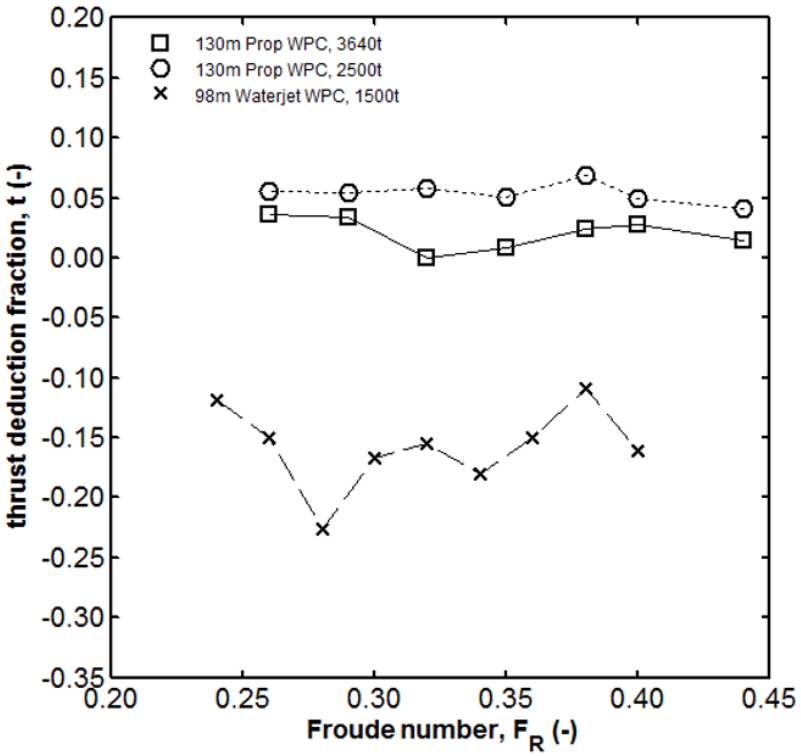


**Figure 6.3** The thrust deduction fractions with respect to the Froude number for the waterjet and propeller propelled catamaran. All of the thrust deduction fractions were calculated using the slope method (Equation 5.2).

In Figure 6.3, the thrust deduction fraction of the propeller driven catamaran ranged from 0.00 to 0.06 depending on the Froude number. The results for the waterjet driven catamaran were negative and range from -0.34 to -0.10, as shown in Figure 6.3. These results were obtained using the slope of the thrust and towing force's regression line. The thrust deduction fractions of the propeller driven vessel were positive as mentioned in Chapter 5. The thrust deduction fractions for both catamarans were obtained using the slope method (using Equation 5.2, Chapter 5).

One reason for the negative values of the thrust deduction fractions may be due to the larger hull transom submergence for the waterjet case. Increasing the submergence of the dry transom increases its hull resistance, thus increasing the slope – *(1 - t)*. As slope – *(1 - t)* increases, the thrust deduction fraction decreases and in some cases negative thrust deduction is observed. Another probable reason is there are forces on the duct of the waterjet that reduce the trim. The common used definition of thrust deduction fraction for waterjet is $t = 1 - (R_{BH}/T_G)$, where $R_{BH}$ and $T_G$ are the bare hull resistance and the gross thrust of the waterjet respectively. When the force on the duct of the waterjet reduce the trim, the gross thrust reduced as the resistance of the hull reduced due to the favourable trim. Hence, the bare hull resistance, $R_{BH}$ will be larger than the gross thrust, $T_G$. Therefore this is why negative thrust deduction is observed.

However the low thrust deduction fractions found in Zürcher (2015) are partially due to errors in the estimation of flow rate as commented in Mustaffa Kamal et al. (2015). The jet flow rate measured by Zürcher (2015) was based on a combination of the static flow measurement test using a tank and the self-propulsion test. The two tests were combined using a reference measurement which used Kiel probes at the nozzle outlet. Estimated errors were found to be at 4% at low shaft speed and at 2% at high shaft speed. More explanation on the estimated errors using uncertainty analysis can be found in Zürcher (2015). Other studies that reported the negative thrust deduction fraction can be found in Svensson (1989), Coop (1995), Terwisga (1996), Eslamdoost (2012), Eslamdoost (2014) and Eslamdoost et al. (2015).

Svensson (1989) has made some interesting comments on the negative thrust deduction fraction. He quoted that the thrust combined with the natural dynamic trim creates an additional aft trim increasing the hull resistance, especially at low speed. Svensson (1989) added that another sources of the negative thrust deduction fraction are influenced by the downforce or the lifting force from the waterjet inlet or the surrounding bottom plating. He reported that the *"The pressure distribution on the bottom plating of the vessel is strongly influenced by the action of the inlets. When the water flow through the inlet is large in relation to the ship speed there is a downward force from the inlet. However, this force is more than balanced by a lifting force on the surrounding bottom plating. When the flow rate is low compared to the vessel speed the inlet creates a substantial lifting force. In this condition the bottom plating contributes less to the lifting force. Thus, the design of the inlet is extremely important to get an optimum performance. The total lifting force generated by the inlets can be in excess of 5% of the displacement for a high speed craft. The lifting force can thus*

*exceed the weight of the units. This will be recognised as a negative thrust deduction reducing vessel resistance."*

Coop (1995) discovered that the line of thrust i.e. where to apply the tow rope pull and in what direction to pull, also affects the thrust deduction fraction. A different towing position effectively changes the LCG and the static displacement. These changes influence the resistance and the thrust deduction fraction. Coop (1995) compared the thrust deduction results with three different towing positions namely (1) the ITTC recommended towing position, (2) MARIN towing position and (3) the net thrust line towing position. The ITTC recommended to use the shaft line where the choice of the shaft line was originated from the conventional screw propeller arrangement where the assumption that the thrust force is primarily applied along the shaft (Savitsky et al., 1987). Sometimes this is not the case in the waterjet line of thrust. In MARIN, the model is towed horizontally through the centre of gravity of the model. In the net thrust line case, the line of thrust is applied through the incoming momentum flux vector which is normally at some distance and a greater angle than the shaft line. Negative thrust deduction fractions are evident in the ITTC and MARIN recommended towing position. The ITTC convention of towing along the shaft line, yielded the most negative thrust deduction fractions, where the negative thrust deduction fractions up to -8% are evident in the hump region for certain towing positions.

Negative thrust deduction fractions were also reported by van Terwisga (1996), Eslamdoost (2012) and Eslamdoost (2014) when using a definition of thrust deduction fraction based on the gross thrust defined as $t = 1 - (R_{BH} / T_G)$. The thrust deductions fractions computed by Eslamdoost (2014) were as low as -0.1 and not as negative as found by Zürcher (2015) as shown here in this thesis.

Eslamdoost et al. (2015) commented that the resistance reduction is not the main source that contributes to the negative thrust deduction. In his study, a numerical method using a RANS solver was employed to study the bare hull and the self-propelled hull resistance. The aim was to investigate whether it is the waterjet hull resistance decrease that contributes to the negative thrust deduction fraction or there are some other effects rather than the resistance increment. It was found from his investigation that there was just a minor change in the resistance of the self-propelled hull compared to the bare hull resistance. Therefore Eslamdoost et al. (2015) concluded that the resistance increment cannot be considered as the main source of the negative thrust deduction fraction. In fact the negative thrust deduction fractions are due to the difference between the net thrust and the gross thrust of the waterjet system. This is mostly due to the non-atmospheric pressure at the nozzle exit. By integrating the non-atmospheric pressure over the nozzle area, a negative exit drag was obtained, where the computed exit drag at Froude number 0.8 is at -10.28N. It was found that the exit drag the nozzle exit has a larger magnitude than the magnitude of the intake drag. It should be noted that the sum of the intake and exit drag is the difference between the gross thrust and the net thrust. As the summation of the intake and the exit drag is negative therefore there is a negative difference between the gross thrust

and the net thrust. The differences between the gross thrust and the net thrust of the waterjet system according to Eslamdoost et al. (2015) are the reasons for the negative thrust deduction fraction.

## 6.4 The propulsive efficiency comparison

It is important to ensure that the definitions for the propulsive efficiency for both propulsion systems are identical for this comparative study. By convention, the propulsive efficiency is defined as the efficiency of the whole propulsion system without taking into account all the mechanical losses in the gearing and the bearings. In this thesis only the hydrodynamic efficiency will be considered without taking into account other efficiencies such as the shaft efficiency and other mechanical losses as mentioned above. Zürcher (2015) in his thesis, described the propulsive efficiency for the waterjet system as

$$\eta_D = \eta_O \eta_{INT} \tag{6.1}$$

where $\eta_O$ is the free-stream efficiency and $\eta_{INT}$ is the total interaction efficiency. This is similar to the propeller driven vessel propulsive efficiency which is defined as

$$\eta_D = \eta_O \eta_H \eta_R \tag{6.2}$$

where the $\eta_O$ is defined as the propeller open water efficiency, $\eta_H$ is the hull efficiency and $\eta_R$ is the relative rotative efficiency. The free-stream efficiency in Equation 6.1 can be identified as the open water efficiency and the total interaction efficiency can be identified as similar to the product of the hull and the relative rotative efficiency.

The propulsive efficiency as in equation 6.2 is originally expanded from the propulsive efficiency in the standard form as shown in Equation 6.3 (Manen & Oossanen, 1988). The propulsive efficiency $\eta_D$, which is also known as the Quasi-Propulsive Coefficient (*QPC*), of the propeller and the waterjet driven catamaran is based on the standard definition of the *QPC*; where it is defined as

$$\eta_D = \frac{P_E}{P_D} \tag{6.3}$$

where $P_E$ is the effective power and $P_D$ is the delivered power. The effective power in the propeller driven vessel is defined as $P_E$ = ½ $C_{TS}$ $\rho_S$ $S_S$ $V_S^3$. The delivered power in the propeller driven catamaran case is defined as

$$P_D = 2\pi\rho D_S^5 n_S^3 K_{QS} \tag{6.4}$$

where $C_{TS}$ is the total ship drag coefficient, $S_S$ is the ship wetted surface area, $V_S$ is the ship speed, $D_S$ is the propeller diameter, $n_S$ is the shaft rotation speed and $K_{QS}$ is the propeller torque coefficient. Therefore, the propulsive efficiency for the propeller driven catamaran can be written as;

$$\eta_D = \frac{C_{TS} S_S V_S^3}{4\pi D_S^5 n_S^3 K_{QS}} \tag{6.5}$$

Equation 6.5 was used for the propulsive efficiency of the propeller driven catamaran.

Zürcher (2015) defined the propulsive efficiency for the waterjet catamaran using the similar equation as in Equation 6.3. Then he expanded the equation into Equation 6.5. In the waterjet powering calculation, the delivered power, $P_D$, was calculated by Zürcher (2015) using the effective pump power, $P_{PE}$, pump efficiency, $\eta_{Pump}$ ,installation efficiency, $\eta_{Inst}$ energy flux at station 7, $E_7$, energy flux at station 1, $E_1$, nozzle efficiency, $\eta_n$, inlet efficiency $\eta_i$ and outlet loss factor between station 5 and 7, $\zeta_{57}$. Further details on the energy flux and stations location on  where each of the energy flux were being calculated can be found in Zürcher (2015).

$$P_D = \frac{P_{PE}}{\eta_{Pump}\eta_{Inst}} = \frac{E_7(1-\zeta_{57}) - \eta_i E_1}{\eta_{Pump}\eta_{Inst}} \tag{6.6}$$

It was suggested by Alexander (1995) to compare waterjets and propeller with the same terms of propulsive efficiency, where the propulsive efficiency needs to be defined in simple terms using the bare hull resistance only, without the appendage drag included. The effective power, $P_E$ can be calculated either using the bare hull resistance data where $P_E = R_{BH}.V$ or using the towing force data at zero thrust, $F_{T=0}$ from the self-propulsion test, where $P_E = F_{T=0}.V$. Therefore to make an equal comparison between the waterjet and the propeller driven vessel, the results of the propulsive efficiency of the waterjet and propeller driven catamaran using the barehull resistance were chosen for this comparative study.

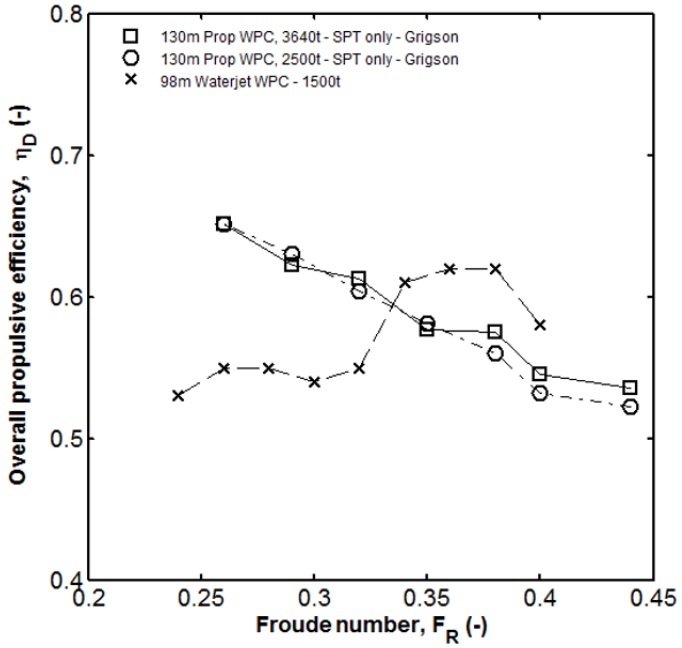


**Figure 6.4** The propulsive efficiency with respect to the Froude number. This plot shows the results for the propeller driven and the waterjet driven catamaran.

In Figure 6.4, the plot of the propulsive efficiency with respect to the Froude number for the 130m propeller driven and the 98m waterjet driven catamaran are shown. The results of the 98m waterjet catamaran and the 130m propeller driven catamaran were extrapolated using correlation allowance $C_A = 0.00035$ (Marin, 2008). The maximum efficiency of the propeller driven catamaran is at 65% at Froude number $F_n = 0.26$ which is equivalent to 18 knots at full scale. The maximum efficiency for the waterjet driven catamaran is at 62% at Froude number $F_n = 0.38$ which is equivalent to 22.4 knots in full scale. At Froude number 0.33, the waterjet and the propeller propulsion have equal propulsive efficiency. The waterjet vessel starts to become more efficient than the propeller catamaran beyond Froude number 0.33. Beyond Froude number 0.33, the propulsive efficiency for the propeller driven catamaran drops from 62% to 53% at Froude number 0.44. Beyond Froude number 0.33, the efficiency of the waterjet driven hull increases up to 62% at Froude number 0.38, before dropping to 58% at Froude number 0.40.

In this comparative study, it was clearly demonstrated that the propeller driven catamaran has a better propulsive efficiency than the waterjet driven catamaran, up to Froude number 0.33. Beyond this Froude number, the propeller catamaran has a higher power requirement than the waterjet propulsion. These results are heavily influenced on the way these both hulls being optimised. The 98m hull was optimised for operation well above the hump resistance and the 130m hull was optimised for operation below the hump. That is the propeller catamaran is more efficient at these slow speeds, but the waterjet catamaran was never designed to go at these low Froude numbers. This will be further discussed and presented in the section 'The residual resistance comparison'.

It was concluded that the 130m propeller driven catamaran performs better in terms of propulsive efficiency than the 98m propeller waterjet catamaran in this lower speed regime below Froude number 0.33.

The variations in resistance with respect to Froude number are due to the required volumetric variations to accommodate the propulsion system variation, resulting from the fact that the 98m hull design was optimised for operation well above hump and the 130m hull was optimised for operation below hump and this may have some influence on the results. The drawbacks with a waterjet hull is the need of excessive transom immersion to keep the waterjet units deep enough below the waterline in order to allow for the waterjet unit to prime. This certainly has a negative effect on the resistance below the hump. Haase et al. (2012a) reviewed investigations on the effects of transom immersion on residuary resistance notably from Fry and Graul (1972), Hadler et al. (2007) and Hadler et al. (2009). Hadler et al. (2009) investigated different transom immersion ratios of the transom stern area over the maximum section area, $A_T/A_X$ which were varied from 1.0 to 0.1. Haase et al. (2012a) in his review concluded that a smaller immersion reduces the residuary resistance of a ship. The 98m waterjet hull has a transom immersion ratio $A_T/A_X$ of 0.69 and the 130m propeller hull has transom immersion ratios $A_T/A_X$ of 0.46 and 0.28 for displacement at 3,640 tonnes and 2.500 tonnes respectively.

The difference in the propulsive efficiency is Froude number dependent and does not take into consideration the power to deadweight ratio. Therefore to make a conclusion on the actual performance we need to look at more complex methods of comparison. The rest of the analysis in this chapter is devoted to this question.

## 6.5 The delivered power and shaft speed

As a first step to attain an equal comparison, the waterjet and propeller vessels were compared by the scaled powering requirements i.e. the delivered power. This provides potential designers with valuable initial design information. The shaft speed for both waterjet and propeller propulsion were also compared as to attain some insight on the magnitude of the rotational speed for the waterjet and propeller propulsion system.

The extrapolated delivered power for the propeller driven catamaran was calculated using Equation 6.4. The delivered power for the waterjet hull was calculated by Zürcher (2015) using Equation 6.6. The powering results had been calculated for the waterjet catamaran using the measurements of the waterjet self-propulsion tests. These results are shown in Figure 6.5. The delivered power for the 1,500 tonnes waterjet driven catamaran were found to be in between 2.8 MW to 11.78MW for Froude number ranged from 0.24 to 0.40. The delivered power for the 3,640 tonnes propeller catamaran were found to be in between 9.5MW and 38.9MW. The delivered power for the 2,500 tonnes propeller catamaran were found to be in between 3.9 MW and 25MW.

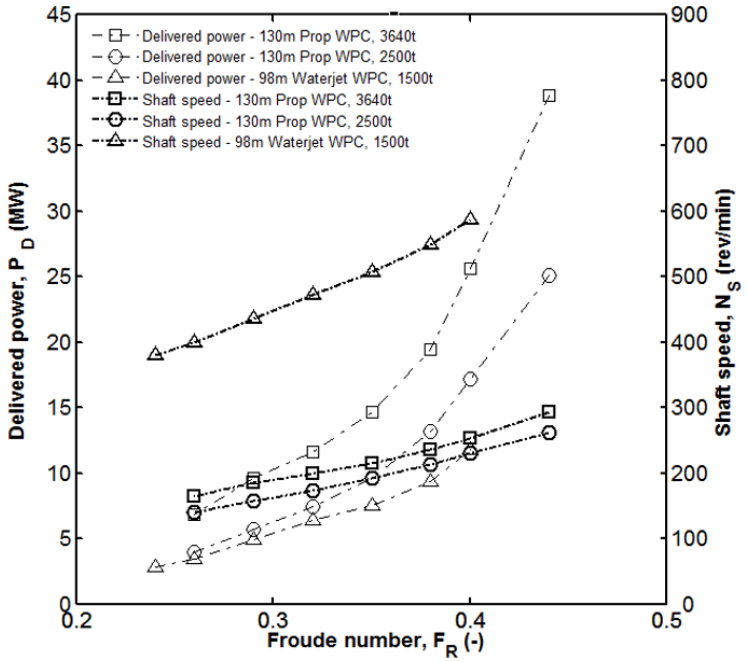


**Figure 6.5** The delivered power and the shaft speed of the propeller driven catamaran and the waterjet driven catamaran. The shaft speed was plotted with bold lines.

The shaft speeds of the propeller driven catamaran were found to be in between 164 rev/min and 293 rev/min for the vessel at a displacement of 3,640 tonnes. The light displacement, 2,500 tonnes vessel's shaft speeds were found to be in between 140 rev/min and 261 rev/min. The waterjet unit required a higher shaft revolution rate than the screw propulsion unit. The shaft speeds of the waterjet vessel were higher, ranged from 381 rev/min to 587 rev/min.

The reason for the waterjet unit operating at a significantly higher rotational speed is that the waterjet unit impellers have a significantly smaller blade area then the equivalent propeller vessel. The shaft revolutions in the waterjet unit were closely related to the power absorption and the impeller rating as explained by Alexander (1995). The power absorbed by the waterjet unit acting as a pump as a function of the shaft revolution follows approximately a cubic law. In contrast, with a screw propeller, the power absorption for a screw propeller follows approximately an absorption law of 2.7 or 3 (Molland et al., 2011, p. 299, p. 299). Hence, to maintain the same power absorption, a waterjet normally requires a higher shaft revolution. In reducing wear and tear of the propulsion machinery of a vessel, a designer may opt for the lower shaft speed option in his design. The propeller propulsion seems to be the better choice here.

From this developed study it is clear that the two systems (waterjet and propeller) are significantly different in terms of the powering and machinery requirements. However, as above, the points at which a designer should consider one over the other are not clear.

## 6.6 The transport efficiency comparison

One of the challenges in this work is making an equivalent comparison between two dissimilar hulls (waterjet and propeller driven hull). Therefore, it is necessary that a performance index is defined to ensure the equivalent comparison is achieved. The performance index of transport efficiency was used in assessing the powering performance merit of both of the propeller and waterjet driven catamarans. Transport efficiency was used to ensure that the assessment of the two catamarans was done on a 'fair' basis. The transport efficiency of a marine vehicle may be defined in various ways and series of researchers have addressed this in the past, such as Akagi (1991), Kennell (1998), Akagi and Morishita (2001), Papanikolaou et al. (2001) and Papanikolaou (2014).

The transport efficiency, *TE* used in this research used the similar approach used by Akagi (1991) as reported by Papanikolaou (2014). The transport efficiency was slightly modified by making it dimensionless by multiplying the nominator with the gravitational acceleration, $g$ in m/s$^2$:

$$TE = \frac{W_D V_{S.} g}{P_D} \tag{6.7}$$

where $P_D$ is the delivered power in kg.m$^2$.s$^{-3}$ or watts, $W_D$ is the displacement in kg and $V_S$ is the vessel speed in m/s.

The transport efficiency (using Equation 6.7) is effectively increased by;

(1) Increasing displacement, $W$ in the movement through the water.

(2) Increasing ship speed $V_S$.

(3) Reducing shaft power $P_S$ or delivered power $P_D$

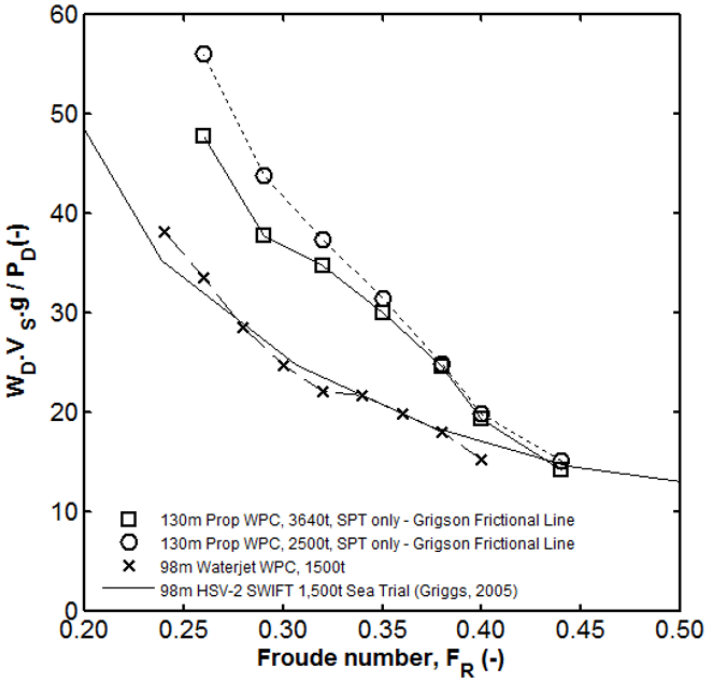


**Figure 6.6** The transport efficiency using equation 6.8, SPT only method and Grigson's Frictional line.

The results of the 130m propeller driven catamaran were presented in transport efficiency using Equation 6.7 are shown in Figure 6.6. These results used the results of the delivered power extrapolated using the SPT only extrapolation method with the Grigson's frictional lines. These results were compared with the 98m waterjet driven catamaran and the 98m HSV-2 Swift powering trial results (Griggs, 2005). The only full scale data that are available is only for the 98m waterjet hull. There are no full scale data for the 130m propeller driven hull as the full scale vessel does not exist. The plots show that the transport efficiency decreased as speed increases. The propeller driven catamaran has larger transport efficiency than the waterjet driven catamaran ranged from 50% to 2.8% depending on the Froude number. Beyond Froude number 0.44, the transport efficiency of the propeller driven catamaran is lower than the transport efficiency of the waterjet hull. This means that the propeller driven catamaran, can carry more weight and with greater ship speed in its movement through the water for a lesser shaft power than the waterjet driven catamaran. Therefore, it can be concluded that in terms of transport efficiency, the waterjet catamaran starts to perform better than the propeller driven catamaran at Froude number 0.44.

As mentioned earlier, to effectively maximise the transport efficiency, the shaft power or the delivered power per deadweight carried must be minimised. This could be achieved by optimising the

hull design for the operation in the medium speed regime. The waterjet catamaran hull was never designed to operate in the medium speed regime, and more suited for high speed regime. Some design recommendations for reducing resistance for medium-speed catamarans can be found in Haase et al. (2012a). Haase suggested that for catamarans operating at Froude number 0.35, a prismatic coefficient, $C_p$ of 0.5 and block coefficient, $C_B$ of 0.4 would be ideal.

## 6.7 Using Telfer's Transport Merit Factor

According to Saunders (1957b), a criterion that can be used to rate ship powering performance, is the Admiralty coefficient, which is given in the form of $(W^{2/3} V^3)/P_E$ or $(W^{2/3} V^3)/P_S$. There is also another variation of Admiralty coefficient, which was proposed by Telfer (1933) and Lammeren (1948). This Telfer merit factor is a combination of the displacement weight $W$, the ship speed $V$, the ship length $L$, and the shaft power $P_S$ or using the delivered power $P_D$. This Telfer merit factor can be written as,

$$\textit{Telfer Merit Factor} = \left(\frac{WV}{P_S}\right)\left(\frac{V}{\sqrt{gL}}\right)^2 = \left(\frac{WV^3}{gLP_S}\right) \tag{6.9}$$

In accordance with Saunders (1957b), if imperial units are used with pound-force, the Telfer merit factor is dimensionless, but it appears that in equation 6.9, where $W$ is in tonnes, $V$ in m/s, $L$ in metre, and $P_S$ in kW, this factor would leave a dimension of $s^2/m$. In order to make this factor to be dimensionless, the gravitational acceleration $g$ will be omitted from the equation. Therefore, equation 6.9 becomes,

$$\text{Telfer Merit Factor*} = \frac{WV^3}{PL} \tag{6.10}$$

This transport factor is increased, by:

(1) Increasing displacement, $W$ in the movement through the water.
(2) The attainment of a greater ship speed $V_S$.
(3) A decrease in the ship length $L$
(4) The movement of the weight $W$ at the speed $V$ by a lesser shaft power $P_S$ or delivered power $P_D$

Essentially the Telfer's merit factor will increase for a short boat which is fast for low power. This does produce an improved vessel in terms of its reduced construction and maintenance costs (largely proportional to length) and increased earning potential, largely by maximising the amount of cargo and the speed at which it is transported at.

The transport factor expressed in equation 6.10 was applied as to make an assessment to the powering performance of the two dissimilar catamarans, as plotted in Figure 6.7. These results were

extrapolated using the self-propulsion test only method with the Grigson's frictional lines. These results were compared with the 98m waterjet driven catamaran. The plots show that the propeller driven catamaran has a larger transport factor than the waterjet driven catamaran up to Froude number 0.45. The transport factors of the propeller driven catamaran were ranged from 2.7 to 3.9 depending on the Froude number. For the waterjet driven catamaran, the transport factor was lower, ranging from 2.2 to 2.6. This indicates that the waterjet driven medium speed catamaran need more power than the propeller driven catamaran to move through the water for a similar given displacement and speed below Froude number 0.45.

There is a crossover of the transport factor curve for the 98m HSV-2 waterjet sea trial results and the propeller catamaran at Froude number 0.44, Beyond Froude number 0.44 the waterjets propulsion begins to have more advantage over the propeller propulsion. Comparing Figure 6.7 and Figure 6.8, it can be seen that regardless of merit function, the cross over between waterjet and propeller under the conditions applied occurs at Froude numbers approximately equal to 0.44.

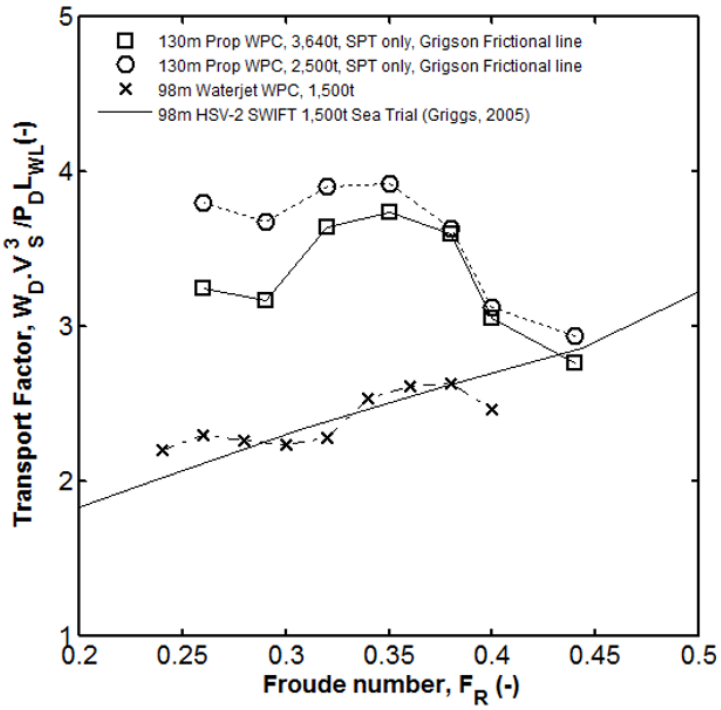


**Figure 6.7** The transport factor with respect to the Froude number. The transport factor used the results extrapolated using SPT only method and Grigson frictional line.

## 6.8 A case study - Extrapolating the propeller driven catamaran to a full-scale 98m vessel

The extrapolation methods used earlier were intended to convert the model test results to a full-scale 130m length catamaran. To further investigate the relative merits of the two designs (the propeller and the waterjet), an additional design scenario was constructed whereby the two vessels were scaled to a similar size. There were two case scenarios chosen for this study, Case 1 was made to

be similar in the weight displacement and Case 2 was made to be similar in the waterline length. The scale ratios used were 21.56 and 21.98 for Case 1 and Case 2 respectively. Hence the model single demihull catamaran was scaled up to a displacement of 1,500 tonnes full scale and 1,589 tonnes full scale. The main particulars of the Case 1 and Case 2 scaled vessel were tabulated in Table 6.3. The comparison of the three scaled vessels was plotted in (1) The delivered power, (2) The overall propulsive efficiency, (3) The Transport Efficiency and (4) The Telfer Merit Factor. In this case study, the extrapolation using the SPT method using Grigson's frictional line was used.

In Figure 6.8, it can be seen that the extrapolated delivered power of the 98m waterjet driven catamaran was higher than the delivered power of the propeller driven catamaran (Case 1 and Case 2) with differences from 11% to 39% depending on the Froude number. In Figure 6.9, the overall propulsive efficiency of the 91.13m 1,500 tonnes propeller driven vessel (Case 1) ranging from 54% to 65% depending on the Froude number. The 92.9m 1,589 tonnes vessel (Case 2) has the same efficiency trend as the 91.13m 1,500 tonnes catamaran. At Froude number 0.33, the waterjet and the propeller propulsion have equal propulsive efficiency. The waterjet vessel starts to become more efficient than the propeller catamaran beyond Froude number 0.33 similar to the finding in the comparative study between the 130m propeller driven and the waterjet driven catamaran in section 6.4. It was clearly demonstrated again that the propeller driven catamaran in Case 1 and Case 2 have a better propulsive efficiency than the waterjet driven catamaran, up to Froude number 0.33. Beyond this Froude number, the propeller catamaran has a higher power requirement than the waterjet propulsion.

**Table 6.3** The main particulars of the 98m full scale propeller driven catamaran with displacements of 1,500 tonnes (Case 1) and 1,589 tonnes (Case 2). Case 1 was set to be similar in the weight displacement. Case 2 was set to be similar in the waterline length, see the shaded cell.

| | ***98m Waterjet driven WPC (1500 tonnes)*** | | ***Case 1: Propeller driven WPC, extrapolated to 91.13m, 1500 tonnes*** | | ***Case 2: Propeller driven WPC, extrapolated to 92.9m, 1589 tonnes*** | |
|---|---|---|---|---|---|---|
| **Particular** | **FS** | **MS** | **FS** | **MS** | **FS** | **MS** |
| $L_{WL}$ (m) | **92.9** | 4.30 | 91.13 | 4.227 | **92.9** | 4.227 |
| $B_{WL,\,DH}$ (m) | 4.50 | 0.210 | 4.76 | 0.221 | 4.86 | 0.221 |
| $T$ (m) | 3.3 | 0.15 | 3.04 | 0.141 | 3.10 | 0.141 |
| $WSA$ ($m^2$) | 704.5 | 1.51 | 672.6 | 1.447 | 699 | 1.447 |
| $\Delta$ (t, Kg) | **1,500** | 145 | **1,500** | 146 | 1,589 | 146 |
| s/L (m) | 0.238 | | 0.200 | | 0.200 | |
| $\lambda$ (-) | 21.6 | | 21.56 | | 21.98 | |

In Figure 6.10, the transport efficiency of the Case 1 and Case 2 vessel were compared with the 98m waterjet driven catamaran and the 98m HSV-2 Swift powering trial results (Griggs, 2005). The transport efficiency of the Case 1 and Case 2 vessel were higher than the 1,500 tonnes waterjet catamaran, up to Froude number 0.44. The crossover point between waterjet and the propeller propulsion is at Froude number 0.44 similar as reported in Section 6.6 in the comparative study between the 130m propeller driven catamaran and the 98m waterjet catamaran. Beyond this Froude number, the HSV-2 Swift waterjet catamaran has a higher transport efficiency than the waterjet propulsion.

In Figure 6.11, the Telfer Merit transport factor of the Case 1 and Case 2 vessel were compared with the 98m waterjet driven catamaran and the 98m HSV-2 Swift powering trial results (Griggs, 2005). The transport factor of the Case 1 and Case 2 vessel were higher than the 1,500 tonnes waterjet catamaran up to Froude number 0.44. The crossover point between waterjet and the propeller propulsion is at Froude number 0.44. This finding is similar to the finding in the earlier comparative study using the 3,640 tonnes and 2,500 tonnes propeller driven catamaran results.

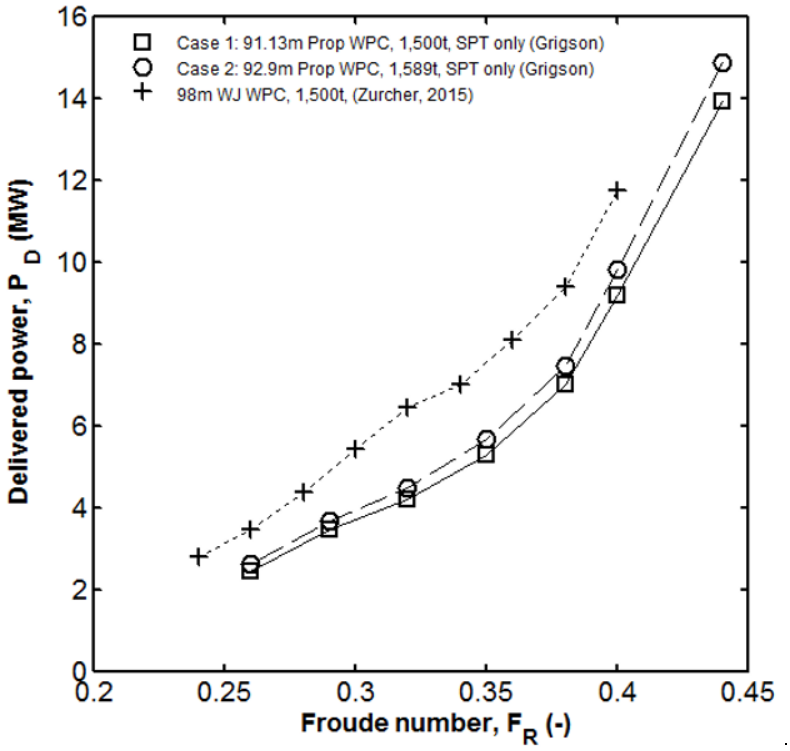


**Figure 6.8** Comparison of the delivered power of the propeller driven catamaran (Case 1 and Case 2) and the waterjet driven catamaran extrapolated to a full scale 98m catamaran

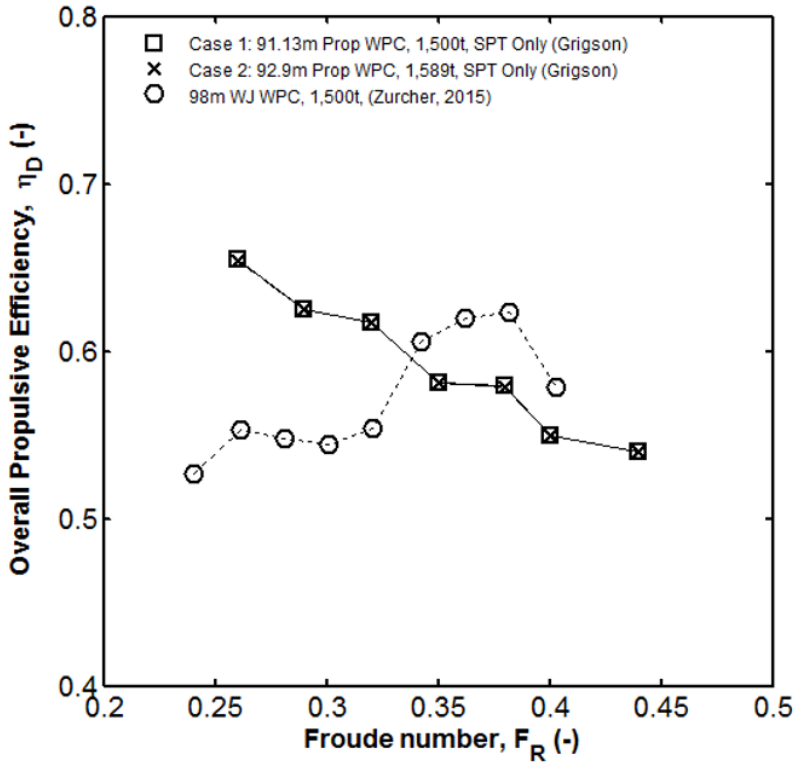


**Figure 6.9** Comparison of the propulsive efficiency of the propeller driven catamaran (Case 1 and Case 2) and the waterjet driven catamaran extrapolated to a full scale 98m catamaran.

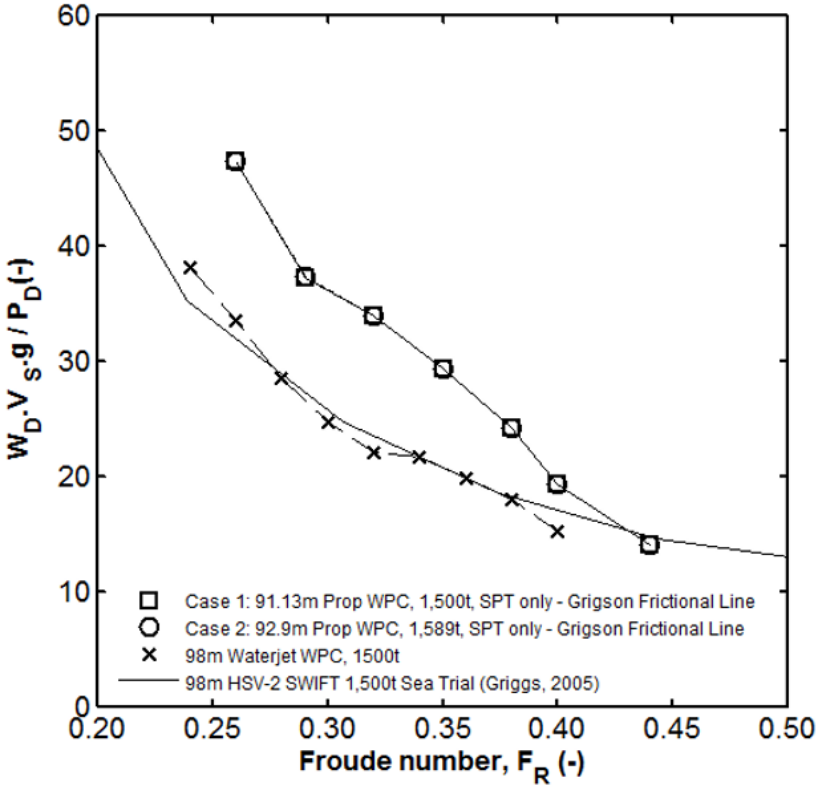


**Figure 6.10** Comparison of the transport efficiency of the propeller driven catamaran (Case 1 and Case 2) and the waterjet driven catamaran extrapolated to a full scale 98m catamaran

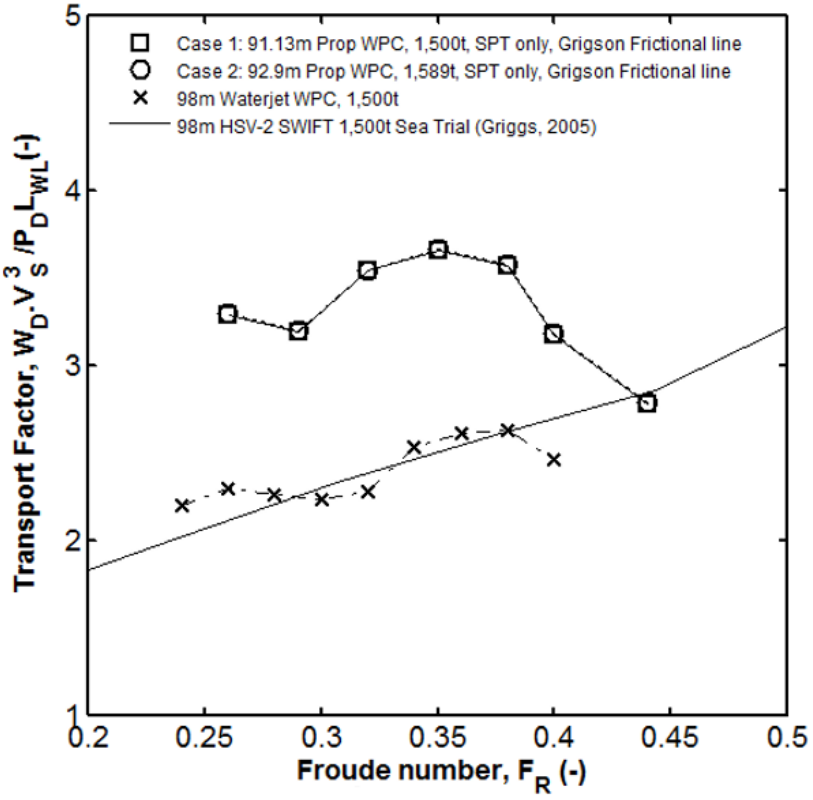


**Figure 6.11** Comparison of the Telfer Merit Factor of the propeller driven catamaran (Case 1 and Case 2) and the waterjet driven catamaran extrapolated to a full scale 98m catamaran.

## 6.9 The total resistance comparison

In an attempt to allow an equivalent comparison between the catamarans, the total resistance of the models has been rendered dimensionless by the specific fresh water density $\rho$, the vessel length squared $L^2$ and velocity squared $V^2$ and plotted with respect to the Froude number as shown in Figure 6.12. The 130m propeller driven catamaran resistance results were compared with the 98m waterjet driven catamaran and the 130m waterjet driven hull tested by Duffy and Lilienthal (2010), which were conducted in January 2010 and September 2010 at the AMC's towing tank. The plots were shown in Figure 6.12 (a) and (b) respectively. Duffy and Lilienthal only conducted a bare hull resistance test on the waterjet hull at the AMC's towing tank. No self-propulsion test yet to be conducted on the waterjet hull.

In Figure 6.12(a), clearly it was observed that the non-dimensional total resistance of the 98m waterjet driven catamaran was higher than the 130m propeller driven catamaran. From Figure 6.12 (b), interestingly, there were some crossover points between the 130m propeller driven catamaran and the 130m waterjet driven hull tested by Duffy and Lilienthal. The crossover points were approximately at Froude number 0.43 at both displacements (2500 tonnes and 3640 tonnes). The hollow speed for both curves were observed at Froude number 0.35, with the propeller catamaran

resistance at the hollow was lower than the waterjet catamaran resistance. These results from the comparison indicate that the propeller driven catamaran has been highly optimised at the highest hollow speed. It was evident from these results that the waterjet catamaran was not optimised to operate in the medium-speed regime.

## 6.10 The residual resistance comparison

In Figure 6.13 (a), it was apparent that the coefficient of the residual resistance for the 98m waterjet catamaran was higher than the 130m catamaran. The residual resistance coefficient of the 1,804 tonnes catamaran apparently having two humps which peak at approximately Froude number 0.32 and Froude number 0.45. The propeller driven catamaran apparently having two humps, approximately at Froude number 0.3 and 0.47. The hollow of the residuary resistance for the 130m propeller driven catamaran occurred much earlier than the waterjet vessel at Froude number 0.35. The hollow for the 98m waterjet driven catamaran occurred at Froude number 0.37. The residuary resistance curves for the propeller driven catamaran rise steadily beyond Froude number 0.35.

In Figure 6.13 (b), the results of the 130m propeller driven catamaran were compared with the results from a series of a 130m waterjet hull model experiments done by Duffy and Lilienthal (2010). The residuary resistance coefficients of the 130m waterjet vessel were higher than the 130m propeller driven vessel from Froude number $F_R$ 0.3 – 0.38. Beyond Froude number 0.38, the residual resistance coefficient of the waterjet catamaran was lower than the residual resistance coefficient of the propeller driven catamaran. The residual resistance coefficient of the waterjet vessel begins to drop beyond Froude number 0.45. This clearly shows that the 130m waterjet hull was specifically design to operate beyond this hump speed at Froude number 0.45, while the 130m propeller driven hull was optimised to operate at the medium speed regime between $F_R$ 0.2 to $F_R$ 0.38. Table 6.4 presents the Froude numbers at which the humps and hollows occur in the wave making resistance.

These differences in the humps and hollows between the two catamarans are caused by the differences in the effective waterline of each vessel. The waterjet catamaran under certain conditions is effectively longer than the propeller driven catamaran on the waterline because of the deeper transom stern. These differences in the effective waterline altered the wave reinforcement or the wave cancellation at stern.

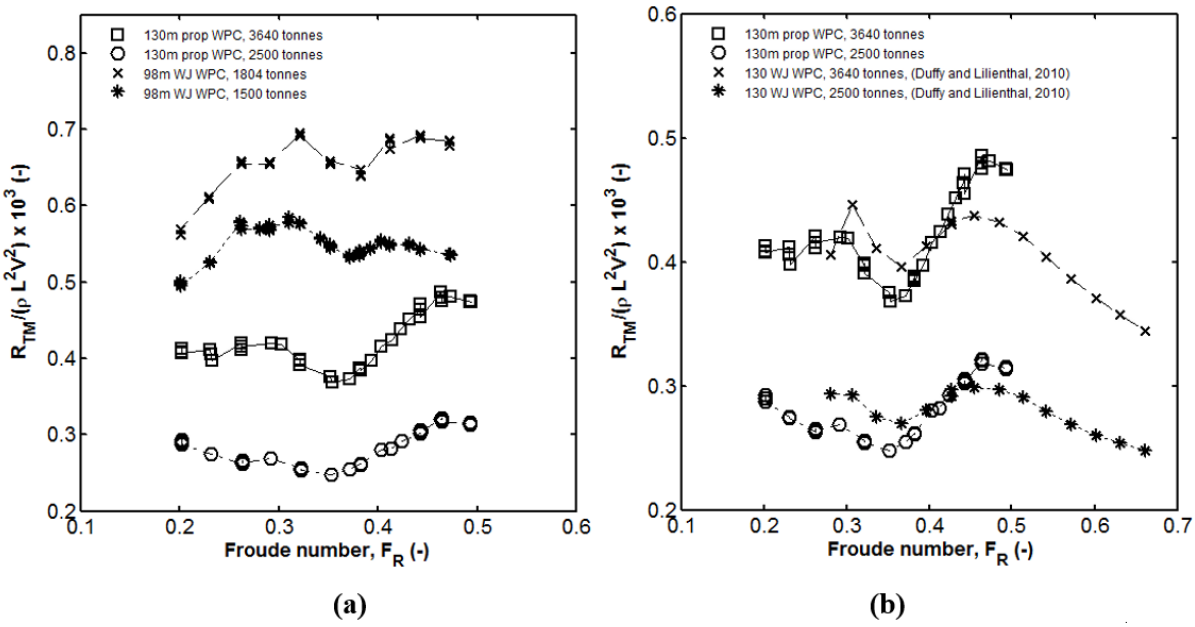


**Figure 6.12** Total normalised resistance results of the three different models from the calm water resistance test. **(a)** The 130m propeller driven catamaran and the 98m waterjet driven catamaran. **(b)** The 130m propeller driven catamaran and the 130m waterjet driven hull (Duffy & Lilienthal, 2010)

**Table 6.4** Froude number corresponding to the wave resistance wave humps and hollow occurrence for the 98m waterjet driven catamaran with displacements at 1,500 tonnes and 1,804, the 130m waterjet hull with displacements at 2,500 tonnes and 3,640 tonnes and the 130m propeller driven hull with displacements at 2,500 tonnes and 3,640 tonnes.

| ***Model*** | ***Occurred at $F_R$*** | | |
|---|---|---|---|
| | **1st hump** | **1st hollow** | **2nd hump** |
| 98m Waterjet 1,500t | 0.32 | 0.37 | 0.45 |
| 98m Waterjet 1,804t | 0.32 | 0.37 | 0.45 |
| 130m Waterjet 2,500t | 0.31 | 0.37 | 0.45 |
| 130m Waterjet 3,640t | 0.31 | 0.37 | 0.45 |
| 130m Propeller 2,500t | 0.30 | 0.35 | 0.47 |
| 130m Propeller 3,640t | 0.30 | 0.35 | 0.47 |

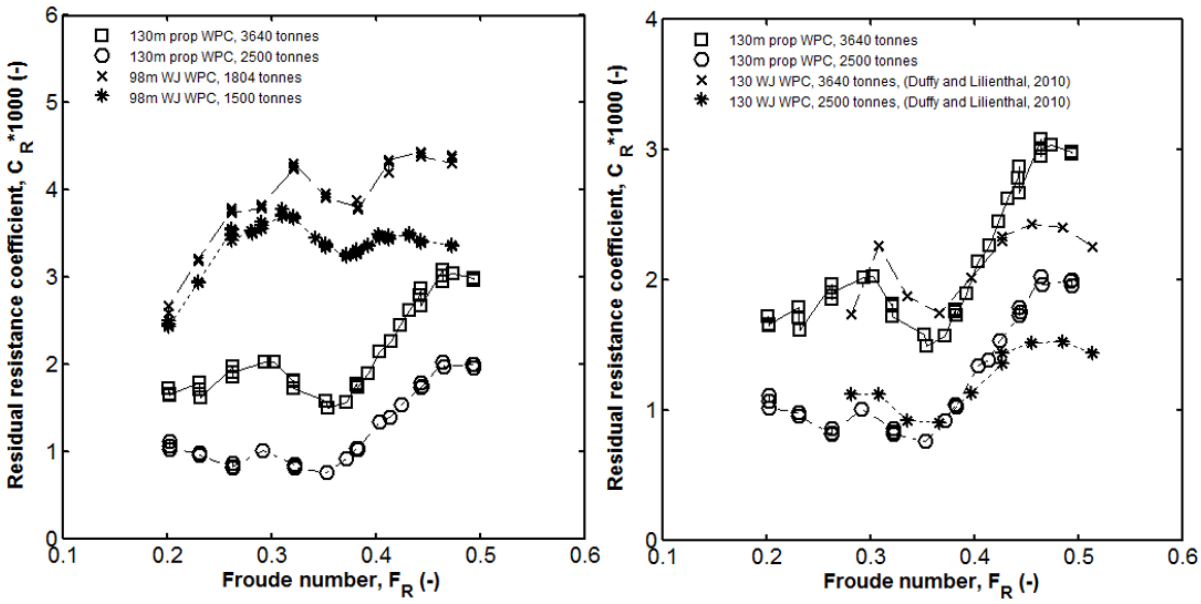


**(a)** **(b)**

**Figure 6.13** The residual resistance, $C_R$ with respect to the Froude number. **(a)** The results of the 130m propeller hull at displacements of 3,640 tonnes and 2,500 tonnes were compared with the results of the 98m waterjet hull tested by Zürcher (2015). **(b)** The results of the 130m propeller hull at displacements of 3,640 tonnes and 2,500 tonnes were compared with the results of the 130m waterjet hull which was tested on 24 September 2010 (Duffy & Lilienthal, 2010)

### 6.11 Sinkage and running trim comparison with the 98m waterjet catamaran.

The comparison of dimensionless sinkage *z/L* between the 130m propeller driven catamaran with the 98m waterjet driven hull is shown in Figure 6.14. The sinkage of the propeller catamaran increased for increasing Froude number and a maximum is reached around Froude number of $F_R$ = 0.48. This coincides with the Froude number at which the maximum hump of the residual resistance occur at $F_R$ = 0.48 as shown in Figure 6.13. The sinkage of the 98m waterjet driven catamaran reached at its maximum around Froude number of $F_R = 0.45$. This is similar to what was found by Haase et al. (2015), where he did a full scale CFD study of design space exploration for five large medium-speed catamarans with varying demihull slenderness ratio and waterline length. It should be noted that all the five large medium catamarans in Haase et al. (2015) investigation closely resembles a propeller driven hull with low transom immersion ratios ranged from 0.21 to 0.28.

The sinkage of the propeller vessel was found to be higher than the waterjet vessel. The differences were significant at Froude number 0.48. In Figure 6.15, the sinkage of the propeller was also compared against the results of Duffy and Lilienthal (2010) waterjet hull. It was noticeable that the propeller hull has a significant sinkage, especially at Froude number 0.48. This was a contrast with the 130m waterjet hull which having a flatter curve at Froude number 0.48 until 0.6.

The running trim results of the 130m propeller hull were also compared with the 98m waterjet driven vessel, see Figure 6.16 (a) and (b). The 1,804 tonnes waterjet vessel's running trim is not much

in differences with the 3,640 tonnes propeller vessel. The 1,500 tonnes waterjet hull has a larger running trim than the 2,500 tonnes propeller hull. In Figure 6.17 (a) and (b), the 130m propeller driven hull running trim was compared with the results of the 130m waterjet hull tested by Duffy and Lilienthal. The running trim of the propeller driven hull was greater than the running trim of the waterjet hull. It is noticeable that the running trim of the waterjet hull stop increasing and stayed constant beyond Froude number 0.5.

These comparative studies show that the propeller driven catamaran sinks more than the waterjet hull, but the 98m waterjet hull trims more than the 130m propeller driven boat. The propeller catamaran experienced more sinkage as it experienced a decrease of pressure distribution around amidship area more than the waterjet driven vessel. The trim however is not affected by the hull wetted surface area, but are more affected by the longitudinal centre of gravity of the vessel.

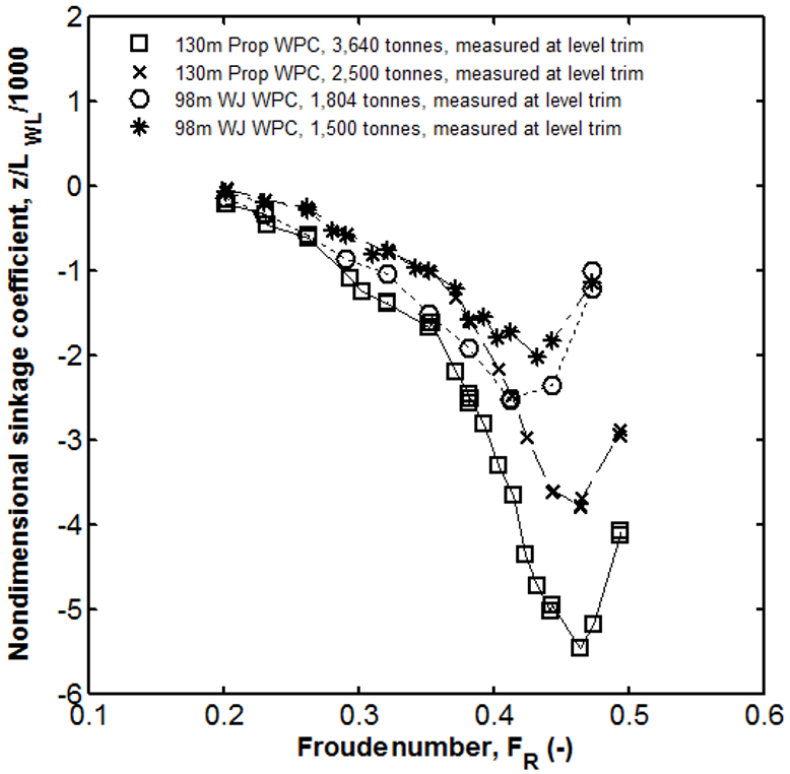


**Figure 6.14** The comparison of sinkage in non-dimensional *z/L* measured in bare hull resistance between the propeller driven catamaran at a displacement of 3,640 tonnes and 2,500 tonnes with the waterjet driven catamaran at a displacement of 1,804 tonnes and 1,500 tonnes.

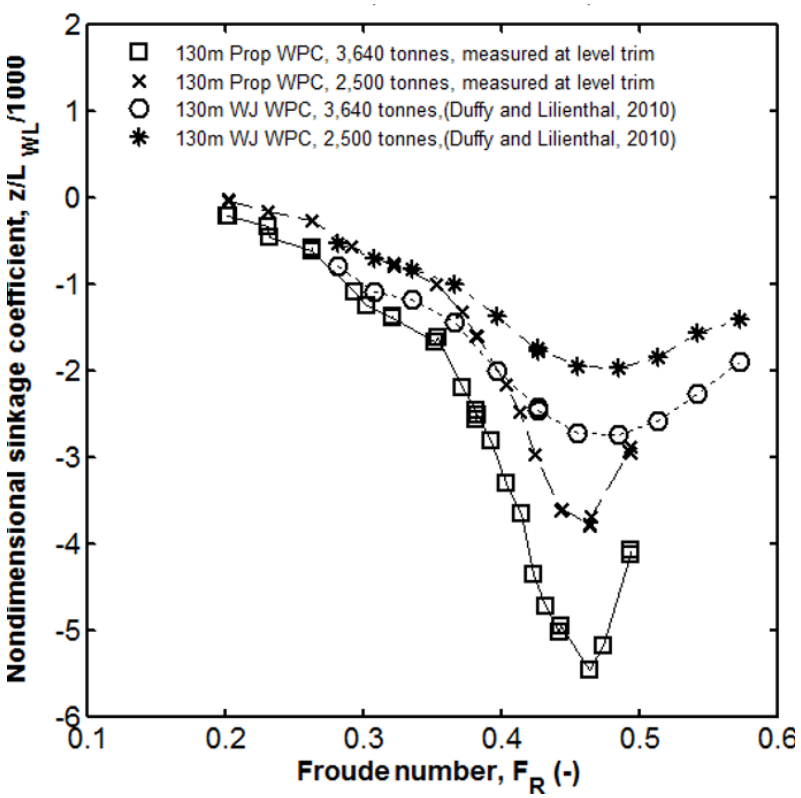


**Figure 6.15** The comparison of sinkage in non-dimensional *z/L* measured between the 130m propeller driven catamaran with a 130m waterjet hull (Duffy & Lilienthal, 2010). Both vessels have two similar displacements at 3,640 tonnes and 2,500 tonnes.

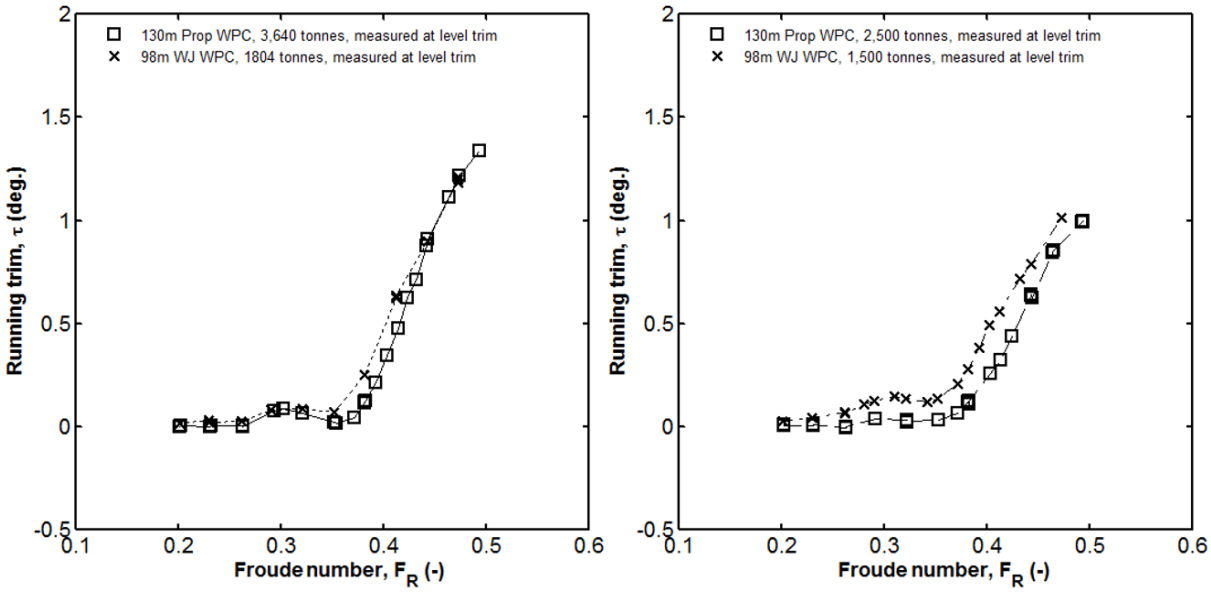


**(a)** **(b)**

**Figure 6.16** The trim in degree with respect to the Froude number - the comparison of running trim angle measured in bare hull resistance **(a)** between the propeller driven catamaran at displacement of 3,640 tonnes with the waterjet driven catamaran at a displacement of 1,804 tonnes **(b)** between the propeller driven catamaran at a displacement of 2,500 tonnes with the waterjet driven catamaran at a displacement of 1,500 tonnes.

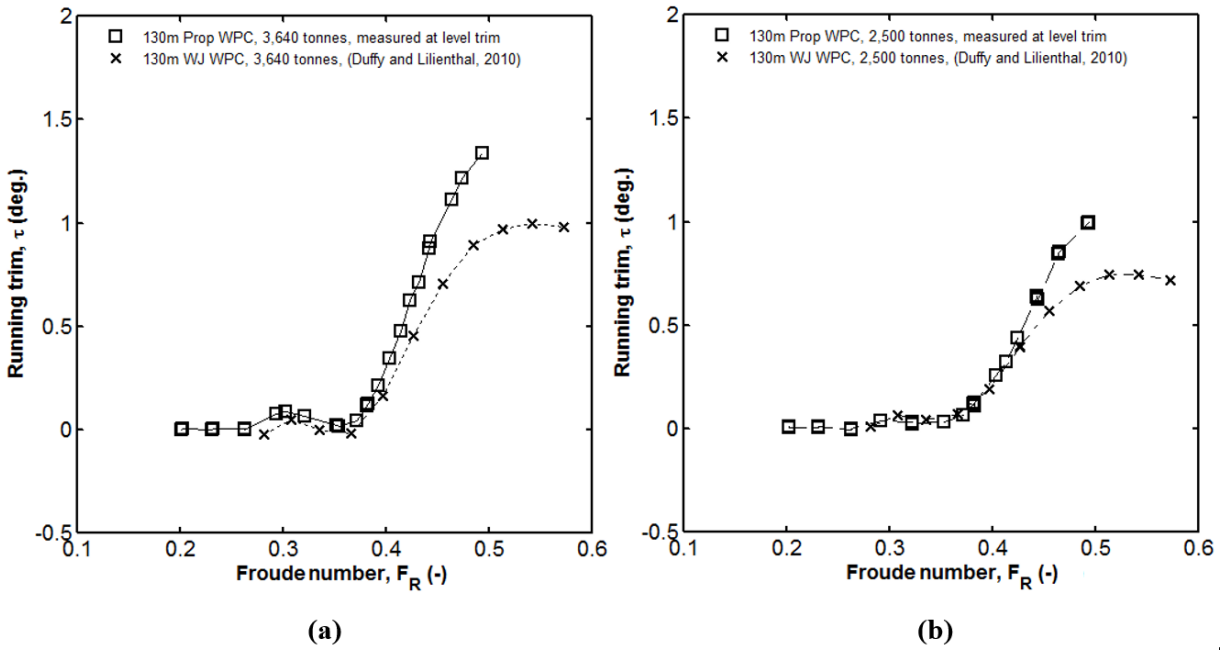


**Figure 6.17** The running trim in degree with respect to the Froude number. Comparison of running trim measured between the 130m propeller driven catamaran with a 130m waterjet hull (Duffy & Lilienthal, 2010) **(a)** Both vessels at a displacement of 3,640 tonnes **(b)** Both vessels at a displacement of 2,500 tonnes

## 6.12 Cavitation consideration

A propeller may experience cavitation at a greater extent compared to a waterjet operating at the same ship's speed (Allison, 1993, pp. 293 - 294). Therefore, a study was made to check the cavitation severity on the propeller blade for the propeller driven catamaran. The study was made using a diagram proposed by Burrill and Emerson (1953). This diagram was reproduced by the author from Burrill and Emerson (1962) and the propeller thrust loading coefficients with respect to the local cavitation number at propeller radius 0.7R were plotted in the diagram.

This diagram was based originally on experience with full-sized propellers and systematic tests of a series of four-bladed merchant ship propeller models in the cavitation tunnel at King's College, in Newcastle. In the diagram as shown in Figure 6.18, there are five diagonal lines indicating 2.5%, 5%, 10%, 20% and 30% back cavitation. Burrill and Emerson (1962) concluded that after making many observations on propellers running at average service condition, that 5% percent back cavitation was a suitable criterion at which to aim in practical design calculations.

The back cavitation for the propeller used in the 130m propeller driven catamaran are well below 5 percent except for the propeller running at Froude number $F_R$ = 0.40 and 0.44 at displacement of 3,640 tonnes. The worst is at almost 20 percent back cavitation for the propeller running at Froude number $F_R$ = 0.44 which is equivalent to about 30 knots full scale. However, the author concluded that the propeller propulsion will still be preferable over waterjet propulsion as medium-speed operation is below Froude number 0.38 which is unlikely to experience excessive cavitation and erosion. It should

be noted that the propeller used in the tests is a propeller based on a systematic series. The cavitation can still be reduced if the propeller(s) of the 130m catamaran are custom designed to minimised cavitation. In considering this cavitation extent, it was felt that the maximum recommended Froude number to be at 0.38.

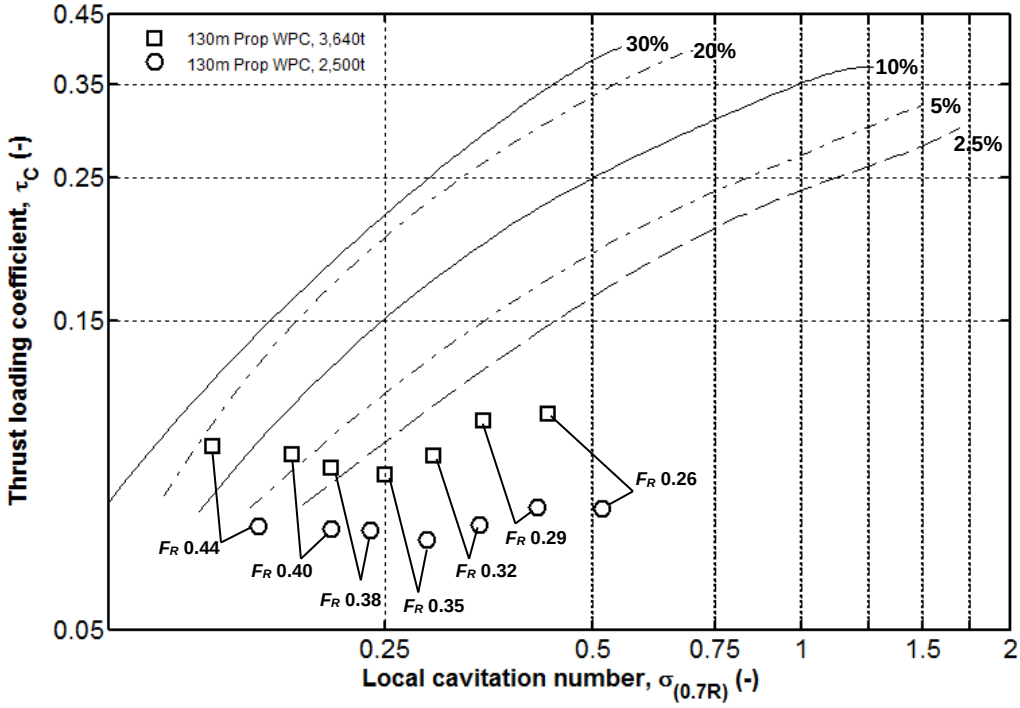


**Figure 6.18** The cavitation severity check of the propeller propulsion using Burrill chart.

## 6.13 Summary

The first approach in making an equal assessment to both propulsors were done by using the propulsive efficiency. It was demonstrated that the propeller driven catamaran has a better propulsive efficiency than the waterjet driven catamaran, up to Froude number 0.33. The changeover point of both propulsors occurred at Froude number 0.33. Beyond this Froude number, the waterjet catamaran has a better propulsive efficiency than the propeller driven catamaran. It is to be noted that the 98m hull was optimised for operation well above the hump resistance at Froude number 0.45 and the 130m hull was optimised for operation below the hump at Froude number 0.47. This was clearly proven by the results of the residuary resistance of both vessel. The residuary resistance of the 98m waterjet catamaran are rather flat beyond Froude number 0.37, which shows that this hull has the intended high speed performance beyond the hump speed at Froude number 0.45. This is in contrast with the the residuary resistance curves for the propeller driven catamaran which increased and rose steadily beyond Froude number 0.35.

The waterjet unit required a higher shaft revolution rate than the screw propulsion unit. The power absorbed by the waterjet unit as a function of the shaft revolution follows approximately a cubic law. For a screw propeller, the power absorption of a propeller follows approximately a law of

3. Therefore, to maintain the same power absorption, a waterjet normally requires a higher shaft speed.

In the second approach, the transport efficiency was used in the comparative study as a method used to assess the merits of both propulsion system in terms of power to weight ratio. The transport efficiency equation was modified by making it dimensionless by adding the gravitational acceleration, $g$ to the equation. The propeller driven catamaran has a higher transport efficiency than the waterjet driven catamaran ranging from 2.8% to 50% depending on the Froude number. Beyond Froude number 0.44, the transport efficiency of the waterjet driven catamaran is higher than the propeller driven catamaran. This means that the propeller driven catamaran, can carry more weight and with greater ship speed in its movement through the water for a lesser shaft power than the waterjet driven catamaran up to a Froude number of 0.44. The results are the same using Telfer's transport factor, where the propeller driven catamaran has a larger transport factor up to Froude number 0.44. The waterjet catamaran was found to be superior to the propeller catamaran beyond Froude number 0.44.

In the third approach, an additional design scenario was constructed whereby the two vessels of the waterjet and the propeller driven catamaran were scaled to a similar size. There were two case scenarios chosen for this study, Case 1 was made to be similar in the weight displacement and Case 2 was made to be similar in the waterline length to the waterjet catamaran. It was found that the propulsive efficiency for both cases, Case 1 and Case 2, of the propeller driven catamaran are higher than the waterjet catamaran up to Froude number 0.33. Beyond this Froude number, the waterjet catamaran was found to be superior to the propeller driven catamaran in terms of propulsive efficiency. In terms of transport efficiency and the Telfer merit factor, the efficiency of the propeller driven catamaran are higher than the waterjet catamaran up to Froude number 0.44. Beyond this crossover, the waterjet catamaran efficiency was found to be higher than the propeller catamaran.

These several approaches are necessary as the comparison in terms of propulsive efficiency is comparing only the hydrodynamic performances of both of the waterjet and propeller catamarans. This efficiency only accounts for the efficiency due to the flow physics, in terms of thrust developed by the propeller and the fact that the propeller acts behind the hull. To make an assessment on the merit of earning potential, which is correlated to the payload capacity of the vessel, the transport efficiency and the transport factor were used.

The study on the propulsive and transport efficiency showed that the propeller catamaran is more efficient than the waterjet catamaran at the medium-speed regime below the hump speed at Froude number 0.45. The cavitation extent will be still insignificant in operating in the medium speed regime up to Froude number 0.38. Therefore, the propeller propulsion is considered the best option for a large energy-efficient catamaran in operating in the medium-speed regime.

# Chapter 7

# Conclusions and recommendations

There is an apparent important need for a research into a better understanding of the powering performance of large medium-speed catamaran, i.e. waterjet and propeller propelled catamaran. This need arises as there are demands from ferry operators and shipbuilders, where they are forced to act and share their responsibility to promote economically viable and environmentally sustainable sea transportation. Therefore, this research was set out to investigate the powering performance of waterjet and screw propeller propulsion in propelling large medium-speed catamarans where the main aim of this research is to answer the question on which propulsion system is more efficient in the medium speed regime. To be precise the research questions are:

1. Will the propeller be more efficient in comparison with the waterjets propulsion in propelling the medium speed catamarans?
2. What is the most accurate way to extrapolate to full scale for the medium-speed catamaran?
3. At what speed is the changeover point between both propulsors?
4. Is it possible to make an equal comparison between both systems?
5. What is the method to be used to make a 'fair basis' comparison?

A comprehensive study into the powering performance of large medium-speed catamarans using experimental data obtained from towing tank model tests has been made. The study are constricted to a single experimental study and the scope does not include any CFD case study. The ship model tests conducted in the towing tank, i.e. calm water resistance and self-propulsion test, were intended to measure the hydrodynamic performance and the propulsion efficiency for both waterjet and propeller driven wave-piercing catamaran. A large amount of data was obtained from these tests. All the results from these tests were extrapolated to full scale. However, there are some issues in extrapolating these results using the traditional approach, the ITTC 1978 procedure. These issues are explained in the next section.

## 7.1 Wake scaling issues

Two methods were chosen initially to extrapolate the model results to full scale, the ITTC 1978 extrapolation procedure and the 'self-propulsion test only' procedure. The self-propulsion test only procedure was chosen over the ITTC 1978 procedure as some of the calculation recommended in the latest revision of the 7.5-02-03-01.4 procedure (ITTC, 2014) simply do not work. There were some issues in the wake fraction in the model scale obtained either using the 'thrust identity' or the 'torque identity' method (Bose, 2008).

The wake fractions obtained using the 'thrust identity' and the 'torque identity' methods as recommended by the procedure, were somewhat strange, exhibiting for some cases unrealistic wake fractions (e.g. negative values of the wake fractions). The method recommended by the 7.5-02-03-01.4 procedure in finding the model wake fraction, $w_{TM} = 1 - (J_O/J_P)$, failed to work properly as the wake fractions for the catamaran vessel are believed to be too small.

The wake fractions are small as the propeller in the behind of the catamaran stern is operating in a less obstructed flow, as a results of approximately 50 – 60 % of the propeller disc area is located below the baseline of the catamaran. In other words, approximately 50 – 60% of the incoming flow into the propeller disc area are not disturbed by the hull aft end shape of the catamaran. As the value of the advance coefficient in the behind the model is too close to the value of the advance coefficient in the open water, sometimes it is not possible to find the wake fraction using the 'thrust identity' or the 'torque identity' method.

An alternative approach was sought in order to obtain the wake scaling using CFD RANS simulation. The wake fractions for both model and full scale were calculated from the radial wake contour of the 130m propeller driven catamaran which was taken from the CFD simulation work of Haase (2015a). This wake fractions values in model scale and full scale then were used for the wake scaling in the SPT only extrapolation method.

## 7.2 Thrust deduction fraction issues

The thrust deduction fractions obtained using the method recommended in the 7.5-02-03-01.4 procedure (ITTC, 2014) were found to have large variation with respect to the ship speed. If these values were used further in the extrapolation, a lower delivered power is obtained which results in a higher propulsive efficiency.

The ITTC recommended method did not work properly and this was mainly as a result of using equation 5.4. In this equation, the thrust deduction fraction was found from a single point of data from the results of the resistance test and the self-propulsion test. The thrust deduction fractions obtained from the calculation of the *F-T* slope from the load-varied test were more accurate since it uses a linear curve fits to a multiple data points of the thrust with respect to the towing force plots. This is far more accurate than getting the thrust deduction fraction from a single data point from the self-

propulsion point of the ship in the self-propulsion point. By using multiple points of data, the random error is reduced by averaging the runs. Therefore, the thrust deduction fraction obtained from the *F-T* slope equation was chosen for the extrapolation to full scale. The ITTC recommended method does not work and should not be used in the extrapolation process.

## 7.3 Propeller scale effect issues

The scale effect corrections on the propeller proposed by ITTC 1978 (ITTC, 2014; Manen & Oossanen, 1988) did not correct the propeller coefficient very well. The corrections method lead to a small change to the propeller coefficient. The correction method proposed by Benedek (1985) was much larger and shifted the coefficients closer to the benchmark propeller than the corrections proposed by the ITTC1978 method. The benchmark propeller chosen in this study is from results tested on a similar Wageningen B5.75 propeller found in Kuiper (1992). The scale effect corrections proposed in the ITTC were meant for model propellers used in the self-propulsion test having diameter typically from 150 mm to 300 mm (ITTC, 2011d). Due to the significant laminar flow existed in a smaller propeller, as in this case using a model propeller having a diameter of 120 mm, the method proposed by Benedek (1985) was used instead of the proposed method by ITTC 1978.

## 7.4 The problem with the ITTC 1978 procedure

A primary source of uncertainty in the ITTC 1978 procedure is in the ship propeller operating point interpolation curve used to determine the ship propeller operating point given by the equation, $K_T/J^2 = S_S.C_{TS}/2.D_S^2(1-t).(1-w_{TS})^2$. This equation used results from the three separate tests. The $K_T/J^2$ is from the open water test, the $C_{TS}$ is from the calm water resistance test and the $(1 - t)$ and the $(1 - w_{TS})$ are from the self-propulsion test. In the SPT method, the ship propeller operating point interpolation equation is obtained from $K_{TS}/ J^2 = T_S/2\rho D_S^2 V_S^2$. All the results for the input in the SPT method are only from the self-propulsion test. The ITTC 1978 procedure in a way, ignored the interaction effects between the hull and the propeller in the behind condition. This is in contrast with the SPT method where the ship propeller operating point is found from the intersection of the required thrust coefficient with the ship propeller curve in the behind condition, where the interactions between the hull and propeller are not neglected. The ITTC 1978 procedure needs to be reviewed and updated. To improve the ITTC 1978 procedure, the load varying test is essential. The use of tow-force with respect to the propeller thrust plot from the load varying test to obtain the thrust deduction fraction is also essential in improving the ITTC 1978 procedure. Alternative methods of obtaining the wake scaling need to be incorporated in the ITTC 1978 procedure, as in this research a CFD RANS

simulation was used to obtain the wake in the model scale and the full scale. There are a number of other options to obtain the wake scaling, such as using an existing database or conducting a wake survey test in a towing tank. In answering the second research question of what is the most accurate way to extrapolate to full scale for the medium-speed catamaran, it was felt that the SPT only extrapolation method was the most reliable extrapolation method to be used in the catamaran self-propulsion data reduction. It is strongly recommended that the SPT extrapolation method and the load varying test need to be incorporated in the new power prediction procedure for wave-piercing catamarans and similar ship forms. The SPT extrapolation method and the load varying test should only be used to similar catamaran vessels with caution.

## 7.5 The proposed SPT only extrapolation method

The proposed SPT only method is based on the work of Holtrop (2001), Bose and Molloy (2001a), Schmiechen (1991) and Kracht (1991). This method works with the British method or the load-varied method of self-propulsion test only as the name implies. There are two changes or modifications in the SPT only method in order to make the prediction to full-scale works, as shown in earlier in Chapter 5, Figure 5.20.

In this modified procedure, the wake scaling from RANS simulation was introduced. From the simulated nominal wake, the nominal wake fractions in model scale, $w_M$ and the nominal wake fractions in full scale, $w_S$ are obtained. These wake fractions then have been used as the input for the advance coefficient for the full-scale propeller, where it is defined as $J_S = J\left(1-w_M\right/1-w_S\left)\right.$.

In the second modification, a method for propeller scale effect corrections from Benedek (1985) was analysed and compared with other methods which are more widely used. The Reynolds scale effect correction using the ITTC method which has been described by Lindgren et al. (1978) and Manen and Oossanen (1988) failed to provide a satisfactory correction to the small propeller used in the self-propulsion test, as explained in Chapter 3. Using these methods, the modification to the model propeller thrust and torque coefficients, to obtain the full-scale propeller thrust and torque coefficient, $K_{TS}$ and $K_{QS}$, are small compared to the correction proposed by Benedek (1985). As explained in Chapter 3, the corrected coefficients using Benedek's method correlates better with the open water propeller coefficient found in Kuiper (1992). The propeller coefficients found in Kuiper is based on a larger 'geosim' propeller with diameter of 220 mm and running at Reynolds number $Re\ 2.0 \times 10^{-6}$. This much larger 'geosim' propeller acts as a benchmark to the 120 mm diameter smaller propeller. The aim is to get the corrected propeller coefficients of the smaller 'geosim' propeller as close as possible to propeller thrust and torque coefficient of the larger 'geosim' propeller. Therefore the

corrections method proposed by Benedek was chosen over the corrections recommended by the ITTC procedure no 7.5-0.2.03-01.4 (ITTC, 2011a).

## 7.6 The proposed comparative method

Is it possible to make an equal comparison between waterjet and propeller propulsion systems? As both of these catamarans cannot be directly compared as the length to displacement ratio and the wetted surface area ratio are not the same, comparative methods that can compare these two catamarans equally, need to be established. Several approaches were made in order to assess the merit of the waterjet and the screw propeller as the propulsor for medium-speed catamarans. These were based on three methods, an approach using the propulsive efficiency, an approach using a transport efficiency or a transport factor and an approach using a scaling to a similar size method. These several approaches are thought to be necessary as the comparison in terms of propulsive efficiency is comparing only the hydrodynamic performances of both of the waterjet and propeller catamarans. This efficiency only accounts for the efficiency due to the flow physics, in terms of thrust developed by the propeller and the fact that the propeller acts behind the hull. The transport efficiency and the Telfer merit factor are efficiency representation of power-speed-deadweight relationship of a vessel. There is a difference between these two efficiencies, the propulsive efficiency and the transport efficiency. The first only accounts the dynamic similarity and the latter considered the dynamic similarity as well as the design similarity. In dynamic similarity we are equalising the ratios of forces, but in design similarity we are looking at equalising the earning potential, which is correlated to the payload capacity of the vessel.

One of the proposed methods mentioned above is to compare both systems through comparing the propulsive efficiency. The propulsive efficiency is defined as the ratio of the output which is the effective power, $P_E$ over the input which is the delivered power, $P_D$. To compare waterjets and propeller with the same terms of propulsive efficiency, the propulsive efficiency were defined in simple terms using the bare hull resistance only, without the appendage drag included. The effective power, $P_E$ was calculated using the bare hull resistance data where $P_E = R_{BH}.V$ and not using the towing force data at zero thrust, $F_{T=0}$ from the self-propulsion test, where $P_E = F_{T=0}.V$.

In the second approach, both of these catamarans were compared in terms of transport efficiency. The transport efficiency is another meaningful parameter that can be used to assess the merits of both propulsion system in terms of power to weight ratio. The transport efficiency equation was modified by making it dimensionless by adding the gravitational acceleration, $g$ to the equation. The numerator in the transport efficiency contains the vessel's deadweight $W_d$ , its service speed $V_S$ and the gravitational acceleration $g$. The denominator in the transport efficiency contains the vessel's total delivered power, $P_D$. This performance index is a measure of a ship's relative capabilities in

terms of carrying its own weight and payload for a given shaft power. A different kind of transport efficiency was also used in this research. A transport factor proposed by Telfer (1933) and Lammeren (1948) was used with some modifications made to the proposed transport factor equation. This Telfer merit factor is a combination of the displacement weight $W$, the ship speed $V$, the ship length $L$, and the delivered power $P_D$. The gravitational acceleration $g$ was omitted from the equation to make this transport factor dimensionless. The results from the transport factor yields the same changeover point between propeller and waterjet catamaran given by the transport efficiency.

The third approach was done by scaling the 130m propeller catamaran model to be similar to the 98m waterjet catamaran. The results were compared in terms of delivered power, propulsive efficiency, transport efficiency and Telfer merit factor.

It should be recalled that the propulsive efficiency is a measure of hydrodynamic efficiency of the propulsor working in the behind condition. The transport efficiency and the transport factor are a measure of a ship's relative capabilities in terms of carrying its own weight and payload for a given shaft power. Therefore it is useful to use the three efficiencies in assessing the merits of both propulsor.

## 7.7 Which is the best propulsor?

Propeller or waterjet? At what speed is the changeover point of both propulsors? In answering these questions on which propulsion system is more efficient in propelling the catamaran in the medium-speed regime, the approaches mentioned earlier were performed to make an evaluation on the merits of both propulsors.

The first approach in making an equal assessment to both propulsor was done by using the propulsive efficiency. It was found that the propeller driven catamaran has a better propulsive efficiency than the waterjet driven catamaran, up to Froude number 0.33. The changeover point of both propulsors is at Froude number 0.33. Beyond this Froude number, the waterjet catamaran is superior to the propeller driven catamaran. It is to be noted that these results are heavily influenced on the way these both hulls being optimised. The 98m hull was optimised for operation well above the hump resistance at Froude number 0.45 and the 130m hull was optimised for operation below the hump at Froude number 0.47. This was clearly proven by the results of the residuary resistance of both vessel. The residuary resistance of the 98m waterjet catamaran is rather flat beyond Froude number 0.37, which shows that this hull was specifically design to operate beyond the hump speed at Froude number 0.45. This is in contrast with the the residuary resistance curves for the propeller driven catamaran which increased and rising steadily beyond Froude number 0.35.

In the second approach using the transport efficiency as a means of assessment, it was found that the propeller driven catamaran has larger transport efficiency than the waterjet driven catamaran ranged from 50% to 2.8% depending on the Froude number. The changeover point of both propulsors occurred at Froude number 0.44. Beyond Froude number 0.44, the transport efficiency of the propeller driven catamaran drops and are much lesser than the transport efficiency of the waterjet hull. Apparently, the waterjet catamaran starts to perform better than the propeller driven catamaran beyond Froude number 0.44. The results are the same using Telfer's transport factor, where the propeller driven catamaran has a larger transport factor up to Froude number 0.44. The waterjet catamaran was found to be superior to the propeller catamaran beyond Froude number 0.44.

In the third approach, an additional design scenario was constructed whereby the two vessels of the waterjet and the propeller driven catamaran were scaled to a similar size. There were two case scenarios chosen for this study, Case 1 was made to be similar in the weight displacement and Case 2 was made to be similar in the waterline length to the waterjet catamaran. It was found that the propulsive efficiency for both cases, Case 1 and Case 2, of the propeller driven catamaran were higher than the waterjet catamaran up to Froude number 0.33. Beyond this Froude number, the waterjet catamaran was found to be superior to the propeller driven catamaran in terms of propulsive efficiency. In terms of transport efficiency and the Telfer merit factor, the efficiency of the propeller driven catamaran are higher than the waterjet catamaran up to Froude number 0.44. Beyond this crossover, the waterjet catamaran efficiency was found to be higher than the propeller catamaran.

The study on the propulsive and transport efficiency showed that the propeller catamaran is more efficient than the waterjet catamaran at these slow speeds specifically below the hump speed at Froude number 0.45. The crossover point in terms of propulsive efficiency, which is a measure of merit in dynamic similarity, occurs approximately at Froude number equal to 0.33, where waterjet propulsion is superior to the propeller propulsion beyond this Froude number. The crossover point in terms of transport efficiency, which is a measure of merit in design similarity, occurs approximately at Froude number 0.44, where beyond this Froude number, the waterjet starts to perform better than the propeller propulsion. Furthermore it was found that through cavitation analysis, the cavitation extent will still be insignificant in operating in the medium speed regime up to Froude number 0.38.

## 7.8 Recommendations for further experimental testing and analysis.

The main objective in this research in carrying out experimental study and analysing on the powering performance of a waterjet and a propeller driven catamaran has been achieved. However, with further time and resources, investigations of the related areas in greater detail has a good chance of providing further understanding and insight to progress designs of medium speed vessels and their propulsion systems. Thus, there are still many areas which are deserving of further attention. Based on

the experience gained in the research project, a few general recommendations are suggested which are as follows:

1. The 98m waterjet driven catamaran were not designed to be efficient at the medium speed range ($F_R$ 0.25 – 0.45). This contributed to the end result of the 130m propeller driven boat to outperform the 98m waterjet driven catamaran. It is recommended that the self-propulsion test for the waterjet hull to be repeated using a waterjet hull which is designed and optimised for medium-speed operation. It is suggested that the waterjet hull to have a close resemblance to the propeller driven hull in terms of *L/B* ratio, *B/T* ratio, prismatic coefficient and block coefficient. It is suggested to use the 130m waterjet hull tested by Duffy and Lilienthal (2010) which was close in length and displacement ratio to the propeller driven hull.

2. To minimise the scale effect of the propeller and the waterjets, higher ship to model scale ratio leading to a larger model size should be employed if possible. A larger testing facility at another towing tank institution could be necessary if the model size cannot be increased due to the blockage effect restrictions in the AMC towing tank.

3. The speed range for the waterjet self-propulsion testing should be extended to a higher speed range. This is to allow an assessment to be made on the powering performance of the waterjet catamaran above the hump speed beyond Froude number 0.47. This will also allow a comparison to be made at this extended high speed range particularly in between the Froude number 0.45 up to 0.55.

4. Further research is needed in investigating the Reynolds scale effect of using small propeller(s) in self-propulsion test. This was found to be one of the major source of uncertainty in the extrapolated powering results. It is recommended to repeat the open water test as in Chapter 4 using a series of larger 'Geosim' model propeller to be the benchmark propeller. It is also recommended that the model propeller to be tested in a series of Reynolds number ranged between low Reynolds number below 200,000 and at high Reynolds number at 2,000,000. By doing this, a customised correction equation could be derived to correct the scale effect in the torque and the thrust coefficients in the self-propulsion test performed at AMC towing tank. This 'Geosim' study can also be performed using RANS-based method and a larger series of propeller testing can be conducted to reduce funding constraints.

## 7.9 Room for improvements in ship powering predictions

This research has given some further insight on what method works and what not in the model testing, the extrapolation procedure and the comparative procedure between two different vessels. There are still areas of mystery in need of further attention and research. Therefore a few suggestions were addressed here for the thoughts of the ITTC Powering Committee and testing facilities around the world.

Obviously, the ITTC 1978 procedure needs to be reviewed and updated. It was found in this research, some of the method in the extrapolation method did not work well especially in predicting the wake fraction and the thrust deduction fraction for wave-piercing catamarans. It was found that alternative methods of obtaining these propulsion factors can be used.

An alternative method of obtaining the wake scaling could be incorporated in the ITTC 1978 method, as in this research CFD RANS simulation was used to obtain the wake in the model scale and the full scale. There are a number of other options in order to obtain the wake scaling, such as using an existing database or conducting a wake survey test in a towing tank.

The scale effect corrections proposed in the ITTC 1978 method did not work well in correcting the propeller torque and the thrust coefficients. Further testing and research would provide a valuable database that can be used to develop an empirical scale effect correction factors tailored for the testing of small propellers as mentioned earlier in section 7.8 (4) in this chapter.

The SPT extrapolation method and the load varying test needs to be incorporated in the new power prediction procedure for catamarans and similar ships. It was felt that the load-varying test is becoming an essential part of the self-propulsion test as it provides multiple data points in finding the thrust deduction fraction. It was found that the thrust deduction fraction obtained using the traditional approach suggested by ITTC 1978 having large variations of the thrust deduction fractions with respect to the Froude number. Therefore it is suggested that the means of getting an accurate thrust deduction fraction is always by using the *F-T* slope. This method in finding the thrust deduction fraction needs to be incorporated in the new powering prediction procedure.

# Appendix A

# Model Experiment Set-up

## A.1 Model hull size estimation and scale ratio

Model hull estimation is important as to determine the optimum size of the ship model to be used in the 130m wave-piercing catamaran powering prediction test. Initially the model length was investigated in the range of 4.16 to 6.24 meters. In determining the appropriate model size, several requirements and restrictions have to be taken into account, such as facility dimensions, depth Froude number and blockage correction. The range was refined to the range of 4.30 to 4.99m, after considering the depth Froude number at not more than 0.8 (Barrass, 1979, pp. 17 - 19) and having a propeller diameter of not more than 120mm. The depth Froude number was defined as

$$F_{nh} = V \Big/ \sqrt{gh} \tag{A.1}$$

where $V$ is the ship or model velocity in m/s, $g$ is the gravitational acceleration in m/s$^2$ and $h$ is the water depth in m.

It was also important to ensure that the maximum model speed does not exceed the AMC's towing tank carriage maximum speed. The target was to get the dimensions of the model of the 130m propeller driven hull as close as possible to the model of the 98m waterjet driven hull used by Zürcher. The length overall of the waterjet single demihull model is 4.27 meters, with a maximum beam on waterline of 0.21 metres, see Table 2.1. The possible scale ratio with maximum speed, depth Froude number and the demihull model length is listed in Table A.1.

In shortlisting the possible model scale ratio further, a preliminary resistance and powering estimation were made using tests data from the Report of Resistance Tests and Powering Estimates for the 130m WP Catamaran for Revolution Design conducted on 24 September 2010 (Duffy & Lilienthal, 2010) and data from the Report of Calm Water Tests for the JHSV Wave Piercing Catamaran (Marin, 2008). By scaling these results to the scale ratios stated in Table A.1, rough estimates of the calm water resistance and the powering propulsion factors were determined. It is important to ensure that the estimated drag, thrust and torque do not exceed the available sensors rated

loads. It was concluded that the most suitable scale ratio is the 1:29 ratio, with the length of overall of the single demihull of 4.30 metres and a breadth of 0.221 metres.

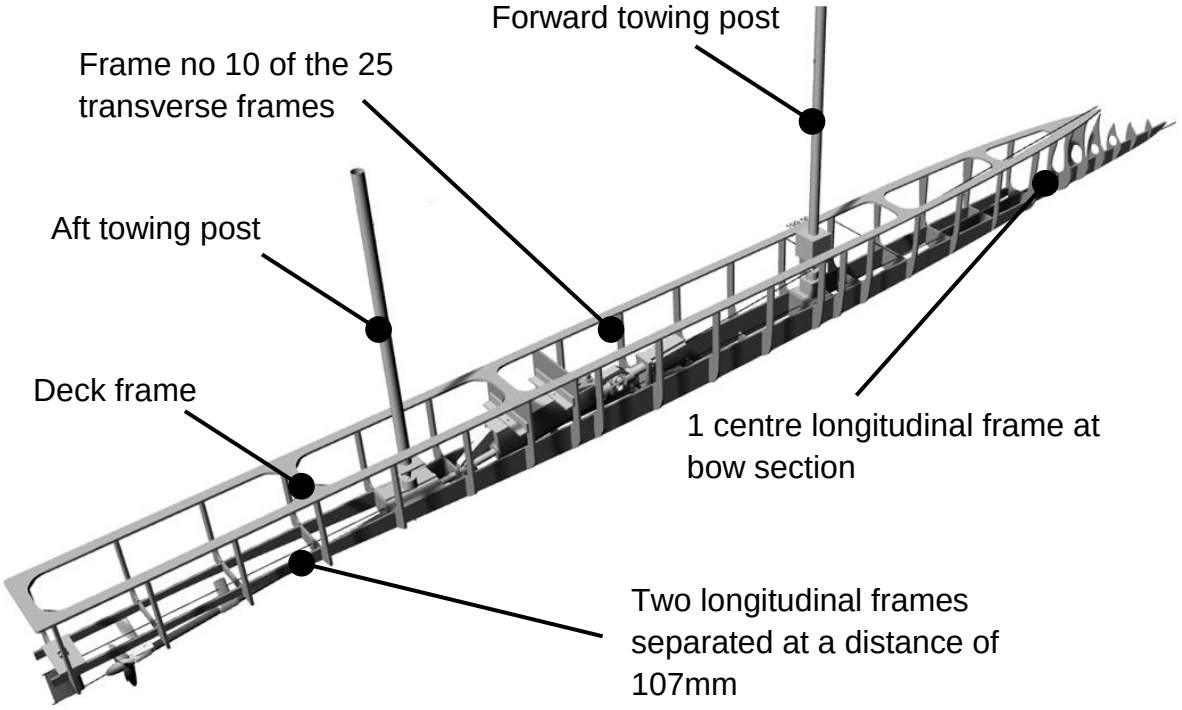


**Figure A.1** Assembled view of the 130m propeller catamaran without the hull body. The internal structure of the model consists of two longitudinal frames, one short centre longitudinal frames at the bow section, 25 transverse frames, and one deck frame.

**Table A. 1** Possible model scale ratio with model length, model speed and model Depth Froude number

| | $\lambda$ = 25, $L_{WL}$=4.99m | | $\lambda$ = 26, $L_{WL}$=4.80m | | $\lambda$ = 28, $L_{WL}$=4.46m | | $\lambda$ = 29, $L_{WL}$=4.30m | |
|---|---|---|---|---|---|---|---|---|
| **Ship Speed (Knots)** | **Model speed (m/s)** | **Depth Froude No** | **Model speed (m/s)** | **Depth Froude No** | **Model speed (m/s)** | **Depth Froude No** | **Model speed (m/s)** | **Depth Froude No** |
| **20** | 2.06 | 0.54 | 2.02 | 0.53 | 1.94 | 0.51 | 1.91 | 0.50 |
| **22** | 2.26 | 0.59 | 2.22 | 0.58 | 2.14 | 0.56 | 2.10 | 0.55 |
| **24** | 2.47 | 0.64 | 2.42 | 0.63 | 2.33 | 0.61 | 2.29 | 0.60 |
| **26** | 2.67 | 0.70 | 2.62 | 0.68 | 2.53 | 0.66 | 2.48 | 0.65 |
| **28** | 2.88 | 0.75 | 2.82 | 0.74 | 2.72 | 0.71 | 2.67 | 0.70 |
| **30** | 3.09 | 0.80 | 3.03 | 0.79 | 2.92 | 0.76 | 2.87 | 0.75 |

## A.2 The ship model fabrication

The single demihull model for the catamaran was fabricated out of carbon fibre reinforced composites similar to the material used by Matsubara (2011). The selection of the carbon fibre composite as the model material provides a reduction in the demihull model mass and rigidness to the model. The composite sandwich consists of high-density foam core and was laminated on both sides with carbon filaments. The carbon filaments were laminated to the foam core using epoxy resins which binds them together. The 'geometrically similar' model was built according to the requirements and manufacturing tolerances as required by ITTC (2011d), ITTC Recommended Procedures and Guidelines - Ship Models. The hull lines in three dimensional surface data were provided by the vessel designer Revolution Design Pty. Ltd.

The framing system of the model consists of two longitudinal frames, a short centre longitudinal frame in the bow section, a deck frame and 25 transverse frames as illustrated in Figure A.1. The two longitudinal frames were separated at a distance of 107mm as to provide adequate

spaces for the ballast weights as most of the standard ballast weights available at AMC are approximately 40mm x 40mm x 100mm in dimensions.

The model was fabricated by Stuart Phillips Model Makers, in Launceston, Tasmania. The structural frames were laser cut from a 7mm thick carbon fibre composite sheet. The material contents of the carbon fibre sandwich are shown in Table A.2. The deck frame was designed to have five large openings for the access of the installation of the propulsion train system, sensors, carriage post attachment, the carriage pin joint and the linear slide mounting. The deck plate was also designed as the datum reference for waterlines marking and precision positioning of the instrumentation and the propulsion train system. The hull body was made using a typical plug and mould method. A set of nesting drawings consists of the demihull stations 2D drawing was given to the model maker for the frame erection of the hull plug.

The frames and the hull strip planks of the plug were made of plywood. The surfaces of the plug were later finished to a high standard of smooth finishing. Using the plug, the mould was created and used for the laying up of the carbon fibre filaments and foam core. Once the carbon fibre hull had dried and cured, the longitudinal, transverse and deck frames were assembled to the carbon fibre hull by means of adhesive applications. The model hull was painted in the AMC towing tank standard colour of yellow. The hull surface was marked with station lines and waterlines on the starboard side of the demihull.

**Table A. 2** The carbon fibre sandwich composite material content, density and sheet thickness.

| Material | Density | Sheet Thickness |
|---|---|---|
| **Carbon Fibre Filament** | 200 g/m2 | 5 – 8 μm |
| **High-Density Closed Cell Core** | 50 – 70 kg/m3 | 7mm |

## A.2 Model ballasting and trimming

Ballasting and trimming of the model were carried according to the ITTC recommended procedure (ITTC, 2011d). The model was ballasted and trimmed for six conditions in the calm water resistance test, i.e. three different static trims at two displacements. The model weight was calculated from full scale displacements using Equation A.2;

$$\Delta_M = \frac{\Delta_S}{\lambda^3}\frac{\rho_S}{\rho_M} \tag{A.2}$$

where $\Delta_M$ is the model displacement in kg, $\Delta_S$ is the full scale displacement in kg, $\rho_S$ is the sea water density of 1,025 kg/m$^3$ and $\rho_M$ is the fresh water density of 1,000 kg/m$^3$. The model was ballasted

according to the full scale displacements i.e. 2500 tonnes, which is equivalent to 50kg per demihull in model scale and 3640 tonnes, which is equivalent to 73 kg per demihull in model scale. The model demihull was weighed on an electronic scale together with all fittings such as carriage mounts and aft slider mount and ballast weights were added onto the scale until the desired weight was reached, i.e. 50 kg or 73 kg. The ballast weights used for ballasting the model were individual weights of 50 grams and 100 grams. The individual weights were in dimension of 50 mm x 50 mm x 50 mm and 100 mm x 50mm x 50mm respectively, which fits in between the two longitudinal frames of the model.

Then the model, including of all outfitting, permanent instrumentation and cabling was placed in the towing tank wet dock. The wet dock is an extension of the towing tank built with transparent glass wall and this wet dock is isolated by an aluminium lock gate to allow for calm water conditions during the process of ballasting and trimming of the model. The transparent glass wall of the wet dock is to allow the viewing of the waterline marked on the model during the process of trimming of the model. To avoid problems with model listing, the ballast weights were distributed symmetrically about the longitudinal centre line of the model. The ballast weights were distributed evenly in the model as to ensure an even trim was achieved. This procedure was repeated for the other testing static trim conditions, i.e. 0.5 and -0.5 degrees of trim angle. The positions of each ballast weights were recorded and marked on the inner hull, to allow trim adjustment for the different static trim conditions, with the model attached to the carriage. This will eliminate the need to transfer the model back to the wet dock for the trim adjustment.

## A.3 Instrumentation of the calm water resistance test

In the calm water resistance test, the measured variables were the model speed, the total resistance force, the sinkage forward and aft, the running trim and running sinkage and the towing tank water temperature. The model speeds were measured by a rotary pulse generator attached to a dedicated wheel of the towing tank carriage. The sinkage and the running trim was calculated from the measured running sinkage fore and aft. The sinkage fore and aft was measured using two Schaevitz 5000 DC-EC Linear Variable Differential Transformers (LVDT). The sinkage was calculated by taking the average values of the forward and aft LVDT readings. The running trim of the model was calculated by taking the arc tangent of the length of the forward LVDT to the aft LVDT. The total resistance forces were measured using an Advanced Mechanical Technology, Inc. (AMTI) load cell.

All the instruments mentioned above were calibrated daily. The calibration of the load cell was done using individual standard weights of 500 grams. The load cell was mounted onto a jig, with the forward side of the load cell facing upward. Then the nominated standard weights of 500 grams were placed one-by-one onto a hanging bucket, with the actual readings of the resistance force in

terms of voltage recorded. This was done up to a total of weights of 6000 grams. Then the nominated standard weights were removed one-by-one with the actual reading recorded as to check for hysteresis error. These readings were then plotted in the LABVIEW program available in the towing tank carriage PC, and the calibration factor was obtained. This calibration factor was later used to convert the voltage values to the total resistance values in Newton.

The calibration of the forward LVDT was done by sliding the LVDT upwards, one at a time in 10 mm increments. This was achieved by means of moving the transformers up with the aid of a row of precisely machined hole slots which is in 10 mm increments as shown in Figure A.2. The calibration of the LVDT starts with the model attached to the towing post and was steady at rest. A locking pin was inserted into the first starting hole slot before any actual reading was recorded. Then the actual readings of the sinkage in mm in terms of voltage were recorded. This was repeated by adjusting the model upwards to the next hole slot until a total of sinkage of 50 mm was recorded. This was repeated once again with the LVDT moving downwards, one at a time in 10 mm increments. Similar to the resistance calibration, these readings were then plotted in the LABVIEW program, and the calibration factor was obtained. This calibration was again repeated for the aft LVDT.

The model was towed at speeds which are equivalent to the Froude numbers of the full scale ship. The model speed was calculated using Froude number, $Fr = V/(gL)^{0.5}$. The acquisition of the data was recorded after a constant speed has been achieved in each run. Generally about 15 to 20 seconds of steady-state condition data was recorded for each run depending on the model speed. The recording time was reduced to 10 seconds, especially with the model running at a velocity greater than 2.9 m/s. The mean values of the measured data were calculated to give an average value of the time series data. A sufficient time was allowed between consecutive runs to achieve consistency in the results. This was due to standing waves in the towing tank which happens after completion of each run, which needs to be brought to a halt before commencing the next run.

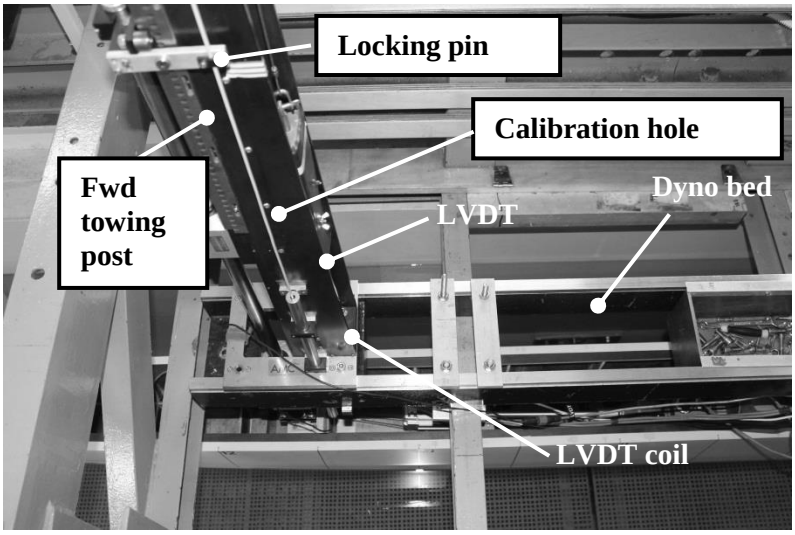


**Figure A.2** The forward LVDT with the forward post attached to the model. Note the sliding core of the LVDT and the calibration hole slots and locking pin hole.

## A.4 Calibration of the dynamometer

Initial thrust and torque coefficient were estimated from the readily available Wageningen B-series $K_T$-$K_Q$-$J$ chart (Kuiper, 1992) to provide an early estimation on the total thrust and torque of the model scale propeller for calibration purposes. Dynamometer calibration setup for both thrust and torque were done by using the static calibration rig which was supplied together with the dynamometer by Cussons as shown in Figure A.3. The static calibration rig comprises of a single post, fitted with two adjustable feet to ensure that the post was in the vertical in x and y planes, with the guide of a built-in bubble level indicator. This adjustment also ensures that the structure was also levelled at its upper end, where a fixed cruciform pad was fitted to enable the dynamometer to be mounted either horizontally or vertically by means of four bolts.

For the calibration of thrust, the dynamometer was mounted vertically onto the cruciform pad, with its output shaft facing upwards as shown in Figure A.3 (a). A yoke extending the length of the dynamometer, which holds the hanging tray was placed on the output shaft. The nominated standard weights were placed one-by-one onto the hanging tray, with the actual readings of the thrust in terms of voltage were recorded. Then the nominated standard weights were removed one-by-one with the actual reading recorded. These readings were then plotted in the LABVIEW program, and the calibration factor was obtained. This calibration factor was later used to convert the voltage values to the thrust values. A similar procedure was completed for the calibration of torque, with the exception that the dynamometer was mounted horizontally as shown in Figure A.3 (b). A double radius arm was used and was mounted on the output shaft. Two hanging trays were used for placing the standard nominated weights. Using these nominated weights the dynamometer was calibrated in torque in angular directions.

**(a)**

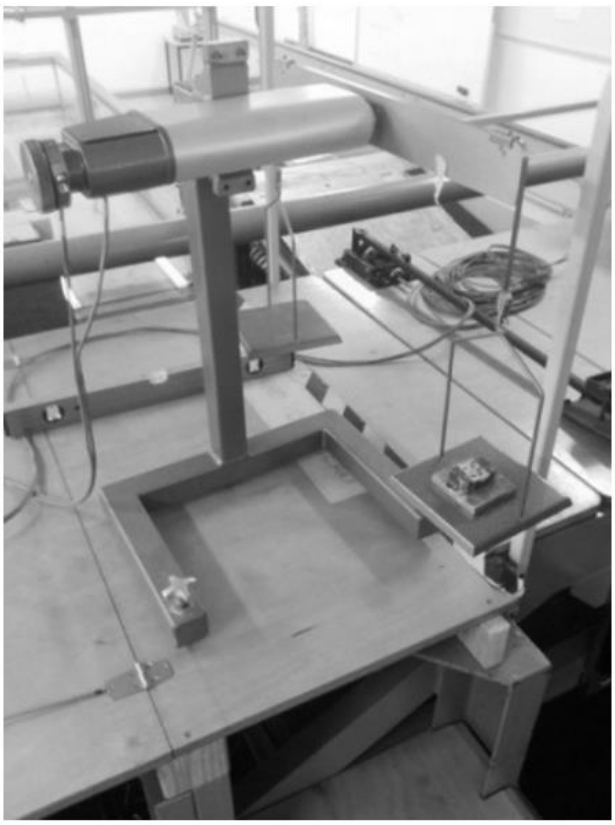

**(b)**

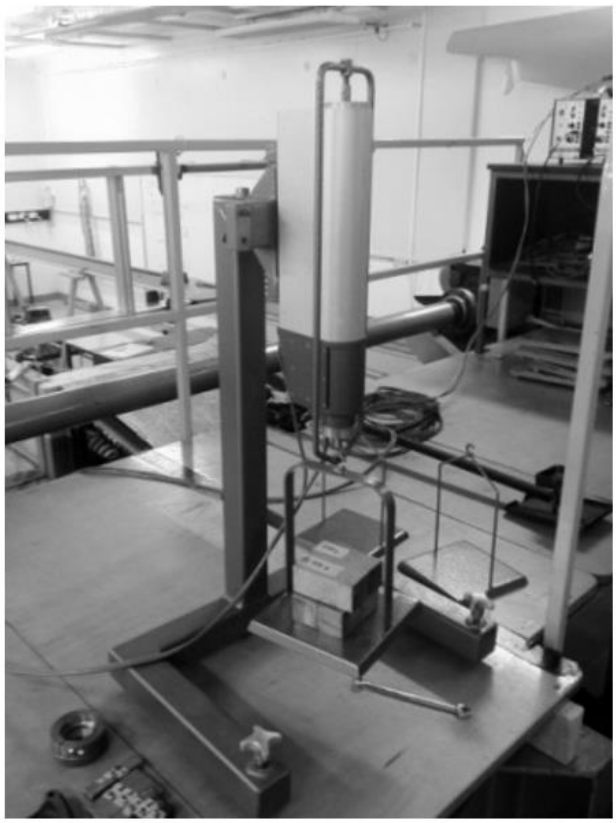

**Figure A.3** The calibration setup. **(a)** Torque calibration set-up using the double radius arm with the input shaft locked with a brass locking-ring. The hanging tray was attached to the both ends of the double radius arm by means of metal tapes. **(b)** Thrust calibration setup using a yoke extension placed on the output shaft which carried the hanging tray for the placement of the standard nominated weights.

## A.5 The propeller design and fabrication

The propeller used in the model testing was based on the Wageningen systematic propeller B series, which can be found in Kuiper (1992). The propeller design was based on the available Wageningen B-series propeller $K_T$-$K_Q$-$J$ charts. These charts were results of the series presented as tabulations of non-dimensional thrust and torque coefficients ($K_T$ and $K_Q$ respectively) with respect to the non-dimensional advance ratio, $J$. Using the ratio of $K_T/J^2$, where the full equation is shown in Equation A.3,

$$\frac{K_T}{J^2} = \frac{T}{\rho n^2 D^4} \cdot \frac{n^2 D^2}{V_A^2} = \frac{T}{\rho D^2 V_A^2} \tag{A.3}$$

with known speed of advance, thrust and the largest possible propeller diameter that fits under the stern, the optimal shaft revolution and the maximum efficiency can be calculated. This was done by plotting the curve $K_T = J^2(T/\rho V_A^2 D^2)$ on the $K_T$-$K_Q$-$J$ diagram. This curve corresponds to the ship requirements. The intersection of this curve with all of the $K_T$-$J$ curves (different $P/D$ ratios) then were identified, and the corresponding efficiency $\eta_O$ were read off. Finally the curve $\eta_O$-$J$ was plotted and the maximum of this curve corresponds to the optimal propeller.

A few assumptions had to be made to the propeller thrust and the velocity of advance in the propeller design calculations. In the propeller design, the following data are to be known: the propeller thrust $T$, the propeller diameter, $D$ and the advance velocity of the propeller $V_A$. The estimated thrust was obtained from test data from the final report of calm water tests for the JHSV wave piercing catamaran (Marin, 2008). The calm water tests were performed by the Maritime Research Institute of Netherlands (MARIN) in November 2008. The B-series selected for the optimisation were propeller B4.70, B4.85, B4.100, B5.60, B5.90 and B5.105. In this design, the right hand propeller was selected. The propeller preliminary designs were done for corresponding speed of 30 knots and 20 knots, which were the highest and the lowest corresponding speed in the towing tank test. In the end, the propeller with best efficiency, low cavitation and optimal shaft revolution was selected. Cavitation checks were performed to the selected propellers based on the Burrill chart (Burrill & Emerson, 1953, 1962) . This chart is also available in Carlton (2007).The cavitation checks were done in full scale.

The results of the open water efficiency, the shaft speed and the severity of the cavitation occurring on the back side of the propeller blade are shown in Table A.3 and A.4. These results are for the model corresponding speed of 30 knots and 20 knots respectively. The selection of the optimum propeller for the Incat model was based on the best open water efficiency, the lowest shaft

revolution and the minimum back cavitation of the propeller. It was concluded that the optimum propeller is the propeller B5.75, with 5 blades and 75% blade area ratio.

The B5.75 propeller surface in three dimensional form was designed in PropCAD (HydroComp, 2010), which is a commercial software used for geometric modelling of marine propellers. The surface model of the B5.75 propeller was available in the PropCad design library. Then the surface model of the B5.75 propeller was exported to Rhinoceros 3D software (Cheng, 2014; van der Kley, 2013) for further detailed design such as the propeller hub design, the propeller bore diameter, the root radii, the propeller blade leading edge radii and the keyway. This was done by transferring the surface profile data into a text file. The software, Rhinoceros was able to read this text file which contains the data for the hub and a single blade profile. In Rhinoceros, the leading edge radii and the root radii of a single blade was created and joined with the surface of the blade, the single blade was copied and rotated to make a complete 5 bladed propeller. Then all surfaces were joined and converted into a solid body. Then the solid body of the propeller data was converted into a Stereolithography (STL) file format. This is the most important step in the Computer Aided Manufacturing (CAM) process later. Then the 120mm diameter model propeller was computer numerical control (CNC) machined by Danford Engineering in Melbourne. The model propeller was machined out of brass. The finished propeller was polished with a fine grade abrasive paper before testing.

**Table A. 3** The performance of B-series propeller propelling the Incat propeller driven catamaran model at a corresponding speed of 30 knots which is equivalent to a model speed of 3.0 m/s.

| | **P/D** | **J** | **$K_T$** | $\eta_O$ | $\eta_M$ | ***$N_M$(rpm)*** | ***$N_S$(rpm)*** | ***Back Cavitation*** |
|---|---|---|---|---|---|---|---|---|
| **B4.70** | 1.1 | 0.77 | 0.20 | 0.65 | 32.47 | 1948 | 361.8 | **<20%** |
| **B4.85** | 1.1 | 0.76 | 0.20 | 0.65 | 32.89 | 1973 | 366.6 | **10%** |
| **B4.100** | 1.1 | 0.76 | 0.20 | 0.64 | 32.89 | 1973 | 366.6 | **10%** |
| **B5.60** | 1.2 | 0.83 | 0.23 | 0.66 | 30.12 | 1807 | 335.4 | <20% |
| **B5.75** | **1.2** | **0.83** | **0.24** | **0.66** | **30.12** | **1807** | **335.4** | **<20%** |
| **B5.90** | 1.2 | 0.83 | 0.23 | 0.65 | 30.12 | 1807 | 335.4 | **<20%** |
| **B5.105** | 1.2 | 0.83 | 0.23 | 0.65 | 30.12 | 1807 | 335.4 | **<20%** |

**Table A. 4** The performance of B-series propeller propelling the Incat propeller driven catamaran model at a corresponding speed of 20 knots which is equivalent to a model speed of 1.91 m/s.

| | **P/D** | **J** | **$K_T$** | $\eta_O$ | $\eta_M$ | ***$N_M$(rpm)*** | ***$N_S$(rpm)*** | ***Back Cavitation*** |
|---|---|---|---|---|---|---|---|---|
| **B4.70** | 1.0 | 0.67 | 0.19 | 0.63 | 23.76 | 1425 | 264.6 | **2.5%** |
| **B4.85** | 1.1 | 0.69 | 0.23 | 0.60 | 23.07 | 1384 | 256.8 | **<2.5%** |
| **B4.100** | 1.1 | 0.72 | 0.22 | 0.61 | 22.11 | 1327 | 246.6 | **<2.5%** |
| **B5.60** | 1.1 | 0.72 | 0.24 | 0.63 | 22.11 | 1327 | 246.6 | **<2.5%** |
| **B5.75** | **1.1** | **0.72** | **0.24** | **0.63** | **22.11** | **1327** | **246.6** | **<2.5%** |
| **B5.90** | 1.1 | 0.72 | 0.23 | 0.63 | 22.11 | 1327 | 246.6 | **<2.5%** |
| **B5.105** | 1.1 | 0.72 | 0.23 | 0.62 | 22.11 | 1327 | 246.6 | **<2.5%** |

# Appendix B

# Uncertainty Analysis

The uncertainty analysis was also done to identify which sources of error had the most influence on the total uncertainty in the measurements as well as to ascertain the overall level of uncertainty in the measurements during the model testing, i.e. calm water resistance test, open water propeller test and self-propulsion test. It will also provide a guide for the uncertainty analysis of further tests of the 130m propeller driven catamaran conducted at other testing facilities.

There are two types of errors were considered for the uncertainty analysis; bias errors and precision errors. These terms of bias and precision errors were adapted from the work of Moffatt (1982). Precision errors are the scatter in the results which is found in the repeated measurements. Bias errors are systematic errors and these errors cannot be measured but have to estimated based on assumptions.

In this appendix, an explanation on how the bias error sources were obtained and the tabulated summaries of the overall uncertainties results are presented.

## B.1 Model length and wetted surface area bias error

The bias error in the model length (on the waterline) due to manufacturing error was assumed to be $\pm$ 0.001m. The bias error in the model wetted surface area (on the waterline) due to manufacturing error in the model geometry was estimated at $\pm$ 0.00041 $m^2$.

## B.2 Propeller geometry bias error

The bias error in the diameter of the propeller model was estimated at $\pm$ 0.0001m. This uncertainty in the propeller diameter was estimated from the error in the CNC machining of the propeller model. Only the bias error on the propeller diameter will be considered here, although there are potential errors from chord length, pitch and blade section shape. The bias errors from the chord length, pitch and blade section are small and therefore are ignored in the estimation of the propeller geometry error.

## B.3 Towing tank water properties bias error

The tank water temperature was measured using a thermometer with a Celsius scale with divisions at every 1 degree Celsius. The thermometer was assumed to be accurate at $\pm$ 0.5 degrees.

The bias error in the water density was obtained by calculating the RSS of the three bias components for the water density, which are the density-temperature relationship (table) error and the data reduction error. The overall bias limit was calculated using the RSS method where it merged all the two bias error to $\pm$ 0.660kg/m$^3$.

The bias error in the fresh water kinematic viscosity was estimated at $\pm$ 4.52E-0.9 m$^2$/s.

## B.4 Carriage speed bias error

The bias errors identified in the carriage velocity measurements were estimated using the standard deviation of the speed measured in the individual test run. The author was not able to follow the procedure provided by the ITTC guidelines (ITTC, 1999b) in estimating bias error using the RSS of the bias error in pulse count, bias error in the carriage wheel diameter and the bias error in the time base as there is no accurate information on this provided in the AMC's towing tank manual. The bias error of the carriage speed is normally very small as reported by Longo and Stern (2005) and Stern et al. (2000). Therefore based on experience from other towing tank institute, the bias error for the carriage speed was estimated at $\pm$ 0.2% of the nominal speed.

## B.5 Resistance measurement bias error

The bias error in the resistance measurement or the drag measured in the model when towed through the water can be divided into four error sources which are (1) the calibration error, (2) the curve fit error, (3) the load cell misalignment error and (4) the towing force inclination error (ITTC, 1999b).

A calibration error existed in the calibration of the load cell (resistance transducer) due to the inaccuracy in the standard weights used in the calibration of the load cell. The individual weights used in the calibration were a set of 500 grams weight. The calibration was performed from 0 to 6000 grams with an increment of 500 grams, which means 12 individual weights of 500 grams were used. The individual weight error was estimated at $\pm$ 0.5 grams. Therefore the total calibration error was calculated to be at $\pm$ 0.006 kg.

The bias for the curve fit error was estimated using the standard error in the regression equation (SEE) as in Equation 4.1 (Coleman & Steele, 1999; ITTC, 1999b),

$$SEE_{m_x} = \sqrt{\frac{\sum_{i=1}^{N}\left(m_i - sv_i - c\right)^2}{N-2}} \tag{B.1}$$

where $m_i$ is the mass increment in the mass/volt relation curve of the load cell calibration, $s$ is the gradient of the mass/volt relation curve, $v_i$ is the volt increment in the mass/volt relation curve, $c$ is the point crossing the y-axis (mass) in the mass/volt relation curve and $N$ is the number of samples or steps taken in the calibration of the load cell. The SEE equation was multiply by two, as $\pm$ 2(SEE) band will contain approximately 95% (95% confidence interval) of the data points (Coleman & Steele, 1999; ITTC, 1999b, 2002a). The bias limit for the curve fit error calculated using Equation B.1, resulted in a bias of $\pm$ 0.046 kg.

The third error was from the load cell misalignment. This misalignment error is basically the difference in the orientation of the load cell between calibration and the test condition itself. The load cell misalignment was estimated by measuring the maximum angle of the mechanical backlash or free play of the load cell relative to the model centreline. This backlash angle was estimated to be at $\pm$ 0.55 degrees. and the bias error equation which can be found in ITTC (2002a) is written as

$$B_{m_{x3}} = m_x - \left[\cos\phi\left(m_x\right)\right] \tag{B.2}$$

where $m_x$ is the resistance measured and $\phi$ is the misalignment angle in degrees. For an example the bias error with the resistance measured at 4 kg was calculated to be at 0.00018kg.

The fourth error was from the load cell inclination error. This inclination happens as the model trims and sinks during a test run, which result in an inclination of the towing force compared to the calibration which is expressed as a bias error $B_{mx4}$. The inclination angle can be obtained from the dynamic trim results. For an example the bias error with the resistance measured at 4 kg and the inclination angle at 1 degree leads to a bias error of 0.0006 kg. Finally, the total bias limit in the resistance was obtained by using the RSS of the four bias components considered earlier, where the total bias limit was calculated to be at $\pm$ 0.046kg.

## B.6 Bias error in the towing force

The bias error identified in the towing force is identical to the bias error estimated in the resistance measurements, see resistance bias error section.

## B.7 Bias error in propeller thrusts

The bias error in the propeller thrust was estimated by calculating the RSS of three bias error component which were the bias for (1) the weight calibration $B_{Tw}$, (2) bias error for the A/D converter $B_{TAD}$ and (3) the bias error in the thrust transducer calibration $B_{Tcf}$. The total bias limit in the propeller thrust can be written as;

$$\left(B_T\right)^2 = \left(B_{Tw}\right)^2 + \left(B_{T_{AD}}\right)^2 + \left(B_{T_{CF}}\right)^2 \tag{B.3}$$

The bias error in the weight calibration was calculated similar to the bias error in the weight calibration for the resistance load cell. The individual weight error was estimated at $\pm$ 0.5 grams. Therefore the total calibration error was calculated to be at $\pm$ 0.006 kg.

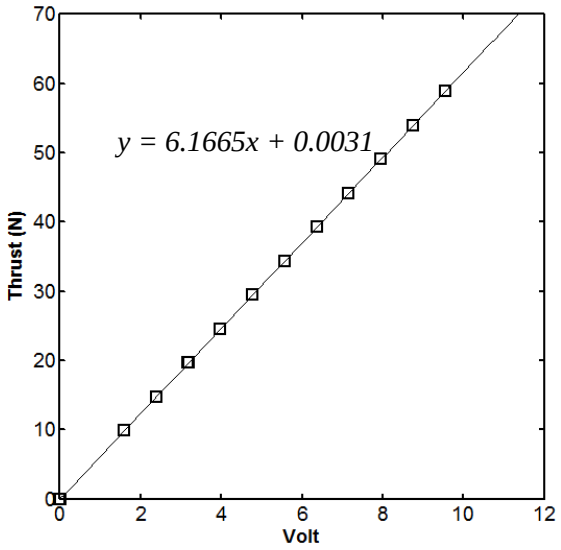


**Figure B.1** The thrust – voltage calibration curves for the R-25 Cussons propeller dynamometer. The slope of the curve was at 6.1665.

The bias error in the A/D converter was estimated using the resolution rate of the 12 bits A/D converter (in volts per total bits) times the slope of the thrust calibration curves (ITTC, 2002a). The thrust calibration curves are shown in Figure B.1 where the slope of the calibration curves was at 6.1665. The A/D converter used in the carriage was a National Instruments A/D converter card. This 12 bits and 16 channels A/D converter card was installed in the PC device in the towing tank carriage. Using the slope of the thrust – volt calibration curves the bias error in the propeller thrust was calculated to:

$$B_{T_{AD}} = \frac{(10volts)}{2^{12}} \times 6.1665 = 0.015N = 0.00153kg \tag{B.4}$$

The bias error in the thrust transducer calibration $B_{Tcf}$, i.e. the R31 Cussons propeller dynamometer, was calculated using the regression equation (SEE) as in Equation B.1. The bias error in the transducer calibration $B_{Tcf}$ was found to be at $\pm$ 0.043kg. Then by calculating the RSS of the three bias error component, the three bias error component was merged into a total thrust bias limit of $\pm$ 0.043kg.

## B.8 Bias error in the propeller torque

The bias error in the propeller torque was calculated similar to the steps shown in the calculation of the bias error in the propeller thrust. The bias error was estimated by calculating the RSS of the three bias error components which were the bias for (1) the weight calibration $B_{Qw}$, (2) the bias error for the A/D converter $B_{QAD}$ and (3) the bias error in the thrust transducer calibration $B_{Qcf}$. The total bias limit in the propeller torque can be written as;

$$\left(B_Q\right)^2 = \left(B_{Qw}\right)^2 + \left(B_{Q_{AD}}\right)^2 + \left(B_{Q_{CF}}\right)^2 \tag{B.5}$$

The three bias error components were calculated using the RSS of the three components, and the three bias error components were merged into a total torque bias limit of $\pm$ 0.0009 Nm.

## B.9 Bias limit in the velocity of advance of the propeller

The bias error identified in the velocity of advance of the propeller is identical to the bias error estimated in the carriage velocity measurements, see carriage speed bias error section.

## B.10 Overall uncertainty in the self-propulsion test

The overall uncertainty in the delivered power, ship's torque and the shaft speed were determined using the Monte Carlo simulation as explained in Chapter 4 – Uncertainty Analysis. Tabulated summaries of the results of uncertainties in the delivered power, ship's torque and the shaft speed for Froude number range from 0.26 to 0.44 at two displacements (3,640 tonnes and 2,500 tonnes) are shown in Table B.1 and Table B.2. These results are for the uncertainties in the delivered power, ship's torque and the shaft speed extrapolated using the ITTC1978 extrapolation procedures. The uncertainties in the delivered power, ship's torque and the shaft speed extrapolated using the SPT procedures are shown in Table B.3 and Table B.4.

The plotted uncertainties in terms of the delivered power, ship's torque and the shaft speed are shown in in Chapter 4 – Uncertainty Analysis, Section 4.8.

**Table B. 1** Overall uncertainty (95% confidence level) in the delivered power, ship torque and ship propeller's shaft speed of the 130m propeller driven catamaran at a displacement of 3,640 tonnes. These values were extrapolated using the ITTC1978 method.

| Fr | $U_{PD}$ (kW) | Percentage error in $P_D$ | $U_{QS}$ (Nm) | Percentage error in $Q_S$ | $U_{nS}$ (rps) | Percentage error in $n_S$ |
|---|---|---|---|---|---|---|
| **0.44** | ± 1828 | ± 8.11 | ± 25553 | ± 6.53 | ± 0.0548 | ± 1.66 |
| **0.40** | ± 1360 | ± 9.06 | ± 21363 | ± 7.88 | ± 0.0557 | ± 1.91 |
| **0.38** | ± 1012 | ± 9.99 | ± 17590 | ± 7.74 | ± 0.0497 | ± 1.83 |
| **0.35** | ± 737 | ± 9.09 | ± 14454 | ± 7.75 | ± 0.0415 | ± 1.74 |
| **0.32** | ± 585 | ± 9.21 | ± 12538 | ± 8.23 | ± 0.0385 | ± 1.57 |
| **0.29** | ± 518 | ± 11.57 | ± 11836 | ± 9.88 | ± 0.0404 | ± 1.98 |
| **0.26** | ± 438 | ± 13.99 | ± 11255 | ± 12.29 | ± 0.0433 | ± 2.36 |

**Table B. 2** Overall uncertainty (95% confidence level) in the delivered power, ship torque and ship propeller's shaft speed of the 130m propeller driven catamaran at a displacement of 2,500 tonnes. These values were extrapolated using the ITTC1978 method.

| Fr | $U_{PD}$ (kW) | Percentage error in $P_D$ | $U_{QS}$ (Nm) | Percentage error in $Q_S$ | $U_{nS}$ (rps) | Percentage error in $n_S$ |
|---|---|---|---|---|---|---|
| **0.44** | ± 1398 | ± 8.92 | ± 22803 | ± 8.37 | ± 0.0521 | ± 1.72 |
| **0.40** | ± 1035 | ± 10.86 | ± 18697 | ± 9.48 | ± 0.0505 | ± 1.84 |
| **0.38** | ± 790 | ± 10.98 | ± 15604 | ± 10.19 | ± 0.0483 | ± 1.89 |
| **0.35** | ± 629 | ± 12.36 | ± 13896 | ± 10.42 | ± 0.0439 | ± 1.83 |
| **0.32** | ± 514 | ± 13.64 | ± 12281 | ± 12.12 | ± 0.0417 | ± 1.99 |
| **0.29** | ± 422 | ± 14.67 | ± 11186 | ± 14.65 | ± 0.0427 | ± 2.09 |
| **0.26** | ± 370 | ± 18.73 | ± 10987 | ± 17.64 | ± 0.0427 | ± 2.38 |

**Table B. 3** Overall uncertainty (95% confidence level) in the delivered power, ship torque and ship propeller's shaft speed of the 130m propeller driven catamaran at a displacement of 3,640 tonnes. These values were extrapolated using the self-propulsion test only method.

| Fr | $U_{PD}$ (kW) | Percentage error in $P_D$ | $U_{QS}$ (Nm) | Percentage error in $Q_S$ | $U_{nS}$ (rps) | Percentage error in $n_S$ |
|---|---|---|---|---|---|---|
| **0.44** | ± 1070 | ± 3.38 | ± 13062 | ± 2.62 | ± 0.0360 | ± 0.894 |
| **0.40** | ± 954 | ± 4.48 | ± 13806 | ± 3.64 | ± 0.0387 | ± 1.084 |
| **0.38** | ± 912 | ± 5.71 | ± 14076 | ± 4.47 | ± 0.0544 | ± 1.556 |
| **0.35** | ± 827 | ± 6.84 | ± 13998 | ± 5.35 | ± 0.0426 | ± 1.390 |
| **0.32** | ± 754 | ± 7.67 | ± 13730 | ± 6.18 | ± 0.0466 | ± 1.619 |
| **0.29** | ± 733 | ± 9.07 | ± 14583 | ± 7.10 | ± 0.0555 | ± 2.008 |
| **0.26** | ± 637 | ± 10.87 | ± 13964 | ± 8.78 | ± 0.0577 | ± 2.305 |

**Table B. 4** Overall uncertainty (95% confidence level) in the delivered power, ship torque and ship propeller's shaft speed of the 130m propeller driven catamaran at a displacement of 2,500 tonnes. These values were extrapolated using the self-propulsion test only method.

| Fr | $U_{PD}$ (kW) | Percentage error in $P_D$ | $U_{QS}$ (Nm) | Percentage error in $Q_S$ | $U_{nS}$ (rps) | Percentage error in $n_S$ |
|---|---|---|---|---|---|---|
| **0.44** | ± 995 | ± 4.83 | ± 13763 | ± 3.76 | ± 0.1295 | ± 3.19 |
| **0.40** | ± 966 | ± 6.66 | ± 15022 | ± 5.29 | ± 0.0423 | ± 1.28 |
| **0.38** | ± 811 | ± 7.27 | ± 13829 | ± 5.94 | ± 0.0332 | ± 1.17 |
| **0.35** | ± 691 | ± 8.64 | ± 13109 | ± 7.05 | ± 0.0469 | ± 1.63 |
| **0.32** | ± 646 | ± 10.07 | ± 13266 | ± 8.31 | ± 0.0410 | ± 1.76 |
| **0.29** | ± 597 | ± 11.88 | ± 13309 | ± 10.04 | ± 0.0548 | ± 2.20 |
| **0.26** | ± 543 | ± 15.63 | ± 13637 | ± 12.87 | ± 0.0504 | ± 2.42 |

# Appendix C

## MATLAB Code for Self-Propulsion Test only extrapolation procedure

```
% ------------------------------------------------------------------------
%# Self-Propulsion Test Extrapolation – SPT only procedure
%# ------------------------------------------------------------------------
%#
%# Author     :  Iwan Mustaffa Kamal (iwanmk@utas.edu.au)
%# Date       :  November 26, 2013
%#
%# %# Facility   :  AMC, Towing Tank (TT)
%-------------------------------------------------------------------------%

% clear workspace and command window

%-------------------------------------------------------------------------%
% clear workspace and command window
clc
clear
%-------------------------------------------------------------------------%
%# ------------------------------------------------------------------------
%# Find and close all plots
%# ------------------------------------------------------------------------
allPlots = findall(0, 'Type', 'figure', 'FileName', []);
delete(allPlots);   % Close all plots
%-------------------------------------------------------------------------%
% ************************************************************************
% START: PLOT SWITCHES: 1 = ENABLED
%                       0 = DISABLED
% ------------------------------------------------------------------------
% Plot titles, colours, etc.
enablePlot                = 1;    % Show plot
%-------------------------------------------------------------------------%
% data reading from excel file

%*************************************************************************

self_prop_data      = xlsread('self_prop_data_Incat_3640t', 'Fr 0.26');
input_data          = xlsread('input_load_varied','Incat_3640t');
%*************************************************************************
scale_ratio         = input_data(1,1);
rho_m               = input_data(2,1);
```

```
rho_s               = input_data(3,1);
formfact            = input_data(4,1);
tanktemp            = input_data(5,1);
seatemp             = input_data(6,1);
diapropMS           = input_data(7,1);
chordL_ship         = input_data(8,1); % m (model scale) x 29 (scale ratio)
CA                  = input_data(9,1);
shipWL              = input_data(10,1);
wsaShip             = input_data(11,1);
wake_model          = input_data(12,1);
wake_ship           = input_data(13,1);
blade_thickness     = input_data(14,1); % m (model scale) x 29 (scale ratio)
blade_roughness     = input_data(15,1);
PD_Ratio            = input_data(16,1);
no_Blades           = input_data(17,1);

velmodel = self_prop_data(:,1);
towing_force = self_prop_data(:,2);
propRPM = self_prop_data(:,3);
thrust = self_prop_data(:,4);
torque = self_prop_data(:,5);

diapropFS = diapropMS*scale_ratio;        % diameter of prop - full scale
modelWL  = shipWL / scale_ratio;
propRPS = propRPM ./60;
wsaModel = wsaShip / (scale_ratio*scale_ratio);

%************************************************************************
%extrapolation starts
%************************************************************************

%************************************************************************
%creating the poly values for the towing force vs thrust plots
%this is for creating the F - T plot
n_linear = 1;
xi = linspace(-40,50,100);

pol_self_prop = polyfit (thrust,towing_force,n_linear);
y_self_prop = polyval(pol_self_prop,xi);
%************************************************************************

%************************************************************************
%viscosity calculation based on ITTC Guidelines
viscosFW = (((0.000585*(tanktemp-12))-0.03361)*(tanktemp-12)+1.235)*0.000001;
viscosSW = ((0.000659*(seatemp-1)-0.05076)*(seatemp-1)+1.7688)*0.000001;
%************************************************************************

%************************************************************************
%matrices of ship speed and model speed taken from self-prop test
velShip = velmodel.*sqrt(scale_ratio);
%************************************************************************

%************************************************************************
% Reynolds number calculation for model and full scale
RNM = velmodel.*modelWL/viscosFW;
RNS = velShip.*shipWL/viscosSW;
%************************************************************************

%************************************************************************
```

```
%Calculation of CFm and CFs which will be used in CFd calculation
CFM = 0.075./(log10(RNM)-2).^2;
CFS = 0.075./(log10(RNS)-2).^2;
%*************************************************************************

%*************************************************************************
%self-propulsion point calculation
FD = mean(0.5*rho_m.*velmodel.^2*wsaModel.*((1+formfact)*(CFM-CFS)-CA));
%*************************************************************************

%*************************************************************************
%selecting the first matrix of pol_self_prop as to obtained the thrust
%deduction fraction from t - 1 = slope gradient
t = pol_self_prop(1,1)+ 1;

%Calculation of method (2) and (3) in chapter 6
Graphical_m = (FD - pol_self_prop(1,2))/ pol_self_prop(1,1);
TF0_FD = -(pol_self_prop(1,2)/pol_self_prop(1,1))- FD;
FT0_FD_1t = (pol_self_prop(1,2)- FD)/(1-t);
%*************************************************************************

%*************************************************************************
%Calculation of CTS as to be used in calculating PE later
RTM = pol_self_prop(1,2);
CTM = RTM ./(0.5*rho_m*wsaModel.*(velmodel.^2));
CTS = CTM +((1+formfact)*(CFS-CFM))+ CA;
%*************************************************************************

%*************************************************************************
%value of model thrust at the value if the towing force equivalent to the
%self propulsion point of the ship
TM = (FD - pol_self_prop(1,2))/(t - 1);
%extrapolation to full scale thrust
TS = TM*scale_ratio^3*(rho_s/rho_m);
TM1 = TM + FD;
%*************************************************************************

%*************************************************************************
%shaft speed calculation
nm = interp1 (thrust,propRPS,TM);
ns = (1/sqrt(scale_ratio)) * nm;
%*************************************************************************

%*************************************************************************
%coefficient form of the thrust and torque
KTP = thrust./(rho_m.*propRPS.^2*diapropMS^4);%/no_prop;
KQP = torque./(rho_m.*propRPS.^2*diapropMS^5);%/no_prop;
%*************************************************************************

%*************************************************************************
%wake scaling
J   = velmodel./(propRPS.*diapropMS);
JS = J.*((1 - wake_model)/(1 - wake_ship));
%*************************************************************************



%*************************************************************************
%Calculation using Benedek correction
```

```
%%*************************************************************************
velship = velmodel.*(sqrt(scale_ratio));
propRPS_S = propRPS./ (sqrt(scale_ratio));
chordL    = chordL_ship/scale_ratio;
r = 0.75*diapropMS/2;

rNCO      = (chordL.* (velmodel.^2+((2*pi().*propRPS*r).^2)).^(0.5))/viscosFW;
rNCO_s    =
(chordL_ship.*(velship.^2+((2*pi().*propRPS_S*r).^2)).^(0.5))/viscosSW;

%Calculation of CFm and CFs which will be used in CFd calculation
CFMo = 0.075./((log10(rNCO)-2).^2);
CFSo = 0.075./((log10(rNCO_s)-2).^2);
%*************************************************************************
phi = atan (1.2/(0.75*pi()));
delkt = (pi()./4).*(0.75).*(CFMo-CFSo).*(J.^2+((0.75*pi())^2))*sin(phi);
delkq = (pi()./4).*(0.75).*(CFMo-CFSo).*(J.^2+((0.75*pi())^2))*0.375*cos(phi);

KTS= KTP - delkt;
KQS= KQP + delkq;
%*************************************************************************

%*************************************************************************
degree = 2;
xii = linspace(0,3.5,100);

KTS_J2 = (TS .*(J.^2)) ./ (rho_s*diapropFS^2.*velShip.^2);%/no_prop;


pol_KTS_J2 = polyfit (J,KTS_J2,degree);
y_KTS_J2 = polyval (pol_KTS_J2,xii);

pol_KTS = polyfit(JS,KTS,degree);
y_KTS = polyval(pol_KTS,xii);

pol_KQS = polyfit (JS,KQS,degree);
y_KQS = polyval (pol_KQS,xii);

%determination of the intersections
J_point = intersections(xii,y_KTS, xii, y_KTS_J2,degree);
KTS_point = interp1(xii,y_KTS,J_point);
KQS_point = interp1(xii,y_KQS,J_point);
%*************************************************************************

%*************************************************************************
%calculation of the remaining full scale operating parameters
n_s = velShip./(J_point*diapropFS);
PDS = 2*pi()*KQS_point*rho_s.*ns.^3*diapropFS^5;
QS = KQS_point*rho_s.*ns.^2*diapropFS^5;
PE = 0.5*CTS*rho_s*wsaShip.*velShip.^3;
eta_D =PE./PDS;
%*************************************************************************
output = [t mean(PE) mean(PDS) mean(n_s) mean(TS) mean(QS) mean(eta_D)]';
save results.txt output -ascii

%%%%%%%%%%%%%%%%%%%%%%%%%%%%%%%%%%%%%%%%%%%%%%%%%%%%%%%%%%%%%%%%%%%%%%%%%%%%
%close;
```

# Appendix D

## The calculation of appendage drag

In this appendix, the formulation used in the calculation of the appendage drag are explained. The catamaran single demihull were attached with a rudder and a shaft bracket as shown in Figure D.1. There are few options in deriving full-scale appendage drag as mentioned in Manen and Oossanen (1988) which are as the following:

1. The full-scale resistance of the naked hull is extrapolated from the model tests and the calculated appendage drag are calculated, at full scale and added to the full-scale resistance.
2. The resistance and the propulsion characteristics of the appended model is measured experimentally. The resistance of the appendages is then calculated at the model Reynolds number using well established formulation from R. W. Peck (1976), Hoerner (1965) and Kirkman and Kloetzli (1980). The calculated appendage drag then are subtracted from the measured total resistance. Then the resulting resistance values are extrapolated to full-scale. The calculated appendage resistance in the full-scale Reynolds number is added to the extrapolated full-scale resistance values.

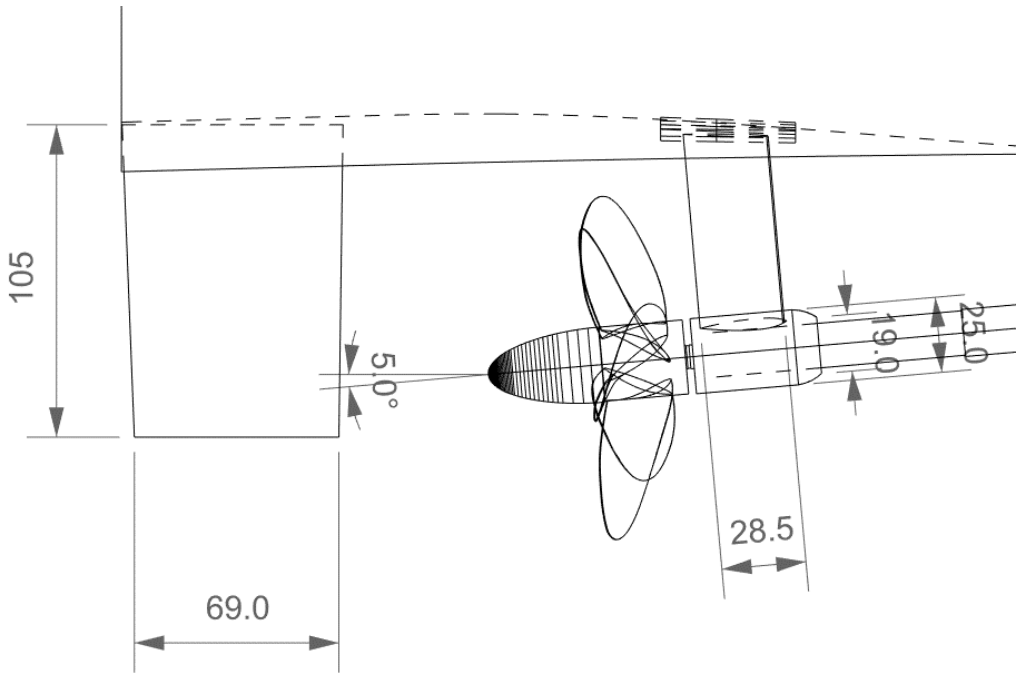


**Figure D.1** The appendages attached to the catamaran model consist of a rudder and a shaft bracket with a barrel. All the dimensions shown above are in millimetres and in model scale.

## D.1 Calculation of appendage drag in model scale

In model scale where the Reynolds number is between 5 x $10^5$ and 1 x $10^7$, the equation D.7 is not accurate enough, since the skin friction coefficient to be used in Equation D.7 is that for a turbulent boundary layer. The drag of the rudder or the shaft brackets in the model scale were calculated using the formulation developed by Kirkman and Kloetzli (1980) to determine the appropriate $C_D$ values for a control surface drag at low Reynolds number as in Equation D.1:

$$C_{D,rudder,bracket} = 0.00293\left[1 + 2\left(\frac{t}{c}\right) + 60\left(\frac{t}{c}\right)^4\right] \tag{D.1}$$

where $c$ = mean chord length

$t$ = maximum thickness of the rudder

The pressure drag of the propeller shaft in model scale was calculated using the approximate formula given by Kirkman and Kloetzli (1980) as in Equation D.2:

$$C_{DP} = 1.1\sin^3\alpha \tag{D.2}$$

where $\alpha$ = angle between the flow lines and shaft axis.

The frictional drag of the propeller shaft in model scale for Re $\leq$ 5 x $10^5$ was calculated using the formulation which can be found in Kirkman and Kloetzli (1980) as in Equation D.3:

$$C_F = 1.327\left(\mathrm{Re}\right)^{-0.5} \tag{D.3}$$

where $Re = \frac{Vlc}{\upsilon}$ and $lc = \frac{l}{\tan\alpha}$, l is the length of the shaft and $\alpha$ is the angle between the flow lines and the shaft axis. Once the pressure and the frictional drag coefficient were calculated, the total drag on the shaft can be found using the formulation as in Equation D.4:

$$D_{shaft} = \frac{1}{2}\rho L_{SH} d V^2 \left(C_{DP} + C_F\right) \tag{D.4}$$

There are interference of the strut bracket appendages with the flow along the hull. The interference drag were calculated using the formulation which can be found in Hoerner (1965):

$$D_{\mathrm{int}} = \frac{1}{2}\rho V^2 t^2\left[0.75\left(\frac{t}{c}\right) - \frac{0.0003}{\left(t/c\right)^2}\right] \tag{D.5}$$

Then the total appendage drag in model scale can be calculated by summing up all the drag calculated in Equation D.1 to D.5:

$$Total\ appendage\ drag = D_{rudder} + D_{bracket} + D_{shaft} + D_{\text{int}} \tag{D.6}$$

## D.2 Calculation of appendage drag in full scale

The resistance of the rudder and the shaft brackets of the propeller driven catamaran in full-scale can be calculated using R. W. Peck (1976) equation for control surfaces which is as in Equation D.7:

$$D_{rudder,bracket} = \frac{1}{2}\rho S V^2 C_F \left[ 1.25\frac{c}{c_f} + \frac{S}{A} + 40\left(\frac{t}{c_a}\right)^3 \right] \tag{D.7}$$

where $c$ = mean chord length = $c_f$ + $c_a$

$c_f$ = chord length from the nose of the rudder or the shaft bracket to the location of the maximum thickness line of the rudder or the shaft bracket

$c_a$ = chord length from the tail of the rudder or the shaft bracket to the location of the maximum thickness line of the rudder or the shaft bracket

$S$ = wetted surface area of the rudder or the shaft brackets

$A$ = frontal area of section of maximum thickness

$t$ = maximum thickness

$V$ = ship speed

The frictional drag of the propeller shaft in full scale was calculated using the formulation which can be found in Kirkman as in Equation D.8:

$$C_F = \frac{1}{\left(3.46\log_{10}\mathrm{Re} - 5.6\right)^2} - \frac{1700}{\mathrm{Re}} \tag{D.8}$$

where $Re = \frac{Vlc}{\upsilon}$ and $lc = \frac{l}{\tan\alpha}$, l is the length of the shaft and $\alpha$ is the angle between the flow lines and the shaft axis. The pressure drag of the propeller shaft in full scale was calculated using the approximate formula given by Kirkman as in Equation D.9:

$$C_{DP} = 0.60 \tag{D.9}$$

Then the total appendage drag in model scale can be calculated by summing up all the drag calculated in Equation D.7 to D.9:

$$Total\ appendage\ drag = D_{rudder} + D_{bracket} + D_{shaft} + D_{\text{int}} \quad \text{(D.10)}$$

## D.3 Results of the appendage drag in full scale and model scale

Tabulated summaries of the results of the total appendage drag in model and full scale for Froude number range from 0.26 to 0.44 at displacements 3,640 tonnes are shown in Table D.1. The percentage of the appendage drag in model scale from the total model drag were ranged from 2.17% to 2.77%. The percentage of the appendage drag in full scale from the total ship drag were ranged from 7.39% to 10.42%.

**Table D. 1** The total appendage drag in model and full scale and its percentage from the total drag.

| Fr | Total appendage drag in model scale (N) | The percentage from total model drag (%) | Total appendage drag in full scale (kN) | The percentage from total ship drag (%) |
|---|---|---|---|---|
| **0.44** | 0.7431 | 2.17 | 48.33 | 7.39 |
| **0.40** | 0.6205 | 2.43 | 40.39 | 8.91 |
| **0.38** | 0.5632 | 2.65 | 36.66 | 9.87 |
| **0.35** | 0.4822 | 2.77 | 31.40 | 10.42 |
| **0.32** | 0.4072 | 2.64 | 26.52 | 9.79 |
| **0.29** | 0.3382 | 2.50 | 22.04 | 9.30 |
| **0.26** | 0.2754 | 2.58 | 17.94 | 9.56 |

# Appendix E

## The calculation of drag correction due to the effect of the turbulence studs

In this appendix, the formulation used in the calculation of the drag correction due to the effect of the turbulence studs are explained. The drag correction due to the effect of turbulence studs on model resistance was based on the work of Hughes and Allan (1951), Hoerner (1965) and Molland et al. (1996). According to Molland et al. (1996) there are three main points that are must be taken into consideration in calculating the effect of turbulence studs on model resistance which are:

(1) The additional drag on the model due to the presence of studs,

(2) The increase in the momentum thickness of the boundary layer due to the presence of the studs

(3) The laminar region in front of the studs.

The drag correction that must be made to the measured resistance according to Molland et al. (1996) is:

$$Drag\ correction = D_{unstimulated\ turbulent} - D_{turbulent} - D_{laminar} - D_{stud} \tag{E.1}$$

The drag of the studs according to Molland et al. (1996) can be calculated as in equation E.2, where $\rho$ is the density of the water in kg/m$^3$, $h$ is the height of the stud in metre, $w$ is the width of the stud in metre, $n$ is the number of studs, $\overline{U}$ is the mean velocity over the stud and $C_D$ is the drag coefficient of the stud which are assumed to be at 0.95.

$$D_{stud} = \frac{1}{2}\rho h w n \overline{U}^2 C_D \tag{E.2}$$

The mean velocity over the stud can be calculated as in equation E.3, where $U_O$ is the model velocity in m/s, $h$ is the height of the stud in metre, $x$ is the distance of the stud from the leading edge at the bow and $\upsilon$ is the kinematic viscosity in m$^3$/s. This is necessary as the stud are in the boundary layer and part in the free stream.

$$\overline{U} = U_O\left[1 - \frac{1.997}{h}\sqrt{\frac{x\upsilon}{U_O}}\right] \tag{E.3}$$

The drag of the turbulent part of the model can be calculated using the formula given in Equation E.4 (Molland et al., 1996), where $S_M$ is the model wetted surface area in metre square, $S_{laminar}$ is the area of the laminar region starting from the leading edge to the studs in metre square and $C_{F_{turbulent}}$ is the coefficient of the frictional resistance at the turbulent region.

$$D_{turbulent} = \frac{1}{2}\rho(S_M - S_{laminar})U_O^2 C_{F_{turbulent}} \tag{E.4}$$

The model and the full scale boundary layers is difference in terms of its boundary layer momentum thickness as shown in Figure E.1. The model boundary layer starts as a laminar boundary layer from the leading edge L.E. and then is tripped by the studs. Beyond this point the drag on the studs increases the momentum thickness of the boundary layer. This reduces the frictional drag coefficient, $C_F$ values over the turbulent part of the model.

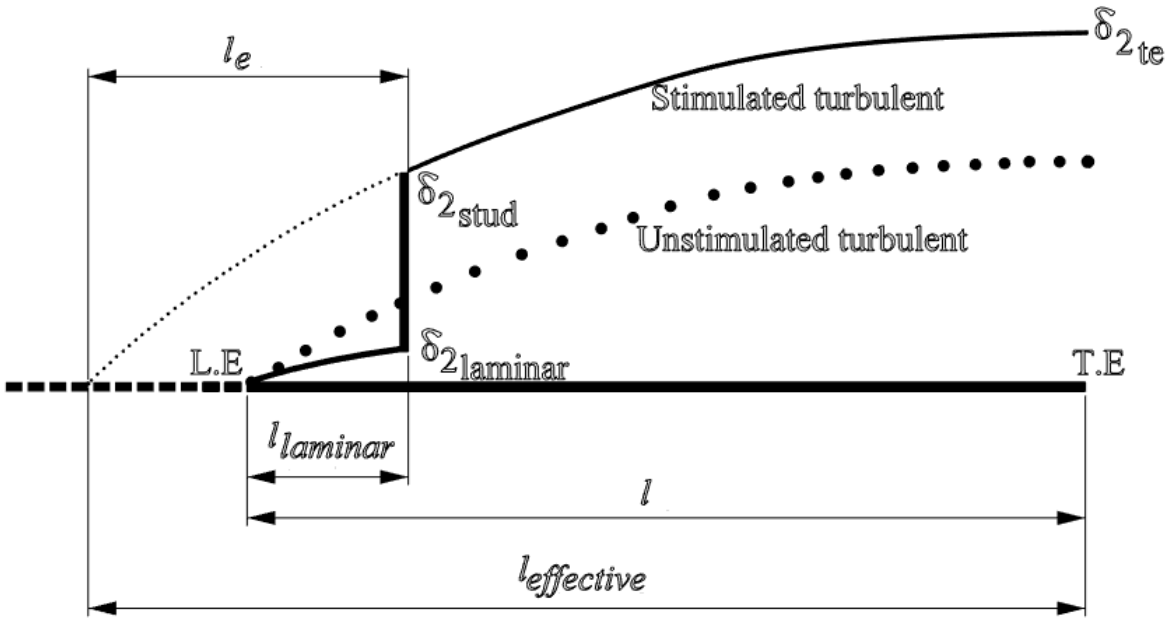


**Figure E.1** The tripping of the boundary layer by the studs (Molland et al., 1996)

The coefficient of the frictional resistance at the turbulent region can be calculated as in Equation E.5, where $\delta_{2_{te}}$ is the momentum thickness at the trailing edge in metre, $\delta_{2_{total.at..stud}}$ is the total momentum thickness at the stud in metre, $l$ is the model length in metre and $l_{laminar}$ is the distance of the studs from the leading edge L.E. in metre.

$$C_{F_{turbulent}} = \frac{2\left(\delta_{2_{te}} - \delta_{2_{total\text{-}at\text{-}stud}}\right)}{\left(l - l_{laminar}\right)} \tag{E.5}$$

The momentum thickness at the trailing edge $\delta_{2_{total.at..stud}}$ can be calculated as in Equation E.6, where $l_{effective}$ is the effective model length as given in Equation E.7. The effective frictional drag coefficient $C_{F_{effective}}$ can be calculated using the ITTC correlation line formulation using the Reynolds number based on the effective model length $l_{effective}$.

$$\delta_{2_{te}} = \frac{l_{effective} C_{F_{effective}}}{2} \tag{E.6}$$

$$l_{effective} = l - l_{laminar} + l_e \tag{E.7}$$

The increase of the momentum thickness caused by the studs can be calculated as in Equation E.8, where $n$ is the number of the studs at both sides of the model and, $h$ is the height of the studs in metre, $w$ is the width of the studs in metre, $C_D$ is the drag coefficient of the studs which are assumed to be at 0.95 and $T_{stem}$ is the draught of the studs.

$$\delta_{2_{stud}} = \frac{hwnC_D}{4T_{stem}} \left( \frac{\overline{U}}{U_O} \right)^2 \tag{E.8}$$

The length from the studs to a fictitious leading edge *le* as shown in Figure E.1 can be obtained using Equation E.9.

$$le = \sqrt[6]{\frac{\delta^7 U_O}{2.054 \times 10^{-6} \upsilon}} \tag{E.9}$$

where the momentum thickness of the boundary layer $\delta$ along the fictitious leading edge is given by Equation E.10.

$$\delta = \frac{(n+1)(n+2)}{n} \delta_2 \tag{E.10}$$

The total momentum thickness at the stud can be calculated by adding the laminar momentum thickness with the increased momentum thickness at the studs. This is given in Equation E.11.

$$\delta_{2_{total.at.stud}} = \delta_{2_{stud}} + \delta_{2_{laminar}} \tag{E.11}$$

The skin friction coefficient $C_{F_{laminar}}$, for the laminar region can be calculated using Equation E.12.

$$C_{F_{laminar}} = \frac{2\delta_{2_{laminar}}}{l_{laminar}} \tag{E.12}$$

The drag on this part of the model, $D_{laminar}$ can be calculated using Equation E.13.

$$D_{laminar} = \frac{1}{2}\rho(A_{laminar})U_O^2 C_{F_{laminar}} \tag{E.13}$$

Results of this correction is given in Table E.1. The correction for the model was seen to amount about 0.82 to 2.54 % of the measured resistance.

**Table E. 1** Stud correction for the propeller driven catamaran at displacement of 3,640 tonnes

| $U_o$ | $R_{measured}$ | $D_{stud}$ | $D_{turbulent}$ | $D_{laminar}$ | $D_{unstimulated\ stud}$ | *Correction* | *Correction* |
|---|---|---|---|---|---|---|---|
| (m/s) | (N) | (N) | (N) | (N) | (N) | (N) | (%) |
| **1.30** | 6.27 | 0.011 | 4.13 | 0.113 | 4.10 | -0.16 | -2.54 |
| **1.88** | 13.57 | 0.001 | 8.05 | 0.197 | 8.05 | -0.20 | -1.46 |
| **2.27** | 17.38 | 0.001 | 11.32 | 0.261 | 11.35 | -0.23 | -1.33 |
| **2.66** | 27.46 | 0.010 | 15.08 | 0.331 | 15.15 | -0.27 | -1.00 |
| **2.99** | 38.59 | 0.024 | 18.60 | 0.393 | 18.70 | -0.32 | -0.82 |

# Appendix F

## Model experimental results

**Table F. 1** The un-appended calm water resistance test results for the propeller driven catamaran model at displacement of 3,640 tonnes with coefficients of total, frictional and residuary resistances

| Fr | Model speed | Sinkage | Trim | $R_{T, m}$ | $C_{T, m}$ *1000 | $C_{F, m}$ *1000 | $C_{R, m}$ *1000 |
|---|---|---|---|---|---|---|---|
| - | m/s | mm | Degrees | N | - | - | - |
| **0.20** | 1.30 | -0.87 | 0.00 | 6.33 | 5.10 | 3.38 | 1.72 |
| **0.20** | 1.30 | -0.85 | 0.00 | 6.27 | 5.04 | 3.38 | 1.66 |
| **0.20** | 1.30 | -0.84 | 0.00 | 6.27 | 5.03 | 3.38 | 1.65 |
| **0.23** | 1.49 | -1.40 | 0.00 | 8.27 | 5.09 | 3.30 | 1.79 |
| **0.23** | 1.49 | -1.39 | 0.00 | 8.16 | 5.01 | 3.30 | 1.71 |
| **0.23** | 1.49 | -1.90 | 0.00 | 8.09 | 4.91 | 3.30 | 1.61 |
| **0.26** | 1.69 | -2.60 | 0.00 | 10.90 | 5.19 | 3.22 | 1.96 |
| **0.26** | 1.69 | -2.45 | 0.00 | 10.67 | 5.07 | 3.22 | 1.85 |
| **0.26** | 1.69 | -2.57 | 0.00 | 10.78 | 5.13 | 3.22 | 1.90 |
| **0.32** | 2.08 | -5.86 | 0.06 | 15.45 | 4.90 | 3.11 | 1.79 |
| **0.32** | 2.08 | -5.81 | 0.06 | 15.52 | 4.93 | 3.11 | 1.82 |
| **0.32** | 2.08 | -5.83 | 0.07 | 15.23 | 4.83 | 3.11 | 1.72 |
| **0.35** | 2.27 | -7.02 | 0.02 | 17.51 | 4.64 | 3.06 | 1.58 |
| **0.35** | 2.27 | -6.84 | 0.01 | 17.38 | 4.55 | 3.06 | 1.49 |
| **0.38** | 2.47 | -10.40 | 0.11 | 21.30 | 4.79 | 3.02 | 1.77 |
| **0.38** | 2.47 | -10.85 | 0.12 | 21.26 | 4.77 | 3.02 | 1.76 |
| **0.38** | 2.47 | -10.63 | 0.12 | 21.16 | 4.75 | 3.02 | 1.73 |
| **0.41** | 2.66 | -15.44 | 0.48 | 27.46 | 5.24 | 2.97 | 2.26 |
| **0.42** | 2.73 | -18.42 | 0.62 | 29.58 | 5.41 | 2.96 | 2.45 |
| **0.43** | 2.79 | -20.01 | 0.71 | 31.75 | 5.57 | 2.95 | 2.62 |
| **0.44** | 2.86 | -21.26 | 0.88 | 34.16 | 5.72 | 2.94 | 2.78 |
| **0.44** | 2.86 | -20.92 | 0.91 | 34.72 | 5.81 | 2.94 | 2.87 |
| **0.44** | 2.86 | -21.50 | 0.86 | 33.61 | 5.61 | 2.94 | 2.67 |
| **0.46** | 2.99 | -22.02 | 1.14 | 39.36 | 6.00 | 2.92 | 3.08 |
| **0.46** | 2.99 | -24.26 | 1.04 | 38.59 | 5.87 | 2.92 | 2.95 |
| **0.46** | 2.99 | -23.10 | 1.11 | 38.96 | 5.92 | 2.92 | 3.01 |
| **0.49** | 3.18 | -16.70 | 1.33 | 43.61 | 5.87 | 2.89 | 2.98 |
| **0.49** | 3.18 | -17.43 | 1.34 | 43.50 | 5.85 | 2.89 | 2.97 |
| **0.49** | 3.18 | -17.25 | 1.34 | 43.56 | 5.86 | 2.89 | 2.97 |

Notes: [Sinkage: increase in draught –ve] [Trim: bow up +ve]

**Table F. 2** The un-appended calm water resistance test results for the propeller driven catamaran model at displacement of 2,500 tonnes with coefficients of total, frictional and residuary resistances

| **Fr** | **Model speed** | **Sinkage** | **Trim** | **$R_{T,m}$** | **$C_{T,m}$ *1000** | **$C_{F,m}$ *1000** | **$C_{R,m}$ *1000** |
|---|---|---|---|---|---|---|---|
| - | m/s | mm | Degrees | N | - | - | - |
| **0.20** | 1.30 | -0.09 | 0.01 | 4.53 | 4.43 | 3.37 | 1.06 |
| **0.20** | 1.30 | -0.14 | 0.01 | 4.48 | 4.39 | 3.37 | 1.02 |
| **0.20** | 1.30 | -0.13 | 0.00 | 4.57 | 4.48 | 3.37 | 1.11 |
| **0.23** | 1.49 | -0.67 | 0.01 | 5.66 | 4.25 | 3.29 | 0.96 |
| **0.23** | 1.49 | -0.64 | 0.00 | 5.68 | 4.27 | 3.29 | 0.98 |
| **0.26** | 1.69 | -1.15 | 0.00 | 6.96 | 4.03 | 3.21 | 0.82 |
| **0.26** | 1.69 | -1.14 | -0.01 | 6.93 | 4.02 | 3.21 | 0.81 |
| **0.26** | 1.69 | -1.09 | -0.01 | 7.02 | 4.07 | 3.21 | 0.86 |
| **0.29** | 1.88 | -2.38 | 0.04 | 8.83 | 4.16 | 3.15 | 1.01 |
| **0.32** | 2.08 | -3.20 | 0.02 | 10.18 | 3.93 | 3.10 | 0.83 |
| **0.32** | 2.08 | -3.33 | 0.03 | 10.14 | 3.91 | 3.10 | 0.82 |
| **0.32** | 2.08 | -3.39 | 0.03 | 10.22 | 3.95 | 3.10 | 0.85 |
| **0.35** | 2.27 | -4.32 | 0.03 | 11.84 | 3.81 | 3.05 | 0.76 |
| **0.37** | 2.40 | -5.63 | 0.07 | 13.63 | 3.94 | 3.02 | 0.92 |
| **0.38** | 2.47 | -6.83 | 0.13 | 14.76 | 4.04 | 3.01 | 1.03 |
| **0.38** | 2.47 | -6.86 | 0.11 | 14.72 | 4.03 | 3.01 | 1.02 |
| **0.38** | 2.47 | -6.90 | 0.12 | 14.75 | 4.05 | 3.01 | 1.04 |
| **0.40** | 2.60 | -9.32 | 0.26 | 17.50 | 4.32 | 2.98 | 1.34 |
| **0.41** | 2.66 | -10.65 | 0.32 | 18.53 | 4.35 | 2.97 | 1.39 |
| **0.42** | 2.73 | -12.77 | 0.44 | 20.15 | 4.49 | 2.95 | 1.54 |
| **0.44** | 2.86 | -15.49 | 0.62 | 23.01 | 4.68 | 2.93 | 1.75 |
| **0.44** | 2.86 | -15.57 | 0.64 | 23.15 | 4.72 | 2.93 | 1.79 |
| **0.44** | 2.86 | -15.56 | 0.63 | 22.83 | 4.66 | 2.93 | 1.73 |
| **0.46** | 2.99 | -15.86 | 0.86 | 26.25 | 4.87 | 2.91 | 1.97 |
| **0.46** | 2.99 | -16.29 | 0.84 | 26.49 | 4.93 | 2.91 | 2.02 |
| **0.46** | 2.99 | -16.32 | 0.85 | 26.56 | 4.94 | 2.91 | 2.03 |
| **0.49** | 3.18 | -12.39 | 0.99 | 29.38 | 4.83 | 2.88 | 1.95 |
| **0.49** | 3.18 | -12.63 | 0.99 | 29.52 | 4.87 | 2.88 | 1.99 |
| **0.49** | 3.18 | -12.71 | 0.99 | 29.61 | 4.87 | 2.88 | 2.00 |

Notes: [Sinkage: increase in draught –ve] [Trim: bow up +ve]

**Table F. 3** The self-propulsion test results for the propeller driven catamaran model at displacement of 3,640 tonnes. The test was conducted at model speed 1.69 m/s at Froude number 0.26.

| **Fr** | **Model speed** | **Shaft speed** | **Sinkage** | **Trim** | **Torque** | **Thrust** | **Towing Force** |
|---|---|---|---|---|---|---|---|
| - | m/s | rev/sec | mm | Degrees | Nm | N | N |
| **0.26** | 1.69 | 8.98 | -1.98 | -0.024 | 0.10 | -0.80 | 15.04 |
| **0.26** | 1.69 | 8.98 | -2.10 | -0.007 | 0.47 | -1.06 | 14.68 |
| **0.26** | 1.69 | 8.98 | -1.70 | -0.012 | 0.42 | -1.78 | 15.22 |
| **0.26** | 1.69 | 8.98 | -1.87 | -0.012 | 0.47 | -1.56 | 15.21 |
| **0.26** | 1.69 | 10.15 | -2.25 | -0.012 | 0.35 | -0.98 | 13.36 |
| **0.26** | 1.69 | 10.15 | -2.16 | -0.005 | 0.35 | -0.46 | 13.50 |
| **0.26** | 1.69 | 10.15 | -2.08 | -0.002 | 0.35 | -0.04 | 13.40 |
| **0.26** | 1.69 | 10.15 | -2.22 | -0.002 | 0.38 | 0.17 | 13.40 |
| **0.26** | 1.69 | 12.03 | -2.48 | 0.004 | 0.12 | 4.33 | 10.39 |
| **0.26** | 1.69 | 12.03 | -2.43 | 0.008 | 0.12 | 2.20 | 10.22 |
| **0.26** | 1.69 | 12.03 | -2.50 | 0.007 | 0.16 | 2.17 | 10.45 |
| **0.26** | 1.69 | 12.03 | -2.76 | 0.009 | 0.16 | 2.18 | 10.23 |
| **0.26** | 1.69 | 14.05 | -2.35 | 0.011 | 0.10 | 8.13 | 6.40 |
| **0.26** | 1.69 | 16.11 | -2.71 | 0.029 | 0.30 | 13.26 | 1.51 |
| **0.26** | 1.69 | 16.11 | -3.03 | 0.035 | 0.13 | 9.84 | 1.70 |
| **0.26** | 1.69 | 16.11 | -2.91 | 0.032 | 0.14 | 8.89 | 1.78 |
| **0.26** | 1.69 | 16.11 | -3.29 | 0.039 | 0.12 | 8.87 | 1.48 |
| **0.26** | 1.69 | 18.02 | -3.13 | 0.053 | 0.40 | 18.61 | -3.68 |
| **0.26** | 1.69 | 18.02 | -3.12 | 0.050 | 0.24 | 16.00 | -3.25 |
| **0.26** | 1.69 | 18.02 | -3.40 | 0.054 | 0.23 | 16.19 | -3.15 |
| **0.26** | 1.69 | 19.01 | -3.41 | 0.068 | 0.50 | 22.03 | -6.83 |

Notes: [Sinkage: increase in draught –ve] [Trim: bow up +ve]

**Table F. 4** The self-propulsion test results for the propeller driven catamaran model at displacement of 3,640 tonnes. The test was conducted at model speed 1.88 m/s at Froude number 0.29.

| Fr | Model speed | Shaft speed | Sinkage | Trim | Torque | Thrust | Towing Force |
|---|---|---|---|---|---|---|---|
| - | m/s | rev/sec | mm | Degrees | Nm | N | N |
| **0.29** | 1.88 | 10.00 | -4.03 | 0.06 | 0.03 | -2.80 | 18.64 |
| **0.29** | 1.88 | 10.60 | -3.93 | 0.05 | 0.10 | -2.10 | 17.67 |
| **0.29** | 1.88 | 11.20 | -4.20 | 0.07 | 0.01 | 4.10 | 16.65 |
| **0.29** | 1.88 | 11.20 | -4.13 | 0.06 | 0.03 | 1.55 | 16.75 |
| **0.29** | 1.88 | 11.20 | -4.22 | 0.06 | 0.02 | 0.80 | 16.68 |
| **0.29** | 1.88 | 11.20 | -4.07 | 0.06 | 0.01 | 0.50 | 16.68 |
| **0.29** | 1.88 | 11.22 | -4.79 | 0.07 | 0.00 | 0.26 | 16.61 |
| **0.29** | 1.88 | 11.90 | -4.02 | 0.05 | 0.00 | 1.54 | 15.56 |
| **0.29** | 1.88 | 11.99 | -4.13 | 0.06 | 0.00 | 0.86 | 15.37 |
| **0.29** | 1.88 | 12.99 | -4.77 | 0.08 | 0.10 | 3.58 | 13.65 |
| **0.29** | 1.88 | 13.00 | -4.58 | 0.07 | 0.00 | 2.81 | 13.59 |
| **0.29** | 1.88 | 13.04 | -4.58 | 0.08 | 0.00 | 3.79 | 13.57 |
| **0.29** | 1.88 | 14.00 | -4.64 | 0.08 | 0.18 | 7.97 | 11.59 |
| **0.29** | 1.88 | 14.90 | -4.76 | 0.08 | 0.10 | 7.20 | 9.47 |
| **0.29** | 1.88 | 14.96 | -4.70 | 0.09 | 0.10 | 7.98 | 9.56 |
| **0.29** | 1.88 | 15.00 | -4.76 | 0.10 | 0.21 | 8.59 | 9.30 |
| **0.29** | 1.88 | 15.04 | -4.70 | 0.10 | 0.20 | 6.00 | 9.37 |
| **0.29** | 1.88 | 15.04 | -4.62 | 0.10 | 0.20 | 8.58 | 9.41 |
| **0.29** | 1.88 | 16.12 | -4.83 | 0.08 | 0.20 | 10.66 | 6.87 |
| **0.29** | 1.88 | 16.12 | -4.78 | 0.09 | 0.20 | 10.63 | 6.77 |
| **0.29** | 1.88 | 17.90 | -5.10 | 0.11 | 0.30 | 14.76 | 1.85 |
| **0.29** | 1.88 | 17.90 | -5.06 | 0.12 | 0.30 | 14.88 | 1.93 |
| **0.29** | 1.88 | 18.00 | -4.97 | 0.11 | 0.40 | 11.07 | 1.76 |
| **0.29** | 1.88 | 18.00 | -5.02 | 0.11 | 0.40 | 11.04 | 1.74 |
| **0.29** | 1.88 | 18.00 | -4.97 | 0.10 | 0.30 | 15.44 | 1.68 |
| **0.29** | 1.88 | 18.02 | -5.07 | 0.12 | 0.40 | 15.17 | 1.55 |
| **0.29** | 1.88 | 18.02 | -5.11 | 0.12 | 0.40 | 14.51 | 1.67 |
| **0.29** | 1.88 | 18.02 | -5.16 | 0.11 | 0.30 | 15.81 | 1.56 |
| **0.29** | 1.88 | 18.04 | -5.04 | 0.11 | 0.40 | 15.68 | 1.49 |
| **0.29** | 1.88 | 18.04 | -5.43 | 0.12 | 0.41 | 13.38 | 1.73 |
| **0.29** | 1.88 | 18.04 | -5.09 | 0.12 | 0.40 | 16.71 | 1.61 |
| **0.29** | 1.88 | 20.00 | -5.33 | 0.13 | 0.54 | 24.39 | -4.56 |
| **0.29** | 1.88 | 20.50 | -5.22 | 0.12 | 0.50 | 24.00 | -6.34 |
| **0.29** | 1.88 | 20.50 | -5.33 | 0.12 | 0.50 | 23.51 | -6.64 |

Notes: [Sinkage: increase in draught –ve] [Trim: bow up +ve]

**Table F. 5** The self-propulsion test results for the propeller driven catamaran model at displacement of 3,640 tonnes. The test was conducted at model speed 2.08 m/s at Froude number 0.32.

| Fr | Model speed | Shaft speed | Sinkage | Trim | Torque | Thrust | Towing Force |
|---|---|---|---|---|---|---|---|
| - | m/s | rev/sec | mm | Degrees | Nm | N | N |
| **0.32** | 2.08 | 12.16 | -5.60 | 0.05 | 0.10 | -1.44 | 19.86 |
| **0.32** | 2.08 | 13.91 | -5.19 | 0.05 | 0.00 | 1.77 | 16.54 |
| **0.32** | 2.08 | 15.07 | -5.72 | 0.07 | 0.10 | 4.81 | 14.09 |
| **0.32** | 2.08 | 17.02 | -5.64 | 0.08 | 0.20 | 9.69 | 9.35 |
| **0.32** | 2.08 | 17.93 | -5.78 | 0.08 | 0.20 | 12.26 | 6.66 |
| **0.32** | 2.08 | 18.99 | -6.14 | 0.09 | 0.30 | 15.28 | 3.91 |
| **0.32** | 2.08 | 20.05 | -6.24 | 0.10 | 0.40 | 20.35 | -1.08 |
| **0.32** | 2.08 | 21.00 | -6.13 | 0.10 | 0.50 | 22.25 | -3.10 |
| **0.32** | 2.08 | 21.06 | -6.25 | 0.10 | 0.50 | 22.21 | -3.26 |
| **0.32** | 2.08 | 22.10 | -6.34 | 0.10 | 0.60 | 25.15 | -6.93 |
| **0.32** | 2.08 | 22.14 | -6.46 | 0.12 | 0.60 | 25.44 | -7.12 |
| **0.32** | 2.08 | 22.16 | -6.24 | 0.11 | 0.60 | 25.53 | -7.26 |

Notes: [Sinkage: increase in draught –ve] [Trim: bow up +ve]

**Table F. 6** The self-propulsion test results for the propeller driven catamaran model at displacement of 3,640 tonnes. The test was conducted at model speed 2.27 m/s at Froude number 0.35.

| Fr | Model speed | Shaft speed | Sinkage | Trim | Torque | Thrust | Towing Force |
|---|---|---|---|---|---|---|---|
| - | m/s | rev/sec | mm | Degrees | Nm | N | N |
| **0.35** | 2.27 | 13.05 | -6.55 | -0.03 | 0.10 | -2.95 | 23.15 |
| **0.35** | 2.27 | 15.06 | -6.21 | 0.00 | 0.00 | 1.55 | 19.04 |
| **0.35** | 2.27 | 16.97 | -6.94 | 0.01 | 0.10 | 6.22 | 14.66 |
| **0.35** | 2.27 | 18.99 | -7.95 | 0.03 | 0.30 | 11.54 | 8.95 |
| **0.35** | 2.27 | 20.30 | -7.58 | 0.05 | 0.40 | 16.41 | 4.95 |
| **0.35** | 2.27 | 22.00 | -7.68 | 0.05 | 0.50 | 21.48 | -1.21 |
| **0.35** | 2.27 | 23.51 | -7.60 | 0.06 | 0.60 | 26.97 | -6.32 |

Notes: [Sinkage: increase in draught –ve] [Trim: bow up +ve]

**Table F. 7** The self-propulsion test results for the propeller driven catamaran model at displacement of 3,640 tonnes. The test was conducted at model speed 2.47 m/s at Froude number 0.38.

| Fr | Model speed | Shaft speed | Sinkage | Trim | Torque | Thrust | Towing Force |
|---|---|---|---|---|---|---|---|
| - | m/s | rev/sec | mm | Degrees | Nm | N | N |
| **0.38** | 2.47 | 15.06 | -9.31 | 0.07 | 0.0 | -2.44 | 26.4 |
| **0.38** | 2.47 | 17.96 | -10.25 | 0.11 | 0.2 | -0.57 | 19.25 |
| **0.38** | 2.47 | 17.98 | -9.94 | 0.12 | 0.1 | 4.82 | 19.21 |
| **0.38** | 2.47 | 17.99 | -10.23 | 0.1 | 0.1 | 5.04 | 18.99 |
| **0.38** | 2.47 | 19.90 | -10.38 | 0.13 | 0.3 | 8.32 | 13.42 |
| **0.38** | 2.47 | 19.93 | -10.39 | 0.12 | 0.2 | 10.69 | 13.53 |
| **0.38** | 2.47 | 19.94 | -10.57 | 0.12 | 0.3 | 11.31 | 13.17 |
| **0.38** | 2.47 | 21.00 | -10.92 | 0.12 | 0.3 | 15.24 | 10.36 |
| **0.38** | 2.47 | 21.00 | -10.73 | 0.11 | 0.3 | 15.48 | 10.33 |
| **0.38** | 2.47 | 21.08 | -11.09 | 0.12 | 0.3 | 15.25 | 9.78 |
| **0.38** | 2.47 | 22.05 | -10.54 | 0.13 | 0.5 | 19.64 | 7.65 |
| **0.38** | 2.47 | 22.80 | -10.94 | 0.12 | 0.5 | 20.34 | 3.45 |
| **0.38** | 2.47 | 23.10 | -11.39 | 0.16 | 0.6 | 23.43 | 2.79 |
| **0.38** | 2.47 | 24.00 | -11.22 | 0.16 | 0.6 | 24.87 | -0.44 |
| **0.38** | 2.47 | 25.00 | -11.34 | 0.16 | 0.8 | 32.66 | -8.23 |
| **0.38** | 2.47 | 25.77 | -11.37 | 0.19 | 0.8 | 32.74 | -7.43 |
| **0.38** | 2.47 | 26.80 | -11.57 | 0.18 | 1.0 | 37.4 | -13.14 |

Notes: [Sinkage: increase in draught –ve] [Trim: bow up +ve]

**Table F. 8** The self-propulsion test results for the propeller driven catamaran model at displacement of 3,640 tonnes. The test was conducted at model speed 2.60 m/s at Froude number 0.40.

| Fr | Model speed | Shaft speed | Sinkage | Trim | Torque | Thrust | Towing Force |
|---|---|---|---|---|---|---|---|
| - | m/s | rev/sec | mm | Degrees | Nm | N | N |
| **0.40** | 2.60 | 17.00 | -12.41 | 0.29 | 0.00 | -0.29 | 28.30 |
| **0.40** | 2.60 | 18.99 | -13.15 | 0.30 | 0.10 | 5.29 | 22.94 |
| **0.40** | 2.60 | 20.40 | -13.52 | 0.30 | 0.20 | 10.06 | 18.95 |
| **0.40** | 2.60 | 22.01 | -13.83 | 0.33 | 0.40 | 14.50 | 13.57 |
| **0.40** | 2.60 | 22.84 | -13.61 | 0.33 | 0.40 | 17.40 | 10.77 |
| **0.40** | 2.60 | 25.05 | -14.29 | 0.34 | 0.60 | 26.40 | 2.02 |
| **0.40** | 2.60 | 26.42 | -14.05 | 0.37 | 0.80 | 32.47 | -3.07 |

Notes: [Sinkage: increase in draught –ve] [Trim: bow up +ve]

**Table F. 9** The self-propulsion test results for the propeller driven catamaran model at displacement of 3,640 tonnes. The test was conducted at model speed 2.86 m/s at Froude number 0.44.

| **Fr** | **Model speed** | **Shaft speed** | **Sinkage** | **Trim** | **Torque** | **Thrust** | **Towing Force** |
|---|---|---|---|---|---|---|---|
| - | m/s | rev/sec | mm | Degrees | Nm | N | N |
| **0.44** | 2.86 | 17.99 | -20.51 | 0.78 | 0.10 | -4.93 | 41.15 |
| **0.44** | 2.86 | 17.99 | -19.51 | 0.83 | 0.20 | -6.32 | 41.37 |
| **0.44** | 2.86 | 17.99 | -19.52 | 0.84 | 0.15 | -7.24 | 41.30 |
| **0.44** | 2.86 | 17.99 | -19.14 | 0.84 | 0.20 | -6.08 | 41.51 |
| **0.44** | 2.86 | 19.96 | -20.86 | 0.81 | 0.10 | 1.55 | 35.54 |
| **0.44** | 2.86 | 22.14 | -20.66 | 0.77 | 0.20 | 8.01 | 27.77 |
| **0.44** | 2.86 | 24.10 | -21.80 | 0.84 | 0.40 | 15.38 | 21.35 |
| **0.44** | 2.86 | 25.00 | -21.01 | 0.88 | 0.37 | 18.09 | 18.53 |
| **0.44** | 2.86 | 25.00 | -20.22 | 0.89 | 0.38 | 17.64 | 19.02 |
| **0.44** | 2.86 | 25.00 | -18.70 | 0.72 | 0.38 | 17.23 | 18.27 |
| **0.44** | 2.86 | 25.74 | -21.16 | 0.83 | 0.60 | 22.10 | 14.91 |
| **0.44** | 2.86 | 25.74 | -21.23 | 0.83 | 0.60 | 21.97 | 14.87 |
| **0.44** | 2.86 | 26.90 | -19.07 | 0.78 | 0.70 | 27.80 | 8.87 |
| **0.44** | 2.86 | 28.20 | -22.53 | 0.87 | 0.80 | 33.40 | 3.60 |
| **0.44** | 2.86 | 28.20 | -19.67 | 0.80 | 0.80 | 34.02 | 2.47 |
| **0.44** | 2.86 | 28.20 | -21.48 | 0.89 | 0.69 | 31.16 | 5.00 |
| **0.44** | 2.86 | 28.20 | -21.26 | 0.91 | 0.69 | 31.20 | 4.59 |
| **0.44** | 2.86 | 28.20 | -21.30 | 0.92 | 0.70 | 31.63 | 4.02 |
| **0.44** | 2.86 | 29.80 | -20.00 | 0.81 | 1.00 | 42.04 | -4.84 |
| **0.44** | 2.86 | 29.90 | -19.43 | 0.80 | 1.00 | 42.34 | -5.71 |

Notes: [Sinkage: increase in draught –ve] [Trim: bow up +ve]

**Table F. 10** The self-propulsion test results for the propeller driven catamaran model at displacement of 2,500 tonnes. The test was conducted at model speed 1.69 m/s at Froude number 0.26.

| **Fr** | **Model speed** | **Shaft speed** | **Sinkage** | **Trim** | **Torque** | **Thrust** | **Towing Force** |
|---|---|---|---|---|---|---|---|
| - | m/s | rev/sec | mm | Degrees | Nm | N | N |
| **0.26** | 1.69 | 7.923 | -0.58 | -0.03 | 0.10 | -2.60 | 12.21 |
| **0.26** | 1.69 | 7.924 | -0.67 | -0.03 | 0.10 | -2.66 | 12.18 |
| **0.26** | 1.69 | 7.925 | -0.57 | -0.03 | 0.10 | -2.56 | 12.12 |
| **0.26** | 1.69 | 8.999 | -0.67 | -0.02 | 0.10 | -1.25 | 10.76 |
| **0.26** | 1.69 | 9.001 | -0.69 | -0.03 | 0.10 | -1.07 | 10.73 |
| **0.26** | 1.69 | 9.001 | -0.66 | -0.02 | 0.10 | -1.01 | 10.70 |
| **0.26** | 1.69 | 10.173 | -0.90 | -0.02 | 0.00 | 0.96 | 9.09 |
| **0.26** | 1.69 | 10.179 | -1.10 | -0.01 | 0.00 | 0.92 | 9.18 |
| **0.26** | 1.69 | 10.179 | -0.97 | -0.01 | 0.00 | 0.99 | 9.10 |
| **0.26** | 1.69 | 13.043 | -1.26 | 0.00 | 0.10 | 5.42 | 4.47 |
| **0.26** | 1.69 | 13.043 | -1.13 | 0.00 | 0.10 | 5.58 | 4.26 |
| **0.26** | 1.69 | 13.051 | -1.05 | 0.00 | 0.10 | 5.65 | 4.22 |
| **0.26** | 1.69 | 14.068 | -1.21 | 0.01 | 0.10 | 7.91 | 2.32 |
| **0.26** | 1.69 | 14.068 | -1.29 | 0.00 | 0.10 | 7.98 | 2.30 |
| **0.26** | 1.69 | 14.070 | -1.30 | 0.00 | 0.10 | 8.16 | 2.12 |
| **0.26** | 1.69 | 15.097 | -1.44 | 0.01 | 0.20 | 10.56 | -0.13 |
| **0.26** | 1.69 | 15.097 | -1.46 | 0.00 | 0.20 | 10.43 | -0.10 |
| **0.26** | 1.69 | 15.100 | -1.42 | 0.01 | 0.20 | 10.47 | -0.10 |
| **0.26** | 1.69 | 16.125 | -1.60 | 0.02 | 0.20 | 13.23 | -2.62 |
| **0.26** | 1.69 | 16.125 | -1.65 | 0.02 | 0.30 | 13.15 | -2.56 |
| **0.26** | 1.69 | 16.131 | -1.66 | 0.01 | 0.20 | 13.25 | -2.75 |
| **0.26** | 1.69 | 18.026 | -1.79 | 0.03 | 0.40 | 19.05 | -8.20 |
| **0.26** | 1.69 | 18.027 | -1.81 | 0.03 | 0.40 | 18.76 | -8.05 |
| **0.26** | 1.69 | 18.052 | -1.84 | 0.03 | 0.40 | 18.89 | -8.23 |

Notes: [Sinkage: increase in draught –ve] [Trim: bow up +ve]

**Table F. 11** The self-propulsion test results for the propeller driven catamaran model at displacement of 2,500 tonnes. The test was conducted at model speed 1.88 m/s at Froude number 0.29.

| Fr | Model speed | Shaft speed | Sinkage | Trim | Torque | Thrust | Towing Force |
|---|---|---|---|---|---|---|---|
| - | m/s | rev/min | mm | Degrees | Nm | N | N |
| **0.29** | 1.88 | 9.140 | -1.73 | 0.01 | 0.10 | -3.39 | 14.70 |
| **0.29** | 1.88 | 10.181 | -2.01 | 0.02 | 0.10 | -1.61 | 13.17 |
| **0.29** | 1.88 | 11.277 | -2.12 | 0.02 | 0.00 | 0.47 | 11.41 |
| **0.29** | 1.88 | 13.003 | -2.24 | 0.03 | 0.00 | 3.49 | 8.24 |
| **0.29** | 1.88 | 15.102 | -2.68 | 0.04 | 0.10 | 8.05 | 3.93 |
| **0.29** | 1.88 | 16.131 | -2.57 | 0.05 | 0.20 | 10.78 | 1.51 |
| **0.29** | 1.88 | 17.002 | -2.67 | 0.05 | 0.20 | 13.28 | -0.86 |
| **0.29** | 1.88 | 18.032 | -2.96 | 0.06 | 0.30 | 16.17 | -3.70 |

Notes: [Sinkage: increase in draught –ve] [Trim: bow up +ve]

**Table F. 12** The self-propulsion test results for the propeller driven catamaran model at displacement of 2,500 tonnes. The test was conducted at model speed 2.08 m/s at Froude number 0.32.

| Fr | Model speed | Shaft speed | Sinkage | Trim | Torque | Thrust | Towing Force |
|---|---|---|---|---|---|---|---|
| - | m/s | rev/sec | mm | Degrees | Nm | N | N |
| **0.32** | 2.08 | 10.181 | -2.53 | 0.00 | 0.10 | -4.66 | 17.51 |
| **0.32** | 2.08 | 11.277 | -2.76 | 0.01 | 0.10 | -2.61 | 15.74 |
| **0.32** | 2.08 | 13.043 | -2.92 | 0.02 | 0.00 | 0.63 | 12.68 |
| **0.32** | 2.08 | 13.047 | -2.86 | 0.02 | 0.00 | 0.50 | 12.55 |
| **0.32** | 2.08 | 13.052 | -2.81 | 0.02 | 0.00 | -1.04 | 12.46 |
| **0.32** | 2.08 | 13.052 | -2.83 | 0.02 | 0.00 | 0.22 | 12.40 |
| **0.32** | 2.08 | 15.099 | -3.04 | 0.03 | 0.10 | 5.35 | 8.10 |
| **0.32** | 2.08 | 15.103 | -3.27 | 0.03 | 0.10 | 5.24 | 8.27 |
| **0.32** | 2.08 | 15.103 | -3.13 | 0.03 | 0.10 | 5.54 | 8.08 |
| **0.32** | 2.08 | 17.004 | -3.35 | 0.04 | 0.20 | 10.56 | 3.63 |
| **0.32** | 2.08 | 17.011 | -3.35 | 0.04 | 0.20 | 10.26 | 3.60 |
| **0.32** | 2.08 | 17.040 | -3.60 | 0.04 | 0.20 | 10.46 | 3.66 |
| **0.32** | 2.08 | 18.025 | -3.64 | 0.04 | 0.30 | 13.28 | 0.87 |
| **0.32** | 2.08 | 18.028 | -3.62 | 0.05 | 0.30 | 13.21 | 0.89 |
| **0.32** | 2.08 | 18.030 | -3.78 | 0.05 | 0.30 | 13.12 | 1.04 |
| **0.32** | 2.08 | 19.546 | -3.84 | 0.06 | 0.40 | 17.61 | -3.69 |
| **0.32** | 2.08 | 20.352 | -3.93 | 0.06 | 0.40 | 20.69 | -6.20 |
| **0.32** | 2.08 | 20.361 | -3.84 | 0.07 | 0.40 | 20.65 | -6.47 |
| **0.32** | 2.08 | 20.368 | -3.89 | 0.06 | 0.40 | 20.41 | -6.41 |

Notes: [Sinkage: increase in draught –ve] [Trim: bow up +ve]

**Table F. 13** The self-propulsion test results for the propeller driven catamaran model at displacement of 2,500 tonnes. The test was conducted at model speed 2.27 m/s at Froude number 0.35.

| Fr | Model speed | Shaft speed | Sinkage | Trim | Torque | Thrust | Towing Force |
|---|---|---|---|---|---|---|---|
| - | m/s | rev/sec | mm | Degrees | Nm | N | N |
| **0.35** | 2.27 | 12.039 | -3.59 | 0.00 | 0.10 | -4.45 | 19.37 |
| **0.35** | 2.27 | 13.045 | -4.01 | 0.00 | 0.10 | -2.69 | 17.40 |
| **0.35** | 2.27 | 15.089 | -3.97 | 0.01 | 0.00 | 1.90 | 12.88 |
| **0.35** | 2.27 | 17.206 | -4.46 | 0.03 | 0.10 | 7.12 | 7.86 |
| **0.35** | 2.27 | 18.953 | -4.82 | 0.05 | 0.30 | 12.74 | 3.19 |
| **0.35** | 2.27 | 20.337 | -5.45 | 0.05 | 0.40 | 17.52 | -1.34 |
| **0.35** | 2.27 | 22.124 | -5.50 | 0.07 | 0.50 | 22.91 | -7.35 |

Notes: [Sinkage: increase in draught –ve] [Trim: bow up +ve]

**Table F. 14** The self-propulsion test results for the propeller driven catamaran model at displacement of 2,500 tonnes. The test was conducted at model speed 2.47 m/s at Froude number 0.38.

| Fr | Model speed | Shaft speed | Sinkage | Trim | Torque | Thrust | Towing Force |
|---|---|---|---|---|---|---|---|
| - | m/s | rev/sec | mm | Degrees | Nm | N | N |
| **0.38** | 2.47 | 15.089 | -5.92 | 0.08 | 0.00 | -1.55 | 19.06 |
| **0.38** | 2.47 | 16.120 | -6.22 | 0.09 | 0.00 | 0.91 | 16.82 |
| **0.38** | 2.47 | 18.079 | -6.82 | 0.11 | 0.10 | 6.09 | 11.92 |
| **0.38** | 2.47 | 20.337 | -7.08 | 0.13 | 0.30 | 13.32 | 5.42 |
| **0.38** | 2.47 | 22.121 | -7.14 | 0.13 | 0.40 | 19.58 | -0.66 |

Notes: [Sinkage: increase in draught –ve] [Trim: bow up +ve]

**Table F. 15** The self-propulsion test results for the propeller driven catamaran model at displacement of 2,500 tonnes. The test was conducted at model speed 2.60 m/s at Froude number 0.40.

| Fr | Model speed | Shaft speed | Sinkage | Trim | Torque | Thrust | Towing Force |
|---|---|---|---|---|---|---|---|
| - | m/s | rev/sec | mm | Degrees | Nm | N | N |
| **0.40** | 2.60 | 6.600 | -6.64 | 0.13 | 0.50 | -23.30 | 41.53 |
| **0.40** | 2.60 | 11.260 | -8.05 | 0.20 | 0.30 | -12.99 | 32.78 |
| **0.40** | 2.60 | 14.059 | -8.68 | 0.20 | 0.10 | -6.97 | 27.11 |
| **0.40** | 2.60 | 16.988 | -8.72 | 0.24 | 0.00 | -0.03 | 20.26 |
| **0.40** | 2.60 | 19.014 | -9.49 | 0.26 | 0.10 | 5.35 | 14.98 |
| **0.40** | 2.60 | 20.500 | -9.67 | 0.27 | 0.30 | 10.26 | 10.74 |
| **0.40** | 2.60 | 22.119 | -9.72 | 0.26 | 0.40 | 16.39 | 4.99 |
| **0.40** | 2.60 | 23.193 | -9.94 | 0.27 | 0.50 | 20.14 | 1.25 |
| **0.40** | 2.60 | 25.763 | -10.63 | 0.28 | 0.70 | 29.79 | -8.98 |

Notes: [Sinkage: increase in draught –ve] [Trim: bow up +ve]

**Table F. 16** The self-propulsion test results for the propeller driven catamaran model at displacement of 2,500 tonnes. The test was conducted at model speed 2.86 m/s at Froude number 0.44.

| Fr | Model speed | Shaft speed | Sinkage | Trim | Torque | Thrust | Towing Force |
|---|---|---|---|---|---|---|---|
| - | m/s | rev/sec | mm | Degrees | Nm | N | N |
| **0.44** | 2.86 | 16.080 | -13.63 | 0.54 | 0.10 | -11.16 | 33.44 |
| **0.44** | 2.86 | 18.000 | -14.00 | 0.56 | 0.00 | -3.18 | 28.10 |
| **0.44** | 2.86 | 18.021 | -13.82 | 0.55 | 0.00 | 3.08 | 27.87 |
| **0.44** | 2.86 | 20.033 | -14.40 | 0.59 | 0.10 | 2.38 | 22.89 |
| **0.44** | 2.86 | 22.167 | -14.64 | 0.58 | 0.30 | 9.73 | 15.74 |
| **0.44** | 2.86 | 25.000 | -14.67 | 0.58 | 0.50 | 18.23 | 6.87 |
| **0.44** | 2.86 | 25.780 | -13.43 | 0.58 | 0.60 | 23.96 | 1.38 |
| **0.44** | 2.86 | 27.000 | -15.31 | 0.57 | 0.70 | 30.72 | -5.32 |

Notes: [Sinkage: increase in draught –ve] [Trim: bow up +ve]

**Table F. 17** Propeller open water test results conducted using Wageningen B-5.75 series propeller. The test was conducted at Reynolds number 2.28 x $10^5$.

| **Carriage speed (Advance speed)** | **Propeller Torque** | **Propeller Thrust** | **Shaft speed** |
|---|---|---|---|
| m/s | Nm | N | rev/sec |
| **0.00** | 1.16 | 53.90 | 21.01 |
| **0.00** | 1.16 | 53.76 | 21.00 |
| **0.29** | 1.10 | 50.58 | 21.00 |
| **0.50** | 1.05 | 48.20 | 21.01 |
| **0.50** | 1.05 | 48.60 | 21.05 |
| **0.50** | 1.05 | 47.97 | 21.01 |
| **0.80** | 0.96 | 43.76 | 21.00 |
| **1.00** | 0.90 | 40.32 | 21.00 |
| **1.00** | 0.91 | 42.34 | 21.01 |
| **1.00** | 0.90 | 40.39 | 21.05 |
| **1.31** | 0.77 | 36.48 | 21.01 |
| **1.50** | 0.74 | 32.14 | 21.05 |
| **1.50** | 0.73 | 31.01 | 21.01 |
| **1.51** | 0.74 | 31.38 | 21.00 |
| **1.81** | 0.63 | 25.70 | 21.00 |
| **2.01** | 0.57 | 22.05 | 21.01 |
| **2.01** | 0.57 | 22.11 | 21.05 |
| **2.01** | 0.57 | 22.14 | 21.01 |
| **2.31** | 0.46 | 16.16 | 21.05 |
| **2.52** | 0.38 | 11.77 | 21.01 |
| **2.52** | 0.38 | 12.11 | 21.00 |
| **2.52** | 0.39 | 12.56 | 21.00 |
| **2.82** | 0.27 | 6.52 | 21.01 |
| **3.02** | 0.18 | 0.76 | 21.05 |
| **3.02** | 0.19 | 1.14 | 21.05 |
| **3.02** | 0.19 | 2.54 | 21.01 |
| **3.52** | 0.05 | 7.91 | 21.00 |

# References


Abbott, I. H., & Doenhoff, A. E. V. (1959). *Theory of Wing Sections*. Dover Publications Inc, New York.

Akagi, S. (1991). *Synthetic Aspects of Tranport Economy and Transport Vehicle Performance with Reference to High Speed Marine Vehicles*. Paper presented at the 1st International Conference on Fast Sea Transportation – FAST'91, Trondheim, Norway.

Akagi, S., & Morishita, M. (2001). *Transport Economy – Based Evaluation and Assessment of the Use of Fast Ships in Passenger – Car Ferry and Freighter Systems.* Paper presented at the 6th International Conference on Fast Sea Transportation – FAST 2001, London.

Alexander, K. (1995). Waterjet versus Propeller Engine Matching Characteristics. *Naval Engineers Journal, Volume 107*(Issue 3).

Allison, J. (1993). Marine Waterjet Propulsion. *Transactions of SNAME, Vol 101*(The Society of Naval Architects and Marine Engineers, New York).

Armstrong, T. (2004). Catamarans. In T. Lamb (Ed.), *Ship Design and Construction Volume II (pp. 45-1 – 45-35)*: The Society of Naval Architects and Marine Engineers, New York.

Aucher, M. (1974). Approximate formulas for the calculation of the drag coefficient and lift correction of the Open Water Charateristics of Propellers. *Working paper prepared for the ITTC Performance Committee*.

Austal. (2004). Austal's First for Sealink, Enthusiastic welcome for Austal's first medium speed ferry, News Release *Austal Ship*.

Bailey, D. (1976). The NPL high-speed round bilge displacement hull series. *Maritime Technology Monograph No.4, Royal Institution of Naval Architects*.

Bailey, D. (1982). *A Statistical Analysis of Propulsion Data obtained from Models of High Speed Round Bilge Hulls.* Paper presented at the Second Symposium on Small Fast Warships and Security Vessels, The Royal Institution of Naval Architects, London. .

Barrass, C. (1979). Ship-handling problems in shallow water. *Marine Engineers Review 3,* pp 17 – 19.

Bazilevski, Y. S. (2001). *On the Propeller Blade Turbulization in Model Tests*. Paper presented at the SP2001: Lavrentiev Lectures, St. Petersburg, Russia.

Bazzi, T., & Benedetti, L. (2009). *Ship model propeller manufacturing by using RPT.* Paper presented at the The 1st International Conference on Advance Model Measurement Technology for the EU Maritime Industry AMT'09, Ecole Centrale de Nantes, France.

Becker, J. F. F., Burgess, A., & Henstra, D. A. (2004). No Need for Speed in Short Sea Shipping. *Maritime Economics and Logistics, Palgrave Macmillan Ltd, London.*

Benedek, Z. (1985). Scale Effect on the Torque and Thrust Coefficients of Screw Propellers. *Periodica Polytechnica Mechanical Engineering, 29*(1-3), 115-120.

Bertram, V. (2000). *Practical Ship Hydrodynamics*. Oxford, UK: Butterworth-Heinemann.

Blasius, H. (1908). Grenzschichten in Flussigkeiten mit kleiner Reibung. *Z. Angew. Math. Phys., 56*, 1-37.

Boorsma, A. (2000). *Improving full scale ship powering performance predictions by application of propeller leading edge roughness.* (Master of Science), University of Technology, Delft.

Bose, N. (2008). *Marine Powering Prediction and Propulsors*. New Jersey, USA: The Society of Naval Architects and Marine Engineers.

Bose, N., Billet, M., Andersen, P., Atlar, M., Dugue, C., Ferrando, M., Qian, W., & Shen, Y. (1999). *The Specialist Committee on Unconventional Propulsors, Final Report and Recommendations to the 22nd ITTC.* Paper presented at the 22nd International Towing Tank Conference, Edinburgh, UK.

Bose, N., Insel, M., Anzbock, R., Hwangbo, S.-M., Mewis, F., Steen, S., Toki, N., & Zhu, D.-X. (2005). *The Specialist Committee on Powering Performance Prediction - Final Report and Recommendations to the 24th ITTC.* Paper presented at the Proceedings of the 24th ITTC

Bose, N., & Molloy, S. (2001a). *Powering prediction for ships with compound propulsors*. Paper presented at the International Conference on Ocean Engineering, Indian Institute of Technology, Madras.

Bose, N., & Molloy, S. (2001b). *Ship powering prediction from self-propulsion load varying tests*. Paper presented at the Proceedings of the SP2001 Lavrentiev Lectures, St. Petersburg State Marine Technical University. St. Petersburg, Russia.

Bowden, B. S., & Davidson, N. J. (1974). Resistance Due to Hull Roughness Associated with Form Factor Extrapolation Methods. *National Physical Laboratory, Ship Technical Manual 3800*.

Broberg, L., & Orych, M. (2011). *Modern Tools for Efficient Hydrodynamic Design of Ships.* Paper presented at the International Conference on Ship and Offshore Technology, ICSOT, RINA conference, India.

Bulten, N. (2008). *A Breakthrough in Waterjet Propulsion Systems*. Paper presented at the Doha International Maritime Defence Exhibition and Conference DIMDEX 2008, Qatar

Burrill, L. C., & Emerson, A. (1953). Propeller Cavitation - Some observations from 16 Inch Propeller Tests in the New King's College Cavitation Tunnel. *Trans., NECI, Vol. 70*.

Burrill, L. C., & Emerson, A. (1962). Propeller Cavitation - Further Tests on 16 Inch Propeller Models in the King's College Cavitation Tunnel. *Trans. NECI, Vol. 79*.

Campana, E. F., Hino, T., Bull, P., Carrica, P. M., Kim, J., Kim, S.-E., Li, D.-Q., Saisto, I., & Starke, B. (2011). *The Specialist Committee on Computational Fluid Dynamics - Final Report and Recommendations to the 26th ITTC.* Paper presented at the 26th International Towing Tank Conference, Rio de Janeiro.

Carlton, J. S. (2007). *Marine Propellers and Propulsion* (2 ed.). UK: Butterworth-Heinemann.

Chapman, L. (2007). Transport and climate change: a review. *Journal of Transport Geography, 15*(5), 354-367.

Cheng, R. K. C. (2014). *Inside Rhinoceros 5*. Stamford, USA: Cengage Learning.

Choi, J. K., & Kinnas, S. A. (2001). Prediction of Non-Axisymmetric Effective Wake by a Three-Dimensional Euler Solver. *Journal of Ship Research, Vol. 45*, pp. 13 - 33.

Coleman, H., & Steele, W. G. (1999). *Experimentation and Uncertainty Analysis for Engineers* (2nd Edition ed.). USA: John Wiley & Sons.

Coop, H. G. (1995). *Investigation of Hull-Waterjet Interaction Effects.* (PhD Thesis), University of Canterbury, Christchurch.

Couser, P., Molland, A. F., Armstrong, N., & Utama, I. K. (1997). *Calm water powering predictions for high-speed catamarans*. Paper presented at the Fourth International Conference on Fast Sea Transportation, Sydney, Australia.

Davidson, G., Roberts, T., Friezer, S., Davis, M., Bose, N., Thomas, G., Binns, J., & Verbeek, R. (2011). *Maximising Efficiency and Minimising Cost in High Speed Craft*. Paper presented at the 11th International Conference on Fast Sea Transportation FAST 2011, Honolulu, Hawaii, USA.

Duffy, J. T., & Lilienthal, T. (2010). Resistance Tests and Powering Estimates for the 130m WP Catamaran *Commercial in Confidence, Report prepared for Revolution Design, AMC Search Ltd Report No. 10/T/01*. Australian Maritime College, Tasmania.

Eca, L., & Hoekstra, M. (2005). On the accuracy of the numerical prediction of scale effects on ship viscous resistance. *International Conference on Computational Methods in Marine Engineering*, 1 - 10.

Emerson, A. (1959). Ship Model Size and Tank Boundary Correction. *Transactions of NECES*, p. 251.

Eslamdoost, A. (2012). *Investigation of waterjet/hull interaction effects.* (PhD Thesis), Chalmers University of Technology, Gothenburg, Sweden.

Eslamdoost, A. (2014). *The Hydrodynamics of Waterjet/Hull Interaction.* (PhD Thesis), Chalmers University of Technology, Gothenburg, Sweden.

Eslamdoost, A., Larsson, L., & Bensow, R. (2015). *Waterjet propulsion and negative thrust deduction fraction*. Paper presented at the Fourth International Symposium on Marine Propulsors smp'15, Austin, Texas, USA.

Fishman, G. S. (1996). *Monte Carlo - Concepts, Algorithms and Applications*. New York: Springer-Verlag.

Froude, W. (1872, 1874). Experiments on Surface Friction. *British Association Reports*.

Fry, E. D., & Graul, T. (1972). Design and application of high-speed catamarans. *Marine Technology, Vol 9, No 3*.

Fu, T. C., Takinaci, A. C., Bobo, M., Gorski, W., Johannsen, C., Heinke, H.-J., Kawakita, C., & Wang, J.-B. (2011) The Specialist Committee on Scaling of Wake Field - Final Recommendations to the 26th ITTC. 26th International Towing Tank Conference, Rio de Janeiro, Brazil.

Garcia-Gomeza, A. (2000). On the form factor scale effect. *Ocean Engineering, Volume 27*(1), 97 - 109.

Gilat, A. (2010). *MATLAB: An Introduction with Applications*: Wiley Publishing.

Giles, W., Dinham-Peren, T., Amaratunga, S., Vrijdag, A., & Partridge, R. (2010). *The advanced waterjet: Propulsor performance and effect on ship design*. Paper presented at the IMAREST's 10th International Naval Engineering Conference, Portsmouth UK.

Goubault, P., & Allison, J. (2004). Advanced Marine Surface Craft. In T. Lamb (Ed.), *Ship Design and Construction Volume II* (pp. 44-41 – 44-21): The Society of Naval Architects and Marine Engineers, New York.

Griggs, D. (2005). HSV-2 SWIFT Combined Standardization and Powering Trials Results. Naval Surface Warfare Center, Carderock Division, West Bethesda, Maryland.

Grigson, C. W. B. (1993). An accurate smooth friction line for use in performance prediction. *Trans. Royal Inst. of Naval Architects, Vol. 135*.

Haase, M. (2015a). *Energy-efficient large medium-speed catamarans hull form design by full-scale CFD simulations.* (PhD), Australian Maritime College, University of Tasmania.

Haase, M. (2015b). *Energy-efficient large medium-speed catamarans hull form design by full-scale CFD simulations.* Australian Maritime College, University of Tasmania, Launceston.

Haase, M., Binns, J., Thomas, G., Bose, N., Davidson, G., & Friezer, S. (2012a). On the Macro Hydrodynamic Design of Highly Efficient Medium-Speed catamarans with Minimum Resistance. *Transaction of the Royal Institution of Naval Architects, Part A - International Journal of Maritime Engineering 154.A3*, pp. 131 - 142.

Haase, M., Davidson, G., Friezer, S., Binns, J., Thomas, G., & Bose, N. (2015). Hydrodynamic Hull Form Design Space Exploration of Large Medium-Speed

Catamarans Using Full-Scale CFD. *Trans. Royal Inst. of Naval Architects, Part A - International Journal of Maritime Engineering 157.A3*, pp. 161 - 174.

Haase, M., Iliopulos, F., Davidson, G., Friezer, S., Thomas, G., Binns, J., Bose, N., Lavroff, J., & Davis, M. (2012b). *Application of RANSE-based simulations for resistance prediction of medium-speed catamarans at different scales.* Paper presented at the Proceedings of the 18th Australasian Fluid Mechanics Conference, 3-7 December, Launceston, Tasmania, Australia.

Hadler, J. B., Cain, K. M., & Singleton, E. M. (2009). *On the effect of transom area on the resistance of high-speed catamaran hulls*. Paper presented at the International Conference on Fast Sea Transportation, Greece.

Hadler, J. B., Kleist, J. L., & Unger, M. L. (2007). *On the effect of transom area on the resistance of hi-speed monohulls*. Paper presented at the International Conference on Fast Sea Transportion, Shanghai, China.

Haglund, K., Svensson, R., & Bjorheden, O. (1982). *Design and Testing of a High-Performance Water Jet Propulsion*. Paper presented at the Second Symposium on Small Fast Warships and Security Vessels, The Royal Institution of Naval Architects, London. .

Hahn, B. D., & Valentine, D. T. (2007). *Essential MATLAB for Engineers and Scientists* (Third ed.): Butterworth-Heinemann.

Hasan, S. M. R. (2011). *Impact of EEDI on Ship Design and Hydrodynamics.* Master of Science thesis, Chalmers University of Technology, Gothenburg, Sweden

Hoerner, S. F. (1965). Fluid Dynamic Drag. *Hoerner Fluid Dynamics, Bricktown, New Jersey*.

Holtrop, J. (2001). Extrapolation of propulsion tests for ships with appendages and complex propulsors. *Marine Technology, Vol. 38*(No. 3), pp. 145 - 157.

Hugel, M. A. (1992). *An Evaluation of Propulsors for Several Navy Ships.* (Master), Massachusetts Institute of Technology, Massachusetts.

Hughes, G. (1954). Friction and Form Resistance in Turbulent Flow and a Proposed Formulation for Use in Model and Ship Correlation. *Trans. RINA, Vol. 96*.

Hughes, G. (1961). Tank Boundary Effects on Model Resistance. *Transactions of RINA*.

Hughes, G., & Allan, J. F. (1951). Turbulence stimulation on ship modesl. *SNAME Transactions, 59*.

HydroComp. (2010). PropCad, 2010 User's Guide. USA.

Iannone, L. (2006). New perspectives in experimentally predicting ships power performance. *Bollettino della Comunita Scientifica in Australasia*(Dicembre 2006), pp 47 - 50.

IMO. (2012). Guidelines on the method of calculation of the attained Energy Efficiency Design Index (EEDI) for new ships *Resolution MEPC. 212 (63), Adopted on 2 March 2012.* International Maritime Organization.

IMO. (2013). Revised proposal for the inclusion of the Ro-Ro Cargo and Ro-Ro passenger ship types into the IMO Energy Efficiency Regulatory framework. *Submitted to MEPC 65th session by Germany, Sweden, Community of European Shipyards Associations (CESA) and Interferry, Agenda Item 4, MEPC 65/4/4.* International Maritime Organization.

Insel, M., & Molland, A. F. (1992). An investigation into resistance components pf high-speed displacement catamarans. *Transactions, Royal Institution of Naval Architects, 134*.

ISO. (1995). Guide to the Expression of Uncertainty in Measurement. Geneve, Switzerland: International Organization for Standardization.

ITTC. (1999a). Recommended Procedures - Performance, Propulsion 1978 ITTC Performance Prediction Method. International Towing Tank Conference.
ITTC. (1999b). Uncertainty Analysis in EFD (Vol. ITTC Recommended Procedure 7.5-02-01-01). 22nd International Towing Tank Conference Seoul / Shanghai.
ITTC. (2002a). ITTC - Recommended Procedures and Guidelines - Testing and Extrapolation Methods Resistance Uncertainty Analysis Example for Resistance Test. International Towing Tank Conference.
ITTC. (2002b). ITTC - Recommended Procedures and Guidelines, Testing and Extrapolation Methods Propulsion, Propulsor Open Water Test. International Towing Tank Conference.
ITTC. (2008). Guide to the Expression of Uncertainty in Experimental Hydrodynamics: International Towing Tank Conference.
ITTC. (2011a). ITTC - Recommended Procedures and Guidelines - 1978 ITTC Performance Prediction Method, International Towing Tank Conference. International Towing Tank Conference.
ITTC. (2011b). ITTC - Recommended Procedures and Guidelines - Resistance Test. International Towing Tank Conference.
ITTC. (2011c). ITTC - Recommended Procedures and Guidelines - Waterjet Propulsive Performance Prediction. International Towing Tank Conference.
ITTC. (2011d). ITTC – Recommended Procedures and Guidelines – Ship Models. International Towing Tank Conference.
ITTC. (2014). ITTC – Recommended Procedures and Guidelines - 1978 ITTC Performance Prediction Method. International Towing Tank Conference.
Jessup, S., Bose, N., Dugue, C., Esposito, P. G., Holtrop, J., Lee, J.-T., Mewis, F., Poustoshny, A., Salvatore, F., & Shirose, Y. (2002). *The Propulsion Committee - Final Report and Recommendations to the 23rd ITTC.* Paper presented at the 23rd ITTC, Venice.
Katsui, T., H. Asai, Himeno, Y., & Tahara, Y. (2005a). *The Proposal of a New Friction Line.* Paper presented at the The 5th Osaka Colloquium on Advanced Research on Ship Viscous Flow and Hull Form Design by EFD and CFD Approaches, Osaka, Japan.
Katsui, T., Himeno, Y., & Tahara, Y. (2005b). *The proposal of a new friction line.* Paper presented at the Proceedings of the 5th Osaka Colloquium on Advanced research on Ship Viscous Flow and Hull form design by EFD and CFD Approaches, Osaka.
Katzman, F. M., Pustoshny, A. F., & Schtumpf, V. M. (1972). *The propulsive performance of seagoing ships*. Leningrad, Sudostroenie. (in Russian).
Kennell, C. (1998). Design Trends in High-Speed Transport. *Journal Marine Technology, Vol. 35, No 3*.
Kim, H. C. (1962). *Blockage Correction in Ship Model Testing*. Paper presented at the ATTC, University of Michigan, Ann Arbor.
Kinoshita, M. (1954). On Restricted Boundary Effect on Ship Resistance. *Transactions of Japan Society of Naval Architects, Vol. 76*, pp. 173 - 213.
Kirkman, K. L., & Kloetzli, J. W. (1980). Scaling Problem of Model Appendages. *ATTC, University of Michigan, Ann Arbor*.
Kiss, T. G., & Compton, R. H. (1989). The effects of transom geometry on the resistance of large surface combatants. *SNAME Transactions, 97*, 339 -373.
Kobylinski, L. K. (2003). Directional stability of ships and safe handling. *Transactions on the Built Environment, Vol 68*.
Korkmaz, K. B., Orych, M., & Larsson, L. (2015). *CFD Predictions including Verification and Validation of Resistance, Propulsion and Local Flow for the Japan Bulk Carrier*

*(JBC) with and without an Energy Saving Device.* Paper presented at the Proceedings, Tokyo 2015 Workshop on CFD in Ship Hydrodynamics, Tokyo.

Kouh, J., Chen, Y., & Chau, S. (2009). Numerical study on scale effect of form factor. *Ocean Engineering, Volume 36*(Issue 5), 403-413.

Kracht, A. M. (1991). Load Variation Tests Improve the Reliability of Ship Power Prediction Based on Model Test Results. *Ship Technology Research, 38*, 181 - 190.

Kristensen, H. O. H., & Hagemeister, C. (2011). Environmental performance evaluation of Ro-Ro passenger ferry transportation. *Trafikdage pa Aalborg Universitet 2011*.

Kuiper, G. (1992). *The Wageningen propeller series*. The Netherlands: Maritime Research Institute Netherlands (MARIN).

Lammeren, W. P. A. v. (1948). *Resistance, propulsion and steering of ships: a manual for designing hull forms, propellers and rudders*: Haarlem, H. Stam.

Lap, A. J. W. (1956). Scale Effects in the Resistance of Bossings and Shaft Brackets. *NSMB Publication 134a. Also Association Technique Maritime et Aeronaitique*.

Larsson, L., & Hoyte, C. R. (2010). *Ship Resistance and Flow, The Principles of Naval Architecture Series*. The Society of Naval Architects and Marine Engineers, New Jersey.

Li, Y., Martin, J. E., Michael, T., & Carrica, P. M. (2015). A Study of Propeller Operation Near a Free Surface. *Journal of Ship Research, Vol. 59*(Number 4).

Lindgren, Aucher, M., Bowen, B. S., Gross, A., Minsaas, K. J., Muntjewerf, J. J., Tamura, K., & Wermter, R. (1978). *Report of Performance Committee.* Paper presented at the Proceedings of the 15th International Towing Tank Conference, The Haque, The Netherlands.

Longo, J., & Stern, F. (2005). Uncertainty Assessment for Towing Tank Tests With Example for Surface Combatant DTMB Model 5415. *Journal of Ship Research, Vol. 49, No. 1, pp. 55-68*.

Mandel, P. (1953). Some Hydrodynamic Aspects of Appendage Design. *SNAME Transactions, Vol. 61*.

Manen, J. D., & Oossanen, P. (1988). *Principles of Naval Architecture: Resistance and Propulsion* (Vol. 2). New Jersey: SNAME.

Marin. (2008). Calm Water Tests for the JHSV Wave Piercing Catamaran. MARIN, Wageningen, Netherlands.

Maruo, H. (1948). On the Shallow Water Effect. *Transactions of Japan Society of Naval Architects*.

Matsubara, S. (2011). *Ship Motions and Wave-Induced Loads on High Speed Catamarans.* (PhD thesis), University of Tasmania, Australia.

McCarthy, J. H., Power, J. L., & Huang, T. T. (1976). *The roles of transition, laminar separation, and turbulence stimulation in the analysis of axisymmetric body drag*. Paper presented at the Eleventh ONR Symposium on Naval Hydrodynamics, London, UK.

McTaggart, K. (2016). Literature Review for Design and Assessment of Directional Stability and Turning Performance of Naval Destroyers, Defence Research and Development Canada.

Moffatt, R. J. (1982). Contributions to the Theory of Single-Sample Uncertainty Analysis. *ASME Journal of Fluids Engineering, Vol. 104, No. 2, pp. 173 - 178.*

Molland, A. F., Turnock, S. R., & Hudson, A. D. (2011). *Ship resistance and propulsion: practical estimation of propulsive power*. Cambridge University Press, England.

Molland, A. F., Wellicome, J. F., & Couser, P. R. (1996). Resistance experiments on a sytematic series of high-speed displacement catamaran forms: Variations of length-

displacement ratio and breadth-draught ratio. *Transactions, Royal Institution of Naval Architects, 138A*.

Molloy, S. (2006). *Uncertainty analysis of ship powering prediction methods using Monte Carlo simulation.* (PhD), Memorial University, Newfoundland Canada.

Muller, S. B., Abdel-Maksoud, M., & Hilbert, G. (2009). *Scale effects on propellers for large container vessels*. Paper presented at the First International Symposium on Marine Propulsors smp'09, Trondheim, Norway.

Mulligan, R., F., & Lombardo, G. A. (2006). Short Sea Shipping - Alleviting the Environmental Impact of Economic Growth. *WMU Journal of Maritime Affairs, Vol. 5, pp. 181 - 194.*

Mustaffa Kamal, I., Binns, J., Bose, N., & Thomas, G. (2013). *Reliability assessment of ship powering performance extrapolations using Monte Carlo methods.* Paper presented at the Third International Symposium on Marine Propulsors SMP'13, Launceston, Tasmania, Australia.

Mustaffa Kamal, I., Zurcher, K., Bose, N., Binns, J., Chai, S., & Davidson, G. (2015). *Powering for Medium Speed Wave-Piercing Catamarans comparing Waterjet and Screw Propeller Performance using Model Testing*. Paper presented at the Fourth International Symposium on Marine Propulsors, SMP'15, Austin, Texas, USA.

Øyan, E. (2012). *Speed and powering prediction for ships based on model testing.* (Master Thesis), NTNU Trondheim.

Papanikolaou, A. (2014). *Ship Design: Methodologies of Preliminary Design*. Springer Science, Dordrecht.

Papanikolaou, A., Georgantzi, N., & Papatzanakis, G. (2001). Regression Analysis and Assessment of Collected Techno-Economic Data of Fast Marine Vessels - EFFISES Report WOR NTUA, Athens.

Passenger Ship Technology. (2012). *Passenger Ship Technology 4th Quarter 2012*, pp. 14 - 18.

Peck, J. G., & Moore, D. H. (1974). Inclined-shaft propeller performance characteristics. Naval Ship Research and Development Center, Bethesda, Maryland.

Peck, R. W. (1976). The Determination of Appendage Resistance of Surface Ships. *AEW Technical Memorandum 76020*.

Preston, J. H. (1958). The minimum Reynolds number fro a turbulent boundary layer and the selection of a transition device. *Journal of Fluid Mechanics, Vol.3, No 04*, pp. 373 – 384.

Psaraftis, H. N., Kontovas, C. A., & Kakalis, N. M. P. (2009). *Speed reduction as an emissions reduction measure for fast ships*. Paper presented at the 10th International Conference on Fast Sea Transportation, FAST2009, Athens, Greece.

Raven, H. C., Ploeg, A. v. d., Starke, A. R., & Eca, L. (2008). *Towards a CFD-based Prediction of Ship Performance - Progress in Prediciting Full-Scale Resistance and Scale Effects.* Paper presented at the RINA Marine CFD Conference, Southamptom, UK.

Regener, P. B., Mirsadraee, Y., & Andersen, P. (2017). *Nominal vs Effective Wake Fields and their Influence on Propeller Cavitation Performance.* Paper presented at the Fifth International Symposium on Marine Propulsors smp'17, Espoo, Finland.

Robert, C. P., & Casella, G. (2004). *Monte Carlo Statistical Methods*. USA: Springer Science.

Rovere, J. E. (1997, 1997). *Catamaran resistance from tests on a single demihull.* Paper presented at the Proceedings of the FAST' 97, Sydney, Australia.

Sanchez-Caja, A., & Pylkkanen, J. V. (2007). *Prediction of effective wake at model and full scale using RANS code with an actuator disk model*. Paper presented at the 2nd International Conference on Maritime Research and Transportation Ischia, Italy.

Sasajima, H., Tanaka, I., & Suzuki, T. (1966). Wake distributions of full ships. *J. Soc. Nav. Arch, Japan*.

Saunders, H., E. (1957a). *Hydrodynamics in ship design. Volume 1*. The Society of Naval Architects and Marine Engineers, New York.

Saunders, H., E. (1957b). *Hydrodynamics in ship design. Volume 2*: The Society of Naval Architects and Marine Engineers, New York.

Savitsky, D., Knowles, P., Alaez, J. A., Koops, B., Muller-Graf, B., Rutgersson, O., Rozhdestvensky, K., Tanaka, H., & Wilson, R. A. (1987). Report of the High-Speed Marine Vehicle Committee: Proceedings of the 18th ITTC.

Schmiechen, M. (1991). Paper presented at the Proceedings of the 2nd International Workshop on the Rational Theory of Ship Hull-Propeller Interaction and its Applications, VWS, Berlin Ship Model Basin, HEFT 56, June 13 - 14.

Schuster, S. (1955). Beitrag zur Frage der Kanalkorrektur bei Modellversuchen Schifftechnik. *Bd. 3, 1955/56*.

Scott, J. R. (1970). On Blockage Correction and Extrapolation to Smooth Ship Resistance. *SNAME Transactions*, pp. 288 - 324.

Steen, S., Bobo, M., Karafiath, G., Insel, M., Anzbock, R., Jang, J., Toki, N., Zhu, D., & Qiu, W. (2008). *The Specialist Committee on Powering Performance Prediction - Final Report and Recommendations to the 25th ITTC*, Fukuoka, Japan.

Stern, F., Longo, J., Penna, R., Olivieri, A., Ratcliffe, T., & Coleman, H. (2000). *International Collaboration on Benchmark CFD Validation Data for Surface Combatant DTMB Model 5415*. Paper presented at the Twenty-Third Symposium on Naval Hydrodynamics, Val de Reuil, France.

Stern, F., Sadat-Hosseini, H., Yang, J., & Mousaviraas, M. (2013). Computational ship hydrodynamics: nowadays and way forward. *International Shipbuilding Progress, 60*, 3 - 105.

Svensson, R. (1987). *Water Jet Propulsion for Navy Vessels.* Paper presented at the Proceedings of the 2nd Pan American Symposium on Design and Construction of Military Vessels, Pan American Institute of Naval Engineering, Rio De Janeiro.

Svensson, R. (1989). Experience with KaMeWa waterjet propulsion system. *American Institute of Aeronautics and Astronautics, Inc. Report No. 89-1440-CP*.

Tagori, T. (1963). *A Study of the Turbulence Stimulation Device in the Model Experiment on Ship Form.* Paper presented at the Proceedings of the 10th ITTC, Teddington UK.

Tamura, K. (1972). Study of the Blockage Correction. *Journal of the Society of Naval Architects of Japan, Vol. 131, Vol. 131*, pp. 17 - 28.

Tanibayashi, H., Collatz, G., Loggia, B. D., Holtrop, J., Lin, W. C., Moor, D. I., Munk, T., Nizery, B., & Varsamov, K. (1984). *Report of the Performance Committee.* Paper presented at the 17th International Towing Tank Conference, Goteborg, Sweden.

Telfer, E. V. (1933). *Miscellaneous Notes.* Paper presented at the International Conference of Tank Superintendents, The Hague.

Terwisga, T. v. (1996). *Waterjet-Hull Interaction.* (PhD), TU Delft Netherlands.

Tzannatos, E., & Stournaras, L. (2014). EEDI analysis of Ro-Pax and passenger ships in Greece. *Maritime Policy & Management, 42*(4), 305-316. doi: 10.1080/03088839.2014.905722

van der Kley, M. (2013). *Working with Rhinoceros 5.0*: Rhinoacademie.

Wartsila. (2014). Wartsila Solutions for Marine Oil & Gas Markets. In Wartsila Corporation (Ed.). Helsinki, Finland.

Watson, D. G. M. (1988). *Practical Ship Design* (Vol. 1). Elsevier Ocean Engineering Book Series, Oxford.

Zürcher, K. (2015). *Waterjet Testing Techniques for Powering Performance Estimation using a Single Catamaran Demihull.* (PhD Thesis), Australian Maritime College, University of Tasmania, Launceston.

Zürcher, K., Bose, N., Binns, J., Thomas, G., & Davidson, G. (2013). *Design and Commissioning Tests for Waterjet Self-Propulsion Testing of a Medium-Speed Catamaran Ferry using a Single Demihull.* Paper presented at the The Third International Symposium on Marine Propulsors SMP'13, Launceston, Tasmania, Australia.